Linking tectonic evolution with fluid history in hyperextended rifted margins : examples from the fossil Alpine and Pyrenean rift systems, and the present-day Iberia rifted margin

Victor Hugo Pinto

UNIVERSITÉ DE STRASBOURG

Ecole et Observatoire des Sciences de la Terre

École Doctorale des Sciences de la Terre et de l'Environnement (ED 413)

Institut de Physique du Globe de Strasbourg (UMR 7516)

Thèse

présentée par :

Victor Hugo PINTO

soutenue le : **3 décembre 2014**

pour obtenir le grade de : **Docteur de l'Université de Strasbourg**

Discipline/ Spécialité : Sciences de la Terre – Géologie

LINKING TECTONIC EVOLUTION WITH FLUID HISTORY IN HYPEREXTENDED RIFTED MARGINS:

Examples from the fossil Alpine and Pyrenean rift systems, and the present-day Iberia rifted margin

THÈSE dirigée par :

M. MANATSCHAL Gianreto	Professeur, Université de Strasbourg
Dr. KARPOFF Anne Marie	Dr. Emeritus, Université de Strasbourg

RAPPORTEURS :

Mme. BERNASCONI-GREEN Gretchen	Professeur, ETH-Zürich
M. POTDEVIN Jean-Luc	Professeur, Université Lille 1

EXAMINATEURS :

BOULVAIS Philippe	Maître de conférence, Université de Rennes 1
MAGNAVITA Luciano	Géologue, Petrobras, Rio de Janeiro
VIANA Adriano	Géologue, Petrobras, Rio de Janeiro

UNIVERSITÉ DE STRASBOURG

UNIVERSITÉ DE STRASBOURG

Ecole et Observatoire des Sciences de la Terre

PETROBRAS

cnrs dépasser les frontières

IPGS Institut de Physique du Globe de Strasbourg

Linking tectonic evolution with fluid history in hyperextended rifted margins:

examples from the fossil Alpine and Pyrenean rift systems, and the present-day Iberia rifted margin

PINTO, Victor Hugo

Advisor: MANATSCHAL, Gianreto — *Professeur, Université de Strasbourg*

Co-advisor: KARPOFF, Anne Marie — *Dr. Emeritus, Université de Strasbourg*

TABLE OF CONTENTS

REMERCIEMENTS

REMERCIEMENTS

Je savais qu'un jour je ferai un doctorat, mais de là à penser que je le ferais en France, celle de Victor Hugo, de la révolution et de toutes les histoires dont j'étais passionné, la France dont la géologie est si remarquable… C'est une belle surprise que la vie m'a réservée. Cela n'aurait pas été possible sans le support de mon entreprise, Petrobras. Un grand merci à tous les Responsables de Petrobras pour avoir permis ma venue en France; ils savent ce que je leur dois.

Voilà, Gianreto Manatschal, il me m'a fallu que cinq jours d'excursion dans les Alpes pour que je dise, "c'est ici que je dois faire une thèse". Pendant mon doctorat, avec ton enthousiasme tu m'as montré tout les "marges" fossiles, et comment on peut développer une recherche dans ces domaines pour aller plus loin dans leur connaissance. C'est toujours accompagnés de tes métaphores "Manatschaliennes" que nous avons mené de passionnantes et fructueuses discussions, réflexions et enseignements. Grazia fitg!

Un grand merci à Anne Marie Karpoff. La géochimie n'est pas une simple affaire et ses liens avec la géologie le sont encore moins. Il n'aurait pas été possible d'avancer dans ma thèse sans tes connaissances, tes différents exemples de plusieurs océans, plusieurs analogues. C'est une connaissance qu'il faut du temps à acquérir. Merci de m'en avoir transmis une partie, merci pour ta patience, pour ton amitié.

Je remercie Gretchen Bernasconi-Green, Jean-Luc Potdevin, Adriano Viana, Phillippe Boulvais et Luciano Magnavita pour l'honneur d'avoir accepté de faire partie du jury de thèse mais également pour leurs suggestions pour les articles.

À mes amis français que m'ont reçu quand je suis arrivé à Strasbourg et avec qui j'ai partagé, pendant ces trois ans et demi, des bureaux et les discussions sur nos projets de thèse: Benoît Petri, Morgane Gillard, Isabelle Haupert, Pierre Dietrich, Pauline Chenin et bien sûr le grand fan de la Seleção Brasileira, Michael Nirrengarten, mais aussi aux thésard et chers amis dont je suis sûr qu'ils vont continuer dans une bonne direction, Pauline Le Maire, Marie-Eva Epin, Médéric Amman et Nicolo Incerpi, …merci! Je pense aussi à Bruno Gavazzi pour son amitié et nos débats politiques de la "salle café".

Un grand merci aux "vieux" thésards, Emmanuel Masini et Geoffroy Mohn pour les nombreuses discussions et les bons moments que nous avons passé sur le terrain, mais aussi à mes chers Adrien Bronner, Émilie Sutra, Julie Tugend, Ludovic Jeanniot pour les échanges sur les

Marges Ibérique et de Terre-Neuve.

Je n'oublie pas les post-doctorants Alessandro Decarlis, Natasha Stanton, Alexis Nutz, Anne-Sophie Tabaud, Etienne Skrzypek et Alexandra Guy. Je souhaite également remercier les étudiants de Master qui ont travaillé sur les mêmes thématiques que celles de mon projet, Danping Hu et Alexandre Schohn.

Je remercie les professeurs, maîtres de conférence et chercheurs de l'EOST pour les nombreuses discussions géologiques et géochimiques, spécialement Hubert Whitechurch, Karel Schulmann, Julia Autin, Marc Ulrich, Philippe Duringer, Mathieu Schuster et Damien Lemarchand.

En grand merci à René Boutin, Amélie Aubert, Fabienne Huber, Elise Kali, Jerome van der Woerd et John Moine pour m'avoir aidé à la préparation des échantillons, lames minces et analyses chimiques.

Merci pour leurs aides techniques et administratives, Annie, Betty, Ghenima, David, Didier et Joëlle.

J'adresse mes remerciements à mes chers collègues d'Austin pour les discussions sur la modélisation et les bons moments dans la Death Valley et dans les Pyrénées: Nick Hayman, Jacqueline Reber, Suzon Jammes, Anna Svartman, Luc Lavier et Guangliang.

Je remercie spécialement mes superviseurs et collègues de Petrobras, certains d'entre eux à la retraite, pour le soutien, pour les discussions et pour m'avoir fait confiance: Sylvia dos Anjos, Henrique Penteado, José Cupertino, Almério França, Luiz Antônio Trindade, Adriano Viana, Luciano Magnavita, Mario Carminatti, Guilherme Estrella, Peter Szatmari, Edison Milani, Isabela Carmo, Mário Neto, Carlos Fracalossi et Laury Medeiros.

Je remercie Cheryl pour les suggestions d'anglais et pour son optimisme constant.

Et pour terminer, je remercie particulierement Joana qui a partagé tous ce temps à Strasbourg avec moi.

« L'esprit de l'homme a trois clefs qui ouvrent tout: le chiffre, la lettre, la note.
Savoir, penser, rêver. Tout est là. »
Victor Hugo, Les rayons et les ombres, 1840

RÉSUMÉ ÉTENDU

RÉSUMÉ ÉTENDU

L'évolution et la formation des marges passives riftées, et des océans, sont intimement liées à des processus magmatiques, tectoniques, structuraux et sédimentaires, aussi bien qu'à des changements climatiques et d'ouvertures de nouvelles mers. L'étude de ces marges documente de constants changements de la Terre au cours des temps géologiques. Les fluides sont des constituants fréquemment associés à ces processus ou sont formés par eux, par exemple, les fluides métamorphiques, magmatiques, météoriques, biogènes et diagénétiques. Les relations entre processus dynamiques et fluides sont souvent étudiées localement dans des sites spécifiques, par exemple dans des zones de cisaillement, fumeurs hydrothermaux, et volcans. Ceux-ci sont souvent associés à la formation de veines métamorphiques, de biométhanogenèse et à l'activité des fumeurs noirs (black smokers).

Les fluides jouent un rôle majeur dans le refroidissement de la croûte le long des rides médio-océaniques, dans les formations des gîtes minéraux mais aussi dans la formation des ressources énergétiques. Ils sont probablement importants dans la formation des premiers composés organiques et par conséquence pour l'évolution de la vie primitive.

Bien que les marges passives constituent une grande part de la surface de la planète, les fluides qui se sont développés lors des premiers stades de leur formation et les transferts eau-roche qui en résultent ont été peu étudiés. Cela est principalement dû aux difficultés d'accès aux données car la formation et la circulation actuelle des fluides ont lieu dans les fonds marins, dans les bassins sédimentaires, ou en grande profondeur dans la croûte terrestre. De plus, dans bon nombre de ces systèmes, les flux de fluides sont déjà inactifs, limitant de fait l'étude et compréhension de ces processus.

Cependant, des empreintes et marques de flux de fluides sont fréquemment observées le long des zones de failles (ex. formation de veines), dans les roches sédimentaires (ex. silicification) et dans le manteau exhumé (ex. serpentinisation). Bien que ces observations soient faites, leur origine, leurs processus de formation ainsi que leur distribution n'ont pas été suffisamment étudiées. Par ailleurs, ces marques sont peu analysées à grande échelle, en particulier à l'échelle d'une marge continentale. D'importantes questions sont fréquemment posées par la communié scientifique, certaines d'entre elles sont abordées dans cette thèse. Quelle est la source des fluides? Comment et quand ont-ils été formés? Quels sont les chemins de migration? Quels sont la source et le piège des ces fluides? Ont-ils interagi avec les roches du socle et du bassin sédimentaire? Quelle est leur

composition et sont leurs signatures chimiques préservées? Pouvons-nous quantifier le volume des fluides ayant circulé dans les marges et l'importance des transferts eau-roche? Quel est le rôle des fluides sur l'évolution des marges riftées?

La difficulté d'étudier la trace et la signature des fluides dans les marges actuelles est due à la rareté des données, en particulier dans la partie distale des marges (actuellement en eau profonde). Actuellement, les forages de ces objets géologiques sont limités par la technologie et/ou pour leur coût élevé. De plus, même lorsque les données sont disponibles, elles peuvent être insuffisantes pour comprendre l'évolution des systèmes de fluides à l'échelle d'une marge. Les problèmes d'échelle peuvent être résolus par l'utilisation des données sismiques par réfraction et réflexion qui permettent d'imager des structures profondes. Cependant, d'épaisses couches sédimentaires peuvent en limiter la visualisation dans des nombreuses marges. Ainsi, les marges conjuguées de l'Ibérie et de Terre-Neuve font partie des meilleurs sites pour répondre à ces questions, de par leur caractère pauvre en magma et leurs bassins à faible taux de sédimentation (starved basin). Ainsi, l'acquisition sismique n'est pas influencée par d'épaisses sections sédimentaires, des couches évaporitiques ou d'épaisses séquences volcaniques. De plus, plusieurs forages de l'Ocean Drilling Program (ODP) ont été réalisés lors des trois dernières décennies. Ils ont permis à l'acquisition d'un ensemble de données uniques bien que locales, et très importantes pour la communauté scientifique. Afin de résoudre le problème de continuité des structures et des séquences sédimentaires, ces données ont été utilisées dans cette thèse conjointement à deux exemples de systèmes anciens de rift appauvris en magma, de la Téthys alpine et des Pyrénées de l'ouest. Ces systèmes fossiles préservent des bassins sédimentaires et des structures liés au rifting, qui permettent de faire des observations de l'empreinte des fluides et de leur circulation dans un domaine plus large, en comparaison à celui des marges conjuguées Ibérie-Terre Neuve. Les marges de la Téthys alpine exposées dans les Alpes de l'Est Suisse et Sud-Est Français présentent des structures et des bassins jurassiques qui ont été préservés de la déformation et du métamorphisme entre le Crétacé supérieur et le Cénozoïque. Il est important de mentionner que plusieurs similitudes ont été identifiées entre les Alpes et la marge ibérique concernant leur caractéristique tectono-sédimentaire (ex. des bassins à faible taux de sédimentation, des bassins supra-détachements, des failles de détachements extensifs et des systèmes de rift pauvres en magma). Par conséquence, ces marges peuvent être utilisées comme des analogues de systèmes de rift pauvres en magma dont l'évolution des fluides peut être similaire. Le bassin de Mauléon dans les Pyrénées de l'ouest préserve des structures crétacées liées au rifting, et est moins affecté par la compression cénozoïque que les sites des Alpes. Néanmoins, à cause de sections sédimentaires épaisses et d'altérations météoriques intenses, les affleurements

sont moins bien exposés et exploitables que ceux des sites des Alpes.

Ainsi, des évidences de circulation de fluides sont présentées et discutées dans cette thèse. J'utilise des exemples des «marges» fossiles riftées exposées dans la Téthys alpine et dans les Pyrénées de l'ouest, ainsi que des marges riftées actuelles d'Ibérie-Terre Neuve. Par les analyses et leurs interprétations, et leur discussion, j'aborde les questions de l'origine et de l'évolution des fluides (c.-à-d. modifiés et enrichis en éléments au cours des réactions eau-roche) dans différents domaines des ces marges au moment de leur formation.

Un résultat majeur est celui de la démonstration que les fluides sont avant tout liés à des structures profondes intimement associées à l'évolution des systèmes hyper-amincis, qui peuvent évoluer dans une marge riftée pauvre en magma. Les fluides migrent au travers de ces structures, provoquent des échanges eau-roche, pour revenir ensuite interagir avec l'eau de mer et les dépôts des bassins sédimentaires sus-jacents. Ces interactions ont de nombreuses implications pour le budget chimique de l'eau de mer, le contrôle de la nature des sédiments, aussi bien que pour les processus diagénétiques.

Ces observations ont permis de proposer des modèles expliquant le lien entre l'histoire de la migration de fluide et l'évolution tectonique des marges riftées. Ces interactions ont un rôle majeur dans les changements rhéologiques de la croûte continentale et du manteau supérieur lors de la phase finale de l'extension, phase qui peut éventuellement résulter en la formation d'une marge riftée pauvre en magma.

La combinaison des différentes méthodes et types de données, comprenant des données structurales/ microstructurales, des études minéralogiques, des analyses chimiques et des données géophysiques, ont permis de caractériser d'anciennes zones de circulation de fluides à grande échelle, dans la partie distale des marges riftées.

Les résultats montrent l'existence de deux types de fluides. Un premier type est dominé par l'interaction entre l'eau de mer et les roches du socle de la croûte continentale, un deuxième type est dominé par l'interaction entre l'eau de mer et des roches mantéliques. Le premier type, lié à la croûte continentale (continental crust related-fluids), est un fluide enrichi en Si et Ca provenant des pertes des éléments causées par l'ensemble des processus de saussuritisation sous l'influence de réactions eau-roche. L'empreinte de ce type de fluide est mise en évidence par la forte chloritisation aussi bien que par les nombreuses occurrences de veines quartz et calcite le long de la zone de faille des systèmes de détachement extensifs. Le deuxième type de fluide, relié

au manteau (mantle-related fluids), est enrichi en Si, Mg, Fe, Mn, Ca, Ni, Cr et V provenant des pertes des éléments en réponse aux processus de serpentinisation, produits par l'interaction l'eau de mer-manteau. La serpentinisation produit d'importants changements minéralogiques menant par exemple à la formation de chrysotile, lizardite et chlorite, et résultant en l'augmentation volumétrique et en la diminution de densité des roches mantéliques. Le fluide relié au manteau peut être tracé par les éléments Ni-Cr-V et Fe-Mn le long des zones des failles des grands détachements extensifs mais aussi dans les roches sédimentaires sus-jacentes. Le fait que les signatures des fluides peuvent être documentées dans tous les systèmes extensifs étudiés m'a permis de conclure que la percolation des fluides est un processus important et caractéristique de ces domaines, intervenant au cours de l'évolution des marges riftées pauvres en magma. Tandis que les fluides liés à la croûte continentale sont actifs lors des stades initiaux à tardifs de l'extension, les fluides liés au manteau sont uniquement actifs pendant le stade tardif de l'évolution de systèmes hyper-amincis et au moment de l'exhumation du manteau. Ensuite, la percolation des ces fluides se produit le plus souvent dans des bassins restreints, qui ne sont pas complètement connectés à des domaines océaniques ouverts, causant ainsi une amplification des interactions chimiques entre l'eau de mer et les sédiments contemporains. Les flux de fluides dans les bassins sédimentaires peuvent également influencer l'évolution diagénétique (précoce) des sédiments et par conséquence leurs propriétés physiques (ex. porosité, perméabilité et densité).

Le flux de fluides dans les domaines hyper-amincis peuvent jouer un rôle majeur dans la rupture crustale, influencer la focalisation des magmas et la rupture lithosphérique postérieure des marges riftées de type pauvre en magma. Comme l'hydratation de la croûte et du manteau est de grande importance dans les marges riftées pauvres en magma, elle peut également avoir un rôle important au cours de leur réactivation et donc sur la formation de zones de subduction, de l'évolution initiale des orogènes aussi bien que sur le magmatisme le long d'arcs orogéniques. Le cycle de l'exhumation mantélique, d'abord suivie par la serpentinisation, l'absorption d'eau et de pertes d'éléments spécifiques (Ni, Cr, V, Si, Fe, Mn), puis la subduction de ces roches modifiées, doit avoir des impacts majeurs dans les changements et budgets géochimiques des grands réservoirs de la Terre au cours de son évolution.

EXTENDED ABSTRACT

EXTENDED ABSTRACT

The evolutions and formation of passive rifted margins and oceans are intimately related to magmatic, tectonic, structural and sedimentary processes as well as change in climate and formation of new seaways. Their investigation reveals the constant changes of the planet through geological time. Fluids are common constituents associated with many of these processes or even formed by them, e.g., metamorphic, magmatic, meteoric, biogenic and diagenetic fluids. These relationships are often studied in specific sites such as shear zones, hydrothermal vents and volcanoes resulting, for example, in the formation of metamorphic veins, in biomethanogenesis and black smoker activity. Fluids are of major importance for the cooling of the planet along mid-oceanic ridges, ore deposit formation, and geothermal and fossil energy sources. They may also played an important role for the formation of earliest organic compounds and consequently for the evolution of primitive life.

Even though passive margins account for an enormous area of the planet, the aforementioned fluids developed during their formation have been little investigated. This is mainly due to difficulties in accessing the data, once the formation and percolation of fluids occur on the seafloor, in sedimentary basins and deep in the Earth's crust. Moreover, fluid flow in many of these systems is no longer active limiting its understanding. Nevertheless, the imprint of fluids is often observed along fault zones (e.g., veining), in sedimentary rocks (e.g., silicification) and in exhumed mantle (e.g., serpentinization). Although these observations have been described, their origins, formation processes and distribution have not been sufficiently studied and are consequently less understood, especially at a margin scale.

Therefore, major questions are frequently posed by the research community, many of which arose during the development of this thesis. What are the sources of these fluids? How and when were they formed? What are their migration pathways? What are the *source and sink* of these fluids? Did they interact with basement rocks and the overlying sediments? What is the composition and what is the amount of these fluids? Do they have a signature? What is the role of fluids for the formation of rifted margins?

The difficulty of studying the imprint of fluids in present-day rifted margins is the lack of data, mainly for distal (deep-water) rifted margins. Usually, drilling in this geological setting is limited by technology and/or high cost. Moreover, even when data are available, they may not be sufficient to understand the evolution of fluid systems at the scale of a margin. The scale problem

may be solved by regional refraction and reflection seismic surveys, which allow imaging of deep structures. But in many margins the thick sedimentary section limits their imaging. In this sense, the Iberia-Newfoundland conjugate margins are the best sites to address those questions because they are magma-poor and sedimentary-starved. Thus, seismic acquisition is not interfered by thick sedimentary sections or salt layers, or the presence of thick volcanic sequences. In addition, many projects carried out by the Ocean Drilling Program (ODP) were performed over the last three decades. They resulted in the acquisition of a unique, but still local, dataset accessible for the scientific community. To override the problem of continuity of structures and sedimentary sequences, this dataset has been used in this thesis together with two examples of former magma-poor rift systems from the Alpine Tethys and the Western Pyrenees. These fossil systems preserve rift-related structures and sedimentary basins that allow the observation of the imprint of fluids in a much more continuous way compared to the Iberia-Newfoundland conjugate margin. The Alpine Tethyan margins exposed in the Eastern Swiss and Southeast French Alps exhibit well-preserved Jurassic structures and sedimentary rocks that escaped Late Cretaceous and Cenozoic deformation, and metamorphism. It is important to mention that many similarities have been identified between the Alps and the Iberian Margin regarding to their tectono-sedimentary characteristics (e.g., sedimentary starved basins, supradetachment basins, extensional detachment faults and magma-poor systems). Consequently, they can be seen as analogues for hyperextended magma-poor rift systems with a comparable fluid evolution. The Mauléon Basin in the Western Pyrenees is less affected by the Cenozoic compression compared to the Alps, preserving Cretaceous rift-related structures. However, due to the thick sedimentary section and weathering conditions, the outcrops are less well-exposed than in the Alpine examples.

Therefore, the evidence for fluids in the fossil rift systems exposed in the Alpine Tethys, and Western Pyrenees as well as in the Iberia-Newfoundland magma-poor rifted margins is primarily presented and discussed in this thesis. In doing so, their origin and how they were formed (i.e., enriched) in different domains of these rifted margins is also addressed here.

As a major result, it is shown that the identified fluids are related to deep structures intimately associated with the evolution of hyperextended systems that can evolve to magma-poor rifted margins. Fluids used these structures as pathways to interact with the seawater and the overlying sedimentary basin. They have important implications for changing the seawater chemistry and the nature of sediments as well as influencing diagenetic processes. These observations enabled the proposition of models that explain the link between the *fluid history* and the tectonic evolution. This link plays an important role in changing the crustal and upper mantle strength in the final

extensional event, which can lead to the formation of magma-poor rifted margins.

The combination of different methods and datasets, including structural/microstructural, mineralogical studies, geochemical analyses and geophysical data, allowed the demonstration of the existence of a large-scale fossil fluid flow in the distal part of the rifted margin. The results point to two types of fluids, one heavily influenced by the interaction of seawater and continental crust rock and another characterized by seawater-mantle interaction. The first one is referred to here as *continental crust-related fluids,* which are enriched in Si and Ca as a result of element losses caused by the assembly of saussuritization processes under the influence of water-rock interaction. The imprint of these fluids are best evidenced by strong chloritization as well as frequent occurrences of quartz veins and less frequent calcite veins along the fault zone of extensional detachment systems. The second fluid type referred to here as *mantle-related fluids* is enriched in Si, Mg, Fe, Mn, Ca, Ni, Cr and V as a result of element loss during serpentinization that occurs during seawater-mantle interaction. Serpentinization produces major mineral changes, which lead to the formation of, e.g., chrysotile, lizardite and chlorite, resulting in volumetric increase and density decrease of mantle rocks. Mantle-related fluids can be traced using Ni-Cr-V and Fe-Mn along fault zones of major extensional detachment faults and in the overlying sedimentary rocks.

Due to the repeated pattern in which these fluids occurred in the studied extensional systems, we conclude that fluid percolation is an important and characteristic process during the evolution of magma-poor rifted margins. While the continental crust-related fluids occur during early to late stages of extension, mantle-related fluids occur in the final stages during the evolution of hyperextended rift systems. The percolation of these fluids often occurs in restricted basins that are not yet completely connected with global oceans. This leads to changes in the chemistry of the seawater and nature of sediments. Fluid percolation in the sedimentary basin also impacts the diagenetic evolution of sediments, and consequently their physical properties.

The fluid flow in the hyperextended domains can play a major role for crustal breakup, focalization of magmatic addition and the subsequent lithospheric breakup of magma-poor rifted margins.

As hydration of both crust and upper mantle is of primary importance in magma-poor rifted margins, their eventual subduction can influence the early evolution of orogens and magmatism along orogenic arcs. The cyclic mantle exhumation accompanied by serpentinization, water absorption, element losses and its later subduction, must have substantial impact on changing the geochemistry of major Earth reservoirs during the evolution of the planet.

INTRODUCTORY PART

1. CONTEXT AND TERMINOLOGY USED IN THIS STUDY

1.1. Some aspects related to the formation of extensional systems

Under the influence of the concepts of plate tectonics in the 1970s, the investigation of rifted margins resulted in the understanding that they were formed by continental lithospheric extension culminating in the formation of oceans. The final margin architecture is usually associated with two main processes. The first one is of tectonic origin, which is best expressed by thinning of the continental crust and lithospheric mantle. The second one is the thermal variation caused by the lithospheric thinning leading to the upwelling of the asthenospheric mantle and magma formation [*McKenzie*, 1978; *Beaumont et al*., 1982; *McKenzie and Bickle*, 1988].

McKenzie [1978] presented a model in which the amount of the lithospheric thinning controls the subsidence history of passive margins and consequently the creation of accommodation space by tectonic and thermal processes. This model predicted that the thermal gradient would be elevated in zones of higher lithospheric thinning, such as in distal margins where the continental crust is thinner and a transition to the oceanic crust is observed. Many models [e.g., *Royden and Keen*, 1980; *Hellinger and Sclater*, 1983] were proposed in the light of these observations. They assumed that the lithosphere is decoupled in layers according to their rheology (upper and lower crust and mantle) (Figure 1A). The major principle behind some of these models is that the deformation of the lithosphere was symmetrical (pure shear). This was contradictory with observations made in the Basin and Range province (Figure 1B) [e.g.,*Wernicke*, 1985] where the deformation of the crust was asymmetrical (simple shear). These two models had different implications not only for the geometry of the margins [*Lister et al*., 1991], but also for their thermal evolution. These observations led *Kusznir et al*. [1991] to propose that the upper crust can be deformed by simple shear manner while the mantle would be thinned following the pure shear principle what is mainly based on rheological properties. This model succeed in explaining the asymmetry observed in many extensional systems where detachment faults are responsible for the extension of the crust but are not necessarily related to thinning of the upper mantle.

These ideas drove initial studies of conjugate rifted margins presenting strong asymmetry [e.g., *Lister et al*., 1986] (Figure 1C) as exemplified by the Iberia-Newfoundland conjugate rifted margins [*Boillot et al*., 1988; *Reston et al*., 1996; *Manatschal and Bernoulli*, 1998; *Manatschal et al*., 2001; *Péron-Pinvidic and Manatschal*, 2009] (Figure 1D).

Apart from the tectonic processes associated with the formation of rifted margins, magmatic

additions that occur during extensional events are also an important geological element that define the type of margin [*Kusznir and Karner*, 2007]. The amount of magmatic addition can influence the architecture of margins and the nature and location of lithospheric breakup [*Geoffroy*, 2005; *Franke*, 2013]. Nevertheless, all the sites studied in the Iberia-Newfoundland, Alps and Western Pyrenees can be classified as magma-poor systems, in which their main characteristics are presented below.

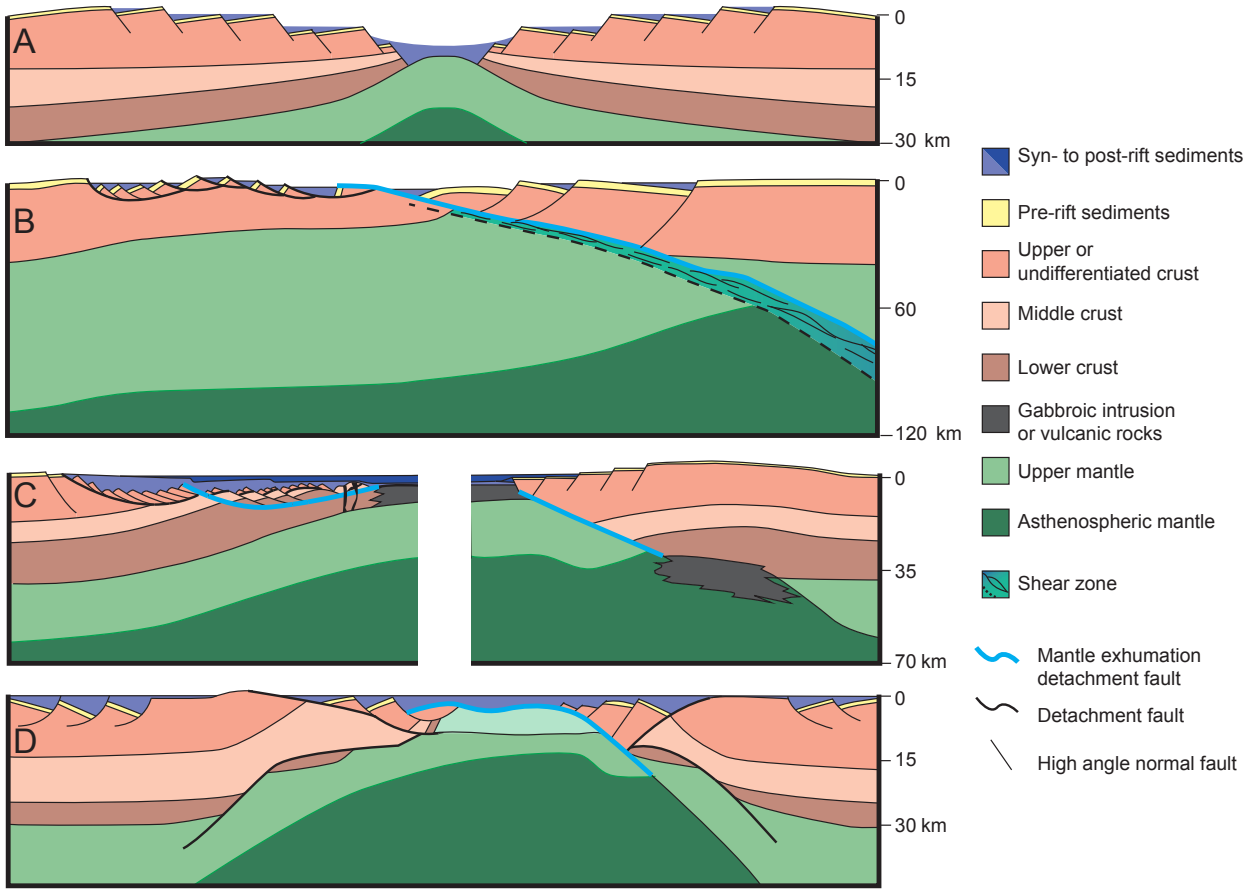

Figure 1. Models of extensions. (A) Conceptual pure shear model based on the work of *McKenzie* [1978] or other depth-dependent-type model [e.g., *Hellinger and Sclater*, 1983]. Note that the extension is symmetrical and that mantle can be exhumed at higher thinning factors. (B) Simple shear model from *Wernicke* [1985]. Note the asymmetry of the extensional system. A first extensional detachment system (black bold line) is responsible for thinning the brittle crust. A second extensional detachment system (blue line) cuts trough the entire crust and upper mantle resulting in a large shear zone. (C) Asymmetrical model used to explain the evolution of rifted passive margins [*Lister et al.,* 1996]. At the first stage, the continental crust is thinned by an extensional detachment system (bold black line) and then a second detachment system cuts through the thinned continental crust creating an asymmetric conjugate margin, referred to as lower plate margin (left) and upper plate margin (right). (D) New concept of development of magma-poor rifted margin [*Péron-Pinvidic and Manatschal*, 2009] based on observations from the Iberia-Newfoundland and the fossil Alpine Tethyan margins. The first detachment system is responsible for thinning the continental crust (black bold line) and then a second one (blue line) cuts the thinned continental crust subsequently exhuming the mantle at the seafloor. Note the asymmetry of the system setting up an lower plate model (left) and upper plate margin (right).

1.2. **The evolution and architecture of magma-poor rifted margins**

More recent studies have shown [*Péron-Pinvidic and Manatschal*, 2009; *Sutra et al*., 2013] that the final architecture of magma-poor rifted margin is a product of three major extensional events followed by the emplacement of a mid-oceanic ridge (Figure 2). The first event (*stretching*) is the extension of the continental crust, which is associated with high-angle normal faults that create grabens and half-graben basins. In this event, the lithospheric thinning process is dominated by pure shear leading to symmetrical rift setting (Figure 2A). The second event (*necking*) is characterized by an important thinning of the middle crust that is controlled by extensional detachment systems leading to the formation of *Necking Zones* [*Mohn et al*., 2012] (Figure 2B). The third event (*coupling*) develops between these necking zones where the crust is usually thinned to less than 10 km. This event is responsible for hyperextension of the continental crust where extensional detachment faults cut through the thinned crust and root in the mantle (Figure 2C) leading to the exhumation of mantle rocks at the seafloor and posterior development of a mid-ocean ridge (Figure 2D).

An essential observation from Figure 2 is that these systems may not necessarily evolve into a rifted margin, in the sense that they do not result in lithospheric breakup and formation of a mid-oceanic ridge. As discussed in the articles, each studied area records a particular evolutionary stage presented in Figure 2. Therefore, through this thesis the term "*extensional system" will be used* to refer to the studied sites. More detailed discussion about the evolution of magma-poor rift systems/margins is addressed in the three articles.

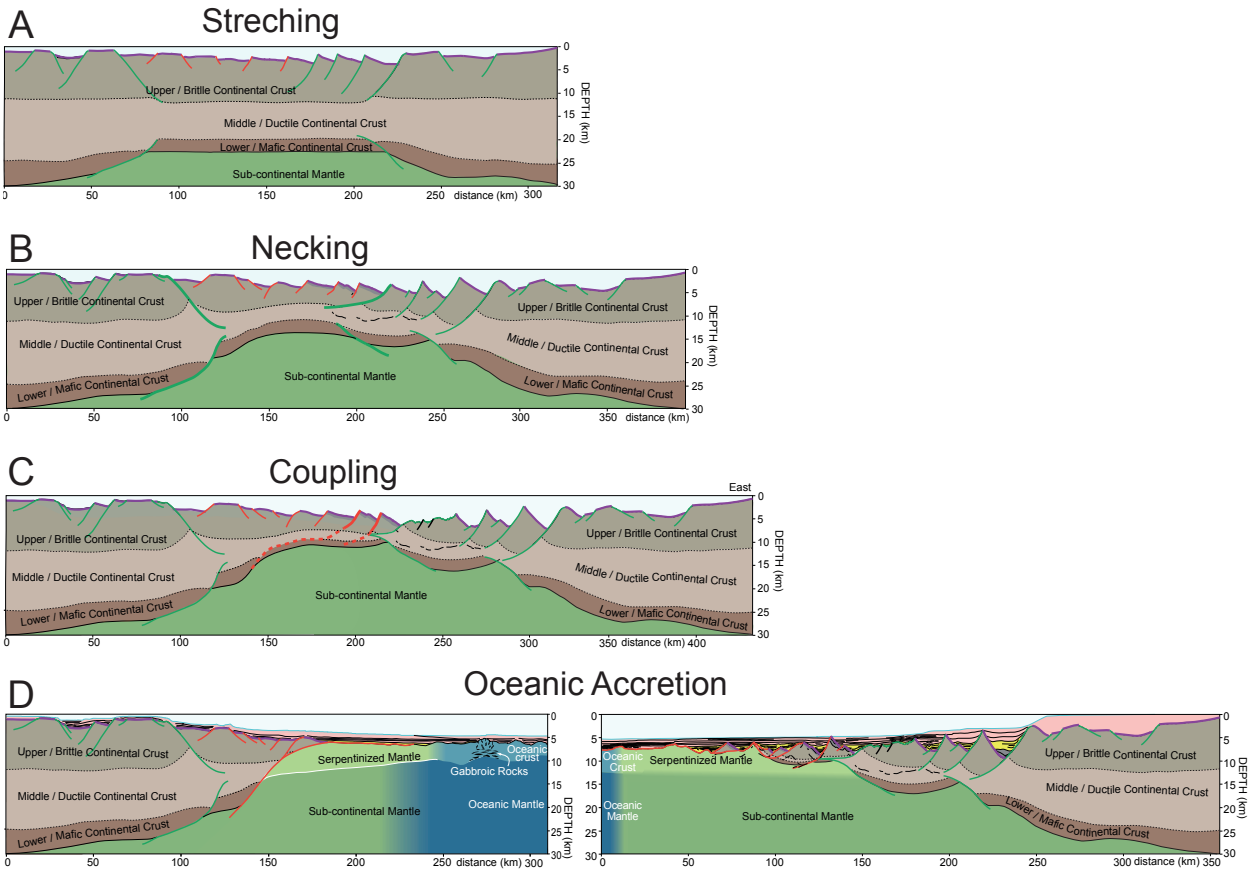

Figure 2. Evolution and architecture of magma-poor rifted margins. The figures show the main stages of magma-poor extensional systems that lead to the formation of magma-poor rifted margins. (A) The extensional system is characterized by symmetrical rifting that creates fault-bounded basins. The thinning of both continental crust and upper mantle are minor. (B) Deformation is focused along the necking detachment faults (bold green lines) leading to major thinning of the middle continental crust. (C) Detachment faults (bold red lines) cut through the hyperextended brittle continental crust rooting in the mantle allowing subsequent exhumation of mantle rocks at the seafloor. (D) Final architecture of a magma-poor rifted margin where the ocean crust is formed. Figures from *Sutra et al.* [2013].

1.3. **Extensional detachment systems**

The previous sections addressed the possible mechanisms responsible for the thinning of the lithosphere. Each mechanism opens and closes possibilities of fluid-rock interaction at different lithospheric levels during extension. Some mechanisms are associated with extensional detachment systems, which are intimately related to the thinning of the continental crust and upper mantle. Detachment fault systems can connect different reservoirs of the Earth, such as the continental crust, the upper mantle and oceans.

Therefore, the aim of the following section is to show some aspects related to extensional detachment faults, which record important information not only about the deformation history but also about the role of fluids in extensional systems. Two examples of active extensional detachment systems are presented in order to introduce their characteristic structures and related fluid activity.

The first is in a continent setting and is exemplified by the detachment system exposed in Death Valley (SW-USA). The second is in an ocean setting, and a good example to illustrate this system is the Mid-Atlantic Ridge at 13°19'N. Both detachment systems are associated with very characteristic fault rocks. They are strongly influenced by fluid-rock interaction that result in the formation of new syn-tectonic mineral phases (mainly phyllosilicates).

1.3.1. **The example of Metamorphic Core Complexes**

Extensional detachment faults are well exemplified in metamorphic core complexes in the Basin and Range province in the SW-USA. The metamorphic core complexes are characterized by deep crustal rocks (amphibolites and granulites) that are exposed along convex upward mylonitic fault zones, which many of them are posteriorly superimposed by brittle structures [Wernicke, 1985b; Lister and Davis, 1989; Scott and Lister, 1992]. These brittle structures are spectacularly exposed along the so-called "Turtlebacks" in Death Valley representing exposed extensional detachment faults (Figure 3A-C).

Many authors have discussed about the origin of these structures, e.g., if they are formed by post-orogenic collapse [*Coney and Harms*, 1984], by flow of upper mantle due to the removal of the upper crustal rocks [*Wernicke and Axen*, 1988] or by lower crustal flow [*Block and Royden*, 1990]. Others suggested that the involvement of magmatism during the extension was responsible for the uplift and the convex upward geometry of the metamorphic core complexes [*Rehrig and Reynolds*, 1980].

An important point about the core complexes is the low-angle nature of the extensional detachment faults. They cannot be explained by classical rock mechanic theory (e.g. Mohr-Coulomb theory). Therefore, *Buck* [1988] and lately, *Lavier et al*. [1999], proposed that the fault starts as a high-angle and by flexural rotation they become low-angle. These models have two main assumptions: (1) a regional extent for the isostatic response of faulting; (2) when the footwall of detachment is rotated to an optimal angle, a new high angle normal fault cuts the upper crust nucleating at the same place the previous detachment fault.

In this thesis, this model is assumed to explain the evolution of the detachment systems in the studied sites for the following reasons: (i) the observation that at the scale of the margin new detachment fault progressively developed oceanwards, (ii) the observation of continental allochthons were formed by high-angle normal faulting that roots in the previous extensional detachment, (ii) extensional low-angle normal fault extends regionally across more than 25 km

(regional isostatic response) (iv) rolling hinge model can explain the usual occurrence of semi-perpendicular fractures and small faults along the footwall of extensional detachment, and (v) they do not need syn-kinematic magmatism, which is not observed in the studied examples, to explain the upwarping of the detachment fault surface.

1.3.2. **The example of Ocean Core Complexes**

Core complexes similar to those observed in the Basin and Range province are often observed along mid-ocean ridges, referred to as Ocean Core Complexes (OCCs). These impressive structures are well imaged at the Mid-Atlantic Ridge [*MacLeod et al*., 2011] where they are characterized by convex upward extensional detachment faults (Figure 3D). These OCCs (Figures 3D-E) are usually about 11 km wide both parallel and perpendicular to the ridge axis, and they have about 9 km of heave [*MacLeod et al*., 2002, 2009; *Boschi et al*., 2006]. Characteristic striations are often observed and well and dredge data show predominantly brittle structures that cut previous high temperature mylonites [*Dick et al*., 2000; *Schroeder and John*, 2004].

The brittle structures along the OCC are best depicted by foliated cataclasites that usually appears as anastomosing zone (Figure 3F) [*Boschi et al*., 2006]. Sedimentary breccias composed by footwall- and hanging wall-derived clasts are often observed, showing that the active fault surface serves as source for these sediments (Figure 3F). Similar breccias are also found in the examples discussed in this study.

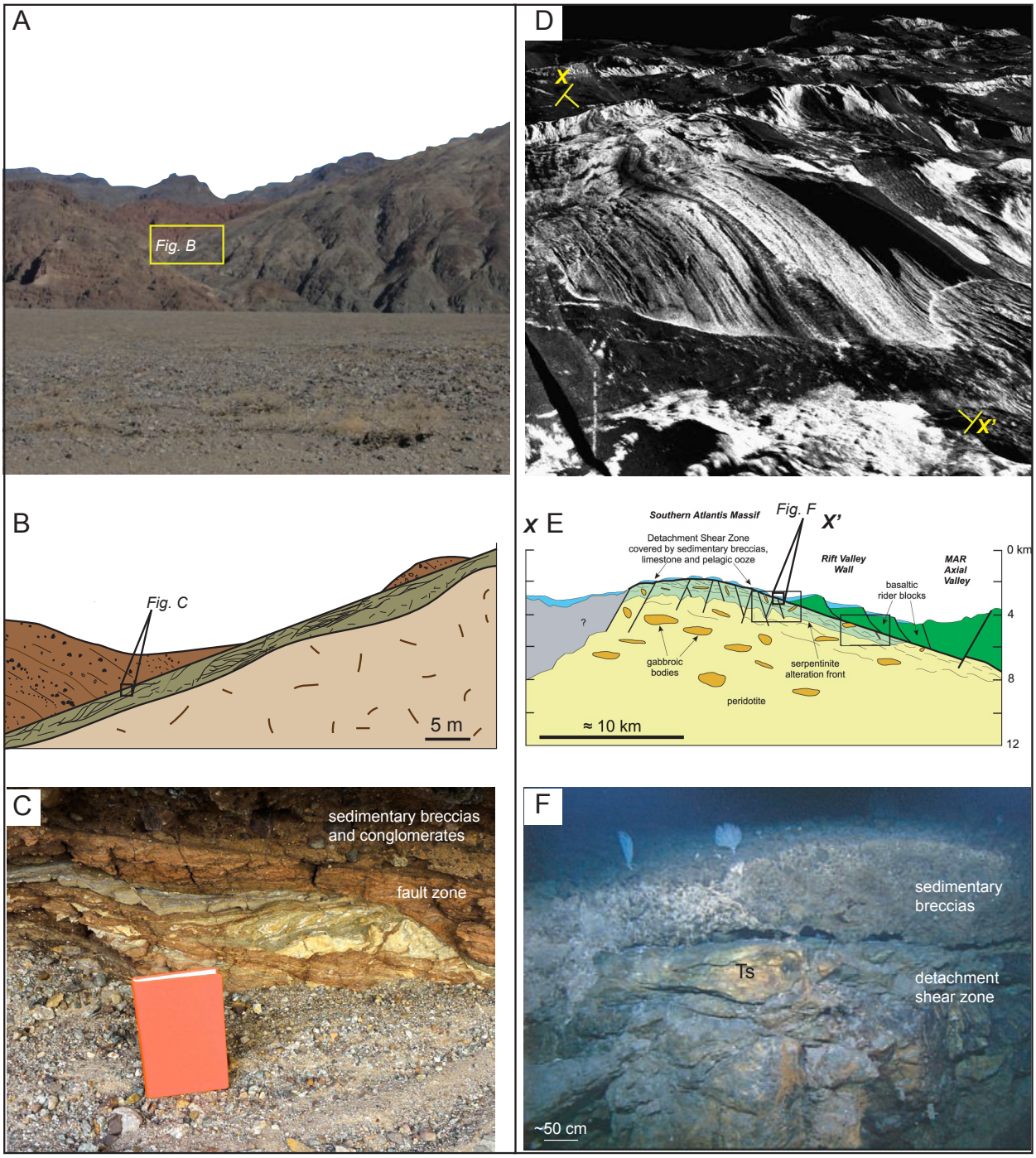

Figure 3. Extensional detachment faults. (A) Extensional detachment fault (Turtleback) in the Death Valley, USA. (B) Small section showing the fault zone and the overlying sediments. (C) Fault zone and the overlying sediments. Note that the fault rocks are rich in clay minerals. (D) 3-D perspective looking NW of the active ocean core complex (13°19'N) [*MacLeod et al.,* 2009]. Note the striated detachment surface emerging from the axial valley floor. The X-X' points to the schematic section from another core complex (Atlantis). (E) Schematic section from the Atlantis massif that can represent the detachment fault from figure D. Note the shear zone along the fault. (F) Top of detachment shear zone (DSZ) and overlaying sedimentary breccias of the Atlantis Massif. The figure shows the deformed metasomatic talc-amphibole rock (Ts). Figures E and F from [*Boschi et al.,* 2006].

1.3.3. **Fault rocks associated with extensional detachment faults**

Many classifications have been proposed for brittle fault rocks [e.g., *Sibson*, 1977; *Wise et al*., 1984; *Schmid and Handy*, 1991]. They manly considered the clast/matrix ratio, the development of foliation, the coherence/incoherence, grains size reduction and recovery processes. In the Articles 1 and 2, some of the established terminologies have been used to describe the fault rocks occurring along the detachment faults studied in this work. Of major importance is to understand the evolution of these fault rocks, at what temperature and pressure conditions they formed and what was the nature of fluid-rock interaction they underwent along the detachment faults during exhumation.

Low temperature recovery and recrystallization processes are usually associated with brittle deformation [*Passchier and Trouw*, 2005]. Although they also depend on the strain rate, they were used as a first order indication of temperature as proposed by *Stipp et al*. [2002]. The observed fault rocks along the studied extensional detachment faults usually present *bulging* and at a less extent *subgrains rotation* both developed at greenschist facies.

Therefore these features were used to distinguish and characterize the fault rock types in the continental crust. Some of these structures are also observed in the mantle, despite the fact that the mineralogical composition is quite different. The following description focus on fault rocks of the continental crust with a granitic/gneissic composition. In the study the following types of fault rocks are distinguished:

- Cataclasite: the most characteristic feature in cataclasite and the other fault rocks is cataclastic flow (cataclasis). They are developed as corridor-like shapes through out the rocks. These corridors are made of angular clasts of variable size and a fine-gain matrix usually made of quartz and feldspars. However, retrograde metamorphic reactions such as chloritization are often observed. These reactions increase with deformation and therefore the matrix can become more clay-rich. Cataclasis is a fractal feature and can be observe at outcrop and microscopic scale. Cataclasites are affected by brecciation that results in typical jigsaw structures and desegregation of the protolithe fabric/structure. In thin section, they usually exhibit intragranular fractures when deformation is less intense, and transgranular fracture when deformation is more intense. This last one is usually accompanied by cataclastic flow. Weak to moderate quartz undulose is often observed. Bulging, when present, is the major recrystallization process.

- Foliated cataclasite: characterized by penetrative cataclastic foliation, which points to considerable

focused deformation along a fault zone. This deformation increases the formation of clay minerals, which are often observed along the foliation. Fractures are transgranular and very pervasive in foliated cataclasites. They are often filled by quartz and calcite veins. Original quartz often shows strong undulose extinction. Bulging is a common recrystallization process while subgrain rotation is less observed.

- Clast-rich chlorite-schist: this rock type shares some characteristic with the foliated cataclasite with the major difference that it is strongly chloritized. This chloritization is a product of strong phyllonitization [*Hippertt and Massucatto*, 1998].

- Ultracataclasite: this rock type presents similar characteristics like foliated cataclasites but their clasts are usually rounded and their matrix are mainly composed by micro quartz and sericitized feldspar. Due to the grain size of the matrix and its dark color, hand specimen samples have similar aspect of gouges.

- Fault breccia: this rock-type shares similar characteristics with the cataclasites, but with higher matrix content that is formed by phyllosilicates or micrometric quartz and feldspars.

- Gouge: gouges are matrix-supported rocks. They are characterized by high content of phyllosilicates and rounded clasts, which can range from few millimeters to about 2 meters (in the case of fault rocks in the mantle). The rounded clasts and strong foliations given by clay minerals indicate strong deformation and high water/rock ratio. Gouges are usually found in the core zone at the top of footwall, marking the strains localization of the extensional detachment faults.

1.3.4. **Evidence for fluid percolation through fault zones**

Evidence for fluid percolation through extensional detachment faults is best exemplified by present-day active off-axis ultramafic-hosted hydrothermal system at Mid-Atlantic Ridges [*Kelley et al*., 2001; *McCaig et al*., 2007; *Kelley and Shank*, 2010]. As discussed in the Article 1, such fluids were directly sampled from hydrothermal vents and present a characteristic composition [*Kelley et al*., 2001; *Edmonds*, 2010].

Apart from direct observations from active systems, fossil fluid flow along fault zones of extensional detachment systems are evidenced by their imprints in new-formed syn-kinematic hydrated minerals. For example, the formation of the brittle structures in Death Valley is usually accompanied by water-assisted reactions resulting in the formation of syn-kinematic clay minerals (e.g., illite and chlorite) observed in the matrix of cataclasites and gouges [*Hayman*, 2006]. In the

OCC syn-kinematic tremolite and chlorite are often described in the fault rocks [Schroeder and John, 2004]. Petrological studies of these fault rocks indicate that pervasive talc-amphibole-chlorite metasomatism in the mafic and ultramafic rocks is a key element of the detachment fault zone of OCC [*Boschi et al*., 2006]. Geochemical analyses show that the interaction of hydrothermal fluids with these rocks produced a fluid-enriched in Si-Al-Ca [*Boschi et al*., 2006].

The imprints of fluids were also described in extensional detachment systems exposed in the Err nappe in the Alps [*Manatschal*, 1999; *Manatschal et al*., 2000], where they show strong chloritization and albitization highlighting the influence of water-assisted reactions. At the Hobby High at the Iberia Margin veins of epidote and new-formed hydrated minerals in the continental crust points also to water-assisted retrograde reactions [*Manatschal et al*., 2001].

The imprints of fluid flow are also observed at extensional detachment systems overlying the exhumed mantle in the Iberian Margin. They are evidenced by veining along the fault zone, mineralization of sulfides, occurrences of oxyhydroxides of Fe and Mn, and Ni-Fe alloys [*Morgan and Milliken*, 1996; *Beard and Hopkinson*, 2000; *Hopkinson et al*., 2004]. The evidence for fossil fluid flow along extensional detachment systems is the main subject of this thesis and a more detailed discussion is addressed in the Articles 1 and 2.

1.3.5. **Temperature and conditions of fluid formation**

Temperature, pH, oxide-redox and pressure are key parameters to understand the environmental conditions in which fluids operate. They control many reactions during fluid-rock interaction not only in the basement but also in the sedimentary rocks.

The temperature and pH conditions of fluids directly measured in active ultramafic-hosted hydrothermal vents show temperatures lower than 90°C and alkaline pH [*Kelley et al*., 2001; *Kelley and Shank*, 2010], but both can vary depending on the amount of magmatic addition.

Nevertheless, many of these conditions are difficult to be determined in *fossil hydrothermal systems*. They are usually described by observing the phase equilibrium of minerals, fluid inclusions or stable isotopes [*Früh-Green et al*., 1990; *Beard and Hopkinson*, 2000; *Hayman*, 2006].

Microstructural studies also give a first-order estimation about the conditions of temperature of fluid percolation. As some of the fault rocks are dominated by fracturing (<250°C), cataclastic flow (~300°C) and low temperature recrystallization, e.g., bulging (~350°C), it can be inferred that the fluids percolated and reacted with rocks that were at an environment with temperatures of

about 300 to 350°C. Nevertheless, the temperature of fluids can easily change along the fault zone when fluids are in contact with cold seawater and can result in very local thermal perturbations (e.g., hydrothermal systems).

The stress field in extensional systems may also exert a strong control not only in the formation of faults and related structures, but also in the differential pressure that controls fluid migration through the fault zone [*Sibson*, 1994; *Caine et al*., 1996; *Evans et al*., 1997]. Extensional detachment faults show a complex evolution that can initiate at the brittle-ductile transition deep in the crust and culminate with its exposure at the seafloor. This exhumation can influence the stress field evolution, which strongly controls the migration of fluids.

1.4. **Some occurrence of fluids in extensional systems and rifted margin**

Fluids of different nature can occur in extensional systems and rifted margins. They are most known to be originated in the sedimentary basins as interstitial fluid, brines or as products of organic maturation (e.g., petroleum) [*Magoon and Dow*, 1994; *Kharaka and Hanor*, 2003]. However, fluids can also originate from deeper crustal levels during magmatic underplating, prograde metamorphic reactions or volcanism [*Ague*, 2003] or even be related to water-rock interaction with deep basement rock [*Evam et al*., 1995; *Manatschal*, 1999; *Boschi et al*., 2006; *Benedicto et al*., 2008].

These fluids formed or modified in deep level of the lithosphere can be directly accessed in present-day rift systems. They are exemplified by mantle-derived (i) CO_2, He_2 and CH_4 in gas pool in Bohai Basin, China [*Anping et al*., 2009], (ii) CO_2, He_2 [*Santos Neto et al*., 2011] and trace elements (e.g., Ni and V) in petroleum reservoirs [*Szatmari et al*., 2011] from Brazilian margins.

In Bohai Basin more than 90% of the gas pool are composed of CO_2, which isotopic signature points out to a mantle source, what is confirmed by He isotopes [*Anping et al*., 2009]. These gas pools occur close to deep faults. The same analyses were performed in Brazilian margin and they also showed a mantle signature for those gases [*Santos Neto et al*., 2011]. Moreover, Brazilian oils present a signature e.g., Ni, V, Fe and Cr ,which exhibit a strong correlation with chondrite and fertile peridotites [*Szatmari et al*., 2011]. They are usually associated with more distal domains of the margins, where recently mantle exhumation have been proposed [*Zalán et al*., 2011].

It is known that Cenozoic volcanism in Bohai Basin [*Anping et al*., 2009; *Hussein and*

Xiaomin, 2014] and Cretaceous volcanism in the Brazilian margin [*Fodor et al*., 1983; *Peate*, 1997; *Thomaz Filho et al*., 2000] were widespread. In these cases, a volcanic source for CO_2 and Helium is most probable and they may be related to partial melting produced by lithospheric thinning [*McKenzie and Bickle*, 1988]. However, due to the strong correlation between the metals in the petroleum and the fertile peridotites [*Szatmari et al*., 2011] the occurrence of e.g., Ni and Cr seem to be related to mantle rocks.

Although the occurrence of these gases and metals are usually described, the understanding of their origin, how and when they were formed and migrated, were not discussed for rifted margins. These were the major points that drove this thesis proposal in its very beginning. Since then, many question about the role of these fluids during the evolution of rifted margins arose based on the new field evidence couple with structural, sedimentological, geophysical and geochemical data discussed in the Articles 1-3.

1.5. **Definition of fluid described in this study**

Innumerous types of fluid can be observed in geological systems. Some of them can be formed or transformed during geological processes. Fluids can be the result of melting leading to CO_2 formation during mantle degasing, they can be formed by prograde metamorphism leading to dehydration of rock and forming a metamorphic fluid (e.g., H_2O). They also can be transformed by the fluid-rock interaction leading to changes in the chemistry of the initial fluid.

The fluids described in this study are products of the interaction between seawater and mantle or crustal rocks. The temperature and pressure conditions about which these interactions occur can change their composition. For example, the temperature environment that fluid flow can change their state (i.e., gas, liquid or supercritic). The interactions with other minerals (e.g., micas) can also exchange main components of seawater like O and H. In addition, fluid-rock interaction can lead to major chemical changes. They can become saturated in e.g., Si, Mg and Fe and become unsaturated in CO_2 or O_2. In this sense to affirm that the fluid were formed or only slight transformed can be difficult and a detailed investigation is necessary.

Therefore, in this thesis we often use the expression "*fluids formed by"*, for the transformation of the initial seawater when it interacted with mantle and crustal rocks in rift systems. Our point is to show that saussuritization and serpentinization reactions lead to losses of elements that saturate the initial seawater in many elements and that these reactions occur at different physical conditions, as it will be addressed in the Article 2.

2. QUESTIONS, METHODS AND SITES RELATED TO THIS STUDY

2.1. Scientific questions

The previous introduction gives the context of the occurrence of fluids in extensional systems and their imprint along extensional detachment faults. It can be observed that although fluid percolation through fault zones have been studied, they were not put in the regional context of distal rifted margins and hyperextended systems (Figure 2). This is due to the difficulty to upscale microscopic and outcrop observations to the scale of a rifted margin and also due to the complexity of its final extensional evolution, which often leads to the superposition of earlier extensional stages. Although fluids have been described in rifted margins from the geochemistry perspective, the relation between their occurrence and the tectonic evolution has not been attempted. In this context, the main objective of this thesis was to make the link between the tectonic evolution of magma-poor rift systems/margins and the fluid history, especially in hyperextended domains.

Therefore, major questions have arisen about the nature, accumulation and the imprint (i.e., fossil evidence) of these fluids in hyperextended domains, as summarized bellow:

(1) Is there evidence for fluids in distal rifted margins and hyperextended systems?

This was the primary question at the origin of this thesis. Is it possible to find evidence for *deep* fluids in liquid or gas phase similar to what has been observed in the Brazilian margin or in Bohai basin for instance? Or can fluids only be observed imprinted in the rocks? If the fluids are imprinted in the rocks, what are the best setting to recognize them (i.e., basement, fault zone, sedimentary basins)? It is likely that the fluid signature is best recorded in the fault rocks as observed on metamorphic and oceanic core complexes. But, are their signature also recorded in the sediments or in the seawater? What are the best methods to recognize the imprint of fluids in a hyper-extensional environment?

(2) How can the nature of fossil fluid systems be understood?

Once the fluids are recognized in the different geological setting, the next question was about their nature. Do the retrograde metamorphic reactions lead to the formation of a metamorphic fluids? Metamorphic fluids are often observed in prograde reactions due to the expelling of water out of the mineral structure. On the other hand, retrograde metamorphic reactions usually consume water. However, an interaction between seawater and the (O-H) from the minerals can also strongly modify the fluid conditions. Is this process able to form a new fluid? Therefore, what are the

reactions and processes related to water-rock interaction that lead to the *formation of fluids*?

Retrograde metamorphic reactions are often observed in fault rocks of extensional detachment systems in metamorphic and oceanic core complexes. In metamorphic core complexes albitization, chloritization and illitization are often described. In oceanic core complexes, serpentinization and chloritization are one of the main reactions observed in the fault rocks. Do these reactions consume or release elements? If they release elements, which ones and what happen to these elements?

In hyperextended domains serpentinization associated with mantle exhumation is a major processes. Is only water absorbed during serpentinization or gains and losses of elements during serpentinization are important as well? Do these reactions form a fluid enriched in elements from the mantle? What are the observations and methods that allow the distinction between fluids with a continental crust signature from fluids with a mantle signature?

(3) Can the migration pathways of fluids be reconstructed?

Once that the fluids migrate through extensional detachment systems, it is possible that their passage are recorded in the fault rocks. But did the fluids leave a signature during their passage? Where and how this signature is recorded? How and where did the migration take place? And finally, can pathways of fluid migration be reconstructed?

(4) Where are the sinks of fluids in hyperextended margins?

Once fluids migrate through extensional systems, what are their final sinks? Are they released to the seawater or are they early retained in the sedimentary basins? Is it possible to know the timing and location where these reactions occur? If fluids migrated through the sedimentary section, did they change the composition of sediments? What are these changes? Is it possible to date this event? Are these events occurring in restricted basins or in basins that are connected to the global ocean?

(5) When does fluid migration occur in hyperextended systems?

One important question of this study was about when the fluid percolation happened. When did fluid migration occur along the extensional detachment systems? When fluids interact with the basement and sedimentary rocks?

(6) What is the volume of fluids involved in the evolution of hyperextended systems?

Considering the size of the ocean, crustal and mantle reservoir, the interaction between them has a potential to change an enormous volume of fluids that can percolate in extensional systems. Is it possible to quantify the volume of fluids involved in this interaction? What are their final compositions? What are the losses and gains of elements involved in these interactions? Can these changes modify the composition of the seawater?

(7) Are there economical implication related to fluid percolation at hyperextended rifted margins?

In the last fifteen years, many petroleum discoveries were associated with distal rifted margins, e.g., Campos and Santos Basin in South Atlantic and Gulf of Mexico. For instance in Brazil, deep fluids has been associated with petroleum systems [*Santos Neto et al*., 2011; *Szatmari et al*., 2011]. What are the relations of these deep fluids with the tectonic evolution of these distal, deep water rifted margins? Where can fluids be observed in the studied sites? Can these fluids impact the reservoir quality or control the source rock quality?

Moreover, fluid-rock interactions often remobilize elements leading to mineralization. What are the potential processes that can result in mineralization and what are their compositions?

(8) What are the implications of fluids for the evolution of hyperextended domains?

Fluids can circulate deep in the continental crust and upper mantle. But at what depth can they penetrate and react with these rocks? What is the volume of fluids necessary to explain the observed volume of hydrated crustal and mantle rocks? What mineralogical and petrological changes can be triggered by these hydration reactions? Could they lead to major rheological changes? What is the impact of these changes in the final evolution of hyperextended systems?

(9) Are there implications of fluids for the evolution of orogens and changes in the reservoirs of the Earth?

Fluids play a major role on subduction zones and magmatism along orogenic arcs. Does the amount of hydrated crust and mantle from distal rifted margin influence the subduction processes? Is it possible that the cyclic mantle exhumation accompanied by hydration and posterior subduction changes the reservoirs of the Earth throughout the history of the planet?

2.2. **How to address these questions?**

In order to answer these questions, it is necessary the access to structures formed at different rifting stages. Extensional detachment systems allow the investigation of fluids that interacted

with continental crust and upper mantle rocks. Moreover, sedimentary rocks that overlie the extensional detachment systems can also show evidence for fluid percolation. The understanding of the diagenetic stage that fluids interacted with sediments would reveal the time span that fluid circulated in the sedimentary basin.

The different approaches used to investigate the role of fluids during the evolution of magma-poor rift systems are addressed in the Articles 1, 2 and 3 but their conceptual bases and methods is discussed in the following section.

2.2.1. **Methods**

2.2.1.1. *Field work and observation*

An important part of this thesis was dedicated to field-based studies. They included: (i) first regional studies of the remnants of the Tethyan margins exposed in the Austroalpine and Penninic nappes in the Alps as well as in the Mauléon Basin in the Pyrenees; (ii) description of basic field relationship between structures, sedimentary rocks, and veins; (iii) sampling of crustal and mantle rocks, fault rocks, sedimentary rocks and veins.

In order to compare the evolution of extensional detachment system and fault rocks, fieldwork and sampling were performed also in Death Valley, (SW-USA) where exceptional extensional detachment faults and fluid-rock reaction can be observed. In addition, field observations in the Cantabrian basin allowed me to study the imprint of fluid in syn-rift carbonate sediments.

2.2.1.2. *Structural geology*

Structural studies included first-order identification of the geological terrains, nappes and major structures. These were an important point once they allowed the distinction between rift-related and compressive Alpine/Pyrenean structures. They were also important to calculate the minimum movements between nappes and therefore estimate the length of original rift domains.

The searching for large-scale fluid flow was mainly based on structural descriptions of the fault rocks along extensional detachment systems. The description of fault rocks allows the identification of areas where the imprint of fluid is higher than others, not only across sections of the footwall but also along the lateral extent of the detachment fault systems. The occurrence of veins was also an important structural element to help identify the first order fluid flow and the preferential zone for migration.

2.2.1.3. *Microstructural methods, petrology and mineralogy*

Microstructural investigations combined with petrological and mineralogical studies were key methods to investigate the relationship between deformation, new-mineral phase formation and fluid percolation. Microstructural investigation allowed detailed observations of the fluid activity associated with deformation specially looking the different vein families and the syn-kinematic phyllosilicates. Microstructural methods were also used to study the brittle deformation, low temperature recrystallization and recovery processes of quartz, which point to an temperature range between 180-380 ºC [*Stipp et al*., 2002].

Petrological and mineralogical studies allowed the identification of the mineral constituents of the rock, which support the subsequently geochemical interpretations. Here, we include all methods used for mineralogical studies such as transmitted light optical microscopy, X-Ray Diffraction (XRD) and Scanning Electron Microscopy (SEM) coupled with EDS (Energy-Dispersive X-ray Spectroscopy) and BSE (Back-Scattered Electrons). These methods were applied in fault and sedimentary rocks.

2.2.1.4. *Geochemistry*

The main geochemistry investigation was based on major and trace elements of bulk rock and clay fractions. However, strontium isotopic analyses were performed in few samples from the Err detachment system (further discussed in the Section 4.2). Analyses were performed on undeformed basement, fault and sedimentary rocks from both mantle and the continental crust. The samples from this study were analyzed using the Inductively Coupled Plasma Mass Spectrometry (ICP-MS) and Atomic Emission Spectroscopy (ICP-AES). Published data, in particular whole X-Ray Fluorescence (XRF) data were used to complement our dataset.

The analyses of the fault and the serpentinized rocks were mainly studied using the Gresens-type plot [*Gresens*, 1967] modified by *Potdevin and Marquer* [1987], which present the gain and loss of elements from a protolith to the altered rock (e.g., granite to gouge or peridotite to serpentinite). The plot proposed by *Potdevin and Marquer* [1987] allows a better estimation of the gain and loss of elements during metamorphic reactions assuming elements such as Ti, Al and Zr as immobile or assuming that during the reaction there are no variations in the volume or mass of the rocks. The immobile behavior of Al, Ti and Zr in alteration zones caused by hydrothermal or metamorphic processes has been widely demonstrated [e.g., *Finlow-Bates and Stumpfl*, 1981; *MacLean and Barrett*, 1993 and references therein]. As shown in the Figure A1 in the Annexes,

these elements have an immobile behavior in both fault rocks and the serpentinized peridotites. A more detailed explanation about how these methods were applied in this thesis is addressed in the appendix of the Article 3.

Chemical analyses of the serpentinized peridotites and their minerals were also used in different geochemical charts associated with immobile elements (e.g., Ti and Al) to show their variation caused by fluid percolations (e.g., Ni/Al, Cr/Ti, Fe/Ti and Si/Ti). They evidenced major losses caused by serpentinization, as addressed in the Articles 1 and 2.

Major and trace elements in the sedimentary rocks from the Alps, Iberia and Newfoundland were used to follow the element variations observed along the extensional detachment systems toward the sedimentary section. In the case of the Iberia Newfoundland margins, all the geochemical data used in this thesis are available in the ODP reports. This includes the data from fault (e.g., ODP Site 1067) and the sedimentary rocks (e.g., ODP Sites 638, 641, 1276). Some of these analyses are restricted to few elements such as Fe and Mn (ODP Sites 638 and 641). The data from the Iberia and Newfoundland margins were mainly from XRF analytical methods.

2.3. **Where are the key places to answer to these questions?**

The access to the previous mentioned data is restricted to few rifted margins. In addition, the lack of data in distal domains reduces the number of locations where direct or indirect access to structures of the deep margin is possible. This is mainly because drilling and seismic acquisitions in distal domains are extremely expensive but it is also due to the fact that drilling in these environments is often beyond current technological possibilities. Usually the resolution of seismic data prevents the imaging of extensional detachment faults and their related syn-tectonic sedimentary rock.

Nevertheless, the Iberia-Newfoundland margins are the most well-investigated magma-poor rifted margins due to the numbers of ODP Sites and seismic data that allow the study of: (i) the exhumed continental and mantle rocks, (ii) the major structures related to the evolution of the margins, and (iii) the overlying sedimentary rocks.

Fossil rifted margin/systems are also preserved in orogenic terrains in the Eastern Swiss Alps and in Mauléon Basin in the West Pyrenees. These systems share similarities with Iberia-Newfoundland margins, such as magma-poor systems and extension detachment faults system associated with mantle exhumation. The main regional characteristics of those sites are described

in the following section.

2.3.1. **The remnants of Jurassic rifted margins exposed in the Alps**

The Alpine mountains represent a classical orogenic belt built during two main stages in the Late Cretaceous and the Cenozoic [see e.g., *Lemoine et al*., 1986; *Froitzheim et al*., 1994; *Schmid et al*., 2004]. They preserve remnants of rifted margins that escaped most of the Alpine deformation and metamorphism. These remnants are best characterized by the Apulian/Adriatic and European margins (Figure 4 A-D), which present structures and geometries of lower and upper plate margin, respectively [*Froitzheim and Manatschal*, 1996; *Masini et al*., 2013]. These rifted margins are divided by the Piemont-Liguria domain, an embryonic oceanic domain formed during Middle to Late Jurassic period [*Lemoine et al*., 1987; *Manatschal and Bernoulli*, 1998]. The Piemont-Liguria domain is characterized by serpentinites, locally associated with basalts, dolerites and gabbros. These rocks are overlain by late Middle to early Upper Jurassic Radiolarian cherts. This sequence led to the Steinmann classification of "ophiolites" from the Alps [see, *Bernoulli et al*., 2003 and references therein].

A second hyperextended basin locally floored by serpentinized mantle occurs in the Alps. This basin, known as Valais, was assumed to have formed during Early Cretaceous between the European and Briançonnais block [*Stampfli*, 1993; *Florineth and Froitzheim*, 1994; *Loprieno et al*., 2010]. Nevertheless, new radiometric data points to a Middle/Upper Jurassic age of this basin, questioning an Early Cretaceous opening of the Valais independently from the Piemont-Liguria [*Manatschal et al*., 2006; *Hauser and Müntener*, 2011]. The Valais is best characterized by a thick Cretaceous sedimentary sequence (e.g., flysch) as well as thin serpentinites and magmatic rocks

---

Figure 4. Tectonic and paleogeographic maps, and cross-section through the former Alpine Tethyan margins. (A) Present-day tectonic map with a simplified subdivision of the main domains of the Alpine Tethyan margins. (B) Paleogeographic map of the Alpine Tethyan margins at Albian times. Figures A and B modified from *Schmid et al.* [2004] and *Mohn et al.* [2010]. (C) Composite cross-section (z-z') through the conjugate margins of Adria and Europe/Briançonnais [*Mohn et al.*, 2010]. The red squares from figures A-C mark the position of the studied sites: 1-The Necking zone, the distal margin and the zone of exhumed mantle exposed in the Austroalpine and Penninic nappes in the Swiss and Italian Alps; 2- The OCT exposed in the Tasna nappe in the Swiss Alps; 3-The distal margin and the exhumed mantle exposed in the Penninic nappes in the French Alps. (D) The distal margin exposed in the Err and Platta nappes (Lower Austroalpine and Upper Penninic Nappes, respectively). Note that in this area, the exhumed mantle, the thinned continental crust, the extensional detachment systems and their related sedimentary section necessary for our investigations are preserved. The pictures correspond to, I: extensional detachment fault in the exhumed mantle. Basaltic layers over the exhumed mantle (Falotta, Lower Platta Nappe). II: the exhumed mantle in the Upper Platta Nappe. III: the Err detachment exposed in the middle Err unit (Piz Laviner). IV: the relationship between the Err detachment fault and the overlying syn-tectonic sedimentary breccias (Fuorcla Cotschana, Middle Err Nappe). The figure at the bottom is the reconstructed section from the Err and Platta nappes, modified from *Schaltegger et al.* [2002] and *Masini et al.* [2011].

that are locally observed [*Loprieno et al.*, 2010].

Although the Piemont-Liguria and the Valais are referred to as *oceans* [*Trumpy*, 1975; *Lemoine et al.*, 1986; *Schmid et al.*, 2004], the lack of clear seafloor spreading system and a Penrose-type oceanic crust, together with the absence of typical depleted mantle, lead to question about the nature of these basins, and consequently if the Adria/Apulia and European margins where separated by a true ocean or a failed embryonic oceanic basin. Nevertheless, due to the well-disseminated terminology we often refer to them as rifted margins divided by oceans.

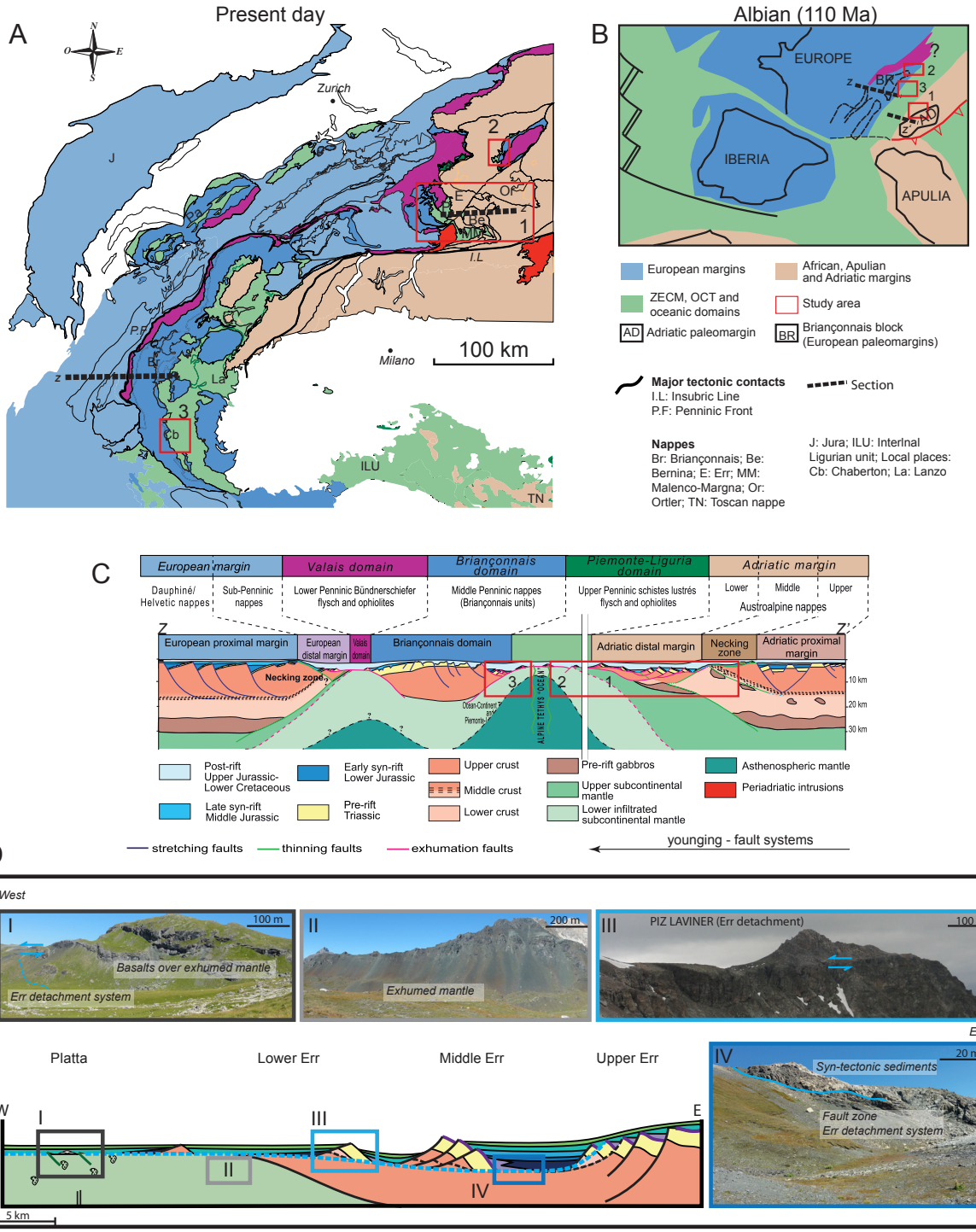

A more detailed description about the studied domains from the Alps is addressed in the Article 1. These areas preserve remnants of Jurassic rift domain with well-exposed extensional detachment systems and overlying syn- to post-tectonic sediments on both mantle and continental crust domains (Figure 4D). They allowed us to investigate the role of fluids not only through the study of fault rocks associated with well exposed detachment systems but also to understand an entire system that couple seawater, mantle, detachment faults and sedimentary basin. Therefore, the Alpine Tethyan margin systems exposed in the Alps represent a *natural laboratory* that can be used to address the questions listed in the previous chapter and investigate the role of fluids during the development of magma-poor hyperextended rift systems.

2.3.2. **Iberia-Newfoundland margin**

The Iberian-Newfoundland conjugate rifted margins present a long history of extension, developed along different segments. This history started with the first rift event from Late Triassic to Early Jurassic, which is characterized by a *wide-rift mode* [*Tucholke and Sibuet*, 2007]. It resulted in distributed graben and half-graben basins bounded by high angle normal faults (e.g., Lusitanian basin) and listric faults (e.g., Jeanne d'Arc basin) [*Driscoll et al*., 1995; *Afilhado et al*., 2008]. This is followed by a regional epeirogenic subsidence until Middle Jurassic times, with few exceptions described in the Lusitanian basin where faulting is observed [*Tucholke and Sibuet*, 2007].

A second rifting event took place from Late Jurassic to Early Cretaceous which is characterized by a change from a wide-rift mode to a more focused deformation that led to extreme thinning of the continental crust followed by mantle exhumation [*Manatschal et al*., 2001; *Wilson et al*., 2001; *Tucholke and Sibuet*, 2007; *Péron-Pinvidic and Manatschal*, 2009] (Figure 5A-B). The second rift event changes along these margins following a regional tendency to become younger to the north [*Tucholke and Sibuet*, 2007]. Furthermore, *Péron-Pinvidic et al*. [2007] highlight that the formation of half-graben basins and supradetachment basins also get younger westward, i.e., towards the future distal margins. This younging is mainly evidenced by the observation that while in the proximal part syn-tectonic sediments were deposited during Tithonian times, at the future distal margin a shallow water platform little affected by faulting was formed [*Shipboard Scientific Party*, 1987; *Wilson et al*., 2001; *Péron-Pinvidic et al*., 2007].

Manatschal et al. [2001] showed, based on reflection seismic and ODP well data (Figure 5A) that during Tithonian, the crust in the future distal margins was thinned to about 10 km and was preserved at shallow level allowing the deposition of the shallow water carbonate platform

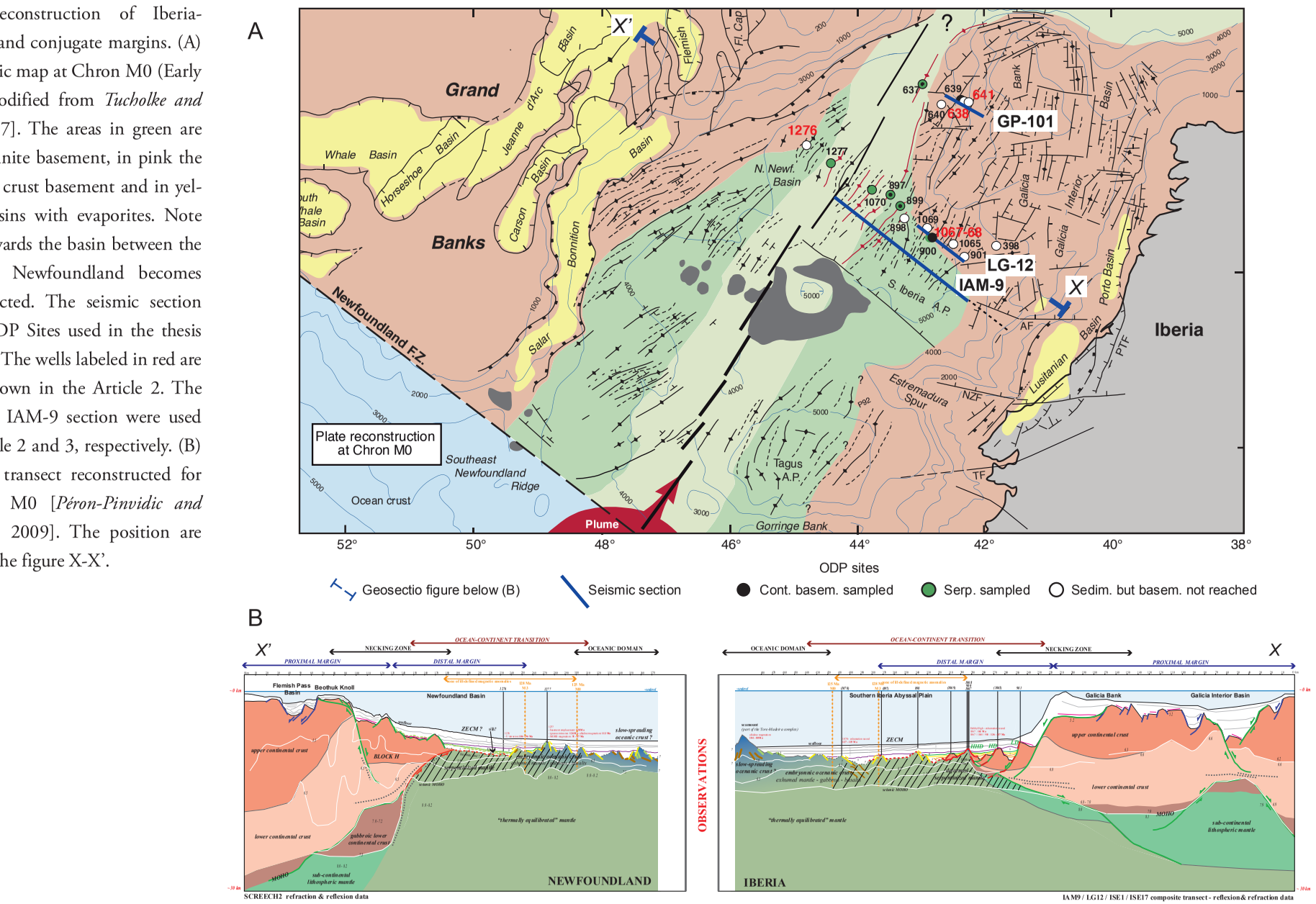

Figure 5. Reconstruction of Iberia-Newfoundland conjugate margins. (A) Paleotectonic map at Chron M0 (Early Aptian), modified from *Tucholke and Sibuet* [2007]. The areas in green are the serpentinite basement, in pink the continental crust basement and in yellow the basins with evaporites. Note that northwards the basin between the Iberia and Newfoundland becomes more restricted. The seismic section and the ODP Sites used in the thesis are plotted. The wells labeled in red are the data shown in the Article 2. The LG-12 and IAM-9 section were used in the Article 2 and 3, respectively. (B) Composite transect reconstructed for the Chron M0 [*Péron-Pinvidic and Manatschal*, 2009]. The position are marked in the figure X-X'.

(e.g., ODP Site 639) little affected by faulting [*Shipboard Scientific Party*, 1987]. The thinning of the future distal margin was supported by thermochronology data from the middle crustal amphibolites of the ODP Site 1067. $^{40}Ar/^{39}Ar$ data on hornblende from these rocks present cooling ages of about 161 Ma (closure temperature ~500 ºC). This shows that the basement was exhumed to shallow levels during Upper Jurassic without major faulting [*Manatschal et al*., 2001]. In the same amphibolites, cooling ages from $^{40}Ar/^{39}Ar$ on plagioclase (closure temperature about ~150 ºC) of 137 Ma evidenced that the basement was exhumed to depths about 5 km in the Early Cretaceous. *Manatschal et al*. [2001] highlighted that this exhumation was associated with brittle deformation formed along extensional detachment faults (Hobby High Detachment) that led to mantle exhumation at the seafloor.

The faulting in the future distal Iberian Margin is well exemplified by seismic and well data (ODP Sites 638 and 641) from Galicia Bank (Figure 6), which show syn-rift sedimentation from Hauterivian to Early Aptian [*Wilson et al*., 2001; *Tucholke and Sibuet*, 2007]. The age of mantle exhumation is interpreted to have also occurred at Barremian to Aptian times [*Péron-Pinvidic et al*., 2007] as evidenced by the exhumation history of the Hobby High [*Manatschal et al*., 2001] and also by the matrix of sedimentary breccias that were dated as Valanginian to Barremian (e.g., ODP Site 1068) [*Shipboard Scientific Party*, 1998].

A regional post-rift sedimentation occurred at Late Aptian/ Early Albian and seems to be well marked along both the Iberian and Newfoundland margins, known as the Aptian event [*Tucholke and Sibuet*, 2007]. Therefore a rifting event associated to a hyperextended domain (i.e., the future distal margin), discussed in the Articles 2 and 3, occurs from Hauterivian to Lower Aptian and is sealed by the first post-rift Upper Aptian/Lower Albian sediments.

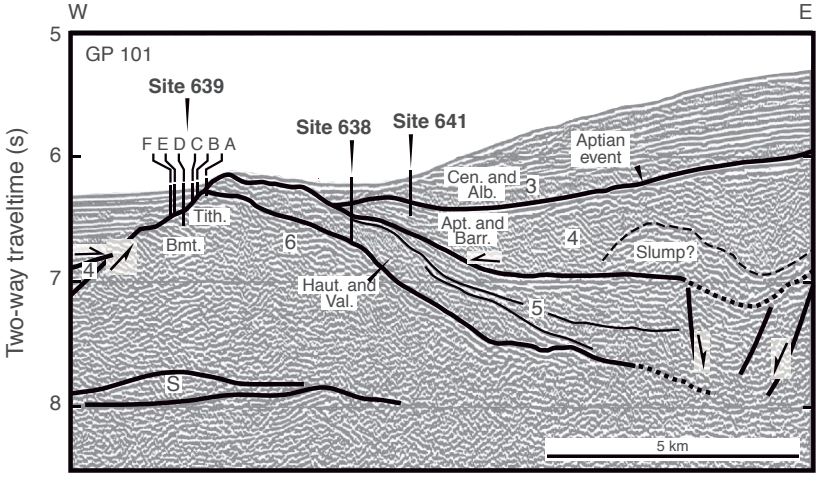

Figure 6. Syn- and post-rift sediments from the Galicia Bank. The figure shows the GP 101 seismic section and the ODP Sites (638 and 641) that drilled into the sedimentary sequences [*Tucholke and Sibuet*, 2007]. The data from these wells were used in the Article 2. Note the unconformity marked by the Aptian event discussed in the Article 2.

2.3.3. **The Mauléon Basin in the West Pyrenees**

In the Pyrenees, the extensional event responsible for extreme thinning of the continental crust and locally mantle exhumation occurred from Late Aptian/Albian to Cenomanian [*Jammes et al*., 2009; *Lagabrielle et al*., 2010]. This event is intimately linked to the opening of the North Atlantic and locally with the Bay of Biscay (Figure 7A) [*Sibuet*, 2004; *Jammes et al*., 2009].

The sedimentary basins preserved in the Pyrenean chain are limited to the south by the Axial zone along the North Pyrenean Fault, and to the North by the North Pyrenean Frontal Thrust. The Pyrenean deformation and metamorphism are lower in the West Pyrenees where the structural relationship and sedimentary facies related to the extensional event are preserved [*Vergés et al*., 2002; *Clerc*, 2012] .

The basement rocks in the Mauléon Basin (Figure 7B) are made of Paleozoic metasediments at the North Mauléon Basin. This basement preserves locally their sedimentary structures and usually are in the anchizone or low greenschist facies. They are best represented by Devonian and Ordovician quartzites and schists from the Axial zone. In the North Mauléon Basin, the basement rocks are best depicted by the same Paleozoic metasediments exposed in the massif of Baygoura as well as by Pre-Cambrian paragneisses exposed in the Massif de l'Ursuya. These paragneisses are in granulite to amphibolite facies, which are in contact with the lower greenschist facies along the Louhossoa lineament.

In the Mauléon Basin, the regional pre-rift sedimentary rocks from Permian to Early Cretaceous are frequently observed. They are generally characterized by (1) Permian/Lower Triassic continental sedimentation (e.g., Buntensandstein), changing to shallow water carbonates and evaporites (e.g., Muschelkalk and Keuper) of Middle to Upper Triassic in age [*Bourquin et al*., 2011]; (2) Jurassic sediments deposited on carbonate platforms (3) Early Cretaceous (Neocomian to Lower Aptian) marls and limestone locally interbedded with sandstones.

During Late Aptian and Early Albian a rifting event affected the South Mauléon Basin [*Masini et al*., 2014] controlled by the South Mauléon Detachment (SMD) (Figure 7C). These authors showed the control of the SMD detachment on the sedimentation, where hanging wall-derived sediments composed by the pre-rift sequence were interfingered with the footwall-derived sediments. These sediments are overlain by post-tectonic Middle Albian to Cenomanian/Turonian sediments.

In Middle Albian, the extension migrated northwards forming the North Mauléon Basins

controlled by the North Mauléon Detachment (NMD) (Figure 7C). This is shown by the first syn-tectonic sedimentary sequence in this basin. The sediments are sealed by Upper Albian to Cenomanian/Turonian post-tectonic sediments [*Masini et al.*, 2014].

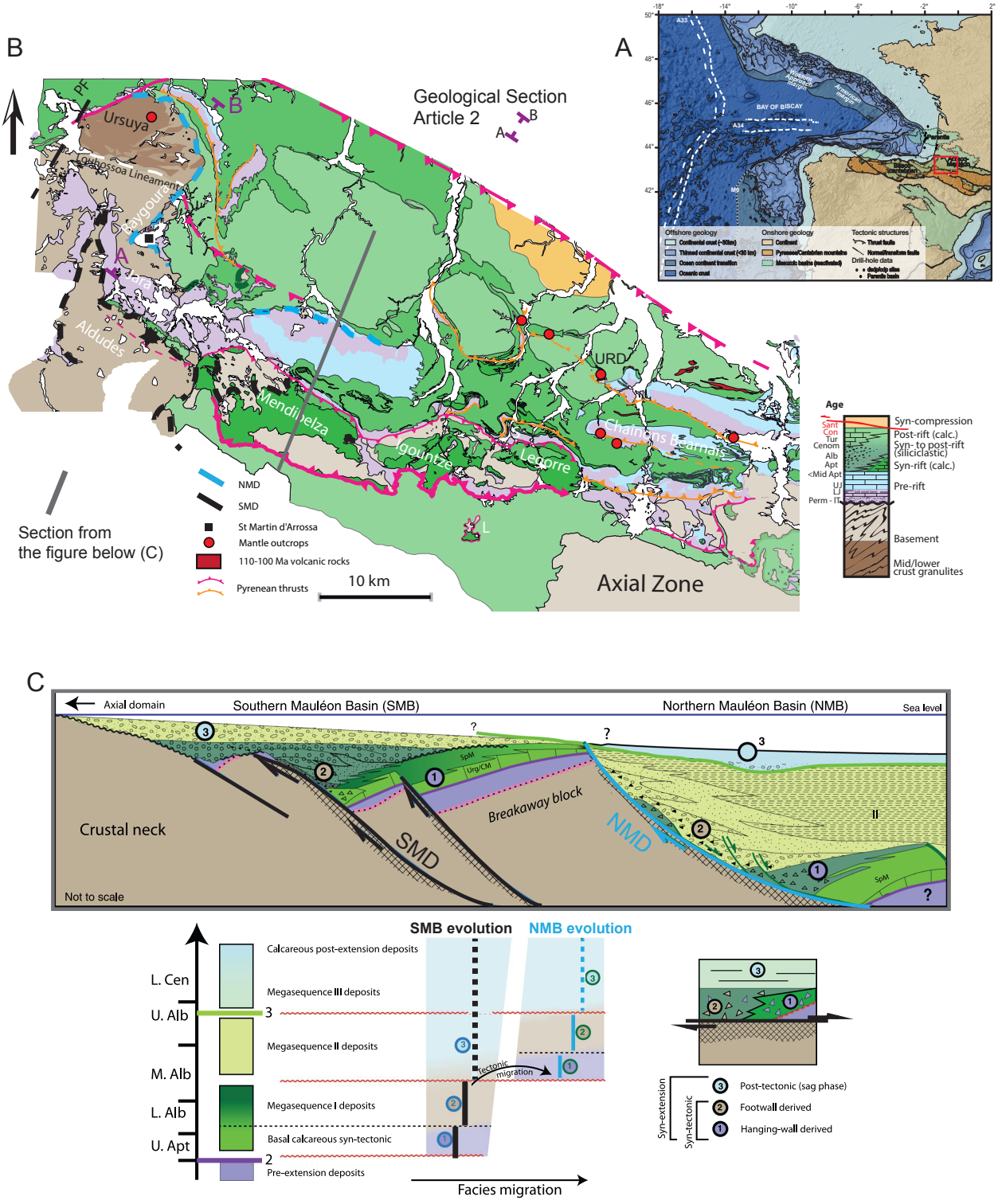

Figure 7. The Mauléon Basin in the West Pyrenees. (A) Location of the Mauléon Basin in the context of the extensional system of the Bay of Biscay and the Pyrenean chain [*Tugend*, 2013]. (B) The geological map of the Mauléon Basin, modified from *Masini* [2011]. Red dots mark the mantle outcrops. Note the indication (A-B) in the map that refers to the geological section shown in the Article 2. (C) Geological section indicated in Figure B by the gray line. The figure shows the Southern and Northern Mauléon Basin, which development were controlled by the activity of their respective detachment systems (SMD and NMD) as shown in the scheme below the section [*Masini* et al., 2014].

The NMD is an important structure in the Mauléon Basin, once it is intimately related to the exhumation of the crustal and locally mantle rocks. The investigation of the NMD permits the understanding of the link between fluids and tectonic evolution in this hyperextended system, which will be addressed in the Article 2.

2.4. Some limitations about the methods and the studied sites

Fluids in its liquid or gas phases were not investigated in this thesis. The primarily reason is due to the access of the data. For instance, fluids are usually trapped in reservoir deep in sedimentary basins. The main studied sites are the fossil extensional systems exposed at the surface in the Alps and Pyrenees. Regarding to the Iberian Margin, the wells were drilled over highs without a structural trap capable to retain fluids. Therefore, the investigation of fluids in this work is restricted to their *imprint* in the basement, fault and sedimentary rocks.

Another limitation is due to the lack of data in present-day distal rifted margins. The few existent data were acquired by the ODP Legs and by petroleum companies. Data from petroleum companies are usually not available for the scientific community.

The Iberia and Newfoundland are the rifted margins with more available ODP data from the distal margin that sampled through sedimentary, basement and fault rocks. Nevertheless, they still cover a small and very local part of the distal margin. This limits the understanding of the volume, variability and composition of fluid along detachment systems and sedimentary rocks.

Many ODP wells did not sample all stratigraphic sections due to technical problems or because wells were drilled over structural highs. Therefore, the investigation of an entire section from the basement rocks passing through extensional detachment faults, finishing with the overlying syn- and post- rift sequences is not possible at the moment. Thus, the study of these rocks was performed on a composite section using different wells.

Regarding to the exhumed mantle in the Iberia-Newfoundland rifted margins, they are more than 90% serpentinized and only up to 100 meter of these rocks were sampled in each ODP site. This strongly limits our study of element losses during serpentinization, as discussed in the three Articles. This was one of the reasons that drove me to use the examples of the Alpine Tethyan margins, where a complete dataset from weak serpentinized peridotites (<5%) to highly serpentinized peridotites (>95%) is exposed.

Although the Mauléon Basin in the Pyrenees is weakly affected by compressional events,

the limitation lies on the fact that the outcrops are only present at specific sites and the fault rocks are relatively less exposed compared to their equivalents in the Alps.

To override the limitation of the exposure of a complete section of rocks (i.e., basement rocks, syn- and post-rift sedimentary rocks, fault rocks) most of the work was focused to the remnants of the extensional systems from the Eastern Alps, Western Iberian Margin and West Pyrenees.

The assembly of petrological, geophysical and geochemical data from the Iberia distal margin allowed us to quantify the amount of fluids involved in serpentinization. However, the high uncertainties regarding the nature of the continental crust limited us to do the same for the continental crust of the Iberian Margin. Therefore, the amount of the continental crust-related fluids involved in the distal margin was not possible.

The geochemical analyses were mainly performed on bulk rock and clay fractions. Small scale mineralogical and isotopic studied were not too much investigated. For instance, the specific conditions (e.g., oxidation state) of development of mineralogical phase was not addressed, although we used published results.

RESULTS

3. **ARTICLES**

3.1. ARTICLE 1: TRACING MANTLE-RELATED FLUIDS IN MAGMA-POOR RIFTED MARGINS: the example of Alpine Tethyan rifted margins

3.2. ARTICLE 2: LINKING TECTONIC AND FLUID HISTORY DURING THE FORMATION OF HYPEREXTENDED DOMAINS: the examples of Tasna in the Alps, Mauléon in the Pyrenees and Hobby High at deep Iberian Margin

3.3. ARTICLE 3: IMPLICATIONS OF ELEMENT LOSS AND MANTLE HYDRATION DURING SERPENTINIZATION IN RIFTED MARGINS

ARTICLE 1

TRACING MANTLE-RELATED FLUIDS IN MAGMA-POOR RIFTED MARGINS:

the example of Alpine Tethyan rifted margins

Victor Hugo G. Pinto[1,2], Gianreto Manatschal[1], Anne Marie Karpoff[1] and Adriano Viana[2]

[1]Institut de Physique du Globe de Strasbourg, CNRS UMR7516, Université de Strasbourg

1 rue Blessig, 67084 Strasbourg Cedex, France

[2]Exploration & Production, Petrobras S.A., Av. República do Chile, 330, Rio de Janeiro, Brazil

ABSTRACT

The thinning of the crust and the exhumation of subcontinental mantle is accompanied by a series of extensional detachment faults. Exhumation of mantle and crustal rocks is intimately related to percolation of fluids along detachment faults leading to changes in mineralogy and chemistry of the mantle, crustal and sedimentary rocks.

Using field observation and analytical methods, we investigate the role of fluids in the former distal margins of the Alpine Tethys. Using Cr-Ni-V, Fe and Mn as tracers, we show that mantle-related fluids used detachment faults as pathways and interacted with the overlying crust and sediments. These observations enable to discuss when, where and how this interaction happened during the formation of the rifted margin. The results show that:

(i) serpentinization of mantle rocks during their exhumation resulted in the depletion of elements and forms mantle-derived fluids that are channeled along active extensional detachment faults, similar to hydrothermal sites at MAR;

(ii) in earlier-stages, these fluids affected the overlying syn-tectonic sediments by direct migration along extensional detachments faults;

(iii) in later-stages, these fluids arrived at the seafloor, "polluted" the seawater and were absorbed by post-tectonic sediments.

We conclude that a significant amount of serpentinization occurred underneath the thinned continental, that the mantle-derived fluids might have modified the chemical composition of the sediments and seawater. We propose that the chemical "signature" of serpentinization occurring during the mantle exhumation is recorded in the sediments and may serve as a proxy to date serpentinization and mantle exhumation in present-day magma-poor rifted margins.

TABLE OF CONTENTS

1. INTRODUCTION

Many studies investigating fluid-rock interactions focused on thrust systems, subduction zones and Mid-Ocean Ridges (MOR), while only few studies investigated fluid systems related to the formation of hyperextended rifted margins [*Manatschal*, 1999; *Manatschal et al*., 2000; *Engström et al*., 2007; *Benedicto et al*., 2008]. In particular, the origin and the time these fluids form and how they interact with different reservoirs (crust, mantle, sedimentary basin and seawater), as well as their migration pathways along distal rifted margins remain little understood.

Fluids can have different origins and their occurrence can be found in a wide range of extensional settings. In the Bohai basin in China, the occurrence of CO_2 and CH_4 accumulations in gas reservoirs has a characteristic mantle or magmatic signature given by C and He isotopes [*Jin et al*., 2004]. Nevertheless, the interplay of the widespread Cenozoic volcanism and the set of major normal faults [*Jin et al*., 2004] suggest that these gases were formed by magmatic activity and migrated through faults. In the southeast Brazilian rifted margins, CO_2 with a mantle signature are also recognized by isotopic composition of C and He [*Santos Neto et al*., 2011]. In the same margins, the trace elements analyzed in petroleum accumulations in Cretaceous and Cenozoic reservoirs suggest a mantle source for those elements [*Szatmari et al*., 2011]. *Manatschal et al*. [2000] described an enrichment of trace elements, typical from mantle composition, in fault rocks from the Err detachment system located in the distal domain of the fossil Adriatic margin of the Alpine Tethys. In the Albian carbonate rocks from the Cantabrian basin, northern Spain, a strong signature of fluids enriched in Pb-Zn-Fe is described [*López-Horgue et al*., 2010; *Dewit et al*., 2012]. These hydrothermal systems occurred over hyperextended crust within a domain where magmatic rocks are found.

Some of those distal domains in rifted margins share similar processes with oceanic domains. Hydrothermal vents at Mid-Atlantic Ridge (MAR) expel fluids enriched in CO_2, H_2S, CH_4 and metals like Cu, Zn, Fe, Au in magmatic systems [*Douville et al*., 2002; *Fouquet et al*., 2010; *Kelley and Shank*, 2010] where they are accompanied by lava flows or by interaction with mafic rocks (e.g., gabbros). Hydrothermal vents resulted from the interaction between seawater and ultramafic rocks are also described [*Kelley et al*., 2001]. Their main fluid compositions are reported as rich in H_2, CH_4 and Si, Ca, Mg, Fe, Mn, Ni [*Delacour et al*., 2008; *Edmonds*, 2010; *Fouquet et al*., 2010; *Kelley and Shank*, 2010].

Sediments associated with exhumed mantle and/or magmatic system in oceanic domains capture the signature of upwelling fluids through the pile or of discharging fluids from

hydrothermal vents that spread out metals in the seawater over long distances. Those fluids lead to the transformation or neoformation of minerals, such as phyllosilicates, oxides and carbonates recording the fluid composition and/or the modified seawater chemistry [*McKenzie et al*., 1990; *Buatier et al*., 1995]. Recently, *Saito et al*. [2013] presented a profile from the Atlantic ocean from the Brazilian margin to the Namibia platform showing a Fe-Mn plume that extends over more than 3000 km. They highlight that the amount of Fe-Mn is much higher at slow spreading systems than in fast spreading systems and that serpentinization is probably one of the major processes controlling it. This is supported by observation of Fe and Mn-rich hydrothermal vents fluids related to serpentinization in the Saldanha field in the South Atlantic [*Dias et al*., 2011]. In this field, low temperature fluids escape from centimetric vent orifices (no chimney structures) that are broadly distributed around the field. Fe and Mn oxyhydroxides precipitate from the seawater due to the cooling and gradually more oxidizing condition and are easily trapped in the contemporaneous sedimentary deposits [*Dias et al*., 2011].

It has also been shown at slow spreading systems and Ocean Continent Transitions (OCT) that serpentinization is intimately related to extensional detachment faults [*Picazo et al*., 2013; *Rouméjon and Cannat,* 2014 and references therein] and that fluids related to these tectonic settings have a characteristic "signature" [*Edmonds*, 2010].

Detachment faults similar to those recognized in oceans [*deMartin et al*., 2007; *Reston and Ranero*, 2011; *Picazo*, 2012; *Whitney et al*., 2012] have also been described in the continental crust of rifted margins [*Froitzheim and Eberli*, 1990; *Manatschal et al*., 2001]. In these settings, fluid circulation seems to be related to extensional events and they are responsible to alteration of basement rocks leading to retrograde metamorphic reactions [*Manatschal et al*., 2000].

This study focus on a well-preserved rift-related extensional detachment system exposed in the Lower Austroalpine and Penninic nappes in the Alps in SE Switzerland (Figure 1). This rift-related detachment system is responsible for the final thinning of the crust and exhumation of the underlying mantle. Along these detachment systems a series of water-assisted retrograde metamorphic reactions associated with hydrothermal circulation and fluid migration can be observed. Some of those reactions are the result of fluid-rock interactions that happened under hydrothermalism during the mantle exhumation, inducing the leaching of elements and their migration along detachment faults into the overlying sedimentary basin and seawater. The fluids derived from mantle serpentinization were enriched in Ni, Cr, V, Fe and Mn; as indicated by their occurrences in fault rocks of extensional detachment faults in the thinned continental crust and

in the overlying sedimentary rocks. In this paper we discuss how and when these mantle-related fluids formed and migrated along the extensional detachment faults, and how they affected the crust and overlying sediments and seawater. We will also show that mantle-related fluids effects can only be observed in the distal margins along the final fault system that is related to mantle exhumation, while earlier fault systems, located further inboard (more proximal) do not show this signature.

2. MAGMA-POOR RIFTED MARGINS

2.1. Present-day magma-poor rifted margins

The architecture of magma-poor rifted margins has been described in many places [*Contrucci et al*., 2004; *Aslanian et al*., 2009; *Péron-Pinvidic and Manatschal*, 2009] using good-quality seismic data. However, only along the Iberia-Newfoundland rifted margins wells penetrated basement rocks in the most distal portions [*Whitmarsh et al*., 1998]. Drill-core data from these margins include exhumed serpentinized mantle, sparse magmatic rocks, faults rocks (cataclasites and gouges) and sedimentary rocks, which document the final evolution stage of magma-poor rifted margins. Present-day oceans have also been broadly studied especially from dredging, DSDP, ODP, and IODP data along slow-spreading mid-ocean ridges (MOR). Although magmatism is thought to be the main process at MOR, mantle exhumation and concomitant serpentinization along detachment faults (oceanic core complexes) and their characteristic hydrothermal vents have been described by many authors and they seem to be more common as previously expected [*Kelley et al*., 2001; *Douville et al*., 2002; *McCaig et al*., 2007; *MacLeod et al*., 2009; *Picazo et al*., 2013; *Castelain et al*., 2014].

The study of well-core and refraction seismic data shows that large portions of the mantle are strongly hydrated (i.e. serpentinized), which leads to question how, where and when fluids were able to penetrate and react with the mantle. However, at present-day rifted margins it is difficult to answer to these questions once the sampling are limited to the first hundreds meters of basement rocks and due to the fact that these margins are no longer tectonically active. As a consequence, direct data and observations are scarce. Nevertheless, the fragments of these hyperextended systems are also exposed in ancient (fossil) magma-poor rifted margins of the Alpine Tethys [*Lemoine et al*., 1986; *Froitzheim and Manatschal*, 1996; *Mohn et al*., 2010]. The well-preserved rift-related structures and sedimentary rocks in these fossil margins have allowed building their main architecture and reveal their complex evolutionary history.

2.2. The Alpine Tethyan Margins

2.2.1. Rift domains and rift evolution

Remnants of the Mesozoic conjugate rifted margins were recognized and described in the Alps. Their different paleogeographic domains (Figure 1) were defined based on the stratigraphic record [*Trümpy*, 1975; *Lemoine et al*., 1986; *Lemoine and Trümpy*, 1987]. More recently [*Mohn et al*., 2010, 2012] reviewed the existing data and proposed the following subdivision:

(i) a proximal domain [*Lemoine et al*., 1986; *Eberli*, 1988] developed over an equilibrated continental crust characterized by grabens and half-grabens overlying a 25 km thick crust, (ii) a necking domain corresponding to a transitional zone between a little extended (> 25 km) and a highly extended (or thinned) continental crust (< 10km), (iii) a highly thinned (~10 km), brittle continental crust characterized by extensional detachment faults and supradetachment basins [*Froitzheim and Manatschal*, 1996; *Masini et al*., 2011], (iv) a zone of exhumed continental mantle [*Desmurs et al*., 2001] grading into (v) an embryonic oceanic domain [*Manatschal and Müntener*, 2009]. The evolution from a continental setting to an embryonic oceanic domain has been studied by many authors [e.g. *Manatschal*, 2004].

The detailed rifting investigation shows a complex 3D time/space evolution resulting in an architecture that includes two hyperextended basins (Piemont-Liguria and Valais) that have separated the Apulia/Adria and European/Briançonnais margins. Despite the Alpine overprint, the preserved remnants of the former rifted margins enable the recognition of the rift-related structures as well as their importance for the evolution of different domains of the alpine Tethyan margins and for their paleogeographic restoration [e.g., *Manatschal and Bernoulli*, 1998; *Schmid et al*., 2004; *Masini et al*., 2013].

2.2.2. The pre-rift stage (inherited condition)

The inherited pre-rift conditions of the Alpine Tethyan margins are characterized by Paleozoic basement and syn- to post-Variscan igneous intrusion [*Raumer*, 1998]. During the Permian an important magmatic event is evidenced by gabbroic rocks intruded in different crustal levels [*Mohn et al*., 2012, and references therein] as well as volcanic rocks associated to fault-bounded basins. The sedimentary record of the pre-rift stage starts in the Late Carboniferous/Early Permian and are commonly associated to the post-orogenic collapse of the Variscan orogeny. During the Permian/Early Triassic, continental siliciclastic sedimentary sequences developed (Verrucano-

Buntsandstein). These sequences is followed by Middle to Upper Triassic marine carbonates and evaporites [*Lemoine et al*., 1986]. The marine carbonate deposition is also associated with a rifting event further to the east/southeast that was related to the opening of the Vadar/Meliata ocean [*Channell and Kozur*, 1997]. However, in the studied area, further to the west/northwest of Alpine Tethys, the onset of rifting did not start before latest Triassic/Early Jurassic. Therefore, the Triassic sequence will be referred to as pre-rift.

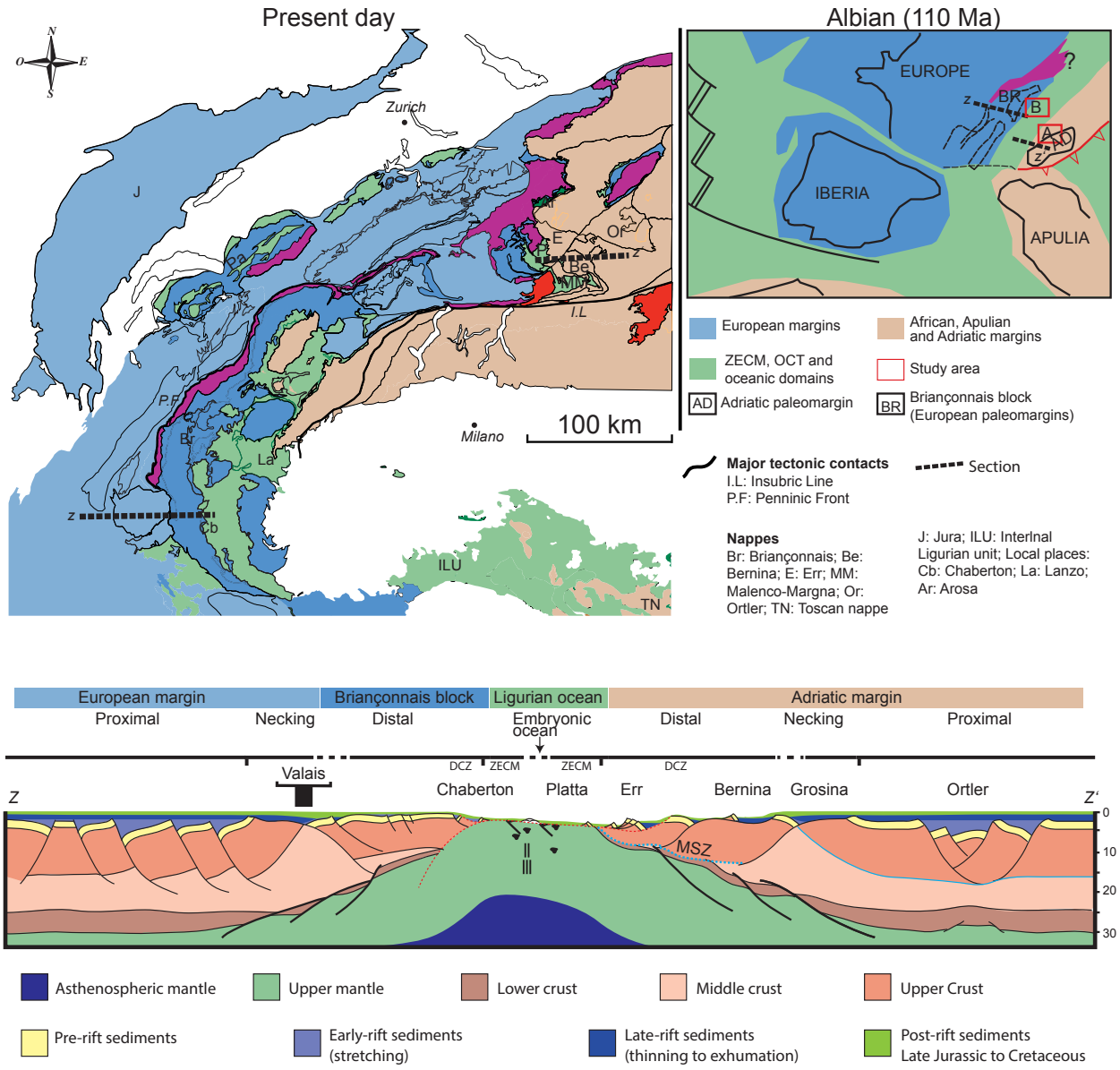

Figure 1. Tectonic and paleogeographic maps, and cross-section through the former Alpine Tethyan margins. The present -day tectonic map (modified from *Schmid et al.* [2004] and *Mohn et al.* [2010]) shows a simplified subdivision of the main domains of the Alpine Tethyan margins. The paleogeographic map shows the continent and margin position at the Albian times. Red squares in the paleogeographic map are the position of the studied areas in Adriatic margin (A) and the Briançonnais (B). The composite cross-section through the conjugate margins of Adria and Europe/Briançonnais in a direction that the Valais domain is not present. The domains in the distal margin are referred as the Zone of Exhumed Continental Mantle (ZECM) and Distal Continental Zone (DCZ). Dotted blue line is the Margna shear zone (MSZ).

2.2.3. **Early rifting event: stretching phase**

The early rift stage (Hettangian/Sinemurian) is best preserved in the proximal domain of the European [*Lemoine and Trümpy*, 1987] and Adriatic margins [*Eberli*, 1988; *Bertotti et al*., 1993]. This event is linked to marine basins that underwent rifting at water-depth that never exceed 1000 m [*Roux et al*., 1988; *Mohn et al*., 2010]. The sediments are mostly characterized by carbonate-bearing thick debris flow and turbiditic sequences bounded by high-angle normal faults [*Lemoine et al*., 1986; *Eberli*, 1988] in a continental crust of about 25 km thick [*Mohn et al*., 2010]. A marl/limestone association dated by ammonites from Pliensbachian/Toarcian [*Eberli*, 1988] seal the high-angle normal faults and mark the end of rifting in the proximal domains.

2.2.4. **Late rifting event: thinning and exhumation phases**

A late rift stage developed in domains that include the future distal part of the margin. This stage is well recorded in the distal Adriatic margin and is characterized by extensional detachment faults that are responsible for the thinning of the crust and mantle exhumation [*Manatschal*, 1995; *Froitzheim and Manatschal*, 1996].

Basal sedimentary sequences onlap onto the exhumed faults at angles <10º indicating a fault-controlled topography. The syn-tectonic sediments are characterized by carbonate bearing turbidites and debris flow deposits, as observed in the Val dal Fain area [cf., Allgäu formation; *Mohn et al*., 2012] and siliciclastic debris flows and turbidite sequences in the Zone of Samedan (ZoS) [cf., Saluver formation; *Masini et al*., 2011]. These sequences were deposited during late Pliensbachian to Bajocian/Bathonian times [*Finger*, 1978; *Eberli*, 1988].

2.2.5. **Embryonic ocean stage**

In the ophiolites from the Alpine Tethyan ocean, thick continuous basaltic layer and sheeted-dikes complexes are absent. Many authors [*Decandia and Elter*, 1972; *Lemoine et al*., 1987; *Lagabrielle and Cannat*, 1990] showed that the Alpine Tethys ocean was not floored by a “classical” oceanic crust, but more likely by exhumed subcontinental serpentinized mantle associated with magmatic additions (gabbros and basalts) of tholeiitic affinity that increase in volume oceanwards [*Lemoine et al*., 1987; *Desmurs et al*., 2001]. This characteristic rock sequence is overlain by Radiolarian cherts dated as Callovian to Bathonian [*Bernoulli and Weissert*, 1985; *Baumgartner*, 1987]. The Radiolarian cherts can be traced from the zone of exhumed continental mantle (ZECM), across the distal margin towards the proximal margin, setting up the first well

marked regional post-rift sequence registered in the Alpine Tethyan margins [*Lemoine et al*., 1986; *Mohn et al*., 2010].

3. THE DISTAL RIFTED MARGIN EXPOSED IN THE ERR AND PLATTA NAPPES

Remnants of the fossil distal domains of the Alpine Tethyan margins are preserved in the Lower Austroalpine Err nappe and in the Upper Penninic Platta nappe in Grisons, southeastern Switzerland (Figure 2). Although the Alps result from different orogenic cycles, the remnants of the fossil distal margins are locally well preserved in the Err-Platta nappes. *Manatschal and Nievergelt* [1997] highlight that the D1-phase, responsible for a west vergent nappe stack, allowed them to restore the main Jurassic rift architecture of the distal margin. The metamorphic overprint in these nappes shows a general increase from north to south [*Trommsdorff and Evans*, 1974; *Ferreiro Mählmann*, 1996]. In the northern Platta nappe the distribution of chrysotile/lizardite shows that the temperature did not exceed 350ºC [*Trommsdorff and Evans*, 1974]. In the Err nappe, the Mesozoic sediments present diagenetic to anchizonal conditions. *Manatschal* [1995] used zircon fission track data from granitoids (118.8 ±8.9 Ma) to show that Alpine deformation never exceeded 250ºC in the Err nappe.

The fact that the basement and the sedimentary rocks are weakly affected by Alpine compressional events and that the Jurassic structures, stratigraphy and overall margin geometry is locally well preserved, makes the Err and Platta nappes one of the best examples world wide to study the structural and stratigraphic evolution of magma-poor rifted margins. As show below, these sites also allowed us to investigate the tectonic and fluid circulation history associated with the formation of this magma-poor rifted margin.

3.1. The Continental Distal Zone (CDZ) and the Zone of Exhumed Continental Mantle (ZECM) exposed in the Err and Platta nappes

The remnants of the former distal margin exposed in the Err and Platta nappes present characteristic zones (sub-domains) that are comparable with present-day magma-poor distal rifted margins. Based on the reconstruction of the Err [*Manatschal*, 1995] and the Platta [*Desmurs et al*., 2001] nappes and their present disposition, these two units preserve a dip section across the former Late Jurassic distal rifted margin that corresponds at least to 50 km in transport direction [*Manatschal*, 1995; *Manatschal and Nievergelt*, 1997]. The distal margin (Figures 1 and 2) preserved in the Err and Platta nappes can be subdivided into the Continental Distal Zone (CDZ;

e.g., Err nappe) and the Zone of Exhumed Subcontinental Mantle (ZECM; e.g., Platta nappe). Both zones are formed by extensional detachment systems (e.g., Err detachment system) that are Early to Middle Jurassic in age as indicated by their relationship with the syn- and post-tectonic sediments [*Eberli*, 1988; *Masini et al*., 2011]. The detailed mapping of the footwall of the detachment systems in the continental and in the mantle domain, the well-preserved sedimentary sequences and the late-rifting magmatism allow us to document and understand the link between detachment faulting and fluids circulation during the evolution of the distal margin.

3.1.1. **The pre-rift continental crust in the future CDZ**

The continental basement in the CDZ is made of Paleozoic gneisses and schists as well as a series of syn- to post-Variscan intrusive and extrusive rocks [*Von Quadt et al*., 1994]. Among these rocks, an intrusive suite of calcalkaline gabbro-diorite-granodiorite-granite referred as the Albula granite [*Manatschal*, 1995] has an important areal distribution in the Err nappe. Among this suite, granites and granodiorites are often found in the footwall of extensional detachment faults (e.g., Err detachment system). Therefore, we will refer to the Albula as granite/granodiorite basement, which are the main protoliths of the fault rocks from the Err detachment. The basement rocks are overlain by a Permo-Triassic pre-rift sequence that initiates with a continental sequence (e.g., Buntsandstein) that develops upsection into Middle to Upper Triassic marine carbonates [*Eberli*, 1988]. In the Err nappe, the most prominent pre-rift sequence is made of Upper Triassic (Norian) dolomites (Hauptdolomit) [*Cornelius*, 1932; *Eberli*, 1988]. The Norian dolomites are overlain by the Rhätian, Kössen, and the Liassic Agnelli formations. This last formation corresponds to the uppermost pre-tectonic (pre-rift) sequence in the distal margin. *Dommergues et al*. [2012] dated the Agnelli formation showing that the top of the sequence has 185 Ma. It is important to note that in the proximal margins, the time equivalent sedimentary sequence of the Agnelli formation is the syn-tectonic Allgäu sequence that is sealed by a Pliensbachian-Toarcian marl/limestone succession [*Eberli*, 1988], which dates the end of rifting in the proximal domains. The top of the Agnelli formation represents an important time marker that dates the onset of detachment faulting and the development of the supradetachment basin in the distal margin [*Masini et al*., 2011].

3.1.2. **Crustal thickness of the future distal domain**

Müntener et al. [2000] showed that locally in the lower Austroalpine nappes, the upper crustal rocks are juxtaposed against lower crustal rocks along a pre-Alpine shear zones (e.g., Margna shear zone). Cooling ages of lower crustal rocks show Jurassic values for this juxtaposition [*Müntener et al*., 2000]. *Mohn et al*. [2012] suggested that this ductile shear zone was part of an

extensional system that thinned the crust to about 10 km (Figure 1). These authors also demonstrate with thermochronological data that the development of this shear zone is contemporaneous with the necking of the continental lithosphere, which is supposed to occur about 190-185 Ma. Furthermore, *Desmurs et al*. [2001] showed that when the extensional detachment faults penetrated the mantle, the latter had already to be in a shallow level. This was mainly concluded from the observation that all the extensional detachment faults found in the crust and mantle only present lower greenschist facies tectonic breccias, indicating that they were only active in the brittle layers of the lithosphere. Therefore, when the extensional detachment faults cut into mantle, the crust had already to be thinned to about 10 km or even less and hence the mantle was already in shallow levels. Very similar observations were also reported for the Iberia margin [*Manatschal et al*., 2001].

3.1.3. **The zone of exhumed subcontinental mantle (ZECM)**

The remnants of the ZECM preserved in the Platta nappe are characterized by subcontinental serpentinized lherzolites with local occurrences of dunite and pyroxenite layers [*Desmurs et al*., 2001; *Müntener et al*., 2010]. The Platta nappe consists of two Alpine units divided by a major D1 thrust fault. These two units, referred to as the Upper and Lower Serpentinite Units (USU and LSU), represent respectively a more proximal and a more distal part of ZECM [*Desmurs et al*., 2001; *Schaltegger et al*., 2002; *Müntener et al*., 2010]. While in the USU magmatic rocks are rare, the LSU presents MORB-bearing magmatic rocks, testifying its embryonic oceanic nature [*Manatschal and Müntener*, 2009].

Key structures and metamorphic reactions observed in the ZECM, record the exhumation path of the mantle rocks to the seafloor. In the USU, pyroxenite dykes parallel to the high-temperature spinel foliation [*Desmurs et al*., 2001] indicate that they equilibrated in the spinel stability field, which would be approximately 40-50 km depth [*Klemme*, 2004]. In the LSU, *Desmurs et al*. [2001] point out the occurrence of high temperature hornblende around Cpx and its cleavage planes, developed under 600-700ºC (about 22 km), followed by a widespread hydration at lower temperature expressed by the crystallization of tremolite at the expense of clinopyroxene and Mg-hornblende. However, the hornblendes could not be dated and their relation to the Jurassic rifting cannot be demonstrated. In contrast, the serpentinization predates the Alpine compression and it is related to the Jurassic rifting [*Desmurs et al*., 2001; *Picazo et al*., 2013]. Serpentine often appears as a mesh-like structure and is associated with magnetite. Spinel is often altered to Cr-chlorite and magnetite, which mark a temperature between 200 and 300ºC [*Klein et al*., 2013]. They are thought to be formed at depths lower than 10 km. At or near seafloor, the serpentine

minerals are partially replaced by calcite + talc, resulting in the so-called ophicalcites [*Bernoulli and Weissert*, 1985; *Picazo et al*., 2013].

Magmatic intrusive rocks also register a final extension/deformation event and some of the extrusive magmatic rocks post-date the extension. Different gabbros intruded the already serpentinized mantle at shallow level at high to moderate temperature [*Desmurs et al*., 2001]. These authors dated some of these rocks in the Platta and other Penninic nappes, which show a crystallization age at 161 ± 1 Ma. This is in agreement with Ar/Ar ages in phlogopite (160 ± 8 Ma) from pyroxenite layers in the peridotites of other Penninic nappes close to the Platta nappe (e.g., Totalp near Davos) [*Peters and Stettler*, 1987]. The crystallization and cooling age are interpreted as the age of mantle exhumation to 10 km depth or less [*Desmurs et al*., 2001].

3.2. **The syn- to post-tectonic sedimentary sequences in the distal margin**

In the Err nappe, the syn- to post-tectonic sedimentary sequences are developed in supradetachment basins [*Masini et al*., 2012] and they are quite different from those described in the proximal margin [*Mohn et al*., 2010; and references therein]. These sediments either overlie the Agnelli formation or are directly deposited over an exhumed basement and are sealed by the post-rift Radiolarian cherts. The syn- to post-tectonic sequences are formed by two main formations, Bardella and Saluver, which were originally distinguished by their clasts composition and grain size [*Finger*, 1978]. *Masini et al*. [2011] subdivided the Bardella and the Saluver formations in three genetic sequences (basal, intermediate and top-facies tracts), which deposition is controlled by the evolution of the Err detachment fault and the development of a supradetachment basin. The basal facies tract is made of Bardella and Saluver A formations, the intermediate corresponds to the Saluver B formation, and the top facies tract is referred to as the Saluver C formation.

The syn-tectonic sequences correspond to the Bardella, Saluver A and Saluver B formations. The post-tectonic sequence corresponds to the Saluver C formation. The Bardella Fm. is composed of breccias with carbonate clasts (mainly the Triassic Hauptdolomit Fm.) that are derived from the hanging wall blocks of the detachment system. The Saluver A Fm. is characterized by polymictic breccias composed of clasts of basement rocks, fault rocks from the Err detachment (e.g. gouges) and carbonates (e.g., Haupdolomit). The Saluver A is related to the exhumation of the detachment footwall at the sea floor and it is frequently found interfingering the Bardella formation, showing a coeval deposition. Both formations correspond to sedimentary deposits that are proximal relative to theirs sources. This observation suggests that they were deposited during early stages of the development of the detachment system. The Saluver B lies above the basal facies tract and is

characterized by thinning and fin-upward sequences that grade from breccias to sandstone-dominated turbiditic sequences, reworking basement and Permo-Triassic rocks. The Saluver C shows interbedding of shales and thin sandstone turbidites at the base (some times mature arkosic beds) and the predominance of shales at the very top (Figure 2). This latter sequence can be partially found, associated to allochthonous continent-derived blocks, in the ZECM in the Platta nappe (e.g. Parsettens area) [*Cornelius*, 1932; *Manatschal et al*., 2003].

The regional post-rift Radiolarite Fm. (RAD) overlies the Saluver C formation. As discussed before, this formation is widely distributed in the Alpine Tethyan domains [*Lemoine et al*., 1986; *Eberli*, 1988; *Bertotti et al*., 1993; *Bernoulli et al*., 2003]. The Radiolarite formation is made of silica-rich radiolarian cherts layers interbedded with thin reddish shales dated as Bathonian to Callovian [*Baumgartner*, 1987; *Cordey and Bailly*, 2007]. The RAD is overlain by the Tithonian to early Berriasian Calpionella formation (the Aptychus limestone from *Cornelius* [1932]), comprising micritic limestone and thin carbonaceous shales [*Bracciali et al*., 2007]. This sequence is overlain by early Berriasian to late Hauterivian-early Barremian Palombini shales [*Marroni et al*., 2000] composed of black shales and levels of marls. The youngest sequence in this domain is made of thin Cretaceous flysch sequences.

3.2.1. **Important time constrain horizons**

Two time horizon (Figure 2) are essential to understand the evolution of the detachment system and its supradetachment basin exposed in Err and Platta nappes [*Masini et al*., 2011]. The first corresponds to the Top of Agnelli Formation (TAF), dated at about 185 Ma. The Bardella and Saluver formations unconformably overlie the TAF. This gives a maximum age for these formations. The second corresponds to the base of the Radiolarite Formation (RAD), dated at about 165 Ma. The Saluver and Bardella formations are unconformably overlain by the RAD and give a minimum age for these formations. The Radiolarite formation also lies above the serpentinites, basalts and exhumed gabbros in the Platta nappe. The crystallization age of gabbros is 161 ± 1 Ma, indicating that the RAD has to be Callovian (161 Ma) or younger in the ZECM. Because no detailed dating was carried in the Radiolarite Fm. in the Platta nappe, the ages used in this study (185 Ma to 165 Ma) can be considered as approximated ages for the formation of distal margin in the Err-Platta.

The observation that fault rocks of the Err detachment systems can be found reworked in the Bardella and Saluver A formations [*Froitzheim and Eberli*, 1990; *Froitzheim and Manatschal*, 1996] and rocks of the Agnelli Formation are truncated by the detachment fault, give maximum

and minimum ages for the Err detachment system in the Err nappe, that is between 185-165 Ma. It is likely that detachment faulting in the Err domain predated exhumation of mantle in the Platta domain that may have lasted at least until 161 Ma, corresponding to the onset of magmatic activity and deposition of Radiolarian cherts.

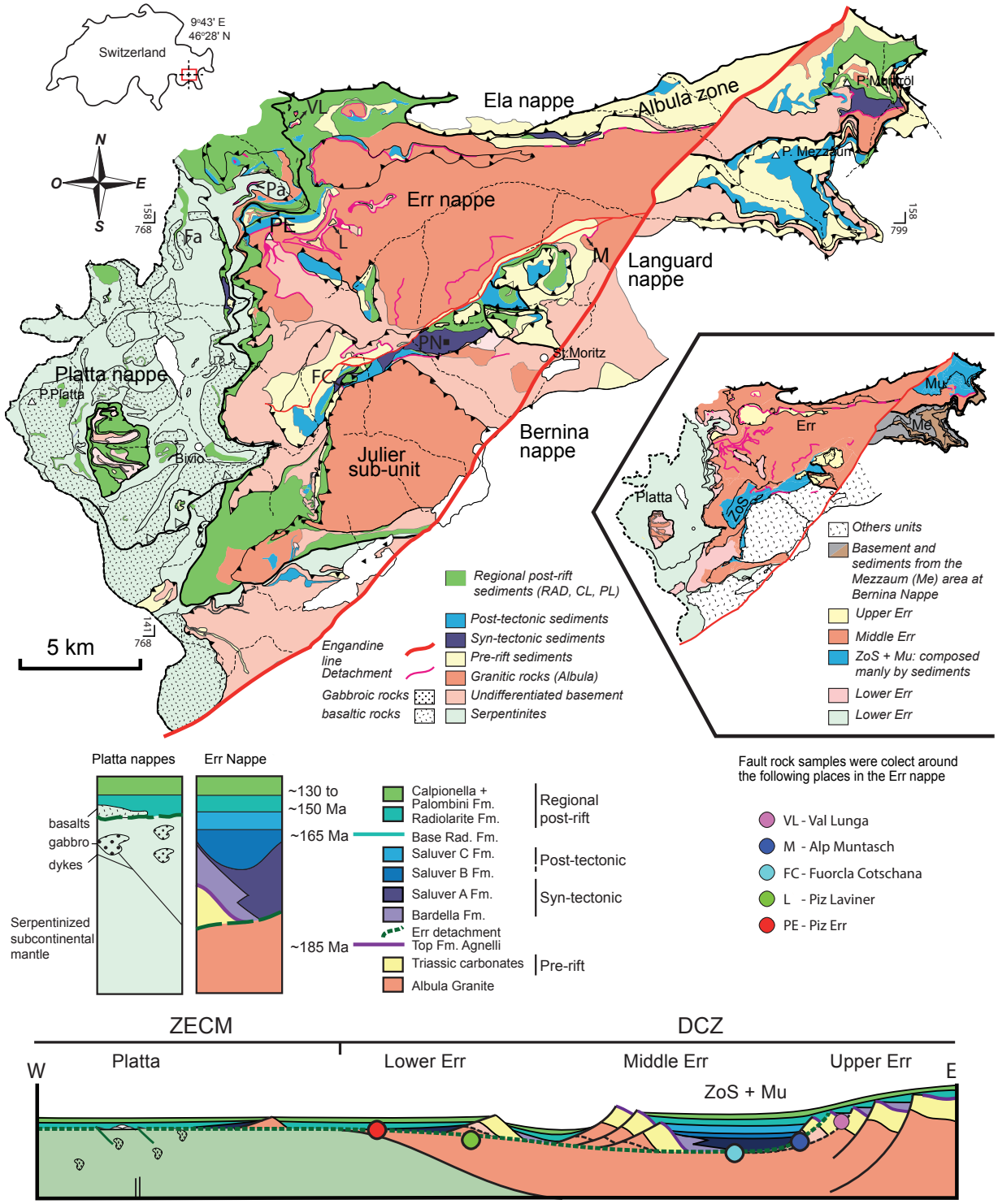

Figure 2. Tectonic map modified from *Mohn et al.* [2011] and cross-section of the Err and Platta nappes. The Err nappe is part of the former DCZ and the Platta nappe is the former ZECM. Notice the distribution of the sedimentary sequences in the ZoS (Zone of Samedan) and Murtiröl (small tectonic map at right). Localities abbreviations are: Fa: Fallota, Pa: Parsettens, PN: Piz Nair, VL: Val Lunga; FC: Fuorcla Cotschana; M: Alp Muntatsch; Mu: Murtirol; Me: Mezzaum. The cross-section (from *Masini et al.* [2012]) passes through the subunits of the Err and the Platta nappes. Colored dots represent the areas where samples were collected along the Err detachment fault (ED). The map is in Swiss grid (CH1903 in km).

3.3. **Extensional detachment faults**

3.3.1. **Fault rocks related to the extensional detachment fault in the mantle**

3.3.1.1. *Macro-scale characteristics*

Extensional detachment faults in the serpentinized mantle from the Platta nappe are characterized by low temperature, brittle fault rocks formed under similar conditions form those in the adjacent continental Err [*Manatschal*, 1999] as well as along other detachment faults in the Penninic nappes [*Picazo et al*., 2013]. The fault zone is roughly composed of foliated serpentinite cataclasites, gouges and ophicalcites (Figure 3G). The foliated serpentinite cataclasites are characterized by a brittle foliation, clasts of highly serpentinized peridotites and veins of serpentine and chlorite. The ophicalcites are composed of partially calcified serpentinites showing clasts of host-rock (serpentinites) cut by millimetric to centimetric calcite veins. Jigsaw clasts present locally in the ophicalcites highlight an *in situ* deformation. Fractures, extensional veins and open space filling veins (Figures 3I, 3J and 3L) are common in these rocks. Gouges occur often at the top of the fault zone containing rounded and sigmoidal clasts in a dark green matrix of serpentines, chlorite and calcite that highlight the localization of deformation (Figures 3G and 3H). The gouges are overlain by tectono-sedimentary breccias (~ 1.5 m) consisting of clasts of reworked serpentinized peridotites within a serpentine-chlorite-calcite matrix that is often cut by millimetric calcite veins. The calcite veins cut the serpentinite foliation and previous chlorite veins, indicating they resulted from a late-fluid migration in the fault zone (Figures 3I, 3J, 3L).

Figure 3. Extensional detachment fault profile and its main fault rocks in the exhumed mantle and in the continent. (A): Rock profile in the continental detachment fault from Err, Bernina, Grosina and Chaberton. Some of the rock types are absent in the mentioned detachments, but cataclasites always occur. White polygons represent the most prominent quartz veins and black lines represent small secondary fault and fractures that, in most of the cases, are filled by quartz veins. (B): Black gouge with clast of Triassic dolomite. (C): Contact chlorite-schist and tabular quartz vein (Grosina). (D) Clast-rich chlorite-schist (Fuorcla Cotschana) showing fracture quartz veins. (E): Foliated cataclasite and different sets of quartz veins (Fuorcla Cotschana). (F): Quartz veins parallel/sub-parallel to the foliation of cataclasites (Parsettens). (G): Rock profile from extensional detachment fault in the exhumed mantle at Platta nappe. Light gray polygons show main calcite veins. Black lines represent small secondary fault and fractures that, in most of the cases, are filled by chlorite, serpentine and calcite veins. (H): Gouges showing rounded clasts of serpentinites. (I): Ophicalcite with centimetric veins of calcite (light gray) parallel to the serpentinite foliation. (J): Ophicalcite with different orientations of calcite veins cutting the serpentinites. (L): Calcite veins (red arrows) cutting previous serpentinite foliation intensely fractured. Ophicaltization is more prominent in (I) compared to (L).

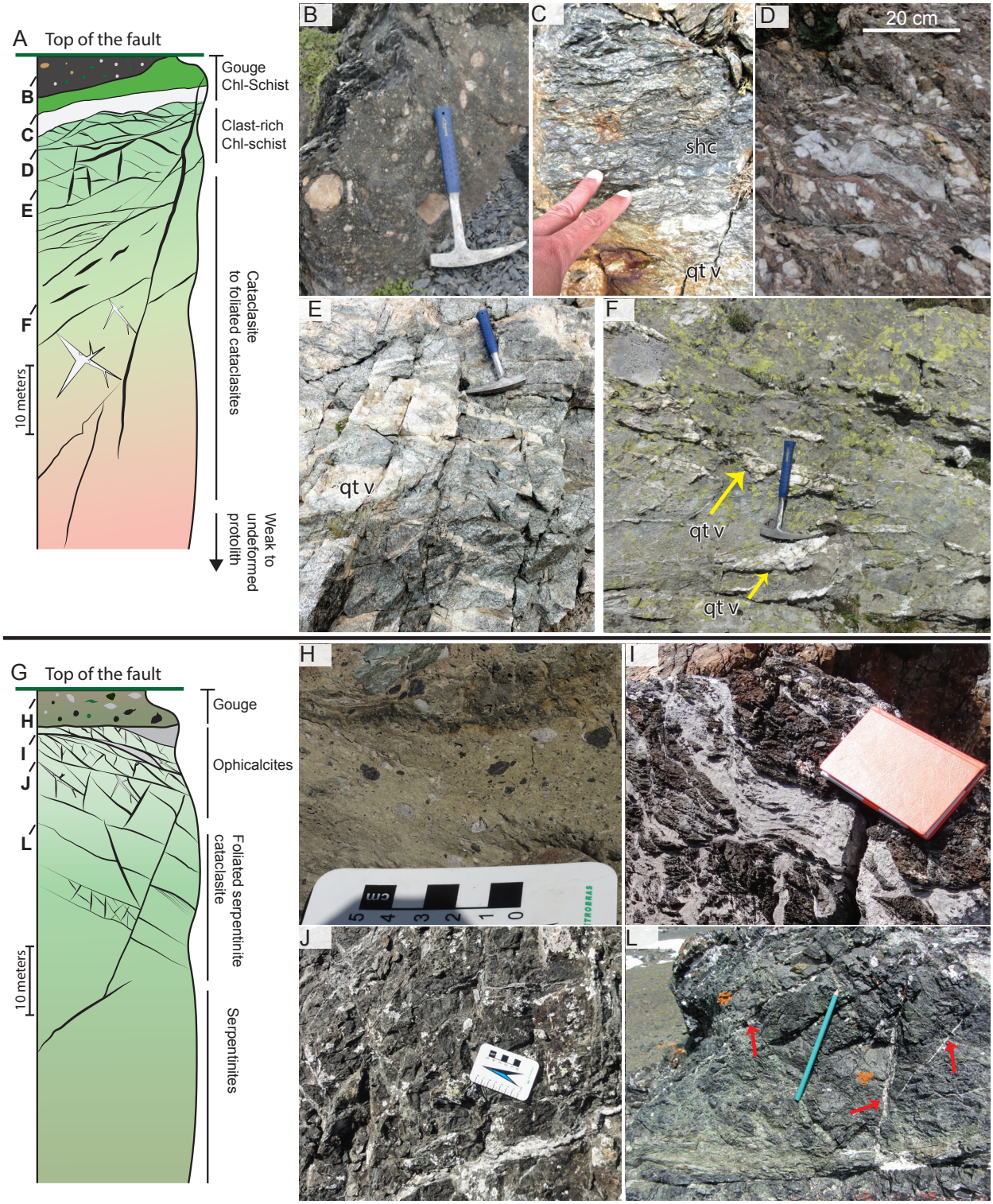

Figure 3.

The formation of ophicalcite was also studied in the present-day Iberia margin [e.g. *Morgan and Milliken*, 1996] and like in the Alps, it implies an important fluid-rock interaction through the fault zone that occurs at final-stage of mantle exhumation at the seafloor [*Bernoulli and Weissert*, 1985; *Picazo et al.*, 2013].

3.3.1.2. *Microstructures and mineralogical characteristics*

Optical microscopy was used to characterize the progressive deformation, the degree of serpentinization and the different types and composition of veins. The fault rocks in the mantle are characterized by a new mineralogical association with hydrated phases (e.g., serpentine and chlorite) that register an important fluid-rock interaction. Analyses of deuterium and oxygen show that this fluid is better defined by seawater with minor and local metamorphic fluids [*Burkhard and O'Neil*, 1988]. These authors showed high water/rock ratio what is also evidenced by the lack of the former minerals from the peridotite protolith (e.g., olivine and pyroxenes), which are completely transformed to phyllosilicates and opaque mineral. However, in the foliated cataclasites, angular to sigmoidal clasts of pyroxene and fully altered plagioclase are locally found in the serpentinite-rich matrix. In the gouges, rounded clasts of pyroxenes and of serpentinites are often observed within a matrix made of serpentine and chlorite. Those rocks are locally affected by a late carbonization [cf., *Picazo et al*., 2013] expressed by calcite veins that often show crack-seal processes and that present a remarkable quantity of Fe-oxides (Figures 4D-F). *Früh-Green et al*. [1990] analyzed similar calcite veins from the ophicalcites in the Arosa unit. They determined a formation temperature lower than 100-150ºC, interpreting that those veins developed under hydrothermalism caused by seawater-serpentinite interaction.

3.3.2. **Fault rocks related to extensional detachment in the continental crust**

3.3.2.1. *Macro-scale characteristics*

The extensional Err detachment system and its fault rocks were previously studied by *Manatschal* [1999] who described two characteristic rocks, the green cataclasites and the black gouges. Similar fault rocks and structures are also observed in the others extensional detachment systems (i.e., Grosina, Bernina and Chaberton detachments) (Figure 3A). The cataclasites are the predominant rock-type and they form most of the damage zones in the footwall of the detachment faults. They are best depicted by their green color, phyllosilicates matrix (e.g., chlorite and sericite), randomly distributed angular clasts, jigsaw structures, and they can also locally display a well-defined cataclastic foliation. The gouges (Figure 3B) are the second most common rock-type and they are best depicted by their black color, millimetric to centimetric rounded clasts and a matrix composed of chlorite and illite. They are found in the uppermost part of fault zones and mark the localization of deformation. Between those layers, two other characteristic rocks not previously described have been observed not only in the Err detachment but also in other Jurassic extensional

detachment systems. They are composed of high contents of chlorite and present a well-developed schistosity, which allow differentiating them from the cataclasites and gouges. Above the foliated cataclasite a clast-rich chlorite-schist occurs. This rock-type has a typical schistosity but with internal brecciated structures (i.e., cataclasis) that differ from the foliation of the cataclasites and from the schistosity of the chlorite-schist. This grades to a completely chlorite schist where cataclasis (hence clasts) is reduced or absent. Field and thin section observations show that all the fault rocks resulted from retrograde metamorphic reactions that become more intense toward the fault core (i.e., from bottom to top). This reaction yields (i) a loss of SiO_2 expressed in different forms of quartz veins in the fault zone, and (ii) chlorite-rich layers.

Quartz veins are remarkable features in the fault zones and their width can range from meters to few millimeters. They often appear parallel to the fault rock foliation (Figure 3F), with tabular shape (Figure 3C) but also without preferred orientation. They are often affected by simple fractures and small fault displacement (Figure 3E). Due to progressive cataclasis, quartz veins are usually intensely fractured and deformed which can be evidenced by angular clasts in cataclasites and rounded clasts in the gouges. The recognition of several generations of veins, some of which are brecciated, shows that veining is a multi-stage processes.

The architecture of fault zone varies from place to place along the studied areas and the overall characteristic of the studied detachment faults is presented in Figure 3A. The differences in the fault zone architecture may result from the initial composition of the protoliths, the deformation history and probably the subsequent flux of fluid through the fault zone. This leads to the presence/absence of one or more fault rock types and also changes in thickness. Nevertheless, in all studied detachment faults, cataclasites are always present. In the Err detachment, the fault zone can vary in thickness from more than 100 meters (Piz Laviner area) to about 20 meters (Alp Muntatsch), but they also change along strike. Cataclasites and foliated cataclasites are widespread as well as gouges, but chlorite-schists can be absent. Along the Bernina detachment, the fault zone is up to 50 m thick and is mainly composed of cataclasites. Gouges are rare and chlorite-schists are not observed. The Grosina detachment consists at least of two detachment faults. In our study, we investigated the lower one described by *Mohn et al*. [2011, 2012]. This detachment fault zone has up to 15 meters of cataclasites. While gouges are not observed at its top, ultracataclasites and chlorite-schist are widespread. The brittle deformation affects a mylonitic zone of unknown age [*Mohn et al*., 2012]. In the Chaberton detachment (see Figure 1 for location) in the pre-Piemont units of the Western Alps, near Briançon, cataclasites and gouges are common.

3.3.2.2. *Microstructures and mineralogical characteristics*

Optical microscopic and powder X-ray diffraction (XRD) analyses were used to better constrain the deformation processes, composition, mineralogical reaction, fluid-rock interaction, fluid migration and to estimate the temperature/depth of formation of the fault rocks.

The mineralogy of fault rocks is manly linked to the protolith type. Nevertheless new mineralogical phases are commonly found (e.g. chlorite and albite) and they provide important evidences for fluid-rock interactions. In the case of the ED, the Albula granite [*Manatschal*, 1999] has an original composition of 40%–60% plagioclase, 10%–30% K-feldspar, 25%–45% quartz, 5%–10% slightly chloritized biotite, and rare amphibole. The Albula granite shows a weak alteration of biotite (chloritization) and K-Feldspar (sericite). It also presents fractures, some of which filled by micrometric calcite veins. Apart from the fractures, no brittle structure (i.e., cataclastic flow) is observed in the Albula granite.

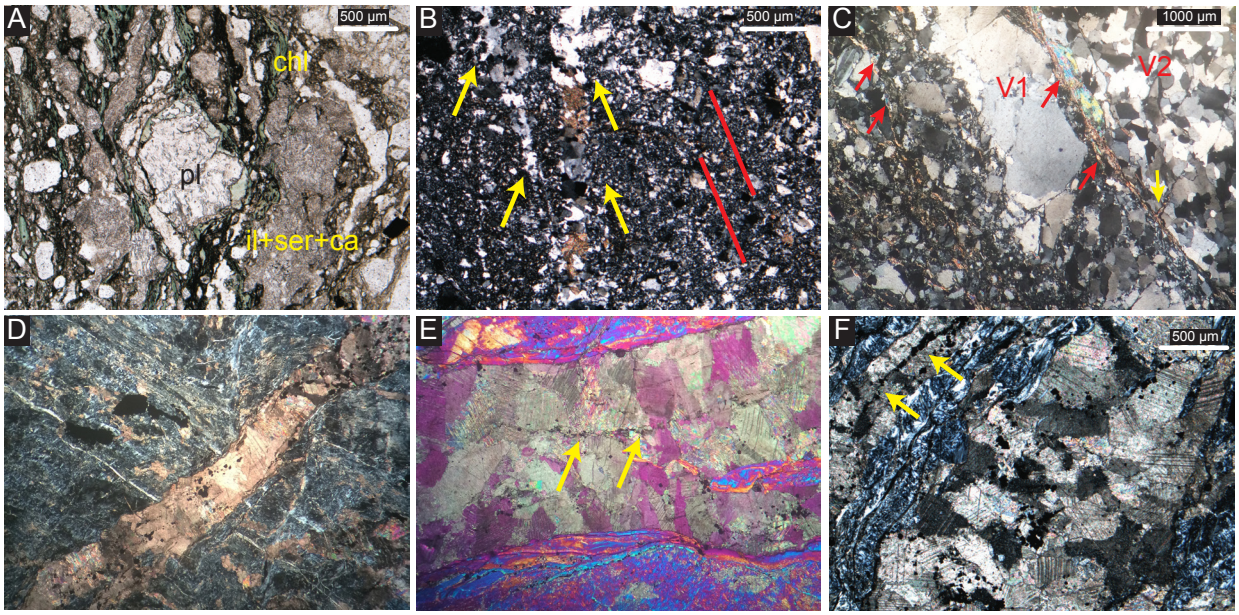

Figure 4. Physical evidences for fluids imprint in fault rocks from Err Detachment. (A): Saussuritization affects mainly the plagioclase (pl) and produces a chlorite (chl) and illite-sericite-calcite (il+ser+ca) rich-matrix that developed along the cataclastic foliation. The syn-tectonic clay minerals (phyllosilicates) register the mantle-related fluid product of serpentinization (e.g., Ni-Cr-V). (B): Evidence for fluid flow in the fault. Quartz and calcite veins (yellow arrows) with the same orientation of the cataclastic foliation (red lines). (C): V1 and V2 are different types of blocky quartz veins. The red arrows points out the phyllosilicates developed in the matrix of the cataclastic foliation cutting the quartz veins, sometimes with different orientation (yellow arrow). From (D) to (F): Calcite veins cutting the serpentinite foliation. Remarkable presence of Fe-oxides in the veins, showing that Fe-rich fluids percolated through fractures. (E) and (F) calcite veins showing the sealing line (yellow arrows) with Fe-oxides.

The cataclasites still preserve similar mineralogy to that of the granites. Nevertheless, saussuritization processes yield alteration of the K-feldspar to albite and to sericite, which can be clearly see in the ED [*Manatschal*, 1999]. Plagioclases are also affected and calcite veins and epidotes are formed during this process.

In thin section, it can be observed that an increase in deformation is related to a grain size reduction and more intense fluid-rock reactions. This later is evidenced by quartz/calcite veins parallel to the cataclastic foliation (Figure 4B) and by clay mineral product of water-assisted saussuritization processes. Saussuritization leads to the formation of illite, chlorite, calcite, albite and quartz-rich matrix especially in foliated cataclasites and gouges (Figure 4A), and a chlorite-muscovite-rich matrix in the clast-rich chlorite-schist. Usually Fe-rich chlorites (chamosite) are found in the rims of plagioclases (Figure 4A). Iron oxides, from the precipitation of Fe-enriched fluid, are often found in the cataclasites following the foliation. The quartz veins in the fault rocks have blocky texture and less frequent directional growth thought to be formed by syntaxial process [*Bons et al*., 2012]. But due to different deformation pulses, the wall rock of the veins is destroyed what makes it difficult to classify the veining processes and therefore to understand the opening evolution of fractures. Where the cataclastic foliation is well developed, syn-tectonic phyllosilicates are formed and become the matrix of the cataclastic fabric. In many cases the well-developed cataclastic foliation cuts different types of veins (Figure 4C).

Deformation processes take place at different degrees. They can start with cataclastic flow that develops in "corridors" preserving the original fabric of the protolith at its borders (e.g., Albula granite). Deformation grades to a situation where the whole rock is brecciated (e.g., cataclasites) and ending to a highly deformed ultracataclasite or gouge. The cataclastic flow itself develops at temperature around 250°C [*Stipp et al*., 2002]. In the fault rocks the quartzes present patchy extinction and in some samples undulose extinction. Quartz grains are also result of locally bulging process and sub-grains can occur. The coexistence of cataclastic flow and these recovery mechanisms indicate a temperature of 280 ±30°C [*Stipp et al*., 2002]. Gouge and chlorite-schists present S-C foliation and/or sigma clasts, which were used as kinematic indicators showing a top-to-W and top-to-NW transport direction in the ED, as previously described [*Froitzheim and Eberli*, 1990; *Manatschal*, 1995]. Similar structures are found in the other detachment faults, like the Bernina, the Chaberton and the Grosina detachments. All these detachment faults formed under similar conditions of the ED, i.e. temperature lower than about 300°C and less than 10 km depth.

4. FLUIDS RELATED TO SERPENTINIZATION

Fluids related to serpentinization processes are directly collected in the present-day hydrothermal vent fields in the Mid-Atlantic Ridge (MAR), and their main chemistry is reported [*Kelley and Shank*, 2010, and references therein]. The formation of such hydrothermal systems at MAR is strongly controlled by extensional detachment faults (e.g., oceanic core complexes) that exert major influence in the interaction between seawater and ultramafic rocks leading to their serpentinization. Even if hydration reactions are well studied [*Evans et al*., 2013], little is known about the mass balance [*Boschi et al*., 2006] related to serpentinization process and its impact on the chemical budget of the seawater, and in the diagenetic/sedimentary process through time. In contrast to MAR, where hydrothermal systems can be investigated in their active state, the study of fossil remnants of the Alpine Tethys, today exposed in the Alps, enables to address some questions related to the evolution of such systems and their interaction with the sediments. As the extensional detachment systems at MAR and the ZECM in the Alpine Tethys share similar processes like serpentinization and mantle exhumation controlled by detachment faults, we assume that present-day MAR is good analogue for what may have occurred during the final rifting and early embryonic Tethyan ocean formation.

4.1. The example of oceanic ultramafic-hosted hydrothermal systems at the Mid-Atlantic Ridge (MAR)

Numerous studies showed that along the MAR the interplay between tectonic, magmatic and hydrothermal activity is much more important than previously thought [*Kelley and Shank*, 2010]. Detachment faults in oceanic domains [*Tucholke and Lin*, 1994; *MacLeod et al*., 2009] are responsible for mantle exhumation [*Cannat*, 1993; *Picazo*, 2012], which accounts for 50-60% of the seafloor observed in some segments at MAR [*Whitney et al*., 2012 and references therein]. These faults can reach 10 km depth [*deMartin et al*., 2007] and are the most characteristic structures in slow-spreading systems [*Whitney et al*., 2012]. Extensional detachment faults control serpentinization and eventually the formation of hydrothermal fields [*Kelley et al*., 2001], in which the expelled fluids have characteristic chemical and isotopic compositions [*Foustoukos et al*., 2008]. Other hydrothermal fields described at MAR expel fluids with similar compositions to those found at magma-dominated, fast-spreading systems [*Fouquet et al*., 2010].

The fluids related to serpentinization are produced by fluid-rock interaction between ultramafic rocks and seawater. But, they can be influenced by the interaction with gabbroic/basaltic rocks that are affected (i.e., truncated) by extensional detachment faults. Whenever fluids

interact with both mafic and ultramafic rocks, quantify and distinguish the influence of each one is not evident. However, qualitative studies at MAR showed that these "mixed" fluids are mainly related to alteration of ultramafic rocks with probably minor influence of gabbroic rocks [*Douville et al*., 2002; *Schmidt et al*., 2007; *Augustin et al*., 2008; *Barnes et al*., 2009; *Seyfried et al*., 2011]. In this case, a third type of hydrothermal system is formed [*McCaig et al*., 2007], which presents a fluid composition that is a mixture of the two end-members, one dominated by serpentinization and another by magmatic process [*Schmidt et al*., 2007].

Therefore, hydrothermal systems at MAR may show differences that are related to the geological context, fluid composition, type of mineralization, biodiversity, temperature of fluids and other factors. Several authors [e.g., *McCaig et al*., 2007; *Fouquet et al*., 2010; *Kelley and Shank*, 2010] proposed a classification for these systems considering these interdependent factors.

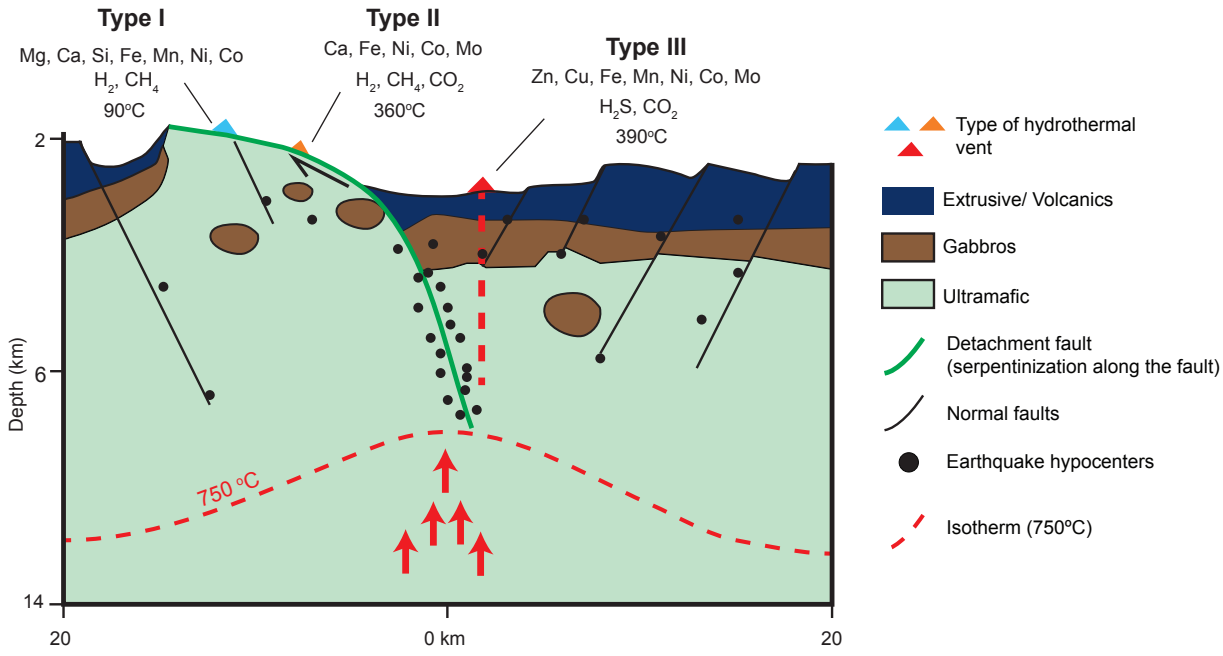

Figure 5. Types of hydrothermal vents and their main fluid composition, modified from *deMartin et al.* [2007]; *Schmidt et al.* [2007]; *Fouquet et al.* [2010]; *Kelley and Shank* [2010]. Type I: fluids are characterized by the presence of H_2 and CH_4 gases, higher content in Si, Ca and Mg [*Kelley et al*., 2001; *Edmonds*, 2010]. Ni and Co are used to distinguish fluids that are more influenced by ultramafic rocks compared to mafic rocks [Fouquet et al., 2010]. Fe-Mn enriched fluids and mineralization are reported for this type of hydrothermal vents. Temperatures are usually lower (< 90°C) than in other types and are attributed to the serpentinization exothermic reaction. Type II: fluids are rich in CO_2, H_2 and CH_4 gases and Ca, Fe and Mn metals [*Kelley et al*., 2001; *Edmonds*, 2010]. Mineral deposits are reported as containing Ni, Co, Fe, Mn, Cu and Zn [*Fouquet et al*., 2010]. Temperatures are ~360°C. Type III: fluids show high amounts of H_2S and CO_2 and are enriched in many metal elements Cu, Zn, Mo, Fe and Mn [*Edmonds*, 2010]. They are characterized by mineralization of Fe, Zn and Cu [*Fouquet et al*., 2010]. The measured temperatures are ~390°C.

However, in the studied context, two geological processes seem to exert major influence on fluid composition: (i) magmatism and (ii) serpentinization. We use them to highlight the differences between these hydrothermal systems and their respective fluid composition as presented in Figure 5.

The Lost City and Saldanha sites [*Kelley et al*., 2001; *Fouquet et al*., 2010] are examples linked to serpentinization processes (Type I). The Snake Pit and TAG sites are examples of a system, with hydrothermal fluids composition influenced by magmatic rocks (Type III). Another type, exemplified by Logatchev site (Type II) represents a system where the composition of fluids is controlled by serpentinization but is also influenced by fluid-rock interaction with magmatic rock (e.g., gabbros).

Although the original fluid composition cannot be determined anymore at fossil examples exposed in the Alps, the fact that they share many similarities with present-day slow-spreading systems allow us to suggest that the hydrothermal fluid systems and their composition may be similar. Because in the Platta nappe (ZECM) serpentinization is far more important than magmatism, in particular during early exhumation stages, a fluid with similar composition to that of the oceanic sites Type I and Type II should be expected.

4.2. **Element losses during serpentinization**

Different degrees of serpentinization are recognized in the exhumed peridotites in the Alps. Many studies have described the replacement of olivine by serpentine and modeled the chemical and mineralogical reactions. However, little attention has been paid to the continuous loss of elements during different degrees (stages) of serpentinization.

Using own data (Table 1) and a set of data from *Müntener et al*. [2010], we were able to track the gains and losses of major and trace elements during different stages of serpentinization using the Gresens-type method [*Gresens*, 1967] proposed by *Potdevin and Marquer* [1987]. Thin section analysis and the loss on ignition (L.O.I) allowed the characterization of the serpentinization degree of the peridotites from the Upper Penninic nappes (Malenco, Platta and Arosa units), which are in the range of 5 to 90% of serpentinization (Figure 6A). The samples were grouped in 3 categories: (1) samples equal or with less than 10% of serpentinization; (2) samples with more than 10% and equal or less than 60% of serpentinization; (3) samples with more than 60% of serpentinization. The results presented in Figure 6 show the gains and losses from group 1 to 2 (Figure 6B), from group 2 to 3 (Figure 6C), and from group 1 to 3 (Figure 6D).

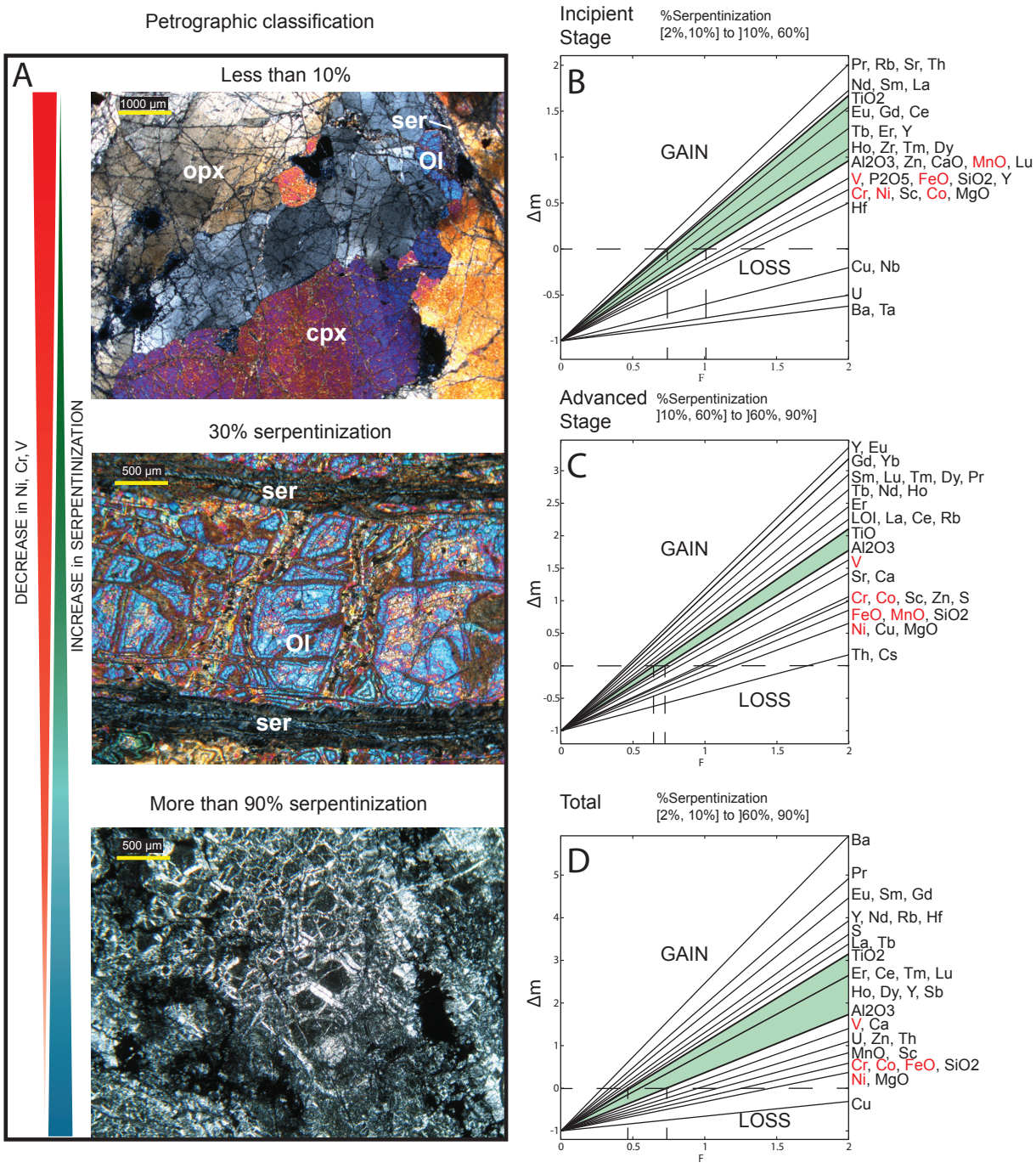

Figure 6. Mineralogical and chemical changes related to serpentinization. (A): The degree of serpentinization (percentage) is based on petrological study and was mainly established by the (olivine+pyroxene)/serpentine ratio. Note in the figure that increase of serpentinization degree is accompanied by the decrease of (olivine+pyroxene)/serpentine ratio. According with this ratio, the samples was grouped in 3 categories. Group 1: samples with less than 10% serpentinized (≤10%). Group 2: samples between more than 10% and equal or less than 60% serpentinized (]10 60]). Group 3: samples higher than 60% serpentinized (>60%). Figures (B) and (C): With the increase of serpentinization, the concentration of Ni, Cr and V decreases. (B): Mass balance at incipient stage defined by weak (group 1) to moderate (group 2) serpentinization degree. (C): Advanced stage defined by moderate (group 2) to strong (group 3) serpentinization. Notice in (D) the total losses of elements from weak (group 1) to strong (group 3) serpentinization. The graphical plot is proposed by *Potdevin and Marquer* [1987]. For calculation, densities are from *Miller and Christensen* [1997] and were assumed to be 3.1 g/cc, 2.8 g/cc and 2.6 g/cc for group 1, group 2 and group 3, respectively.

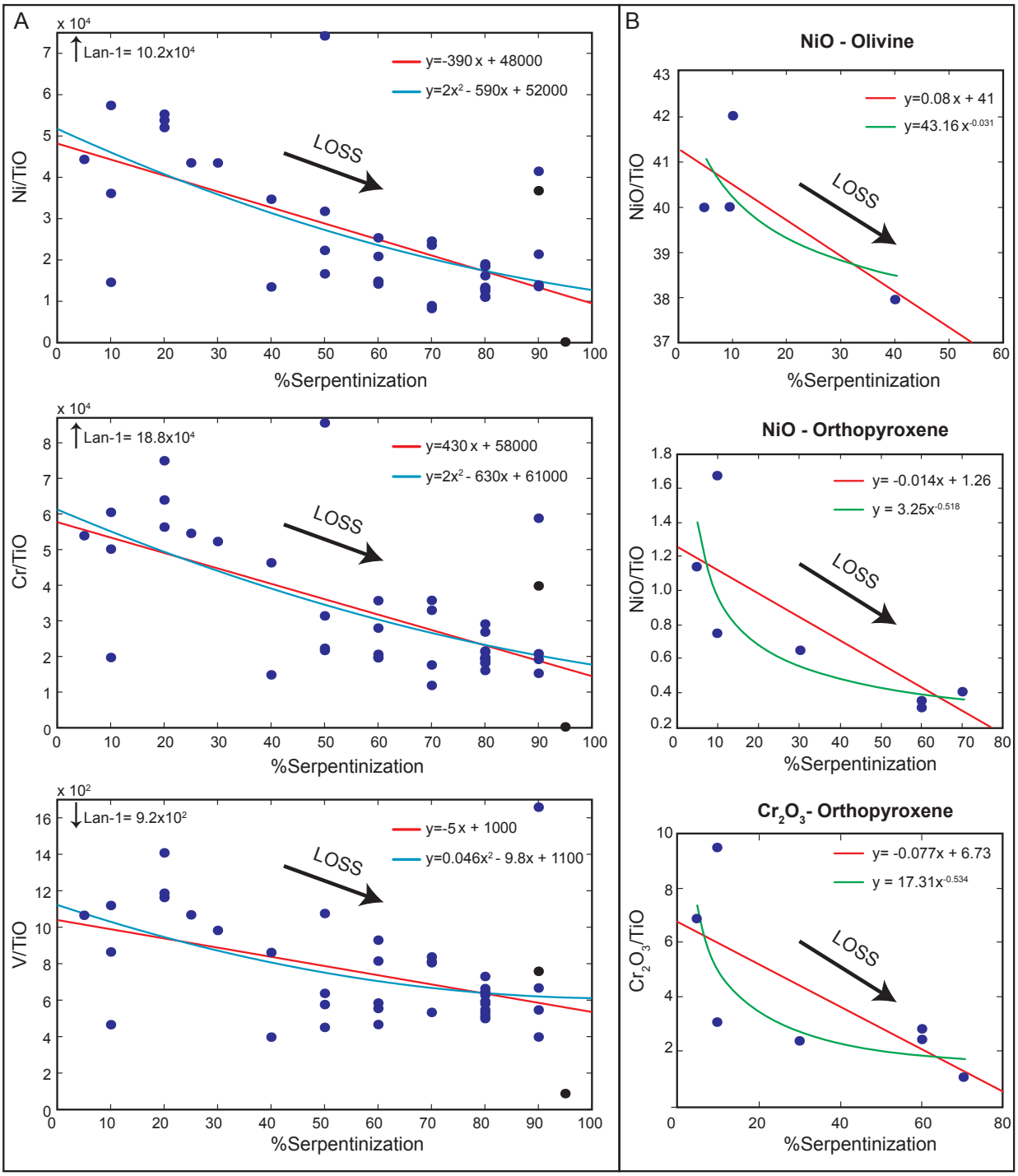

Figure 7. Losses of Ni-Cr-V related to serpentinization. (A): losses of Ni-Cr-V from bulk rock analyses. Data are from Table 1 (this work), Table 10 and 11 from *Müntener et al.* [2010]. (B): losses of NiO and Cr_2O_3 in olivine and orthopyroxene as function of serpentinization. The data from the Table 3 and 4 are from *Müntener et al.* [2010], which were measured using electron microprobe.

The behavior of each element during serpentinization was studied (Figure 6). Among them, Ni, Cr and V are some of the main trace elements that mark element losses at incipient (Figure 6B) and advanced (Figure 6C) stage of serpentinization. As shown in Figure 7A, samples with low degree of serpentinization have elevated values while the samples with high degree of serpentinization present low values of Ni-Cr-V, indicating the depletion of these elements during serpentinization. These element losses are also observed at mineralogical scale. The chemical analysis of olivine and pyroxene shows that these elements (e.g., Ni and Cr) go out of the crystal lattice during the serpentinization process (Figure 7B).

Apart from Ni-Cr-V, major elements like Fe, Mn, Mg, Si, and Ca also show important losses, especially at advanced stages (Figure 6C) compared to more initial stages of serpentinization (Figure 6B). These observations are supported by the presence of Fe-oxides in late calcite veins (Figures 4D-F) in ophicalcites and by the occurrences of Fe-oxides spots of about few thousands of square meters and few meters thick in the serpentinites from the Platta nappe. A similar situation is described in present-day ZECM in magma-poor rifted margins [e.g., *Gibson et al*., 1996] and MAR [*Dias and Barriga*, 2006]. In oceanic core complexes at MAR, *Jöns et al*. [2013] described late-stage quartz veins (Si-rich fluids) that cut the serpentinite foliation. In the Platta nappe, quartz veins are rare and we assume that most of the Si-rich fluids escaped through faults toward the sedimentary basin and seawater.

Another interesting result derived from Figure 6 is that for different degrees of serpentinization there are groups of elements that show much higher losses compared to others. However, a key observation is that serpentinization processes lead to an important overall loss of elements, which is best characterized by Ni, V, Cr, Co, Sc, Fe, Mn Mg, Ca and Si.

The mobility and solubility/precipitation of these elements can be complex, and usually depend on temperature, salinity, pH and concentration. For example, Cr is assumed to be immobile during serpentinization. However, *Klein-BenDavid et al*. [2011] highlighted that saline hydrous fluids are an important and an efficient agent in Cr mobility in the mantle. In addition, the observed losses of Cr in the orthopyroxene (Figure 7B) can be one of the explanations for the depletion of Cr in the serpentinites (Figure 7A). The detailed analysis of mobility and solubility/precipitation is beyond the scope of this work. But, the fact that these elements are discharged through ultramafic-hosted hydrothermal vents in present-day MAR sites shows that conditions like temperature, pH and salinity can be favorable for the element mobility during serpentinization.

Because serpentinization is intimately linked with fluid circulation along detachment faults, we investigate the physical and chemical evidence for fluid-flow (migration) through detachment faults by tracing the element losses during serpentinization.

5. FLUID SIGNATURE IN EXTENSIONAL DETACHMENT FAULT ROCKS

The geochemical composition of the extensional detachment fault rocks from the distal domain (ZECM + CDZ) and the necking zone were analyzed in order to understand the relationship between fault activity, deformation, fluid-rock interaction and fluid migration. The studied sites comprise the detachment faults of the distal margin, (i) the Err detachment (Err-Platta nappes) [*Froitzheim and Manatschal*, 1996], (ii) the Bernina detachment (Bernina nappe) [*Mohn et al*., 2012], (iii) the Chaberton detachment (Pre-Piemont); and the Grosina detachment from necking zone (Grosina nappe) [*Mohn et al*., 2012] (Figures 1 and 2).

5.1. The chemical composition of the detachment fault rocks

The result of major and trace elemental analysis of bulk rock and clay fraction (<2 μm) from detachment fault rocks are shown in the Table 2 and 3 (for general information about the samples, see the annexes of this thesis). The Gresen's type plot [*Gresens*, 1967] proposed by *Potdevin and Marquer* [1987] was used to quantify the gain and losses using Al, Ti and Zr as immobile elements (Figure A1, see the annexes of this thesis).

Using gains and losses of elements that took place during the deformation (fault activity), we identified and "mapped" distinctive elements that entered (i.e., gains), remained (immobile elements) and left (i.e., losses) the system. Comparing results from bulk rock (Figure 8) and clay fraction (Figure 9), we show that trace elements are mainly hosted in syn-tectonic phyllosilicates (Figures 4A and C). Because the calculations are based on the immobility of Al and Ti that are mainly present in phyllosilicate minerals, the results of gain and losses from clay fraction and bulk rock are similar, what lead us to prefer bulk rock analyses due to the easier and faster analytical procedures (i.e., clay fraction separation is time consuming). In addition, the bulk rock data give the opportunity to compare our results with those available in the literature [*Manatschal et al*., 2000]. Although many analyses were done on different rock types, further interpretations are mainly based on the results of gain and losses during the transformation of the protolith into cataclasite and gouge.

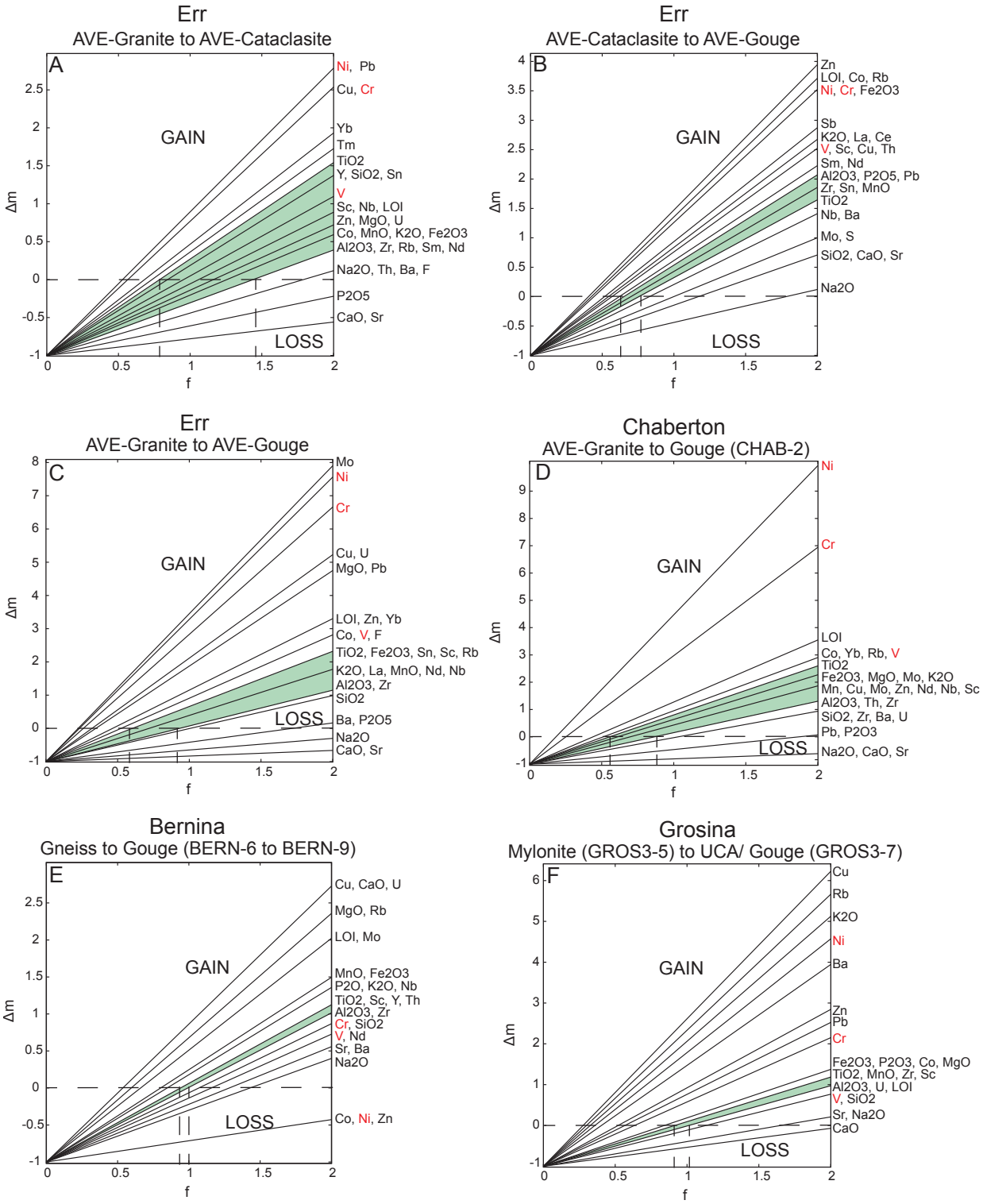

Figure 8. Gain and losses estimated by Gresens-type plot [*Potdevin and Marquer*, 1987]. The results from (A) to (C) are based on average values of fault rocks from Err detachment (ED). The results from (D) to (F) are based on single values of Chaberton, Bernina and Grosina detachments. The results from Err detachment (C) can be used to compare the differences between other detachment faults (D-F). Observe that gains in Ni-Cr-V from ED are higher than the other detachments. Bernina detachment shows losses of Ni-Cr-V and Grosina shows losses in V. For the Err detachment, we use average values from all the Albula granite, cataclasites and gouges (Table 2) together with averages values from *Manatschal et al.* [2000]. All lines (elements) above the green area (limited by Al_2O_3 and TiO_2) are related to element input from outside of the system (gain), which means they are not from the protolith (Albula granite). All lines below that area represent losses, meaning they migrated and precipitated elsewhere. Data resulted from ICP-AES/MS analyses (this work) and XRF analyses from *Manatschal et al.* [2000].

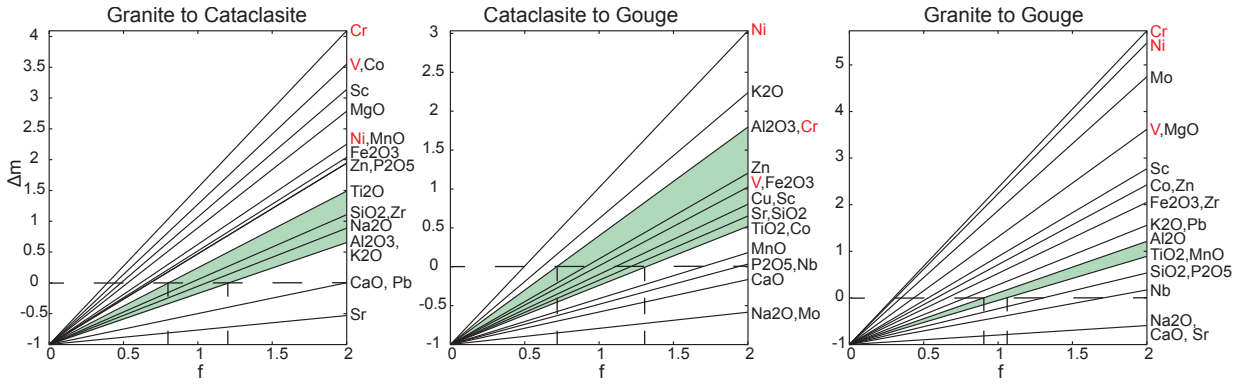

Figure 9. Gain and losses in clay fractions (< 2μm) from Err detachment fault rocks. The figures show that Ni-Cr-V are present in the neoformed clay minerals. The samples used are L-9a for granite, L-7 for cataclasite, and the average values presented in Table 3 for gouge.

5.1.1. **Gains and losses in fault rocks from the Err detachment (ED)**

A systematic and elevated gain of elements such Ni, Cr, V, Co and Cu (Figures 8 A-C) is observed in the fault rocks from the ED. It implies that from protolith to cataclasite (i.e., moderate deformation and chloritization) to the gouge (strong deformation and chloritization) the concentration of these elements increases. Detailed analyses of the ED fault rocks allowed to "map" the variation of these elements along the footwall of the detachment relative to its distance from the former breakaway supposed to be in the Mezzaun area [*Masini et al*., 2012]. Because the concentration of these elements is higher in clay-rich fault rocks (gouges), the gain of Ni-Cr-V is plotted in Figure 10 in order to outline the variation along the detachments (as a function of its distance from the breakaway parallel to transport direction).

Ni, Cr and V were chosen because they are systematically present in all ED fault rocks and, as discussed below, these elements are likely to have originated from the underlying serpentinized mantle. The results in Figure 10 indicate that the more distant the location of the samples is relative to the breakaway of the fault, the higher the concentration of Ni, Cr, and V. Average and individual values of samples are both plotted to show the regional coherence of the results. Data from ICP-MS (this work) and XRF from *Manatschal et al*. [2000] are plotted as well and confirm the consistence of the results. In order to test if other faults show the same trend, we also analyzed samples from other detachment faults from the Alpine Tethys.

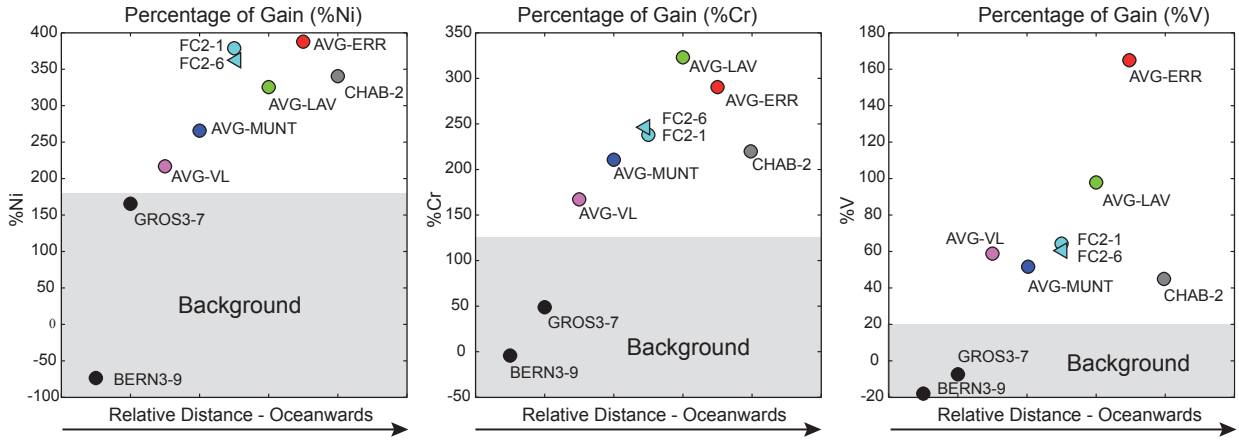

Figure 10. Calculated gain of Ni-Cr-V. It was used the gain values from protolith to gouges assuming an average factor f between Zr, Al and Ti ($f_{Zr}+f_{Al}+f_{Ti}$)/3 where these immobile elements have no mass changes (Δm=0). After, we calculate the mass variation (Δm) that was multiplied by 100 to give the results in percentage. We use average values (AVG) of gouges and single samples (see name of samples). Gouges are represented by dots and chlorite-schist by triangles. It was used the average values of Albula granite for calculate the gain in the gouge from different parts of the ED. ERR (around Piz Err) were obtained based on the samples 1 to 3 from *Manatschal et al.* [2000], LAV (around Piz Laviner) is from our samples in Table 1 and samples 3 to 5 and 8 to 12 from *Manatschal et al.* [2000], VL (area in Val Lunga) is based on our samples from Table 1 and samples 13 to 19 from *Manatschal et al.* [2000], FC (area in Fuorcla Cotschana) and MUNT (area in Alp Muntatsch) are from Table 1. Samples from other detachments (Table 1): GROS (Grosina), BERN (Bernina), CHAB (Chaberton). The gneiss (BERN3-6) and the mylonite (GROS3-5) were used as a protolith for Bernina and Grosina detachment, respectively. For Chaberton it was used the Albula granite as a protolith reference. Notice that samples from Bernina present losses of Ni-Cr-V and those from Grosina present little gain of Ni-Cr and loss of V. The values calculated for the Grosina detachment is used to establish a background value, due to the characteristics of the geological setting. See text for discussion.

5.1.2. **Gains and losses from detachment fault rocks outside the Err nappe**

The Chaberton detachment exposed on the conjugated European margin (at the present located in the Pre-Piemont unit in SE France; Figure 1) exhibit contents of Ni-Cr-V in gouges (Figure 8D) comparable to the ones from the ED what is in agreement with the geological setting from these two places. Since only fault rocks are preserved in the Chaberton area, we assume that they originated from similar protolith as the ED, which is justified by the similarities of their composition and mineralogy. Therefore, in order to plot the Figure 8D we used the average values from the Albula granite as protolith and the gouge (CHAB-2) as the altered rock.

In the Bernina detachment, located further continentwards in the former distal margin, the transformation from the gneiss protolith (BERN3-6) to a clay-rich ultracataclasite (BERN3-9) from the detachment surface shows no gain in Ni-Cr-V. On the contrary, these elements are lost in the fault zone, which is an opposite trend to that observed along the ED (Figure 8E).

In the Grosina detachment (Figure 8F), related to the necking zone, we used the mylonite

(GROS3-5) as the protolith and the ultracataclasite (GROS-7) from the fault zone as the altered rock. However, the record of the fluid composition in the Grosina detachment can be complex by three main reasons: (i) the mineralogical composition, specially the clay content, of the mylonitic protolith changes from place to place, meaning different primary quantity of (Ni-Cr-V); (ii) the mylonite was already a previous fault zone and may have an earlier alteration imprint; and (iii) the interplay between the different detachment systems in the necking zone is not fully understood and a fluid flow interaction between them is possible. Nevertheless, Ni and Cr present minor gain, and V show losses what is opposite to that observed along the ED. These observations allowed delineate a "background" zone in Figure 10 that differs from the one presenting large gains.

6. THE FLUID SIGNATURE (FLUID CONTAMINATION) IN THE SEDIMENTS

Representative sediments through all the sequences in the ZoS and the basal sequence in the Murtiröl were also analyzed (Table 4 and Figure 2 for location). They include the Bardella, Saluver A, B and C, Radiolarite, Calpionella and Palombini formations. The main objective is to observe whether those fluids that circulated through the extensional detachment system also migrated toward the overlain sedimentary basin and affected the sediments.

The Figure 11 exemplifies the increase in Ni-Cr-V concentration from bottom to top of the sedimentary sequence. Although internal variations (spike) can be observed in the Bardella, Saluver A and Saluver B sequences, the average trace metals display a general increase upsection. The Saluver C has a continuous increase in these elements, but the shale-dominated sequence of the Saluver C starts to record a decrease in these elements from the last centimeters (just bellow the Radiolarite). From this point onwards, the regional post-rift

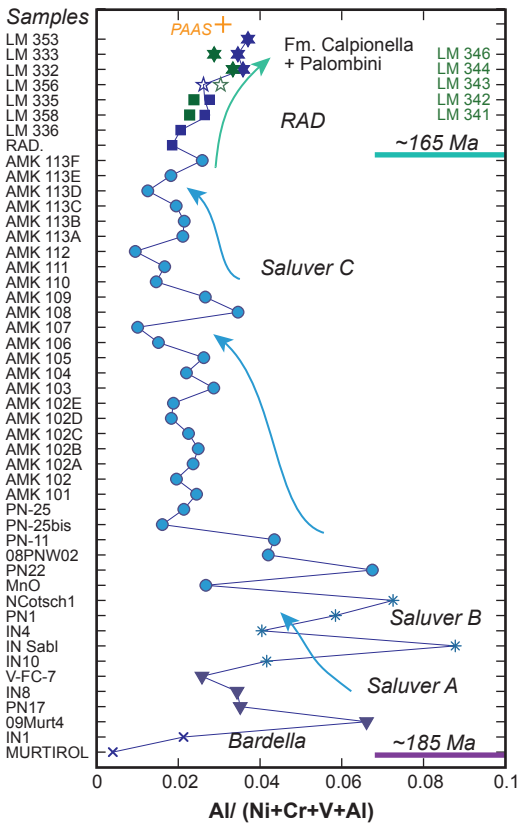

Figure 11. Ni-Cr-V trends from the sedimentary rocks. Samples are located in the ZoS and Murtiröl in the Err nappe (blue symbols). Samples from Platta nappe are from *Bracciali et al.* [2013] (green symbols) and the PAAS (black cross) data from *Condie* [1993] are used as references. See the caption in Figure 12.

sequence (Radiolarite, Calpionella and Palombini formations) records a continuous decrease in these elements.

The Figure 12 shows a continuous increase in Fe and Mn concentrations from the fault rocks to the Saluver C (path1) and a decrease in the regional post-rift Radiolarite, Calpionella and Palombini formations (path 2). These results are compared to results from other units from the Liguria-Piemont ocean as well as the reference values (NASC and PAAS).

As observed in SEM-BSE images, some of these Fe and Mn are found as brunite and oxides over recrystallized quartz (Figure 13A-B), showing the cogenetic relationship between Fe, Mn and Si. In fact, their concentration are relatively high in the Saluver C formation, which presents variable Fe/Mn ratios and some enrichments in Mn-contents. This formation presents similar values from the Mn- and Fe-rich hydrothermally-sourced metalliferous deposits [in *Karpoff et al.*, 1988; *McKenzie et al.*, 1990], as shown in Figure 13C.

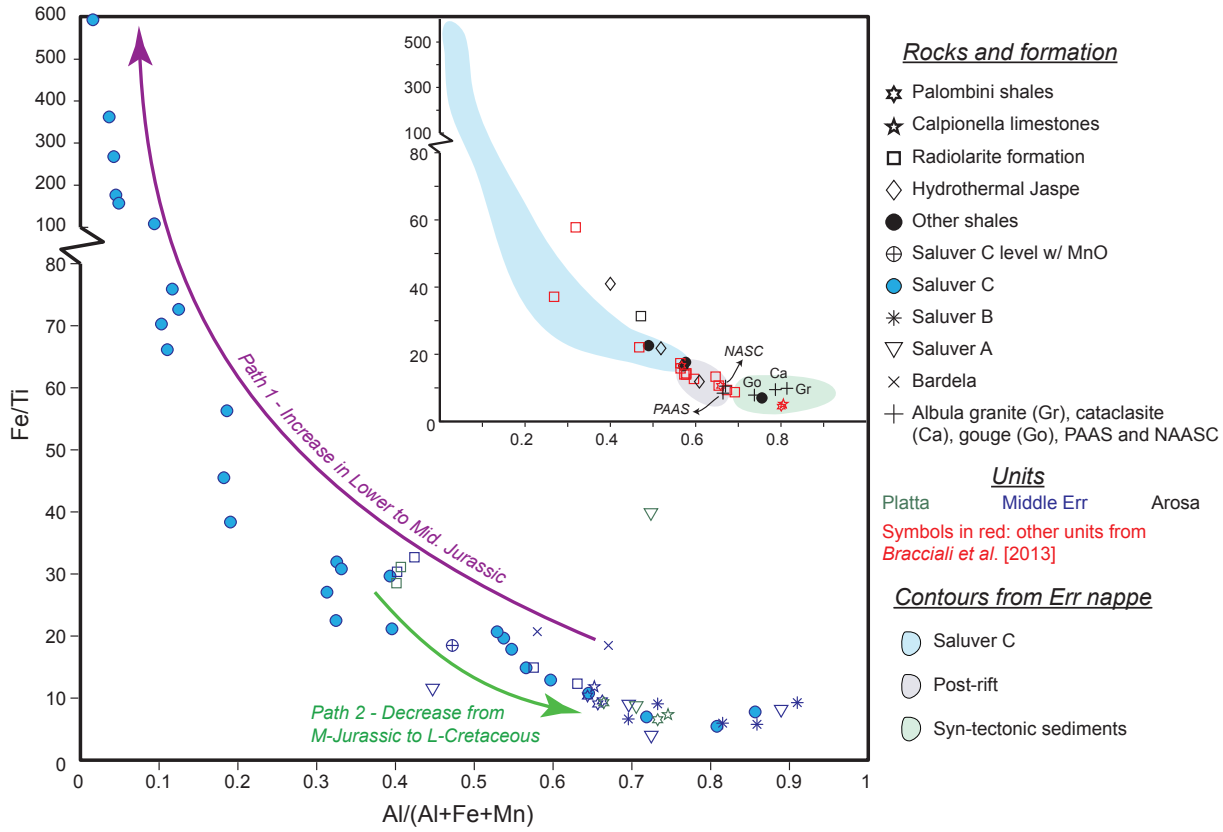

Figure 12. Increase in Fe and Mn contents registered in the post-tectonic Saluver C sediments. The decrease in Fe and Mn is well marked from the Radiolarite to the Calpionella and Palombini formation (both in Err and Platta nappes). The Radiolarite formation data is from this study and *Bracciali et al.* [2013]. Data from Calpionella and Palombini formations are from *Bracciali et al.* [2013]. Reference data are: PAAS (Post-Archean Australian Shale) and NASC (North American Shale Composite) from *Condie* [1993], the Internal Ligurian Units (ILU) and Toscan nappe (TN) in Italy, and Balagne nappe in Corsiga are from *Bracciali et al.* [2013] (see Figure 1 for location).

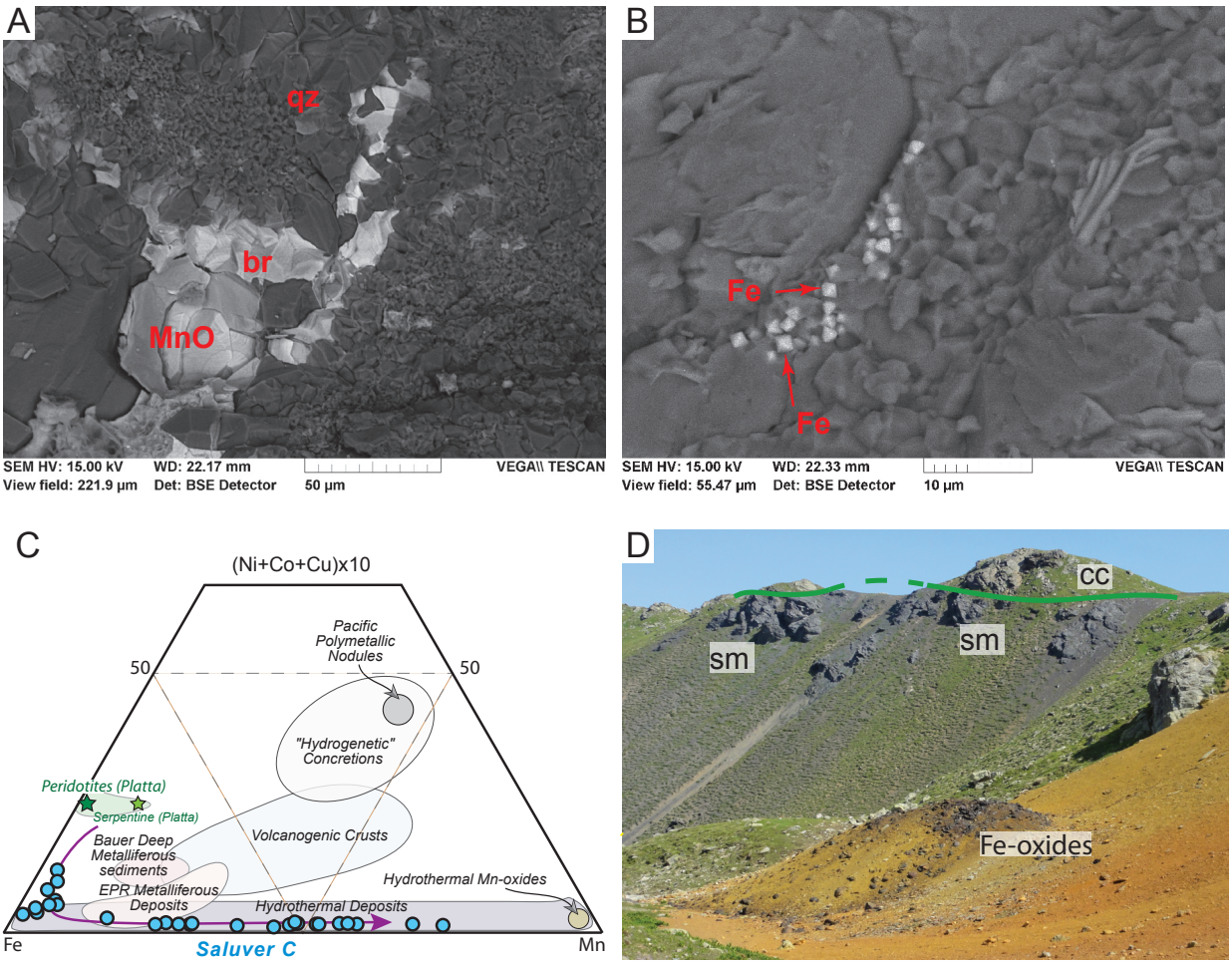

Figure 13. Evidence for Fe and Mn. (A) and (B): SEM-BSE images from Saluver C at ZoS. (A): Shows braunite (br), Mn-oxide (MnO) and quartz (qz), highlighting the cogenetic relationship between Mn and Si. (B): iron oxides (Fe) marked by red arrows. (C): Comparison of geochemical data from Saluver C with Fe and Mn oceanic deposits. Fields in Bonatti diagram from *Karpoff et al.* [1988] and *McKenzie et al.* [1990]. (D): Continental allochthonous block in the ZECM (Parsettens at Platta). The surrounding mantle contains Fe-oxides and high Barium content (sample P7 in Table 1). Continental crust (cc); serpentinized mantle (sm).

7. DISCUSSION

7.1. Tracing fluids along the evolving distal margins

Gains of trace elements (Ni-Cr-V) registered in the fault rocks within the thinned continental Err domain indicate that they should have their source outside the continental "system". In this study, we were able to show that these elements (e.g., Ni-Cr-V and Fe-Mn) are lost during serpentinization leading to the depletion of mantle in many elements (e.g., Si, Fe, Mn, Ni, Cr and V). Since these elements are also found in the sedimentary rocks in the supradetachment basin, we can also get some insights on the age of serpentinization, the formation of a hydrothermal system and the migration of mantle-related fluids.

Indeed, our results show that serpentinization leads to the enrichment of fluids in the

aforementioned elements and that Ni-Cr-V as well as Fe-Mn can be used as tracer of a large-scale fluid migration across the thinned crust, where fluids were channelized along detachment systems. These fluids can also be traced in the overlying sedimentary basins where they affected the syn-tectonic sediments by direct migration and the post-tectonic sediments by the "pollution" of the seawater. In the following sections we discuss the different parts of this large-scale hydrothermal system that accompanied the mantle exhumation.

7.1.1. **Evidence for mass transfer and fluids circulation along extensional detachment faults**

Physical (Figures 3 and 4) and chemical (Figures 8, 9 and 10) evidence for "fossil" fluid percolation in the extensional detachment system are recognized. Physical evidences are best depicted by (i) quartz and calcite veins; (ii) iron oxides precipitated in the cataclastic foliation; (iii) syn-tectonic phyllosilicate minerals transformed or neoformed in the damage zone, which become more abundant toward the core zone of the extensional detachment faults.

Chemical evidences for fluid migration are depicted by water-assisted saussuritization process in the continental basement of extended crust. These processes are responsible for removing and losses of Ca and Si (Figure 8B-F) that percolate the fault zone and precipitate in veins (Figures 3A, 3C-F and 4B-C) along extensional detachment faults. Iron oxides found in the foliated cataclasites seem to be the by-product of alteration of biotite and they precipitate locally along the fault zone, once they have a less mobile behavior in the cataclasites (Figure 8). Nevertheless, the occurrence of Fe-oxides and the gain of Fe in the gouges and in the cataclasites in distal segments of the ED points out to an external source of iron. In addition, fluid circulation can be demonstrated by the gain of elements registered in the syn-tectonic phyllosilicate minerals from the fault rocks. As these elements came from outside the continental system (i.e. not from the surrounding continental basement), they had to be carried by fluids through the active fault zone simultaneously to the formation of the syn-tectonic phyllosilicate minerals (Figure 14A).

7.1.2. **Ni-Cr-V: tracers for mantle-related fluids produced by serpentinization**

Nickel, chromium and vanadium can be considered as tracers of mantle-related fluids for the following reasons: (i) their concentration are much higher in mantle than continental rocks, (ii) they display highest gains in the analyzed continental fault rocks and in contrast to most of the other elements they are always observed along the ED; (iii) their concentration is unusually high in the sediments of the distal margin.

The elevated gain of Ni-Cr-V in the continental fault rocks along the ED cannot be explained by dissolution/precipitation processes in the surrounding continental basement. Therefore, such enrichment leads to the question about the origin, and how and when the elements were released and migrated toward continental units. These elements are typical from mantle rocks with higher concentrations compared to that of continental rocks. In our samples, highly serpentinized peridotites have about 2000 ppm of Ni, 2500 ppm of Cr and 100 ppm of V (total 4600 ppm), and fresh peridotites have even higher contents (Table 1). In the Albula granite, Ni is ~6 ppm, Cr is ~20 ppm and V is ~45 ppm (total 71 ppm, Table 2). Another key observation is that Ni-Cr-V depletion in the mantle (losses) is a function of increasing serpentinization. This result is further in accordance with the data of fluids from ultramafic-hosted hydrothermal fields at MAR where Ni and Co are important elements expelled through the vents (e.g. Rainbow field) [*Fouquet et al*., 2010].

Since the syn- to post-tectonic sedimentary sequence overlying the detachment fault is also enriched in Ni-Cr-V (Figure 11) and that the post-tectonic sequence (Saluver C and Radiolarite formations) is contemporaneous to mantle exhumation a direct link can be made between the losses of Ni-Cr-V in the mantle and its exhumation in the distal margin.

Although Ni-Cr-V elements are good proxies because of their presence and behavior in all studied systems (i.e. mantle, continent, fault rocks and sediments), other trace elements like Cu, Sc and Co present very similar behavior.

Enrichments of Fe and Mn, as distinct oxides, are also found in the post-tectonic sediments (Saluver C) and in the mantle (Figures 4D-F and 13D). They also suggest a close relationship between serpentinization, mantle exhumation, and fluid transfer as is often observed at hydrothermal sites at MAR.

7.1.3. **Formation and migration of mantle-related fluids associated with serpentinization**

Detachment faults in the distal margins cut through a previously thinned, less than 10 km thick, continental crust and root in the underlying mantle. This triggers a seawater-mantle interaction resulting in the leaching of mantle-derived elements during serpentinization, which creates a mantle-related fluid that migrates through extensional detachment fault.

The details of how seawater migrates downward into the mantle are not fully understood. But the observation that the signature of the mantle-related fluids is registered along the Err

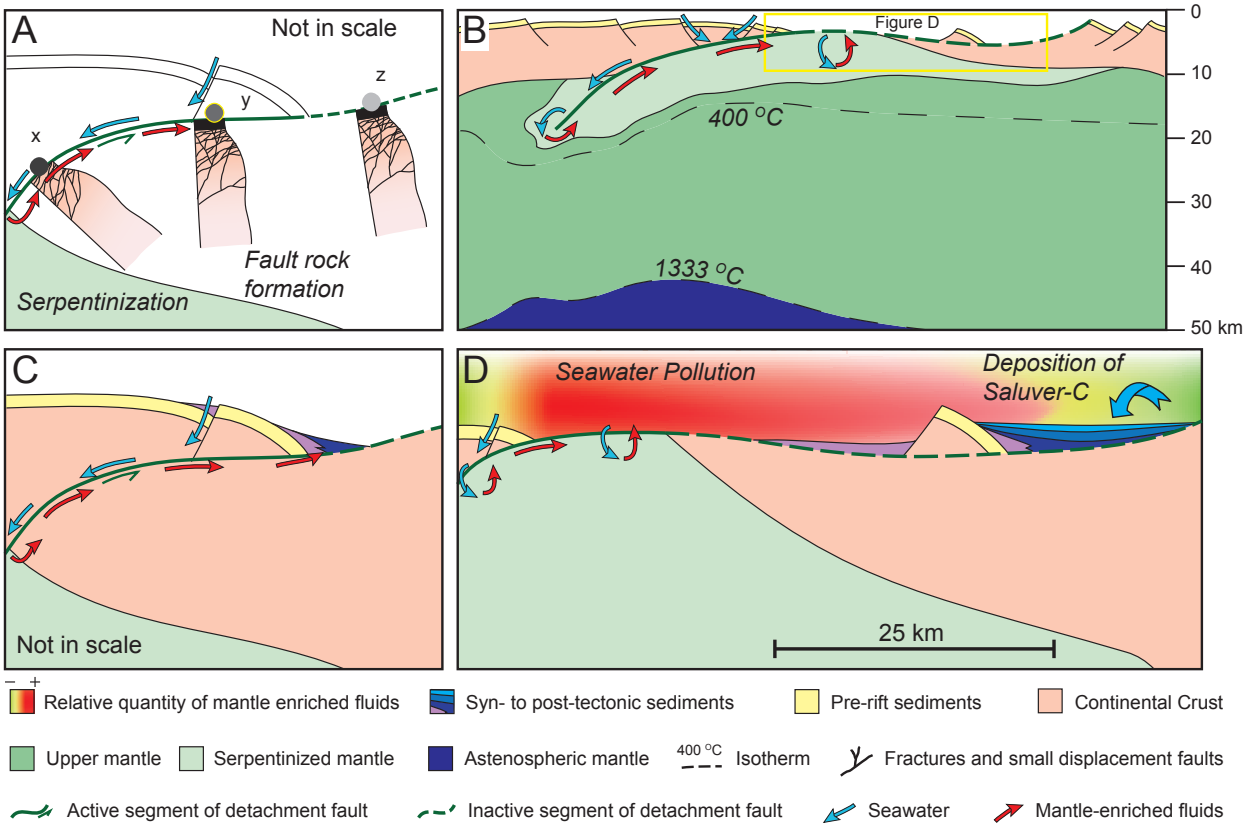

Figure 14. Conceptual processes. (A): Record of mantle-related fluids in the active segment of the detachment fault. At point x the detachment is active and probably with undeveloped gouges. At point y the detachment is active and gouge are well developed. At point z the detachment is inactive. Fluid migration is recorded at points x and y but not in z. (B): Maximum depth for serpentinization is limited around the 400°C isotherm. The elevated geothermal gradient may play an important role in the remobilization of elements by controlling the convective system. (C): Direct migration that affects the syn-tectonic sediments in the supradetachment basin. (D): Seawater pollution by serpentinization that spreads through the seawater and affects the contemporaneous sediments. The segment of detachment fault is active in the ZECM but inactive bellow the supradetachment basin.

detachment fault, shows that the seawater somehow percolate downward through the detachment system. Two possibilities for this downward migration or the combination of the two can be envisaged: (i) seawater percolates downwards through synthetic and antithetic high-angle normal faults that are formed in the hanging wall of the detachment; (ii) seawater percolates downward only through detachment faults.

We interpret that the high-angle normal faults also acted as conduits for seawater downward migration as illustrated in the Figures 14A-D and Figure 15. The progressive downward water migration and serpentinization were intimately linked to the activity of extensional detachment. The interaction between seawater and mantle rocks had to occurs at relatively shallow depths and lower temperatures according to the observations discussed in the Section 3.1.3. Nevertheless, considering the stability field of serpentine minerals [e.g., *Moody*, 1976], the temperature and depth of the fluid-rock interaction and related serpentinization (hydration and chemical exchange)

probably were not higher than about 420ºC and 20 km, respectively.

The beginning of serpentinization (low temperature hydration) occurred below the previously thinned crust (about <10 km) and is evidenced by the gain/enrichment in Ni-Cr-V along the ED (Figure 10) and the overlying syn-tectonic sediments (see following discussion). The mantle hydration below the crust is also supported by high temperature hornblendes (i.e., high temperature hydration) that preceded serpentinization [*Desmurs et al*., 2001]. Considering the formation of hornblendes is related to the rifting event with an elevated geothermal gradient, this high temperature hydration can be assumed to happen at depths around 15 km or more, which suggest how deep the seawater penetrates.

Detachment faulting in the distal margin controls the progressive mantle exhumation, the expansion of the serpentinized area, the increasing degree of serpentinization and the related losses of elements such as Ni-Cr-V (Figures 15). These losses (leaching) in the mantle may be more efficient under hydrothermal advection (Figure 14B) that is probably controlled by a high thermal gradient produced by the thinning of the lithosphere as well as by exothermic serpentinization reaction [*Schuiling*, 1964], similar to what has been described from the MAR [*Kelley et al*., 2001]. Hydrothermal chemical exchange is supported by spots of Fe-oxide crusts (Figure 13 D) that are often observed in the serpentinized mantle of the ZECM (Platta) and by high content of Ba (9%) and barite (see sample P-7 in Table 1, in standard serpentinite Ba=5 ppm).

The fluid circulation is strongly linked and conditioned by the activity along the detachment fault, which also forms the pathways for the fluid enriched in mantle-derived elements (Ni-Cr-V). The upwelling of these fluids along the detachment fault registers the progressive development of serpentinization (in area and degree) that happens when faults were able to cut through the brittle and thinned crust reaching the subcontinental mantle. It is important to emphasize that is unlike this upward migration occurred only at final stage, when the mantle is exhumed to the seafloor. In this context, two major points have to be considered:

(i) when the footwall of the detachment fault is exhumed to the seafloor, this segment starts to become tectonically inactive (Figure 15), and therefore the fluid circulation may decrease due to the healing of fractures [*Tenthorey and Fitzgerald*, 2006; *Mitchell and Faulkner*, 2012]. In this case fluids would scape to the seawater in the ZECM and it would not be registered all along the ED fault rocks as it was showed in the Figure 10;

(ii) since fault gouges have low permeability [*Morrow et al*., 1984; *Evans et al*., 1997] the

fluid migration toward the breakaway throughout the gouge layer seems highly improbable.

However, during fault activity, the permeability can be enhanced [*Tenthorey and Fitzgerald*, 2006]. This is because the fault movement enables fracture opening, especially in the damage zone of the fault characterized by cataclastic rocks. The increase of permeability by fracture opening is evidenced by quartz and calcite veins (Si- and Ca-rich fluids) parallel to the brittle foliation in the cataclasites (Figures 3F and 4B).

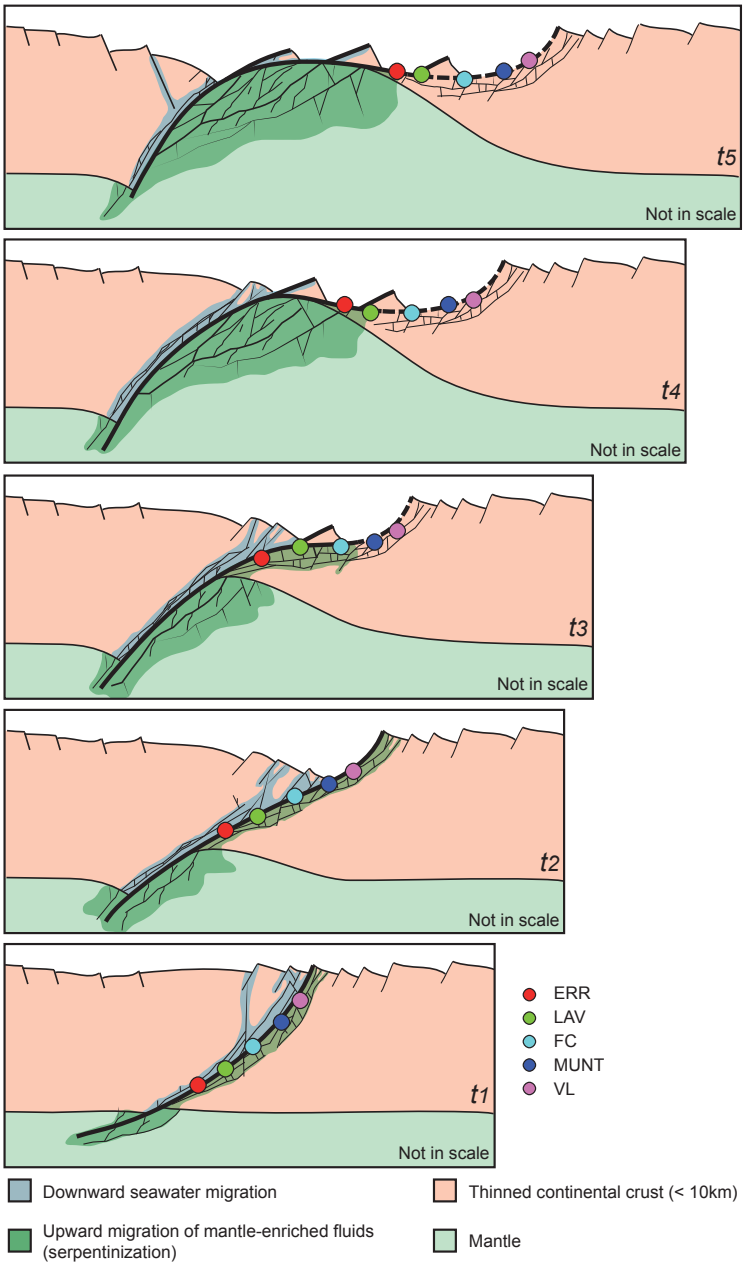

Figure 15. Progressive gain of Ni-Cr-V in different segments of the Err detachment fault. The figures show the concept of the progressive increase of serpentinized area and degree of serpentinization that are linked to the detachment fault evolution. This increase is registered in different segments of the ED (colored dots) according to the results presented in Figure 10. The light blue zone shows the seawater downward migration in the hanging wall that interacts with mantle rocks and induces serpentinization yielding mantle-related fluids that migrate upward, as illustrated by the dark green zone. In t1 stage, the deformation is distributed along a high angle normal fault and a set of fractures. From t2 to t5, the deformation is localized along the detachment fault.

7.1.4. **Fluid migration toward the sedimentary basin**

Direct fluid migration through detachment faults toward the sedimentary basin are evidenced by Ni-Cr-V enrichments (Figure 11) in the syn-tectonic sediments (Bardella, Saluver A and B Fm.). The Figure 14C illustrates the concept of directed flow of mantle-related fluids toward the sedimentary basin. The Figure 16 shows the relationship between the evolution and fluid circulation affecting the syn-tectonic sedimentary sequences in the distal margin from the Err-Platta nappes. The flow path in the sedimentary sequences may be very complex due to the porosity-permeability control of sedimentary rock. In addition, the sediments, particularly the oldest deposit lying directly onto the exhumed fault surface, may have been continuously reworked during movements along the underlying detachment fault. Therefore, they may have been affected by small increments of fluid pulses during upward fluid migration. These observations may explain the variation (spikes) of Cr-Ni-V values of the syn-tectonic Saluver A and Bardella formations (Figure 11). However, the rocks were sampled in different places (along strike) in the Zone of Samedan and Murtiröl areas where clasts of fault rocks are locally found in the basal sequences (i.e. Saluver A and Bardella). But, values of Ni, Cr and V in fault rocks are lower than in the overlying sediments and as the percentage of fault rock clasts in the basal sedimentary sequences is never high, the values measured in these sequences cannot be explained by reworking of fault rocks. Thus, a direct contribution of external, mantle-related fluids needs to be envisaged.

7.1.5. **The "pollution" of seawater by mantle-related fluids: a record of mantle exhumation in post-tectonic sediments**

Evidence for seawater "pollution" by mantle-related fluids (i.e. mixing flow) is given by the geochemical data of the post-tectonic sediments (Saluver C) and the first regional post-rift sequence (Radiolarite Fm.) in the Alpine Tethys (Figures 11, 12 and 13A-C).

Masini et al. [2011] discussed that at the time of the deposition of the post-tectonic sediments (Saluver C), the segment of the ED was already inactive beneath the basin. This implies that the fluids enriched in Ni-Cr-V and Fe-Mn no longer came from the underlying segment of the ED (Figures 15 and 16). This is supported by the fact that Ni-Cr-V enrichment is also observed in the post-rift Radiolarite formation deposited over the exhumed serpentinites and the magmatic rocks, showing that the detachment fault was no longer active in the ZoS and Mürtirol (Err nappe) at that time. Indeed, the data show that the contamination persisted even after the end of extension in the continent (Err nappe) and during the mantle exhumation in the Platta nappe. This is supported by the study of *Perseil and Latouche* [1989] that discuss the occurrence of Ni-Co-Cu as well

as botryoidal Mn-silicates developed under hydrothermal influence in the Platta nappe. Thus, in contrast to the observations made along the continental segment of extensional detachment faults and the syn-tectonic sequence, this "contamination" cannot be affected by the aforementioned direct fluid upwelling through detachments. A possible explanation is that fluid flow stooped along the already exhumed segment of the ED and moved with the deformation to distal parts, it means toward the future embryonic ocean (Figures 15 and 16).

In order to explain the almost continuous enrichment in Ni-Cr-V of the Saluver C we interpret that those elements were dissolved in the seawater, such as in plume systems created by vents and diffuse hydrothermal flows, and the coeval deposited shales from the Saluver C formation "capture" the modified-seawater signature. The "absorption" of elements in present-day oceans is well exemplified by *Torfstein* [2012] who shows the control of clay minerals in the absorption of He in the Pacific Ocean.

The Figure 11 shows a continuous enrichment in Ni-Cr-V recorded from the basal level to the top of the Saluver C followed by a decrease from the final centimeters of the Saluver C to the regional post-rift sequences. It is important to mention that the amount of Ni-Cr-V in the Saluver C from the Middle Err nappe is higher than the values of the shales from the Radiolarite formation that is in direct contact with the serpentinites and seals the exhumed mantle in the Platta nappe. This establishes that when the Radiolarite formation was deposited, the exhumed mantle was more depleted in Ni-Cr-V compared to the stage registered by the Saluver C. This is supported by the depletion of Ni-Cr-V at advanced stages of serpentinization, as previously discussed. From the Calpionella to the Palombini Fm. the system registered a progressive decrease of Ni-Cr-V, which values are comparable to those from the Post-Archean Australian Shale (PAAS). This decrease suggests either the end of the hydrothermal activity or a progressive moving of the source (hydrothermal system) oceanwards. These observations are also valid for Fe and Mn, which have similar trend behavior of Ni-Cr-V (Figure 12). Therefore, mantle exhumation toward the seafloor marks a geochemical event that is related to the release of Ni-Cr-V together with Fe and Mn that is mixed in the seawater and recorded by the Saluver C and, relatively less, by the Radiolarite formation. This is related to the aforementioned hydrothermal reactions that occurred during serpentinization and corroborated by physical evidences in the serpentinized mantle in the ZECM (Figures 4D-E and 13D) and in the sediments (Figures 13A-B). It is worthwhile to mention that the Fe- and Mn-oxides behavior in the Saluver C is comparable to the hydrothermal mineralization in oceanic domains (Figure 13C). The dispersal of hydrothermal Fe-Mn in present-day seawater is exemplified by recent data (see Figure 1 from *Saito et al*. [2013]), which show a Fe and Mn plume

that affects huge distances in the South Atlantic Ocean.

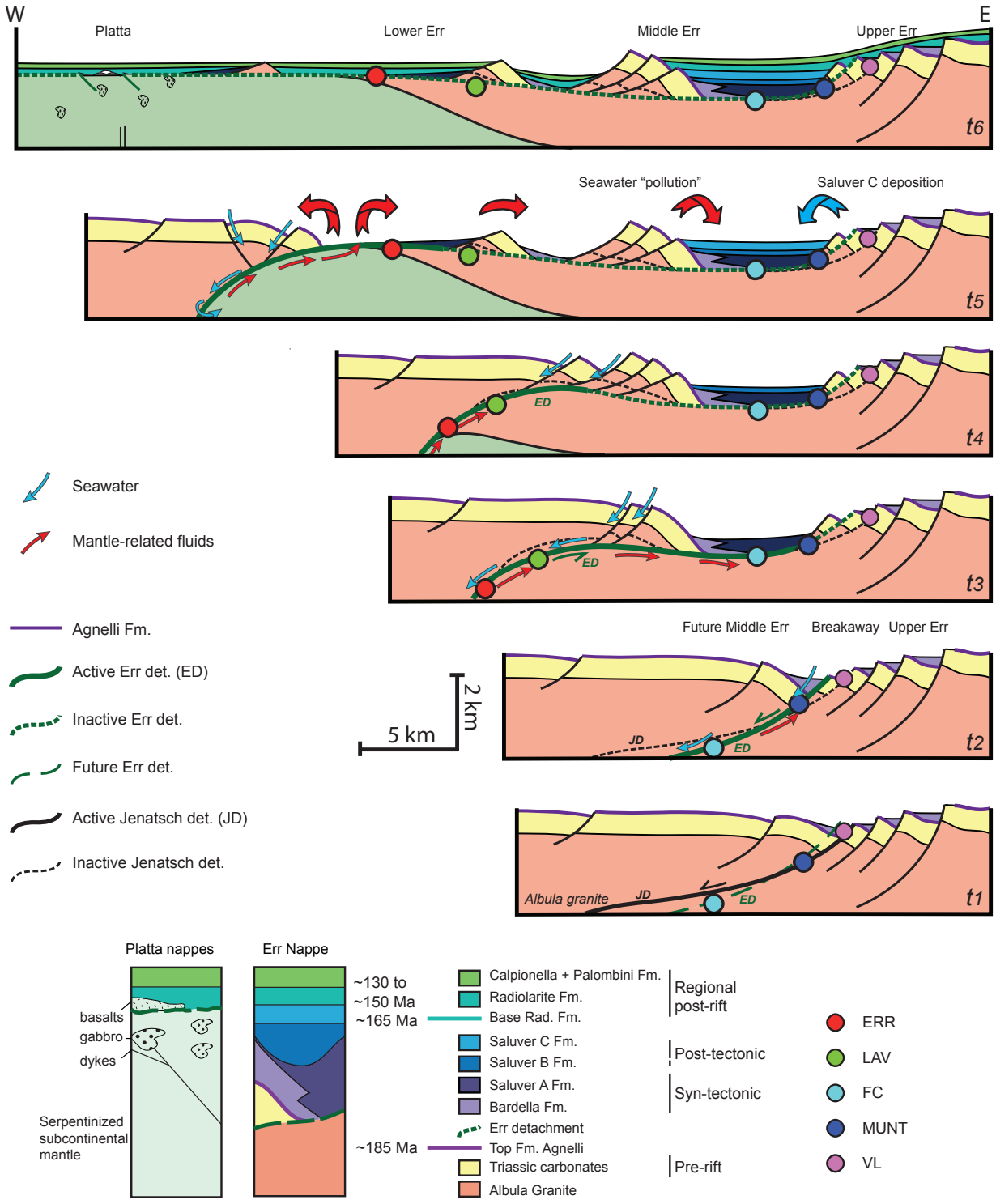

Figure 16. The link between fluid migration and the supradetachment basin evolution in the Err-Platta nappes. The initial stage (t1) starts with listric normal fault system that cuts through the thinned continental crust (<10 km). When the ED becomes active (t2), the mantle-related fluids migrate along the fault zone and are recorded in the fault rocks and the overlying syn-tectonic sediments (t2 and t3). At t3 the ED is convex up in the deformation zone due the upwarping of the footwall. When the deformation starts to move toward the future ZECM (from t4) the ED segment below the ZoS and Mürtirol become inactive. The continuous deposition of the post-tectonic Saluver C (t5) records the seawater "pollution" by mantle-related fluids. During the deposition of the Radiolarite Fm., the hydrothermal system starts to become less active and after evolves to a situation where probably is "shutdown", as observed by the data from Calpionella and Palombini formations (t6). Geological evolution after *Masini et al.* [2012].

These observations lead us to interpret that Fe, Mn and Ni-Cr-V were released by serpentinization (Figures 6 and 7) and were spread in the seawater by hydrothermalism (Figure 14B), and that the post-tectonic sediments registered (Figure 14D) this process. Therefore, the occurrence of Ni-Cr-V, Fe, and Mn trends may be used as proxies for mantle exhumation and related serpentinization in hyperextended rifted margins (Figure 16).

7.2. **Composition of mantle related fluids**

It is difficult to "reassemble" the whole fluid composition involved during the evolution of the distal margin from the sole chemical analyses of the mantle, sedimentary and fault rocks. However, a first-order composition can be envisaged by the observations that syn-tectonic phyllosilicates can register partially the fluid flow in the fault rocks and that these fluids also affect the sediments. In addition, the data set of serpentinized peridotites show that the progressive serpentinization leads to leaching of elements that must outflow through fault systems or be mixed with the seawater. It is important to notice that chemical reactions involved in the fault rocks in the continent and in the mantle domains as well as the serpentinization are water-assisted. Therefore, Jurassic seawater is always involved.

In the Platta Nappe, the serpentinization creates a fluid enriched in mantle elements (e.g. Ni, Cr, V, Fe, Mn, Co and Sc) that migrates through the detachment system and enriches the fault rock and the sediments in the distal domain. Losses of Si, Mg and Ca from progressive serpentinization in the Platta nappe is always observed and these elements are characteristic of the fluids from the ultramafic-hosted hydrothermal systems and oceanic core complexes at MAR [*Kelley et al*., 2001; *Boschi et al*., 2006].

Although fluid inclusions were not investigated, it is well-known from MAR that serpentinization produces strongly reduced H_2-rich fluids with lower CH_4 content formed under relatively low temperature and higher pH. We think that these gases and conditions probably made part of such mantle-related fluids in the Platta nappe. However, in order to better constrain the conditions at which the fluid-rock reactions took place, more detailed mineralogical and chemical analyses and phase equilibrium modeling would be necessary (e.g., *Destrigneville et al*. [1998]).

In the sediments from the distal domains, similar fingerprints of the fluid contribution are conveyed through time. The Radiolarite Fm. in the Platta nappe and post-tectonic Saluver C and Radiolarite formations in the Err nappe, reveal that Fe and Mn are key components linked to a mantel-related fluid. The enrichment in both fractioned elements (distinct Fe- and Mn-oxides),

locally related with secondary silicification, is typical of the hydrothermal source.

Therefore, based on these observation and in line with ultramafic-hosted hydrothermal systems at MAR the fluid composition may be best depicted by Fe, Mn, Si, Mg, Ca, Ni, Cr, V, Co and Sc as well as H_2 and CH_4 gases. Although the overall concentration of these elements in the fluid could not be determined, the observations in the Alpine Tethys suggest that mantle exhumation and related serpentinization had a significant impact on the chemical budget of the seawater during the final stages of mantle exhumation in yet narrow Tethyan basins.

7.3. Temporal and spatial relationships between mantle exhumation, serpentinization and the formation-migration of the mantle-related fluids during the tectonic evolution of the margin

The relationship between detachment fault rocks, sedimentary records, radiometric ages and geochemical data allowed to propose a model of the temporal and spatial distribution of fluids in the margin.

The pre-tectonic Agnelli formation and the regional post-rift Radiolarite formation constrain the age of the supradetachment basin in the distal margin (ZoS). This basin was developed in a time-interval of approximately 20 my, between Pliensbachian and Bathonian (Figure 2). The ED fault cut the Agnelli pre-rift sequences, and clasts from the ED fault rocks are found reworked in the syn-tectonic Bardella and Saluver A formations. As the Radiolarite formation overlies the Bardella and Saluver formations, the age of the ED must be between 185 and 165 Ma. This gives a maximum time-interval of approximately 20 my for the activity of the ED.

Because fluid flow is registered in the fault rocks of the ED, the age of fluid migration through ED also had to happen between 185 and 165 Ma. The progressive enrichment in Ni-Cr-V registered along the ED fault (Figure 10) and in the syn-tectonic sediments (Figure 11) suggests that this gain had to occur at early stages between 185-165 Ma due to the stratigraphic position of the syn-tectonic sequences and the fault segment of ED (e.g. Alp Muntatsch and Fuorcla Cotschana; for location see Figure 2).

When the segment of the ED under the Zone of Samedan was no longer active and deformation moved oceanwards, the fault rocks in the active segments of the ED continued to register the increasing serpentinization (e.g. samples from Laviner and Err, Figures 10, 15 and 16). From this moment onward the post-tectonic Saluver C registered an elevated enrichment in Ni-Cr-V and Fe-Mn by the “pollution” of seawater linked to the ongoing serpentinization and mantle

exhumation oceanwards. Due to the stratigraphic position of Saluver C, we interpret that this could be happened at final stages between 185-165 Ma.

On the other hand, the mantle-related fluid flow is not registered during the formation of the Grosina detachment at about 190 Ma [*Mohn et al*., 2012] and the Bernina detachment at about 185 Ma [*Eberli*, 1988; *Mohn et al*., 2012]. It means that these detachments were not connected to the mantle or if they were connected, they did not lead to significant serpentinization. However, these detachments record the fluids that interacted with continental rocks what is evidenced by quartz and calcite veins, product of the saussuritization processes along the fault zone.

These observations enable to summarize when and where fluids were active along the evolving Alpine Tethyan margin (Figure 17):

Around 190-185 Ma: Occurrence of first continental-sourced fluids found along the Grosina and Bernina detachment.

Early stages between 185-165 Ma: Serpentinization under thinned continental crust leading to progressive Ni-Cr-V enrichment from the breakaway to the end-most segment of ED and direct flow of mantle-related fluids to the sedimentary basin that are registered in the syn-tectonic sequences.

Late stage around 165 Ma: Important serpentinization stage and mantle exhumation probably accompanied by hydrothermal activity that is registered by higher input of Ni-Cr-V, Fe, and Mn in the Saluver C.

After 165 Ma: Decreasing influence of the hydrothermal activity in the Err and Platta nappes evidenced by the decreasing Ni-Cr-V and Fe-Mn inputs in the Radiolarite formation.

During Late Jurassic and Early Cretaceous: Progressive decrease in Ni-Cr-V and Fe-Mn inputs, reaching PAAS background values, in the Calpionella and Palombini Fm., which are no longer under hydrothermal influence.

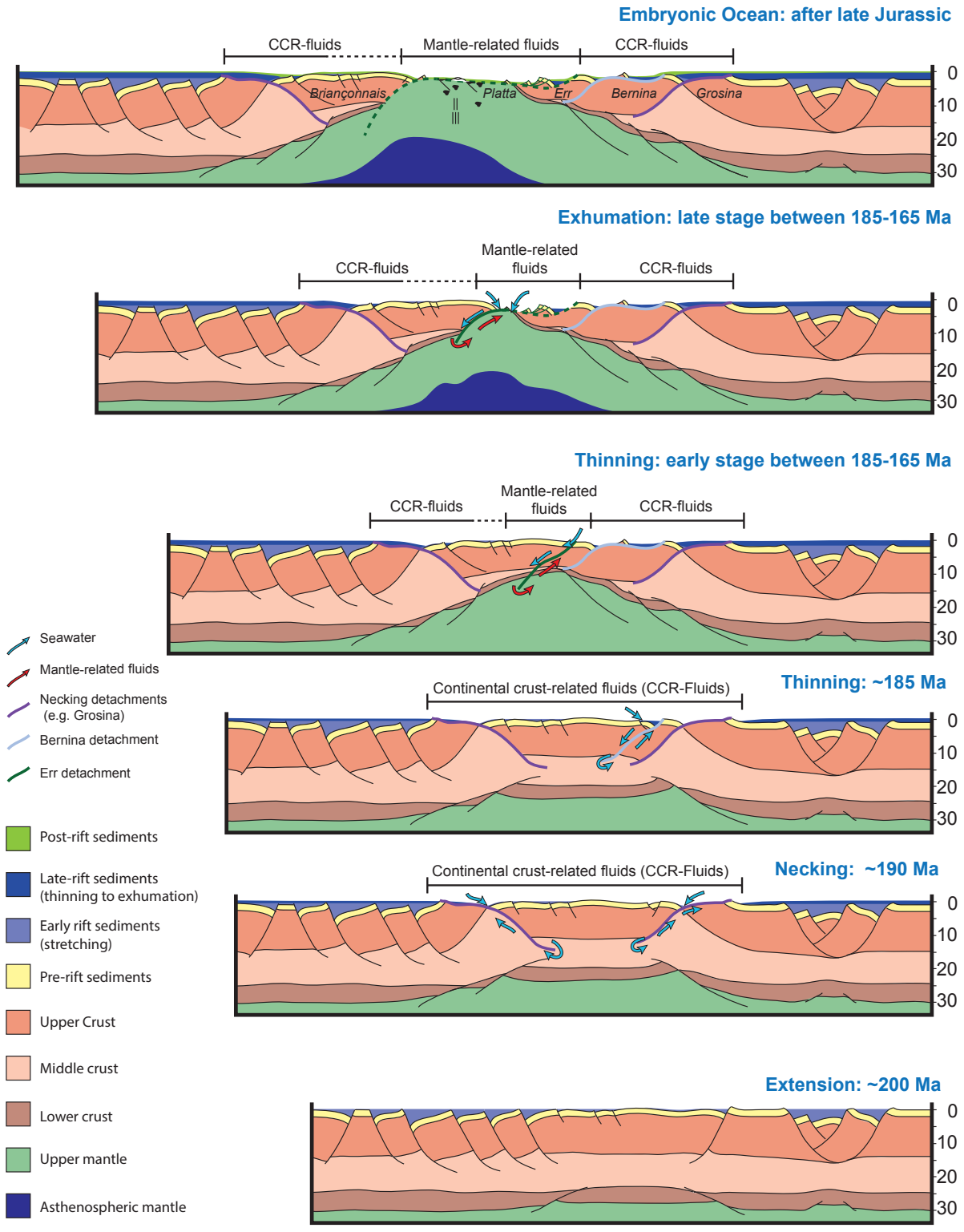

Figure 17. The link between the tectonic evolution and fluid migration along the Alpine Tethyan margin. The Grosina and Bernina detachments record a fluid with a continental composition (about 190-185 Ma). Between 185 and 165 Ma, the ED fault rocks and the supradetachment basin record mantle-related fluids that are produced by initial serpentinization under thinned continental crust. Serpentinization and fluid flow evolve with the progressive mantle exhumation toward the seafloor. During this process, not only the sedimentary basin is affected but also the sea/ocean reservoir. After late Jurassic the hydrothermal system at the Platta nappe becomes inactive. Geological evolution after *Mohn et al.* [2011] and *Masini et al.* [2013].

8. CONCLUSION

The formation and migration of fluids are registered along the margin and can be recognized by different methods. Continental fault rocks registered gain of elements that are not coming from continental rocks alteration process but are the product of serpentinization.

We presented a set of data from the Err and Platta nappes exposing the remnants of a CDZ and ZECM that records a large-scale fluid-flow system. The fluid-rock interaction between seawater and mantle produces a fluid with a mantle composition, that is best depicted by Fe, Mn, and Ni-Cr-V trends. Many of these elements are being expelled in active ultramafic-hosted hydrothermal sites at MAR, which share similar tectonic processes (e.g. mantle exhumation along detachment faults) with the Alpine Tethys domains.

Fluids that are released during serpentinization migrate through detachment faults as traced by the enrichment (gain of elements) of specific mantle-derived elements in the fault rocks. Fluids with same composition but with different relative concentrations are found in the syn-, post-tectonic and in the regional post-rift sedimentary rocks, tracing the coeval evolution of serpentinization and basin formation.

The relationship between structural and stratigraphic data allowed us to understand when and where this fluid circulated in the distal margin.

The determined link between the margin evolution and fluid flow history enabled us to establish the importance of coupling the seawater and mantle reservoirs for the formation and migration of mantle-related fluids along the distal margin and during its evolution. The described fluids may have a considerable impact on the chemical budgets of the seawater during final stages of rifting.

Our results suggest that the sedimentary sequence of present-day magma-poor rifted margins can register the main serpentinization stage and also the age of mantle exhumation. This may have implications for understanding when and how mantle exhumation occurs in present-day magma-poor rifted margins (e.g., South Atlantic margins).

Table 1. Peridotite and serpentinites.[a]

Sample		Lan-1	F3-01	F3-02	P-7
Lithology		Peridotite	Serpentinite	Serpentinite	Serpentinite
Unit		Lanzo	Platta	Platta	Platta
Place		Lanzo	Falotta	Falotta	Parsettens
Serpent. Degree		*2%*	*95%*	*90%*	*95%*
SiO_2	%	38.81	32.70	39.58	52.00
Al_2O_3	%	0.96	20.41	2.08	17.20
Fe_2O_3	%	10.72	12.67	8.00	12.00
MnO	%	0.15	0.25	0.12	0.15
MgO	%	46.38	13.85	36.57	6.83
CaO	%	0.10	9.39	0.21	1.07
Na_2O	%	0.02	0.40	<0.01	3.05
K_2O	%	0.02	<0.01	<0.01	1.89
TiO_2	%	0.03	1.76	0.06	1.08
P_2O_5	%	0.02	0.12	<0.01	0.29
LOI	%	1.50	8.20	12.70	4.26
Ba	ppm	4.00	7.00	3.00	**90600**
Ce	ppm	0.40	17.50	0.40	41.90
Co	ppm	140.80	57.20	96.10	22.30
Cr	ppm	5747.28	383.15	2415.23	98.80
Cs	ppm	<0.1	<0.1	1.10	0.70
Cu	ppm	166.30	2.60	10.40	125.20
Dy	ppm	0.07	6.26	0.20	4.06
Er	ppm	0.04	4.50	0.09	2.35
Eu	ppm	<0.02	1.83	0.04	-
Gd	ppm	0.05	5.39	0.18	4.74
Hf	ppm	<0.1	2.70	<0.1	5.94
Ho	ppm	<0.02	1.45	0.04	0.89
La	ppm	0.30	6.90	0.50	17.89
Lu	ppm	0.01	0.68	0.02	0.35
Nb	ppm	0.10	3.10	<0.1	15.80
Nd	ppm	<0.3	13.60	0.30	19.73
Ni	ppm	3107.20	261.10	2230.50	168.00
Pb	ppm	0.90	0.40	0.50	28.90
Pr	ppm	0.03	2.67	0.04	4.75
Rb	ppm	0.90	0.20	0.60	66.50
S	ppm	200.00	<L.D	600.00	-
Sc	ppm	5.00	49.00	8.00	15.28
Sm	ppm	<0.05	4.26	0.11	5.37
Sr	ppm	0.90	68.30	5.70	4370.00
Ta	ppm	<0.1	0.10	<0.1	1.36
Tb	ppm	<0.01	0.98	0.03	0.59
Th	ppm	<0.2	0.30	<0.2	10.40
Tm	ppm	<0.01	0.70	0.02	0.39
U	ppm	<0.1	0.20	<0.1	1.48
V	ppm	28.00	156.00	46.00	144.60
Y	ppm	0.40	35.90	1.20	27.10
Yb	ppm	<0.05	4.58	0.10	2.43
Zn	ppm	34.00	71.00	20.00	191.10
Zr	ppm	1.20	119.10	2.30	227.40
Cd	ppm	<0.1	<0.1	<0.1	0.40
Mo	ppm	<0.1	<0.1	<0.1	-
Sb	ppm	<0.1	<0.1	<0.1	0.90
Sn	ppm	<1	1.00	<1	4.50
W	ppm	<0.5	<0.5	<0.5	1.00

[a]Notes: Samples used as end-members. Used method ICP-MS and ICP-AES. Sample P-7 analyzed at LHyGeS-CNRS Strasbourg and the others at Acme Analytical Laboratories Ltd. Sample P-7 shows exceptional high Ba content and correspond to a zone extremely rich in chlorite, quartz veins and barite.

Table 2. Bulk composition of fault rocks[a]

Sample	L-9a	L-9b	BI3-1	AVE-M	Total AVE	MUNTA-1	L-07	FC2-05	FC2-5a	L-7a
Lithology	Granite	Granite	Granite	Granite	Granite	Cataclasites	Cataclasites	Cataclasites	Cataclasites	Cataclasites
Unit	Middle Err	Middle Err	Middle Err	Middle Err	Middle Err	Middle Err	Middle Err	Middle Err	Middle Err	Middle Err
Place	Laviner	Laviner	Val Bever	-	-	Alp Muntatsch	Laviner	Fuorcla Cotschana	Fuorcla Cotschana	Laviner
Lab	SARM	LHyGeS	ACME	Zurich	-	SARM	SARM	SARM	SARM	SARM
SiO_2	67.45	67.60	56.87	68.76	65.17	69.49	73.34	78.87	79.16	74.25
Al_2O_3	15.84	15.80	20.59	14.85	16.77	13.60	12.37	12.82	12.21	12.13
Fe_2O_3	2.70	3.14	4.89	3.52	3.56	3.67	2.48	1.83	1.72	2.18
MnO	0.04	0.05	0.06	0.05	0.05	0.07	0.04	0.02	0.01	0.04
MgO	1.05	1.04	1.41	1.05	1.14	1.94	1.27	0.27	0.26	1.17
CaO	1.53	1.64	6.13	1.75	2.76	0.33	0.62	< L.D.	< L.D.	0.59
K_2O	3.88	3.82	2.35	3.22	3.32	2.91	3.12	3.22	3.08	3.32
Na_2O	4.03	3.83	3.96	2.65	3.62	4.23	4.01	0.28	0.27	3.88
TiO_2	0.32	0.38	0.62	0.41	0.43	0.35	0.31	1.04	0.99	0.26
P_2O_5	0.17	0.23	0.18	0.58	0.29	0.11	0.22	0.04	0.04	0.21
LOI	1.78	1.61	2.70	1.44	1.88	1.93	1.40	2.29	2.04	1.26
As	2.13	-	<0.5	-	2.13	5.11	2.48	6.44	6.25	2.25
Ba	724.80	820.90	602.00	543.00	672.68	451.70	324.50	312.90	306.50	340.00
Be	2.77	-	2.00	-	2.38	2.13	1.08	2.30	2.13	1.23
Bi	< L.D.	-	<0.1	-	<LD	0.32	< L.D.	0.33	0.33	< L.D.
Cd	< L.D.	0.30	<0.1	-	0.30	< L.D.	< L.D.	< L.D.	< L.D.	< L.D.
Ce	77.35	118.00	16.60	20.00	57.99	23.96	19.40	73.43	72.63	18.63
Co	3.95	7.00	6.80	10.00	6.94	4.08	3.82	2.79	2.88	3.73
Cr	15.00	31.70	20.53	10.00	19.31	5.42	15.66	60.27	59.41	17.23
Cs	1.79	1.81	3.80	-	2.47	2.13	1.10	2.94	2.89	1.25
Cu	< L.D.	24.70	5.60	3.00	11.10	8.45	9.89	17.42	21.80	13.71
Dy	3.08	4.08	3.70	-	3.62	3.04	3.10	6.15	6.13	3.01
Er	1.34	1.92	2.10	-	1.79	1.84	1.64	3.83	3.75	1.61
Eu	1.20	1.48	1.65	-	1.44	0.70	0.55	1.41	1.39	0.58
F	-	-	-	647.00	647.00	-	-	-	-	-
Ga	20.07	-	24.80	13.00	19.29	17.90	14.43	17.12	16.68	14.42
Gd	4.29	6.38	3.65	-	4.77	2.66	2.69	6.14	5.89	2.67
Ge	1.43	-	-	-	1.43	0.83	1.01	1.78	1.50	0.97
Hf	3.71	5.01	7.50	-	5.41	3.84	2.53	4.14	4.28	2.81
Ho	0.51	0.77	0.77	-	0.69	0.62	0.59	1.28	1.26	0.57
In	< L.D.	-	-	-	<LD	< L.D.	< L.D.	< L.D.	< L.D.	< L.D.
La	40.00	62.61	7.60	20.00	32.55	11.39	9.16	34.50	34.57	8.86
Lu	0.17	0.23	0.33	-	0.24	0.32	0.22	0.62	0.60	0.22
Mo	< L.D.	*	0.20	-	0.20	< L.D.	< L.D.	< L.D.	< L.D.	< L.D.
Nb	11.01	16.03	9.40	6.00	10.61	9.02	8.38	14.93	14.42	7.89
Nd	31.19	47.27	11.90	25.00	28.84	10.80	9.79	32.08	32.44	9.52
Ni	9.78	10.00	3.60	3.00	6.59	< L.D.	5.08	8.72	7.95	5.26
Pb	17.86	30.20	5.20	7.00	15.06	5.83	10.91	16.95	16.94	12.29
Pr	8.61	13.10	2.42	-	8.04	2.88	2.48	8.39	8.46	2.39
Rb	115.70	133.60	141.00	103.00	123.33	94.25	77.94	110.00	107.40	84.20
S	-	-	-	53.00	53.00	-	-	-	-	-
Sb	< L.D.	0.50	<0.1	-	0.50	< L.D.	0.20	0.49	0.56	0.21
Sc	7.30	8.46	13.00	11.00	9.94	9.80	8.48	12.49	11.95	7.87
Sm	5.63	8.20	3.26	-	5.70	2.63	2.62	6.62	6.60	2.59
Sn	1.19	2.70	4.00	-	2.63	4.19	2.20	2.48	2.65	2.18
Sr	204.50	207.30	340.50	168.00	230.08	70.41	45.50	47.71	47.40	47.20
Ta	1.27	1.87	1.00	-	1.38	1.16	1.14	1.47	1.41	1.06
Tb	0.59	0.77	0.64	-	0.67	0.48	0.49	1.01	0.99	0.49
Th	14.19	19.80	3.10	-	12.36	8.38	4.95	11.15	11.26	4.62
Tm	0.18	0.26	0.34	-	0.26	0.29	0.25	0.60	0.58	0.24
U	2.04	2.64	4.40	-	3.03	3.51	3.92	2.62	2.56	2.70
V	28.25	37.50	59.00	70.00	48.69	40.31	37.84	62.79	61.90	34.54
W	0.70	*	0.90	-	0.80	1.98	0.90	2.05	1.66	0.73
Y	15.36	20.60	19.60	18.00	18.39	18.18	16.75	38.10	37.25	16.42
Yb	1.15	1.57	2.07	-	1.60	2.03	1.58	4.08	4.04	1.57
Zn	44.32	47.90	61.00	46.00	49.81	62.84	45.89	31.78	32.51	44.42
Zr	145.80	159.70	347.20	123.00	193.93	135.40	91.01	162.00	165.30	98.19

[a]Notes: Granite is related to Albula granite, cataclasite also refers to foliated cataclasites. AVE-M means average values from *Manatschal et al.,* [2000] (Zurich) and Total AVE refers to the total average from each rock type. Analyses were carried using ICP-MS and ICP-AES in the LHyGeS- CNRS Strasbourg, Service d'Analyse des Roches et des Minéraux (SARM)-CNRS-CRPG at Nancy and Acme Analytical Laboratories Ltd. Major elements are in oxide %wt and trace elements in ppm.

TABLE 2. CONT.

L-14	FC-8C	FC-8M	AVE-M	Total AVE	FC2-6	MUNTA-2	MUNTA-3	L-18	VL-06	VL-07
Cataclasites	Cataclasites	Cataclasites	Cataclasites	Cataclasites	Clast-rich chl-sch	Gouges	Gouges	Gouges	Gouges	Gouges
Middle Err	Middle Err	Middle Err	Middle Err	Middle Err	Middle Err	Middle Err	Middle Err	Middle Err	Middle Err	Middle Err
Laviner	Fuorcla Cotschana	Fuorcla Cotschana	-	-	Fuorcla Cotschana	Alp Muntatsch	Alp Muntatsch	Laviner	Val Lunga	Val Lunga
LHyGeS	LHyGeS	LHyGeS	Zurich	-	SARM	SARM	SARM	SARM	SARM	SARM
73.10	85.50	81.00	75.12	76.65	59.88	66.46	62.99	62.55	69.65	62.80
11.40	7.16	10.90	11.50	11.57	19.34	14.57	16.79	17.61	12.95	18.13
3.75	2.48	2.91	2.24	2.58	8.40	4.23	5.29	6.25	4.99	4.79
0.08	0.03	0.03	0.03	0.04	0.11	0.05	0.04	0.07	0.06	0.04
1.75	0.34	0.31	0.92	0.92	2.11	2.93	3.43	3.33	2.58	2.90
1.28	0.06	0.10	1.32	0.61	0.16	0.34	0.91	0.37	0.50	0.67
2.30	1.44	2.34	1.69	2.60	3.64	5.13	4.96	4.73	1.76	4.96
2.84	0.65	0.69	3.68	2.28	0.42	1.49	0.77	0.79	3.24	0.90
0.53	0.47	0.73	0.27	0.55	0.92	0.48	0.68	0.80	0.44	0.71
0.18	0.06	0.06	0.11	0.11	0.16	0.16	0.17	0.17	0.16	0.16
2.12	1.30	1.86	1.54	1.75	4.15	3.75	4.91	4.17	3.19	4.51
-	-	-	-	4.51	8.35	18.16	72.57	98.78	2.54	5.02
731.70	621.50	284.00	361.00	414.87	472.40	467.60	464.10	493.20	128.20	519.70
-	-	-	-	1.77	2.93	3.33	3.83	5.00	1.85	3.75
-	-	-	-	0.33	0.34	0.55	0.58	0.70	0.13	0.40
0.50	*	0.40	-	0.45	< L.D.	0.49	0.28	0.22	< L.D.	0.13
23.52	54.71	79.50	32.00	44.20	92.33	49.16	71.22	87.70	48.78	82.08
10.10	6.50	9.10	7.00	5.56	18.24	8.49	10.93	11.55	12.72	11.42
36.40	44.40	59.40	8.00	34.02	88.32	47.36	73.10	77.48	15.35	64.04
2.19	1.52	2.49	-	2.06	5.20	12.98	20.10	13.10	2.67	9.23
38.80	41.60	22.00	5.00	19.85	26.33	30.54	31.75	32.62	< L.D.	24.96
2.38	2.68	4.19	-	3.84	5.93	4.45	4.88	6.27	2.80	5.45
1.29	1.73	2.66	-	2.29	3.30	2.59	2.74	3.43	1.40	3.15
0.59	0.52	0.79	-	0.81	1.61	0.73	1.04	1.25	0.90	1.20
-	-	-	416.00	416.00	-	-	-	-	-	-
-	-	-	8.00	14.76	25.94	18.85	22.18	24.40	14.90	23.95
2.39	2.46	4.10	-	3.63	6.44	4.33	5.27	6.42	3.43	5.66
-	-	-	-	1.22	2.54	1.46	1.80	2.40	1.47	2.55
3.44	2.48	5.29	-	3.60	5.43	4.22	4.77	6.08	3.18	4.92
0.51	0.62	0.97	-	0.80	1.14	0.89	0.93	1.22	0.51	1.09
-	-	-	-	< L.D.	0.08	0.08	0.10	0.10	< L.D.	0.08
12.77	28.19	41.46	25.00	22.88	46.36	23.84	36.01	43.58	23.57	42.05
0.19	0.26	0.39	-	0.35	0.49	0.40	0.44	0.50	0.21	0.47
*	0.80	1.00	-	0.90	< L.D.	< L.D.	0.71	0.70	1.52	< L.D.
7.50	8.39	13.19	4.00	9.75	15.90	9.21	11.72	13.62	7.66	12.84
12.54	24.80	35.35	27.00	21.59	38.95	21.98	31.55	38.30	20.65	35.46
23.00	23.00	24.00	4.00	12.63	41.45	17.81	30.58	27.05	8.70	25.15
28.10	44.70	60.90	59.00	28.40	31.91	41.29	22.82	51.12	6.87	26.02
3.20	6.49	9.30	-	5.45	10.63	5.84	8.46	10.40	5.60	9.71
107.20	56.90	94.60	42.00	86.05	142.70	204.30	214.60	198.20	81.92	192.10
-	-	-	454.00	454.00	-	-	-	-	-	-
0.50	0.60	1.00	-	0.51	0.90	0.50	1.84	1.20	< L.D.	0.33
10.52	6.75	10.54	7.00	9.49	18.87	11.61	15.48	17.05	7.68	15.53
2.83	4.16	6.39	-	4.30	7.59	4.63	6.14	7.59	4.27	6.92
3.50	2.90	3.80	-	2.99	3.62	4.67	5.52	5.43	1.89	4.41
52.80	40.70	30.30	56.00	48.67	52.39	34.25	39.93	38.94	59.35	33.77
0.65	0.75	1.26	-	1.11	1.49	1.05	1.15	1.26	1.02	1.31
0.29	0.35	0.58	-	0.59	1.00	0.72	0.82	1.03	0.51	0.91
4.10	6.40	11.00	-	7.73	16.71	10.02	13.12	14.93	6.18	15.02
0.19	0.28	0.42	-	0.36	0.49	0.39	0.41	0.50	0.21	0.47
2.79	1.20	2.01	-	2.66	3.40	3.18	4.54	6.04	2.09	5.38
76.90	43.40	64.40	44.00	51.79	103.70	59.78	88.35	89.96	53.46	71.41
2.10	*	1.20	-	1.52	1.97	3.47	6.44	3.76	1.45	3.49
18.00	16.90	26.00	11.00	22.07	32.64	26.86	27.61	35.08	15.81	32.10
1.18	1.75	2.72	-	2.37	3.22	2.56	2.80	3.35	1.34	3.08
46.10	38.40	46.10	42.00	43.34	133.70	111.40	111.40	116.70	54.21	88.28
137.40	82.30	175.60	95.00	126.91	207.50	152.10	178.60	226.10	118.40	174.30

TABLE 2. CONT.

FC2-1	VL-07	L-16	AVE-M	Total AVE	BERN3-6	BERN3-9	GROS3-05	GROS3-07	CHAB-2
Gouges	Gouges	Gouges/ UCA	Gouges	Gouges	Gneiss	UCA	Mylonite	UCA	Gouges
Middle Err	Middle Err	Middle Err	Middle Err	Middle Err	Bernina	Bernina	Grosina	Grosina	Chaberton
Fuorcla Cotschana	Val Lunga	Laviner	-	-	Val da Fain	Val da Fain	Grosina	Grosina	Chaberton
SARM	SARM	LHyGeS	Zurich	-	ACME	ACME	ACME	ACME	ACME
61.82	62.59	60.40	62.34	63.51	71.50	67.78	68.75	64.80	62.02
18.69	18.10	16.40	17.28	16.72	14.57	15.72	14.93	15.70	18.45
6.52	4.78	6.59	5.75	5.46	2.48	3.07	4.07	5.18	5.72
0.05	0.03	0.11	0.06	0.06	0.03	0.04	0.07	0.08	0.07
2.82	2.87	4.05	3.07	3.11	0.93	1.57	1.24	1.51	1.88
0.21	0.60	0.60	0.56	0.53	0.20	0.37	2.40	1.19	0.52
5.13	5.02	4.06	4.97	4.52	5.60	6.39	1.90	6.21	5.15
0.21	0.89	2.33	0.55	1.24	2.29	1.59	4.32	2.79	0.85
0.87	0.72	0.88	0.77	0.71	0.41	0.45	0.38	0.44	0.78
0.14	0.16	0.21	0.16	0.17	0.14	0.16	0.08	0.10	0.11
4.24	3.84	3.44	3.69	3.97	1.70	2.70	1.70	1.80	4.20
26.93	4.94	-	-	32.71	26.20	707.00	<0.5	2.00	226.80
336.40	551.60	674.90	642.00	475.30	657.00	508.00	376.00	992.00	645.00
3.68	3.78	-	-	3.60	5.00	3.00	5.00	<1	<1
0.44	0.46	-	-	0.47	0.30	1.10	<0.1	0.20	0.30
0.12	0.18	1.90	-	0.48	0.10	<0.1	<0.1	0.30	<0.1
92.54	87.48	110.00	75.00	78.22	52.50	45.30	43.40	75.30	90.00
16.13	12.38	17.70	13.00	12.70	2.70	0.90	7.00	9.00	13.30
80.71	66.11	149.00	80.00	72.57	20.53	20.53	20.53	34.21	75.26
8.43	10.03	36.62	-	14.14	4.00	11.10	2.30	5.90	12.20
32.87	27.02	73.60	18.00	33.92	18.20	34.90	1.40	5.40	15.10
5.26	5.82	10.80	-	5.72	5.91	6.27	4.89	7.20	5.09
2.89	3.34	7.30	-	3.36	3.71	3.99	3.36	4.45	2.92
1.48	1.27	1.24	-	1.14	0.71	0.70	0.98	1.44	1.31
-	-	-	1211.00	1211.00	-	-	-	-	-
24.33	25.15	-	17.00	21.35	16.20	19.10	16.70	17.60	21.80
6.11	6.05	9.04	-	5.79	5.09	5.46	5.27	6.91	6.02
2.29	2.59	-	-	2.08	-	-	-	-	-
4.86	4.99	6.89	-	4.99	4.50	4.70	4.10	4.60	5.40
1.00	1.15	2.60	-	1.17	1.22	1.38	1.09	1.44	1.06
0.08	0.09	-	-	0.09	-	-	-	-	-
46.53	44.79	53.80	53.00	40.80	26.00	23.10	25.80	41.80	47.10
0.45	0.48	0.89	-	0.48	0.47	0.55	0.53	0.63	0.44
< L.D.	0.55	0.90	-	0.87	0.40	0.60	<0.1	<0.1	0.30
14.36	13.62	12.60	7.00	11.40	7.80	8.90	7.10	8.80	15.20
39.70	38.59	46.60	27.00	33.31	25.90	21.70	25.50	39.10	40.50
37.15	26.95	45.00	31.00	27.71	4.80	1.40	7.50	22.30	35.40
36.00	27.83	147.60	23.00	42.51	26.60	221.00	12.60	23.70	7.90
10.75	10.37	12.50	-	9.20	6.70	5.86	6.24	10.51	10.79
213.30	204.50	228.40	211.00	194.26	186.10	307.40	75.90	270.00	220.40
-	-	-	415.00	415.00	<L.D.	500.00	<L.D.	<L.D.	1400.00
1.01	0.42	1.40	-	0.96	0.30	1.30	0.10	0.20	0.40
17.14	15.50	19.21	23.00	15.80	8.00	9.00	12.00	14.00	13.00
7.61	7.40	9.34	-	6.74	5.50	5.10	4.87	8.19	7.36
3.74	4.61	4.80	-	4.38	9.00	30.00	4.00	5.00	4.00
26.30	36.29	44.00	28.00	37.87	41.10	32.60	252.40	175.90	34.70
1.33	1.34	1.03	-	1.19	0.60	1.00	0.90	0.90	1.10
0.92	0.97	1.66	-	0.94	0.89	1.00	0.83	1.23	0.91
16.00	15.39	13.60	-	13.03	12.00	13.30	10.40	15.70	14.50
0.43	0.50	1.18	-	0.51	0.55	0.58	0.54	0.67	0.47
3.12	5.44	42.51	-	9.04	3.10	5.60	4.10	4.30	2.70
97.19	76.43	120.30	139.00	88.43	42.00	36.00	54.00	56.00	86.00
4.62	3.23	4.90	-	3.92	11.20	19.20	<0.5	0.70	4.70
29.04	33.56	70.30	30.00	33.37	32.80	36.50	33.20	37.50	28.60
2.86	3.28	7.02	-	3.29	3.48	3.69	3.41	4.32	3.05
107.90	88.66	137.30	120.00	103.98	81.00	23.00	39.00	80.00	71.00
181.50	184.70	235.60	185.00	181.81	162.30	160.90	134.10	153.40	187.50

Table 3. Composition of clay fraction from Err detachment fault rocks

Sample	L-9b	L-07	L-18	MUNTA-2	MUNTA-3	VL-06	VL-07	FC2-1	AVE-GO
Lithology	Granite	Cataclasite	Gouge	Gouge	Gouge	Gouge	Gouge	Gouge	Gouge
Unit	Middle Err	Middle Err	Middle Err	Middle Err	Middle Err	Middle Err	Middle Err	Middle Err	Middle Err
Place	Laviner	Laviner	Laviner	Alp Muntatsch	Alp Muntatsch	Val Lunga	Val Lunga	Fuorcla Cotschana	-
SiO_2	55.11	58.05	46.39	49.22	46.33	51.11	47.51	46.99	47.93
Al_2O_3	21.68	17.41	24.50	21.21	23.83	21.20	26.38	26.84	23.99
Fe_2O2	4.92	7.47	8.23	7.48	7.77	8.71	6.00	7.35	7.59
MnO	0.08	0.13	0.09	0.10	0.06	0.11	0.04	0.06	0.08
MgO	2.14	4.05	4.75	5.34	5.20	5.57	4.06	3.70	4.77
CaO	1.89	0.89	0.31	0.39	0.52	0.40	0.43	0.18	0.37
Na_2O	3.38	3.15	0.33	0.74	0.36	1.92	0.36	0.21	0.65
K_2O	5.51	4.34	7.59	6.82	7.05	4.56	8.11	8.03	7.03
TiO_2	0.49	0.61	0.40	0.59	0.41	0.55	0.48	0.35	0.46
P_2O_5	0.17	0.25	0.17	0.18	0.09	0.12	0.07	< L.D.	0.13
LO.I	4.33	4.28	6.40	6.43	6.91	5.73	6.24	5.99	6.28
As	9.92	7.51	240.90	29.24	120.50	6.12	6.61	50.03	75.57
Ba	734.40	492.90	848.50	513.20	688.70	385.20	923.00	532.40	648.50
Be	4.61	2.74	8.05	6.06	6.47	3.54	5.70	5.28	5.85
Bi	< L.D.	0.11	1.49	1.10	1.07	0.26	0.52	0.54	0.83
Cd	0.28	0.14	0.25	0.88	0.42	< L.D.	0.12	0.12	0.36
Ce	56.24	28.40	46.59	65.29	74.75	98.97	125.30	49.36	76.71
Co	13.73	31.24	26.22	28.13	25.46	19.23	16.61	25.44	23.52
Cr	29.68	75.57	128.00	91.33	119.90	33.41	99.41	127.40	99.91
Cs	6.43	3.23	30.08	29.62	45.41	9.95	18.21	15.11	24.73
Cu	8.12	52.90	65.78	58.63	65.99	10.82	39.30	51.33	48.64
Dy	2.66	5.74	6.22	8.04	6.45	4.59	6.11	2.70	5.69
Er	1.14	3.03	3.68	4.53	3.51	2.13	3.03	1.48	3.06
Eu	1.33	1.10	0.92	1.20	1.20	1.69	1.59	0.71	1.22
Ga	36.50	32.90	36.07	34.45	34.75	28.88	37.58	36.67	34.73
Gd	3.44	5.40	6.06	7.19	6.19	6.07	7.26	2.91	5.95
Ge	1.60	1.51	3.23	2.64	2.25	2.51	3.45	2.56	2.77
Hf	0.76	0.90	1.08	1.88	1.15	0.82	0.75	1.87	1.26
Ho	0.45	1.10	1.28	1.59	1.26	0.81	1.11	0.52	1.10
In	< L.D.	0.18	0.17	0.15	0.16	0.11	0.13	0.12	0.14
La	28.53	14.30	21.92	31.59	37.95	48.16	65.43	27.18	38.71
Lu	0.14	0.42	0.55	0.64	0.50	0.30	0.39	0.24	0.44
Mo	0.57	9.00	1.46	< L.D.	1.56	2.92	0.61	< L.D.	1.64
Nb	16.62	18.80	9.07	11.64	8.04	9.25	12.23	8.09	9.72
Nd	22.91	17.39	22.41	30.55	33.17	39.47	54.67	19.60	33.31
Ni	16.27	26.09	128.00	36.71	52.03	19.78	32.36	46.88	52.63
Pb	46.77	19.35	109.09	80.68	32.74	14.55	36.47	47.70	53.54
Pr	6.21	3.99	5.59	7.97	8.96	10.99	14.91	5.50	8.99
Rb	241.10	135.10	351.10	322.80	343.00	215.00	349.00	367.00	324.65
Sc	12.60	26.07	23.06	23.45	24.71	21.43	23.43	24.93	23.50
Sb	0.42	0.45	2.10	0.76	3.06	0.39	0.48	1.29	1.35
Sm	4.22	4.99	5.61	7.01	6.66	7.98	10.06	3.61	6.82
Sn	2.04	6.44	8.40	9.19	8.81	5.77	6.94	5.58	7.45
Sr	168.50	39.54	38.12	24.78	38.79	34.63	41.40	27.83	34.26
Ta	1.96	2.60	0.76	1.27	0.70	1.25	0.99	0.65	0.94
Tb	0.51	0.94	0.99	1.28	1.06	0.88	1.09	0.47	0.96
Th	25.20	15.43	28.34	18.84	19.32	15.16	23.53	10.89	19.35
Tm	0.16	0.45	0.56	0.68	0.53	0.32	0.43	0.22	0.46
U	2.25	7.52	10.69	5.30	4.98	2.37	6.77	2.31	5.40
V	56.55	130.00	141.90	112.20	146.20	123.10	116.20	143.80	130.57
W	0.96	11.65	2.87	3.98	4.67	1.34	3.55	3.55	3.33
Y	13.17	31.40	36.29	45.78	36.17	24.39	29.11	14.44	31.03
Yb	0.99	2.95	3.66	4.45	3.49	2.03	2.71	1.57	2.99
Zn	95.39	140.40	173.50	215.70	188.80	116.50	112.70	130.10	156.22
Zr	27.34	28.34	38.38	62.29	38.62	24.88	22.62	63.44	41.71

[a]Notes: Granite is related to Albula granite. AVE-GO refers to the average of gouges samples. The clay fraction separation (<2 μm) were carried at LHyGeS-CNRS Strasbourg using centrifugation technic. Elemental analyses results from ICP-MS and ICP-AES at SARM-CNRS-CRPG at Nancy.

Table 4. Composition of bulk sedimentary rocks[a]

Name	Murtirol	IN1	09Murt4	PN17	IN8	VA-FC-7	IN10	IN Sabl	IN4	PN1
Lithology	Bardella	Bardella	Saluver A	Saluver A	Saluver A	Saluver A	Saluver B	Saluver B	Saluver B	Saluver B
Unit	Middle Err	Middle Err	Middle Err	Middle Err	Middle Err	Middle Err	Middle Err	Middle Err	Middle Err	Middle Err
Sample	Murtirol	Il Nes	Murtirol	Piz Nair	Il Nes	Fuorcla Cotschana	Il Nes	Il Nes	Il Nes	Piz Nair
SiO_2	6.70	15.71	79.44	69.99	83.69	61.80	61.28	58.32	86.80	76.04
Al_2O_3	0.68	2.45	12.38	14.21	7.76	15.30	13.07	8.13	7.26	10.69
Fe_2O_3	0.19	1.30	1.13	4.65	2.13	14.10	3.54	0.58	2.38	1.77
MnO	0.06	0.04	0.03	0.04	0.09	0.19	0.06	0.03	0.02	0.06
MgO	24.40	15.50	0.63	1.95	0.70	0.84	4.14	6.33	0.50	1.69
CaO	29.00	25.30	0.32	0.31	0.21	0.02	4.15	8.16	0.13	2.00
Na_2O	0.55	0.41	3.09	1.36	0.76	0.65	1.40	1.74	0.25	2.12
K_2O	2.21	0.59	2.04	2.93	1.41	1.85	2.40	2.56	1.68	2.36
TiO_2	0.01	0.07	0.16	0.60	0.62	1.42	0.46	0.07	0.42	0.35
P_2O_5	0.62	0.24	0.43	0.37	0.39	0.07	0.36	0.58	0.33	0.36
L.O.I	34.84	38.59	1.45	2.54	1.41	3.06	8.91	13.84	1.31	3.92
Total	99.26	100.20	101.11	98.95	99.17	96.24	99.76	100.34	101.08	101.34
Sr	111.70	154.50	16.70	39.30	22.40	33.90	50.60	42.00	31.20	64.00
Ba	32.90	30.80	84.80	359.20	277.20	289.90	248.90	87.10	130.60	110.80
V	9.90	21.80	16.60	83.60	38.00	119.90	65.20	9.30	29.00	32.60
Ni	66.20	24.80	59.00	51.60	37.30	100.00	41.90	25.40	36.10	36.50
Co	5.00	1.70	3.30	9.60	4.50	25.00	7.50	1.50	3.40	5.10
Cr	14.00	13.00	17.00	71.00	40.00	85.90	52.00	10.00	26.00	22.00
Zn	70.00	20.00	30.00	80.00	100.00	200.20	70.00	40.00	50.00	50.00
Cu	10.00	20.00	10.00	30.00	10.00	65.90	30.00	20.00	20.00	30.00
Sc	-	-	-	-	-	20.92	-	-	-	-
Zr	4.00	20.00	73.00	149.00	484.00	235.20	113.00	35.00	120.00	119.00
Y	8.60	6.20	16.20	27.80	13.70	47.00	26.60	23.20	12.60	18.20
Th	0.70	1.50	4.50	11.70	11.80	14.60	9.60	5.70	7.40	6.80
U	0.73	2.69	0.78	1.69	2.20	3.68	1.44	1.06	1.34	1.14
Rb	34.20	18.30	111.20	151.40	72.30	60.40	124.00	102.50	103.60	104.50
Cs	2.03	0.54	1.97	2.18	1.52	1.30	2.25	0.98	2.35	2.12
Nb	0.62	1.94	5.54	12.78	10.97	18.11	9.78	3.81	7.29	9.15
Mo	-	-	-	-	-	0.50	-	-	-	-
Sb	-	-	-	-	-	0.90	0.30	-	0.40	-
Hf	0.11	0.55	2.28	4.37	12.49	5.76	3.25	1.52	3.23	3.34
Ta	0.03	0.20	0.96	1.05	0.91	1.93	0.92	1.12	0.77	1.22
W	1.50	0.90	2.90	4.90	1.10	1.40	2.20	1.10	2.10	1.70
As	2.70	-	1.30	1.30	3.80	*	7.50	2.80	9.70	1.40
Pb	-	-	0.60	2.40	2.30	67.40	2.60	0.50	1.20	1.00
Cd	0.15	-	-	0.07	0.13	0.40	0.06	-	-	0.06
Sn	1.10	1.00	1.90	2.80	3.50	3.90	2.40	1.80	3.70	2.30
La	5.51	5.10	9.29	33.85	22.41	41.27	25.59	23.06	19.92	8.61
Ce	10.09	11.14	19.48	69.78	45.08	82.45	58.35	26.88	38.39	24.51
Pr	1.17	1.41	2.32	8.20	5.26	9.62	5.98	5.22	4.42	2.63
Nd	4.56	5.54	8.50	30.30	19.24	36.04	22.28	19.33	16.20	10.23
Sm	0.96	1.19	1.99	5.80	3.30	7.86	4.33	3.55	2.71	2.27
Eu	0.21	0.18	0.25	1.01	0.58	1.18	0.77	0.34	0.49	0.35
Gd	0.92	1.05	1.89	5.00	2.59	7.07	3.76	2.93	2.16	2.09
Tb	0.16	0.17	0.40	0.81	0.38	1.11	0.63	0.48	0.36	0.41
Dy	0.86	1.01	2.52	4.88	2.14	6.61	4.08	2.95	1.98	2.60
Ho	0.20	0.21	0.52	1.00	0.46	1.47	0.90	0.66	0.41	0.57
Er	0.48	0.54	1.38	2.72	1.31	3.92	2.50	1.75	1.09	1.59
Tm	0.08	0.09	0.25	0.45	0.24	0.63	0.44	0.30	0.20	0.29
Yb	0.46	0.53	1.53	2.84	1.65	3.77	2.65	1.87	1.23	1.85
Lu	0.07	0.08	0.21	0.41	0.28	0.54	0.39	0.28	0.18	0.28

[a]Notes: Analyses were carried using ICP-MS and ICP-AES in the LHyGeS-CNRS Strasbourg. Major elements are in oxide %wt and trace elements in ppm.

TABLE 4. CONT.

NCotsch1 Saluver B Middle Err Fuorcla Cotschana	MnO Saluver C Middle Err Piz Nair	PN22 Saluver C Middle Err Piz Nair	08PNW02 Saluver C Middle Err Piz Nair	PN-11 Saluver C Middle Err Piz Nair	PN-25bis Saluver C Middle Err Piz Nair	PN-25 Saluver C Middle Err Piz Nair	AMK 101 Saluver C Middle Err Piz Nair	AMK 102 Saluver C Middle Err Piz Nair	AMK 102A Saluver C Middle Err Piz Nair	AMK 102B Saluver C Middle Err Piz Nair
77.86	58.68	82.92	73.54	78.97	48.92	77.13	67.68	53.83	76.19	75.57
10.64	2.60	8.08	8.68	9.12	2.48	7.03	11.00	6.20	11.00	11.20
1.30	1.64	1.01	1.51	2.55	17.58	6.95	8.84	16.50	6.23	5.62
0.02	0.51	0.01	0.04	0.14	20.07	1.14	3.51	14.80	0.14	0.09
1.34	6.93	0.59	2.32	1.75	0.50	1.85	1.61	0.69	1.80	1.66
1.03	11.00	0.35	2.77	0.49	0.61	0.82	0.39	0.57	0.18	0.29
1.82	0.58	2.25	3.06	1.44	0.53	0.26	1.17	0.75	0.99	1.30
3.36	0.51	1.77	1.38	2.66	0.66	1.14	2.48	1.63	2.38	2.39
0.26	0.10	0.15	0.33	0.43	0.12	0.27	0.49	0.27	0.49	0.51
0.42	0.16	0.32	0.32	0.04	0.16	0.11	0.16	0.17	0.16	0.21
2.92	17.64	1.12	5.32	2.18	7.72	2.45	3.64	5.82	2.29	2.14
100.97	100.36	98.57	99.27	97.58	91.63	96.70	100.96	101.23	101.86	100.98
16.50	87.10	16.40	74.80	36.90	199.20	60.10	112.40	180.90	32.60	46.80
131.50	55.60	114.30	96.50	166.30	39.00	99.70	311.30	145.40	208.60	229.30
17.80	22.80	11.80	40.50	53.10	43.40	61.60	104.80	80.60	122.50	124.70
34.20	11.30	34.30	40.30	21.00	27.00	66.00	77.30	54.90	60.30	52.60
3.00	2.30	2.00	27.10	7.53	62.87	32.44	30.92	61.43	28.03	23.89
20.00	16.00	13.00	24.00	32.00	10.00	43.00	50.00	29.00	58.00	55.00
40.00	10.00	40.00	40.00	82.00	82.00	115.00	87.00	109.00	96.00	89.00
20.00	10.00	20.00	20.00	31.96	40.58	65.74	70.70	72.60	53.70	54.10
-	1.00	-	-	7.50	4.50	7.20	11.00	7.00	10.00	11.00
83.00	17.00	91.00	105.00	156.00	32.00	64.00	108.00	66.00	99.00	123.00
13.20	3.20	26.10	16.90	24.80	33.80	26.20	25.40	29.80	18.80	28.30
7.00	-	9.90	6.10	10.60	2.06	4.95	8.83	5.01	8.25	9.38
1.08	-	1.57	2.06	2.61	1.01	1.23	1.85	1.52	1.45	1.62
122.40	13.90	83.40	60.90	117.72	19.12	43.29	103.50	64.30	96.20	106.10
1.57	11.71	1.22	1.06	4.11	0.96	1.86	5.91	2.90	4.05	4.16
6.92	1.55	6.58	6.78	9.85	2.34	5.10	12.25	7.47	11.87	13.37
-	1.60	-	-	0.60	2.47	0.76	0.97	0.97	0.38	0.41
-	5.43	-	-	0.31	0.30	0.33	1.20	0.80	1.40	1.20
2.43	-	3.48	3.14	4.76	0.75	1.70	2.86	1.75	2.67	3.23
0.87	3.90	0.99	0.80	1.30	0.21	0.47	0.86	0.50	0.80	0.91
1.70	1.70	1.50	1.90	8.07	6.37	7.67	2.80	1.80	2.40	2.50
1.00	2.80	-	1.30	*	*	*	1.20	12.80	1.20	1.40
0.50	1.26	-	2.10	13.02	45.74	56.99	16.10	56.40	19.40	18.40
-	0.60	-	-	*	*	*	*	*	*	*
1.60	0.14	1.70	9.50	*	*	*	*	*	*	*
12.07	1.24	10.23	12.56	15.64	14.17	18.77	28.74	20.71	25.04	31.36
31.09	4.71	25.77	25.31	37.27	38.41	50.13	69.83	50.14	56.45	75.57
3.19	0.87	2.74	3.07	4.00	3.60	4.66	6.14	4.76	5.46	7.42
11.76	0.17	9.84	11.60	15.17	15.51	18.62	21.20	19.40	19.70	28.80
2.33	0.73	2.11	2.53	3.15	4.06	4.11	3.70	4.64	3.64	5.95
0.29	0.10	0.22	0.37	0.50	1.00	0.83	0.91	1.21	0.82	1.36
1.94	0.63	2.10	2.26	2.72	3.66	3.35	3.83	4.66	3.43	5.55
0.32	0.13	0.44	0.42	0.52	0.60	0.57	0.59	0.68	0.50	0.80
1.99	0.40	3.30	2.60	3.49	3.90	3.53	3.83	4.21	3.06	4.69
0.43	0.06	0.78	0.56	0.77	0.89	0.74	0.88	0.98	0.67	0.98
1.20	0.37	2.32	1.49	2.24	2.47	1.98	2.26	2.62	1.72	2.38
0.21	0.05	0.45	0.27	0.38	0.43	0.31	0.38	0.45	0.27	0.36
1.31	0.50	2.94	1.65	2.59	2.66	1.80	2.42	2.91	1.75	2.18
0.19	0.13	0.46	0.25	0.37	0.38	0.28	0.40	0.49	0.27	0.34

TABLE 4. CONT.

AMK 102C Saluver C Middle Err Piz Nair	AMK 102D Saluver C Middle Err Piz Nair	AMK 102E Saluver C Middle Err Piz Nair	AMK 103 Saluver C Middle Err Piz Nair	AMK 104 Saluver C Middle Err Piz Nair	AMK 105 Saluver C Middle Err Piz Nair	AMK 106 Saluver C Middle Err Piz Nair	AMK 107 Saluver C Middle Err Piz Nair	AMK 108 Saluver C Middle Err Piz Nair	AMK 109 Saluver C Middle Err Piz Nair	AMK 110 Saluver C Middle Err Piz Nair
70.97	58.23	48.30	74.10	81.64	76.11	41.22	65.75	45.27	87.58	78.48
12.30	4.73	6.50	7.46	3.20	7.18	1.85	1.30	5.88	3.83	1.98
4.94	15.30	17.70	7.14	5.26	8.09	20.50	10.10	10.30	4.08	4.93
0.16	14.40	17.60	4.16	4.53	2.59	15.10	11.10	8.74	1.73	6.43
1.60	0.54	0.76	1.08	0.51	1.58	2.14	0.99	5.12	0.90	0.87
0.38	0.68	0.80	0.90	1.46	0.58	1.55	1.82	6.14	0.38	0.79
1.54	0.84	0.66	1.30	0.47	0.58	0.27	0.38	1.03	0.42	0.47
2.96	1.04	1.77	1.35	0.75	1.32	0.36	0.27	0.87	0.78	0.49
0.54	0.25	0.27	0.37	0.16	0.31	0.07	0.04	0.26	0.15	0.09
0.24	0.26	0.14	0.28	0.66	0.23	0.28	0.42	0.13	0.23	0.15
2.39	5.34	6.75	3.22	2.42	2.87	17.74	9.03	17.11	1.61	6.46
98.03	101.62	101.25	101.35	101.05	101.42	101.08	101.20	100.87	101.69	101.13
50.80	224.00	292.50	238.70	291.00	108.60	100.00	187.90	209.10	79.20	49.10
246.90	118.80	156.40	125.20	69.50	116.70	41.40	35.80	95.30	66.90	34.20
161.20	61.20	87.80	52.70	30.30	69.90	26.70	14.10	37.50	39.60	19.90
55.60	44.30	62.70	50.90	19.00	40.00	29.10	46.60	32.30	15.50	32.80
24.93	48.92	75.06	37.51	20.04	39.43	44.38	62.83	33.43	15.43	58.09
66.00	29.00	29.00	30.00	26.00	31.00	8.00	7.00	17.00	19.00	18.00
89.00	92.00	119.00	5.00	26.00	13.00	11.00	20.00	52.00	20.00	5.00
97.00	120.40	72.20	55.90	50.40	46.50	60.20	86.00	61.00	33.70	42.60
11.00	6.00	8.00	7.00	5.00	7.00	3.00	3.00	4.00	4.00	3.00
112.00	124.00	64.00	150.00	65.00	88.00	18.00	15.00	58.00	38.00	41.00
32.50	42.60	28.70	50.60	63.70	36.00	23.40	26.40	19.60	24.20	15.00
9.10	5.79	4.89	8.43	3.39	6.40	1.28	0.91	5.38	3.27	2.02
1.96	2.33	1.42	2.02	2.01	1.63	0.86	0.72	1.38	0.80	0.59
114.40	40.10	71.70	49.00	25.50	49.50	11.10	6.00	30.30	28.40	15.50
4.85	2.29	3.47	1.75	0.78	1.80	0.32	0.08	0.61	1.32	0.43
13.05	6.33	7.36	8.70	4.25	6.71	1.60	0.91	5.06	3.58	2.09
0.33	1.18	1.24	0.57	0.62	0.21	1.33	0.51	1.29	0.26	0.25
1.10	0.90	0.70	0.05	0.05	0.05	0.05	0.05	0.05	0.05	0.05
3.00	2.99	1.71	3.87	1.59	2.31	0.41	0.37	1.52	1.06	1.12
0.89	0.47	0.49	0.80	0.33	0.56	0.10	0.08	0.43	0.29	0.19
2.20	1.20	1.10	8.50	2.50	2.10	1.00	0.05	1.80	1.40	0.05
2.80	16.70	13.20	1.20	1.10	1.70	0.05	0.80	0.05	0.05	0.80
24.90	84.30	42.30	1.40	2.00	2.00	1.70	1.40	0.90	0.80	0.90
*	*	*	*	*	*	*	*	*	*	*
*	*	*	*	*	*	*	*	*	*	*
34.32	23.08	18.56	358.00	48.18	30.07	11.65	30.75	16.49	18.82	12.73
82.81	61.09	43.42	91.53	102.00	76.39	31.31	29.73	37.26	45.51	27.46
8.01	6.40	4.06	9.02	9.38	6.90	3.16	2.80	4.22	4.84	2.62
30.30	29.20	16.00	36.90	40.40	26.70	14.50	11.80	17.00	19.50	10.40
5.91	7.97	3.85	8.41	10.40	5.68	3.91	2.77	3.78	4.17	2.22
1.36	2.00	1.04	2.18	3.48	1.47	1.30	1.09	0.91	1.12	0.57
5.73	7.48	4.10	8.54	11.24	5.81	4.11	3.38	3.60	4.38	2.40
0.86	1.07	0.63	1.26	1.56	0.86	0.55	0.50	0.53	0.62	0.36
4.95	6.08	3.99	7.42	8.64	5.13	3.16	3.22	3.10	3.69	2.29
1.08	1.31	0.93	1.58	1.86	1.14	0.70	0.74	0.67	0.80	0.50
2.67	3.25	2.60	3.91	4.30	2.85	1.77	1.89	1.69	1.89	1.28
0.40	0.51	0.47	0.61	0.58	0.43	0.30	0.29	0.28	0.29	0.20
2.46	3.19	3.21	3.70	3.29	2.81	1.98	1.78	1.76	1.67	1.28
0.38	0.52	0.56	0.60	0.51	0.46	0.35	0.29	0.28	0.26	0.21

TABLE 4. CONT.

AMK 111 Saluver C Middle Err Piz Nair	AMK 112 Saluver C Middle Err Piz Nair	AMK 113A Saluver C Middle Err Piz Nair	AMK 113B Saluver C Middle Err Piz Nair	AMK 113C Saluver C Middle Err Piz Nair	AMK 113D Saluver C Middle Err Piz Nair	AMK 113E Saluver C Middle Err Piz Nair	AMK 113F Saluver C Middle Err Piz Nair	RAD. Radiolarite Middle Err Piz Nair	VA-P-5 Saluver A Platta Parsettens	VA-P-6 Saluver A Platta Parsettens
78.27	55.20	86.70	83.73	82.33	78.62	72.75	60.23	87.78	69.40	74.30
3.94	0.80	6.10	6.81	7.44	1.06	2.26	9.92	4.27	15.40	12.70
6.61	12.20	3.60	4.41	4.65	4.31	7.62	11.30	4.68	4.80	3.59
5.82	22.70	0.19	0.16	0.17	10.20	8.04	4.67	0.11	0.05	0.06
0.87	0.35	1.24	1.51	1.61	0.55	0.51	2.24	0.78	2.01	1.11
0.80	2.42	0.16	0.23	0.20	0.46	1.97	1.74	0.13	0.19	0.79
0.45	0.36	0.62	0.53	0.73	0.20	0.28	1.91	0.18	1.35	4.15
1.03	0.34	1.41	1.61	1.66	0.35	0.58	1.42	1.36	3.73	1.48
0.14	0.02	0.24	0.25	0.28	0.03	0.08	0.49	0.18	0.64	0.11
0.31	0.81	0.16	0.17	0.18	0.14	1.12	0.70	0.33	0.20	0.16
3.05	6.64	1.55	1.74	1.75	5.65	3.28	4.59	0.96	2.88	1.77
101.29	101.83	101.96	101.15	100.99	101.57	98.49	99.21	100.76	97.77	98.45
259.50	821.80	20.30	20.80	24.50	42.80	235.50	204.80	6.80	32.70	19.50
81.30	21.90	121.50	129.60	141.30	26.80	47.80	139.90	115.10	376.40	49.50
58.20	12.40	88.40	91.40	102.10	22.20	28.10	86.40	28.40	73.70	21.50
47.80	27.80	31.30	38.00	41.90	9.80	26.50	69.50	52.50	19.00	53.00
55.77	54.46	24.23	25.46	27.46	33.85	30.59	43.00	18.50	9.00	7.40
17.00	4.00	30.00	35.00	54.00	12.00	10.00	42.00	39.00	63.80	56.40
12.00	17.00	6.00	17.00	12.00	8.00	29.00	54.00	40.00	362.90	105.40
42.60	82.20	95.40	353.50	192.80	42.50	53.00	107.50	20.00	50.20	86.50
5.00	2.00	6.00	7.00	7.00	2.00	3.00	9.00	-	11.76	4.06
31.00	7.00	44.00	53.00	47.00	11.00	19.00	108.00	51.00	217.50	69.80
30.10	31.80	12.40	14.50	17.80	10.20	55.80	61.20	11.40	37.60	15.00
3.01	0.50	5.13	5.19	5.71	0.64	1.67	12.68	3.70	12.60	6.10
1.07	2.41	1.14	1.31	1.52	0.35	3.83	2.34	0.66	3.45	0.91
37.90	5.10	54.70	62.60	66.00	13.70	23.00	62.50	64.00	146.60	69.80
1.28	0.12	1.66	2.31	2.50	0.59	0.85	3.07	1.80	4.71	1.41
3.12	0.52	4.70	5.86	4.99	0.73	1.58	12.53	3.78	10.87	5.54
0.38	1.04	0.17	0.13	0.12	0.37	0.48	0.55	-	0.70	*
0.05	0.05	0.05	0.05	0.05	0.05	0.05	0.80	-	1.10	*
0.83	0.17	1.21	1.43	1.27	0.28	0.49	3.18	1.14	5.79	2.54
0.25	0.05	0.39	0.43	0.47	0.06	0.15	1.05	0.25	1.07	1.01
0.05	0.05	1.40	1.40	9.20	2.50	1.80	4.90	1.00	4.30	1.90
0.05	0.80	0.05	0.05	0.05	0.05	0.05	1.40	7.50	*	*
2.20	0.50	1.50	6.50	2.60	1.30	5.30	6.60	3.30	638.50	148.10
*	*	*	*	*	*	*	*	0.11	0.30	*
*	*	*	*	*	*	*	*	1.10	7.30	5.80
25.58	19.31	17.03	17.70	321.00	50.29	41.33	50.86	18.00	33.53	6.21
63.83	37.30	39.60	41.13	47.92	13.25	73.30	136.00	37.17	67.47	12.76
5.87	3.17	3.81	4.09	4.86	1.23	5.39	12.70	4.30	7.96	1.61
24.00	13.20	14.40	15.60	18.80	4.91	21.00	51.30	16.28	29.70	5.94
5.46	2.92	2.79	3.17	3.98	1.09	4.12	11.29	3.25	5.98	1.36
1.57	1.20	0.65	0.74	0.93	0.29	1.55	3.01	0.65	1.00	0.15
5.95	4.04	2.59	2.91	3.80	1.22	5.68	12.45	2.71	5.32	1.03
0.88	0.64	0.36	0.42	0.52	0.20	0.85	1.83	0.42	0.81	0.17
4.98	3.95	2.09	2.48	3.00	1.29	5.38	10.40	2.25	4.96	1.81
1.01	0.90	0.46	0.53	0.63	0.31	1.34	2.15	0.46	1.15	0.45
2.23	2.25	1.12	1.30	1.55	0.86	3.35	4.94	1.21	3.06	1.35
0.32	0.34	0.18	0.20	0.23	0.14	0.49	0.72	0.21	0.48	0.26
1.85	2.07	1.11	1.21	1.40	0.95	2.73	4.27	1.19	2.85	1.76
0.29	0.34	0.17	0.19	0.22	0.15	0.44	0.66	0.18	0.42	0.26

TABLE 4. CONT.

B1-1 Shale Arosa Arosa	B1-2 Shale Arosa Arosa	B2 Shale Arosa Arosa	B6-1 Jaspe Arosa Arosa	B6-2 Jaspe Arosa Arosa	D3 Jaspe Arosa Arosa	D5 Radiolarite Arosa Arosa	D10 Shale Arosa Arosa
69.70	89.00	56.20	68.80	88.90	87.80	83.50	59.10
12.20	4.90	14.30	13.00	4.00	3.30	5.10	16.10
7.00	1.20	11.40	6.30	2.80	3.80	4.30	9.00
0.00	0.00	0.13	0.02	0.01	0.01	0.02	0.08
2.91	1.12	8.13	1.95	0.53	0.73	0.81	3.63
0.30	0.11	0.48	0.03	0.02	0.01	0.07	0.57
0.67	0.30	0.68	2.39	1.00	0.28	1.36	2.57
4.41	1.86	2.99	3.44	1.04	0.92	0.92	4.12
0.49	0.20	0.57	0.62	0.15	0.11	0.16	0.60
0.04	0.00	0.13	0.03	0.01	0.05	0.01	0.16
2.67	1.11	4.95	3.11	1.62	1.39	1.06	3.07
100.39	99.80	99.96	99.69	100.08	98.40	97.31	99.00
13.00	8.00	18.00	18.00	10.00	8.00	16.00	31.00
133.00	70.00	169.00	206.00	6.00	52.00	83.00	213.00
88.00	229.00	227.00	366.00	106.00	41.00	64.00	128.00
98.00	37.00	488.00	14.00	3.00	38.00	56.00	335.00
28.00	11.00	78.00	9.00	3.00	3.00	5.00	29.00
78.00	65.00	69.00	102.00	49.00	36.00	38.00	63.00
99.00	39.00	129.00	38.00	18.00	32.00	41.00	88.00
9.00	33.00	286.00	13.00	7.00	28.00	22.00	116.00
12.00	5.00	14.00	14.00	4.00	5.00	5.00	13.00
104.00	45.00	123.00	134.00	28.00	28.00	36.00	158.00
*	*	*	*	*	*	*	*
8.41	3.14	11.94	9.22	3.03	2.30	3.18	11.09
1.23	10.09	2.07	1.47	0.80	0.41	0.39	1.78
161.50	65.09	175.63	153.27	51.91	42.35	41.68	159.20
4.67	2.46	9.96	9.32	3.14	1.98	2.45	5.90
*	*	*	*	*	*	*	*
*	*	*	*	*	*	*	*
*	*	*	*	*	*	*	*
*	*	*	*	*	*	*	*
*	*	*	*	*	*	*	*
*	*	*	*	*	*	*	*
*	*	*	*	*	*	*	*
*	*	*	*	*	*	*	*
*	*	*	*	*	*	*	*
*	*	*	*	*	*	*	*
23.57	10.39	42.41	36.00	18.56	9.34	12.33	32.62
59.26	25.64	99.18	72.89	36.92	19.66	27.76	75.92
5.54	2.38	9.66	7.99	4.05	2.11	2.91	7.70
21.14	9.24	34.61	30.31	14.50	7.98	10.36	28.22
4.95	2.19	7.05	5.19	2.28	1.44	1.92	5.96
1.08	0.47	1.46	1.07	0.49	0.25	0.41	1.18
4.11	2.66	6.03	3.74	1.53	1.07	1.67	4.80
0.76	0.47	0.99	0.59	0.21	0.16	0.28	0.78
4.18	2.67	5.54	3.26	1.12	0.89	1.65	4.39
0.84	0.56	1.25	0.78	0.26	0.23	0.45	0.96
2.16	1.38	2.89	2.16	0.72	0.59	1.05	2.24
0.30	0.18	0.52	0.43	0.14	0.12	0.20	0.44
1.77	1.08	3.05	2.66	0.85	0.67	1.24	2.40
0.29	0.16	0.42	0.42	0.14	0.11	0.20	0.39

9. ACKNOWLEDGMENTS

Some of the serpentinized peridotite data are from *Müntener et al*. [2010] and part of the ED fault rocks data are from *Manatschal et al*. [2000]. We thank Emmanuel Masini and Geoffroy Mohn for earlier discussions. We also thank René Boutin and Damien Lemarchand for helping with the ICP-MS/AES analyses performed in the LHyGeS at Strasbourg University. We are in debt with former master students Martin Stub and Myriam Mahabot from the University of Strasbourg for helping with the analyses of some samples from the sedimentary section. This research was funded by Petrobras S.A.

10. REFERENCES

Aslanian, D. , M. Moulin, J.-L. Olivet, P. Unternehr, L. Matias, F. BAchet, M. RAbineau, H. Nouzeé, F. Klingelheofer, I. Contrucci, and C. Labails (2009), Brazilian and African passive margins of the Central Segment of the South Atlantic Ocean: Kinematic constraints, *Tectonophysics*, *468*(1-4), 98–112. doi: 10.1016/j.tecto.2008.12.016

Augustin, N., K. S. Lackschewitz, T. Kuhn, and C. W. Devey (2008), Mineralogical and chemical mass changes in mafic and ultramafic rocks from the Logatchev hydrothermal field (MAR 15°N), *Mar. Geol.*, *256*(1-4), 18–29, doi:10.1016/j.margeo.2008.09.004.

Barnes, J. D., H. Paulick, Z. D. Sharp, W. Bach, and G. Beaudoin (2009), Stable isotope ($\delta^{18}O$, δD, $\delta^{37}Cl$) evidence for multiple fluid histories in mid-Atlantic abyssal peridotites (ODP Leg 209), *Lithos*, *110*(1-4), 83–94, doi:10.1016/j.lithos.2008.12.004.

Baumgartner, P. O. (1987), Age and genesis of Tethyan Jurassic Radiolarites, *Eclogae Geol. Helv.*, *80*(3), 831–879.

Benedicto, A., V. Plagnes, P. Vergely, N. Flotte, and R. A. Schultz (2008), Fault and fluid interaction in a rifted margin: integrated study of calcite-sealed fault-related structures (southern Corinth margin), *Geol. Soc. London, Spec. Publ.*, *299*(1), 257–275, doi:10.1144/SP299.16.

Bernoulli, D., and H. Weissert (1985), Sedimentary fabrics in Alpine ophicalcites, south Pennine Arosa zone, Switzerland, *Geology*, 13, 755-758, doi:10.1130/0091-7613(1985)13<755.

Bernoulli, D., G. Manatschal, L. Desmurs, and O. Müntener (2003), *Where did Gustav Steinmann see the trinity? Back to the roots of an Alpine ophiolite concept. In: Special Paper 373: Ophiolite concept and the evolution of geological thought.*, edited by Y. Dilek and S. Newcomb, Geological Society of America.

Bertotti, G., V. Picotti, D. Bernoulli, and A. Castellarin (1993), From rifting to drifting: tectonic evolution of the South-Alpine upper crust from the Triassic to the Early Cretaceous, *Sediment. Geol.*, *86*(1-2), 53–76, doi:10.1016/0037-0738(93)90133-P.

Bons, P. D., M. a. Elburg, and E. Gomez-Rivas (2012), A review of the formation of tectonic veins and their microstructures, *J. Struct. Geol.*, *43*, 33–62, doi:10.1016/j.jsg.2012.07.005.

Boschi, C., G. L. Früh-Green, A. Delacour, J. A. Karson, and D. S. Kelley (2006), Mass transfer and fluid flow during detachment faulting and development of an oceanic core complex, Atlantis Massif (MAR 30°N), *Geochemistry, Geophys. Geosystems*, *7*(1), n/a–n/a, doi:10.1029/2005GC001074.

Bracciali, L., M. Marroni, P. Luca, and R. Sergio (2007), Geochemistry and petrography of Western Tethys Cretaceous sedimentary covers (Corsica and Northern Apennines): From source areas to configuration of margins, *Geol. Soc. Am. Spec. Pap.*, *420*, 73–93, doi:10.1130/2006.2420(06).

Bracciali, L., L. Pandolfi, and S. Rocchi (2013), A snapshot of the Late Jurassic Western Tethys seafloor composition and morphology provided by the geochemistry of pelitic sediments (Corsica, Central Alps and Northern Apennines), *Basin Res.*, *25*, 1–25, doi:10.1111/bre.12036.

Buatier, M. D., G. L. Früh-Green, and A. M. Karpoff (1995), Mechanisms of Mg-phyllosilicate formation in a hydrothermal system at a sedimented ridge (Middle Valley, Juan de Fuca), *Contrib. to Mineral. Petrol.*, *122*(1-2), 134–151, doi:10.1007/s004100050117.

Burkhard, D. J. M., and J. R. O'Neil (1988), Contrasting serpentinization processes in the eastern Central Alps, *Contrib. to Mineral. Petrol.*, *99*, 498–506.

Cannat, M. (1993), Emplacement of mantle rocks in the seafloor at mid-ocean ridges, *J. Geophys. Res.*, *98*(B3), 4163, doi:10.1029/92JB02221.

Castelain, T., A. M. McCaig, and R. A. Cliff (2014), Fluid evolution in an Oceanic Core Complex: A fluid inclusion study from IODP hole U1309 D-Atlantis Massif, 30°N, Mid-Atlantic Ridge, *Geochemistry, Geophys. Geosystems*, *15*(4), 1193–1214, doi:10.1002/2013GC004975.

Channell, J., and H. Kozur (1997), How many oceans? Meliata, Vardar and Pindos oceans in Mesozoic Alpine paleogeography, *Geology*, *25*(2), 183–186, doi:10.1130/0091-7613(1997)025<0183.

Condie, K. C. (1993), Chemical composition and evolution of the upper continental crust: Contrasting results from surface samples and shales, *Chem. Geol.*, *104*(1-4), 1–37, doi:10.1016/0009-2541(93)90140-E.

Contrucci, I., L. Matias, M. Moulin, L. Géli, F. Klingelhofer, H. Nouzé, D. Aslanian, J.-L. Olivet, J.-P. Réhault, and J.-C. Sibuet (2004), Deep structure of the West African continental margin (Congo, Zaïre, Angola), between 5°S and 8°S, from reflection/refraction seismics and gravity data, *Geophys. J. Int.*, *158*(2), 529–553, doi:10.1111/j.1365-246X.2004.02303.x.

Cordey, F., and A. Bailly (2007), Alpine ocean seafloor spreading and onset of pelagic sedimentation: new radiolarian data from the Chenaillet-Montgenèvre ophiolite (French-Italian Alps), *Geodin. Acta*, *20*(3), 131–138, doi:10.3166/ga.20.131-138.

Cornelius, H. P. (1932), Geologische Karte der Err-Julier-Gruppe 1:25000., *Schweiz geol Komm Spezialkarte*, *115A*.

Decandia, F. A., and P. Elter (1972), La zona ofiolitifera del Bracco nel settore compreso fra Levanto e la Val Graveglia (Appennino Ligure), *Mem. Soc. Geol. Ital*, *11*, 503–530.

Delacour, A., G. L. Früh-Green, S. M. Bernasconi, P. Schaeffer, and D. S. Kelley (2008), Carbon geo-

chemistry of serpentinites in the Lost City Hydrothermal System (30°N, MAR), *Geochim. Cosmochim. Acta*, *72*(15), 3681–3702, doi:10.1016/j.gca.2008.04.039.

deMartin, B. J., R. A. Sohn, J. Pablo Canales, and S. E. Humphris (2007), Kinematics and geometry of active detachment faulting beneath the Trans-Atlantic Geotraverse (TAG) hydrothermal field on the Mid-Atlantic Ridge, *Geology*, *35*(8), 711, doi:10.1130/G23718A.1.

Desmurs, L., G. Manatschal, and D. Bernoulli (2001), The Steinmann Trinity revisited: mantle exhumation and magmatism along an ocean-continent transition: the Platta nappe, eastern Switzerland, *Geol. Soc. London, Spec. Publ.*, *187*(1), 235–266, doi:10.1144/GSL.SP.2001.187.01.12.

Destrigneville, C., A. M. Karpoff, and D. Charpentier (1998) Modelling the halmyrolytic formation of palygorskite from serpentinite. *Water-Rock Interaction-WRI 9 Proc.*, G. Arehart and J. Hulston (eds), *Balkema Publ.*, pp. 715-718

Dewit, J., A. Foubert, H. A. El Desouky, P. Muchez, D. Hunt, and R. Swennen (2012), Dolomitisation model of hydrothermal dolomites (HTD) hosted by Aptian-Albian carbonates of the Ramales platform (Basque-Cantabrian basin, northern Spain), in *GEOFLUIDS VII – International Conference*, pp. 75–78, Paris, Fance

Dias, Á. S., and F. J. A. S. Barriga (2006), Mineralogy and geochemistry of hydrothermal sediments from the serpentinite-hosted Saldanha hydrothermal field (36°34′N; 33°26′W) at MAR, *Mar. Geol.*, *225*(1–4), 157–175, doi:http://dx.doi.org/10.1016/j.margeo.2005.07.013.

Dias, Á. S., G. L. Früh-Green, S. M. Bernasconi, and F. J. A. S. Barriga (2011), Geochemistry and stable isotope constraints on high-temperature activity from sediment cores of the Saldanha hydrothermal field, *Mar. Geol.*, *279*(1–4), 128–140, doi:http://dx.doi.org/10.1016/j.margeo.2010.10.017.

Dommergues, J.-L., C. Meister, and G. Manatschal (2012), Early Jurassic ammonites from Bivio (Lower Austroalpine unit) and Ardez (Middle Penninic unit) areas: a biostratigraphic tool to date the rifting in the Eastern Swiss Alps, *Rev. Paléobiologie*, *Genève*, *11*, 43–52.

Douville, E., J. L. Charlou, E. H. Oelkers, P. Bienvenu, C. F. J. Colon, J.P. Donval, Y. Fouquet, D. Prieur and P. Appriou (2002), The Rainbow vent fluids (36°14'N, MAR): the influence of ultramafic rocks and phase separation on trace metal content in Mid-Atlantic Ridge hydrothermal fluids, *Chem. Geol.*, *184*, 37–48, doi:10.1016/S0009-2541(01)00351-5.

Eberli, G. (1988), The evolution of the southern continental margin of the Jurassic Tethys Ocen as recorded in the Allgäu Formation of the Austroalpine Nappes of Graubünden (Switzerland), *Eclogae Geol. Helv.*, *81*(1), 175–214.

Edmonds, H. N. (2010), Chemical signatures from hydrothermal venting on slow spreading ridges, in *Diversity of Hydrothermal Systems on Slow Spreading Ocean Ridges*, vol. 188, pp. 27–42, AGU, Washington, DC.

Engström, A., A. Skelton, and N. Grassineau (2007), Isotopic and petrological evidence of fluid-rock interaction at a Tethyan ocean-continent transition in the Alps: implications for tectonic processes and carbon transfer during early ocean formation, *Geofluids*, *7*(4), 401–414, doi:10.1111/j.1468-8123.2007.00194.x.

Evans, B. W., K. Hattori, and A. Baronnet (2013), Serpentinite: What, Why, Where?, *Elements*, *9*(2), 99–106, doi:10.2113/gselements.9.2.99.

Evans, J. P., C. B. Forster, and J. V. Goddard (1997), Permeability of fault-related rocks, and implications for hydraulic structure of fault zones, *J. Struct. Geol.*, *19*(11), 1393–1404, doi:10.1016/S0191-8141(97)00057-6.

Ferreiro Mählmann, R. (1996), The pattern of diagenesis and metamorphism by vitrinite reflectance and illite“ crystallinity” in Mittelbünden and in the Oberhalbstein: Part 2: Correlation of coal petrographical and of mineralogical parameters, *Schweizerische Mineral. und Petrogr. Mitteilungen, 76*, 23–46.

Finger, W. (1978), Die Zone von Samaden (unterostalpine Decken, Graubünden) und ihre jurassischen Brekzien, PhD thesis, ETH Zürich, doi:10.3929/ethz-a-000164017.

Fouquet, Y., P. Cambon, J. Etoubleau, J.-L. Charlou, H. Ondreas, F.J.A.S. Barriga, G. Cherkashov, T. Semkova, I. Poroshina, M. Bohn, J.-P. Donval, K. Henry, P. Murphy, and O. Rouxel, (2010), Geodiversity of hydrothermal processes along the Mid-Atlantic Ridge and ultramafic-hosted mineralization: A new type of oceanic Cu-Zn-Co-Au volcanogenic massive sulfide deposit, in *Diversity of Hydrothermal Systems on Slow Spreading Ocean Ridges*, vol. 188, pp. 321–367, AGU, Washington, DC. doi: 10.1029/2008GM000746

Foustoukos, D. I., I. P. Savov, and D. R. Janecky (2008), Chemical and isotopic constraints on water/rock interactions at the Lost City hydrothermal field, 30°N Mid-Atlantic Ridge, *Geochim. Cosmochim. Acta*, *72*(22), 5457–5474, doi:10.1016/j.gca.2008.07.035.

Froitzheim, N., and G. P. Eberli (1990), Extensional detachment faulting in the evolution of a Tethys passive continental margin, Eastern Alps, Switzerland, *Geol. Soc. Am. Bull.*, *102*(9), 1297–1308.

Froitzheim, N., and G. Manatschal (1996), Kinematics of Jurassic rifting, mantle exhumation, and passive-margin formation in the Austroalpine and Penninic nappes (eastern Switzerland), *Geol. Soc. Am. Bull.*, *108*(9), 1120–1133.

Früh-Green, G. L., H. Weissert, and D. Bernoulli (1990), A multiple fluid history recorded in Alpine ophiolites, *J. Geol. Soc. London.*, *147*, 959–970, doi: 10.1144/gsjgs.147.6.0959

Gibson, I. L., M. Beslier, G. Cornen, K. L. Milliken, and K. E. Seifert (1996), Major- and trace-element seawater alteration profiles in serpentinite formed during the development of the Iberia margin Site 897, *Proc. ODP, Sci. Results*, *149*, in Whitmarsh, R. B., Sawyer, D. S., Klaus, A., and Masson, D. G. (Eds.), College Station, TX (Ocean Drilling Program), 519–527, doi: 10.2973/odp.proc.sr.149.219.1996

Gresens, R. (1967), Composition-volume relationships of metasomatism, *Chem. Geol.*, *2*, 47–65.

Jin, Z., L. Zhang, L. Yang, and W. Hu (2004), A preliminary study of mantle-derived fluids and their effects on oil/gas generation in sedimentary basins, *J. Pet. Sci. Eng.*, *41*(1-3), 45–55, doi:10.1016/S0920-4105(03)00142-6.

Jöns, N., W. Bach, M. Rosner, and B. Plessen (2013), Formation of late-stage mineral veins in the footwall of an oceanic detachment fault (ODP Leg 304/305), *Geophysical Research Abstracts, 15*,

EGU2013-5457, EGU General Assembly Vienna, Austria

Karpoff, A. M., A.-V. Walter, and C. Pflumio (1988), Metalliferous sediments within lava sequences of the Sumail ophiolite (Oman): Mineralogical and geochemical characterization, origin and evolution, *Tectonophysics*, *151*(1-4), 223–245, doi:10.1016/0040-1951(88)90247-8.

Kelley, D. S., and T. M. Shank (2010), Hydrothermal systems: A decade of discovery in slow spreading environments, in *Diversity of Hydrothermal Systems on Slow Spreading Ocean Ridges*, vol. 188, pp. 369–407, AGU, Washington, DC.

Kelley, D. S., A. Jeffrey, D. K. Blackman, G. L. Früh-Green, D. A. Butterfield, M. D. Lilley, E. J. Olson, M. O. Schrenk, K. K. Roe, G. T. Lebon, and P. Rivizzigno, (2001), An off-axis hydrothermal vent field near the Mid-Atlantic Ridge at 30 degrees N., *Nature*, *412*(6843), 145–149, doi:10.1038/35084000.

Klein, F., W. Bach, S. E. Humphris, W.-A. Kahl, N. Jons, B. Moskowitz, and T. S. Berquo (2013), Magnetite in seafloor serpentinite--Some like it hot, *Geology*, *42*(2), 135–138, doi:10.1130/G35068.1.

Klein-BenDavid, O., T. Pettke, and R. Kessel (2011), Chromium mobility in hydrous fluids at upper mantle conditions, *Lithos, 125*(1-2), 122-130, doi: 10.1016/j.lithos.2011.02.002

Klemme, S. (2004), The influence of Cr on the garnet–spinel transition in the Earth's mantle: experiments in the system $MgO–Cr_2O_3–SiO_2$ and thermodynamic modelling, *Lithos*, *77*(1-4), 639–646, doi:10.1016/j.lithos.2004.03.017.

Lagabrielle, Y., and M. Cannat (1990), Alpine Jurassic ophiolites resemble the modern central Atlantic basement, *Geology*, *18*, 319–332, doi:10.1130/0091-7613(1990)018<0319.

Lemoine, M., and R. Trümpy (1987), Pre-oceanic rifting in the Alps, *Tectonophysics*, *133*, 305–320.

Lemoine, M., T. Bas, M. Bourbon, P.-C. Graciansky, J.-L. Rudkiewicz, J. Megard-Galli, and P. Tricart (1986), The continental margin of the Mesozoic Tethys in the Western Alps, *Mar. Pet. Geol.*, *3*, 179–199.

Lemoine, M., P. Tricart, and G. Boillot (1987), Ultramafic and gabbroic ocean floor of the Ligurian Tethys (Alps, Corsica, Apennines): In search of a genetic imodel, *Geology*, *15*(7), 622.

López-Horgue, M. A., E. Iriarte, S. Schröder, P. A. Fernández-Mendiola, B. Caline, H. Corneyllie, J. Frémont, M. Sudrie, and S. Zerti (2010), Structurally controlled hydrothermal dolomites in Albian carbonates of the Asón valley, Basque Cantabrian Basin, Northern Spain, *Mar. Pet. Geol.*, *27*(5), 1069–1092, doi:10.1016/j.marpetgeo.2009.10.015.

MacLeod, C. J., R. C. Searle, B. J. Murton, J. F. Casey, C. Mallows, S. C. Unsworth, K. L. Achenbach, and M. Harris (2009), Life cycle of oceanic core complexes, *Earth Planet. Sci. Lett.*, *287*(3-4), 333–344, doi:10.1016/j.epsl.2009.08.016.

Manatschal, G. (1995), *Jurassic rifting and formation of a passive continental margin (Platta and Err nappes, Eastern Switzerland): geometry, kinematics and geochemestry of fault rocks and a comparision with the Galicia margin*, PhD Thesis, ETH Zürich. http://dx.doi.org/10.3929/ethz-a-001533748

Manatschal, G. (1999), Fluid-and reaction-assisted low-angle normal faulting: evidence from rift-related brittle fault rocks in the Alps (Err Nappe, eastern Switzerland), *J. Struct. Geol.*, *21*(7), 777–793.

Manatschal, G. (2004), New models for evolution of magma-poor rifted margins based on a review of data and concepts from West Iberia and the Alps, *Int. J. Earth Sci.*, *93*(3), 1–35. doi: 10.1007/s00531-004-0394-7

Manatschal, G., and D. Bernoulli (1998), Rifting and early evolution of ancient ocean basins: the record of the Mesozoic Tethys and of the Galicia-Newfoundland margins, *Mar. Geophys. Res.*, 371–381.

Manatschal, G., and O. Müntener (2009), A type sequence across an ancient magma-poor ocean–continent transition: the example of the western Alpine Tethys ophiolites, *Tectonophysics*, *473*(1-2), 4–19, doi: 10.1016/j.tecto.2008.07.021

Manatschal, G., and P. Nievergelt (1997), A continent-ocean transition recorded in the Err and Platta nappes (Eastern Switzerland), *Eclogae Geol. Helv.*, *90*(1), 3–27.

Manatschal, G., D. Marquer, and G. L. Früh-Green (2000), Channelized fluid flow and mass transfer along a rift-related detachment fault (Eastern Alps, southeast Switzerland), *Geol. Soc. Am. Bull.*, *112*(1), 21. doi: 10.1130/0016-7606(2000)112<21:CFFAMT>2.0.CO;2

Manatschal, G., N. Froitzheim, M. Rubenach, and B. D. Turrin (2001), The role of detachment faulting in the formation of an ocean-continent transition: insights from the Iberia Abyssal Plain, *Geol. Soc. London, Spec. Publ.*, *187*(1), 405–428.

Manatschal, G., O. Muntener, and L. Desmurs (2003), An ancient-ocean-continent transition in the Alps: the Totalp, Err-Platta, and Malenco units in the eastern Central Alps (Graubünden and northern Italy), *Eclogae Geol. Helv.*, *96*(1), 131–146, doi:10.5169/seals-169013.

Marroni, M., L. Pandolfi, and N. Perilli (2000), Calcareous nannofossil dating of the San Martino formation from the Balagne ophiolite sequence (alpine Corsica): comparison with the Palombini shale of the northern Apennine, *Ofioliti*, *25*(2), 147–155.

Masini, E., G. Manatschal, G. Mohn, J. Ghienne, and F. Lafont (2011), The tectono-sedimentary evolution of a supra-detachment rift basin at a deep-water magma-poor rifted margin: the example of the Samedan Basin preserved in the Err nappe in SE Switzerland, *Basin Research, 23* (6), 652–677, **doi:** 10.1111/j.1365-2117.2011.00509.x

Masini, E., G. Manatschal, G. Mohn, and P. Unternehr (2012), Anatomy and tectono-sedimentary evolution of a rift-related detachment system: The example of the Err detachment (central Alps, SE Switzerland), *Geol. Soc. Am. Bull.*, *124*(9-10), 1535–1551, doi:10.1130/B30557.1.

Masini, E., G. Manatschal, and G. Mohn (2013), The Alpine Tethys rifted margins: Reconciling old and new ideas to understand the stratigraphic architecture of magma-poor rifted margins, edited by H. Weissert, *Sedimentology*, *60*(1), 174–196, doi:10.1111/sed.12017.

McCaig, A. M., R. a. Cliff, J. Escartin, A. E. Fallick, and C. J. MacLeod (2007), Oceanic detachment faults focus very large volumes of black smoker fluids, *Geology*, *35*(10), 935, doi:10.1130/G23657A.1.

McKenzie, J., A. Isern, A. M. Karpoff, and P. Swart (1990), Basal dolomitic sediments, Tyrrhenian sea,

ODP Leg 107, *Proc. ODP, Sci. Results*, *107*, in: Kastens, K. A., Mascle, J., et al., (Eds), College Station, TX (Ocean Drilling Program), 141-152, doi:10.2973/odp.proc.sr.107.124.1990

Miller, D. J., and N. I. Christensen (1997), Seismic velocities of lower crustal and upper mantle rocks from the slow-spreading Mid-Atlantic ridge south of the Kane transform zone (MARK), in *Proc. ODP Sci. Results*, *153*, in: Karson J. A., Cannat M., Miller D. J., Elthon D. (Eds), College Station, TX (Ocean Drilling Program), 437–454.

Mitchell, T. M., and D. R. Faulkner (2012), Towards quantifying the matrix permeability of fault damage zones in low porosity rocks, *Earth Planet. Sci. Lett.*, *339-340*, 24–31, doi:10.1016/j.epsl.2012.05.014.

Mohn, G., G. Manatschal, O. Müntener, M. Beltrando, and E. Masini (2010), Unravelling the interaction between tectonic and sedimentary processes during lithospheric thinning in the Alpine Tethys margins, *Int. J. Earth Sci.*, *99*, 75–101, doi: 10.1007/s00531-010-0566-6

Mohn, G., G. Manatschal, and E. Masini (2011), Rift-related inheritance in orogens: a case study from the Austroalpine nappes in Central Alps (SE-Switzerland and N-Italy), *J. Earth Sci. 100* (5), 937-961, doi: 10.1007/s00531-010-0630-2

Mohn, G., G. Manatschal, M. Beltrando, E. Masini, and N. Kusznir (2012), Necking of continental crust in magma-poor rifted margins: Evidence from the fossil Alpine Tethys margins, *Tectonics*, *31*(1), TC1012, doi:10.1029/2011TC002961.

Moody, J. B. (1976), Serpentinization: a review, *Lithos*, *9*(2), 125–138, doi:10.1016/0024-4937(76)90030-X.

Morgan, J. K., and K. L. Milliken (1996), Petrography of calcite veins in serpentinized peridotite basement rocks from the Iberia abyssal plain, Sites 897 and 899: kinematic and environmental implications, *Proc. Ocean Drill. Program, Sci. Results*, *149*, in: Whitmarsh, R. B., Sawyer, D. S., Klaus, A., and Masson, D. G. (Eds.), College Station, TX (Ocean Drilling Program), 559–569. doi: 10.2973/odp.proc.sr.149.230.1996

Morrow, C. A., L. Q. Shi, and J. D. Byerlee (1984), Permeability of fault gouge under confining pressure and shear stress, *J. Geophys. Res.*, *89*(B5), 3193, doi:10.1029/JB089iB05p03193.

Müntener, O., J. Hermann, and V. Trommsdorff (2000), Cooling history and exhumation of lower-crustal granulite and upper mantle (Malenco, eastern Central Alps), *J. Petrol.*, *41*(2), 175–200, doi:10.1093/petrology/41.2.175.

Müntener, O., G. Manatschal, L. Desmurs, and T. Pettke (2010), Plagioclase peridotites in ocean-continent transitions: refertilized mantle domains generated by melt stagnation in the Shallow mantle lithosphere, *J. Petrol.*, *51*(1-2), 255–294, doi:10.1093/petrology/egp087.

Péron-Pinvidic, G., and G. Manatschal (2009), The final rifting evolution at deep magma-poor passive margins from Iberia-Newfoundland: a new point of view, *Int. J. Earth Sci.*, *98*(7), 1581–1597.

Perseil, E. A., and L. Latouche (1989), Découverte de microstructures de nodules polymétaliques dans les minéralisations manganésifères métamorphiques de Falotta et de Parsettens (Grisons-Suisse), *Miner. Depos.*, *24*, 111–116.

Peters, T., and A. Stettler (1987), Radiometric age , thermobarometry and mode of emplacement of the Totalp periodite in the Eastern Swiss Alps, *Schweizerische Mineral. und Petrogr. Mitteilungen*, *67*(3), 285–294.

Picazo, S. (2012), *Déformation des roches ultramafiques liée à l'exhumation dans les dorsales et les transitions océan continent,* PhD thesis, Institut de Physique du Globe, Paris, 258 pp.,

Picazo, S., G. Manatschal, M. Cannat, and M. Andréani (2013), Deformation associated to exhumation of serpentinized mantle rocks in a fossil Ocean Continent Transition: The Totalp unit in SE Switzerland, *Lithos*, *175-176*, 255–271, doi:10.1016/j.lithos.2013.05.010.

Potdevin, J. L., and D. Marquer (1987), Quantitative methods for the estimation of mass transfers by fluids in deformed metamorphic rocks, *Geodin. Acta*, *1*(3), 193–206.

Von Quadt, A., M. Grünefelder, and H. Büchi (1994), U-Pb zircon ages from igneous rocks of the Bernina nappe system (Grisons, Switzerland), *Schweizerische Mineral. und Petrogr. Mitteilungen*, *74*, 373–382.

Raumer, J. Von (1998), The Paleozoic evolution in the Alps: from Gondwana to Pangea, *Geol. Rundschau*, *87*, 407–435.

Reston, T. J., and C. R. Ranero (2011), The 3-D geometry of detachment faulting at mid-ocean ridges, *Geochemistry, Geophys. Geosystems*, *12*(7), 1–19, doi:10.1029/2011GC003666.

Rouméjon S., and M. Cannat (2014), Serpentinization of mantle-derived peridotites at mid-ocean ridges: Mesh texture development in the context of tectonic exhumation, *Geochem.Geophys. Geosyst., 15*, doi:10.1002/ 2013GC005148

Roux, M., J. P. Bourseau, T. Bas, T. Dumont, P. C. de Graciansky, M. Lemoine, and J. L. Rudkiewicz (1988), Bathymetric evolution of the Tethyan margin in the Western Alps (data from stalked crinoids); a reappraisal of eustatism problems during the Jurassic, *Bull. Soc. Geol. France*, *IV* (4), 633–641, doi:10.2113/gssgfbull.IV.4.633.

Saito, M. A., A. E. Noble, A. Tagliabue, T. J. Goepfert, C. H. Lamborg, and W. J. Jenkins (2013), Slow-spreading submarine ridges in the South Atlantic as a significant oceanic iron source, *Nat. Geosci.*, *6*(9), 775–779, doi:10.1038/ngeo1893.

Santos Neto, E. V., J. R. Cerqueira, and A. Prinzhofer (2011), Natural gas geochemistry of the southern offshore Brazilian Basins, in *International Meeting on Organic Geochemistry*, p. 264.

Schaltegger, U., L. Desmurs, G. Manatschal, O. Muntener, M. Meier, M. Frank, and D. Bernoulli (2002), The transition from rifting to sea-floor spreading within a magma-poor rifted margin: field and isotopic constraints, *Terra Nova*, *14*, 156–162.

Schmid, S. M., B. F Genschuh, E. Kissling, R. Schuster, and B. Fugenschuh (2004), Tectonic map and overall architecture of the Alpine orogen, *Eclogae Geol. Helv.*, *97*(1), 93–117.

Schmidt, K., A. Koschinsky, D. Garbe-Schönberg, L. M. de Carvalho, and R. Seifert (2007), Geochemistry of hydrothermal fluids from the ultramafic-hosted Logatchev hydrothermal field, 15°N on the Mid-Atlantic Ridge: Temporal and spatial investigation, *Chem. Geol.*, *242*(1–2), 1–21, doi:http://

dx.doi.org/10.1016/j.chemgeo.2007.01.023.

Schuiling, R. D. (1964), Serpentinization as a possible cause of high heat-flow values in and near the oceanic ridges, *Nature*, *201*(4921), 807–808, doi:10.1038/201807b0.

Seyfried, W. E., N. J. Pester, K. Ding, and M. Rough (2011), Vent fluid chemistry of the Rainbow hydrothermal system (36°N, MAR): Phase equilibria and in situ pH controls on subseafloor alteration processes, *Geochim. Cosmochim. Acta*, *75*(6), 1574–1593, doi:10.1016/j.gca.2011.01.001.

Stipp, M., H. Stünitz, R. Heilbronner, and S. Schmid (2002), The eastern Tonale fault zone: a "natural laboratory" for crystal plastic deformation of quartz over a temperature range from 250 to 700°C, *J. Struct. Geol.*, *24*(12), 1861–1884, doi: 10.1016/S0191-8141(02)00035-4

Szatmari, P., T. C. O. Fonseca, and N. F. Miekeley (2011), Mantle-like trace element composition of petroleum – Contributions from serpentinizing peridotites, in: *Tectonics*, Closson D., editor, ch.13, 1–28. doi: 10.5772/14063.

Tenthorey, E., and J. Fitzgerald (2006), Feedbacks between deformation, hydrothermal reaction and permeability evolution in the crust: Experimental insights, *Earth Planet. Sci. Lett.*, *247*(1-2), 117–129, doi:10.1016/j.epsl.2006.05.005.

Torfstein, A. (2012), Size fractionation, reproducibility and provenance of helium isotopes in north-equatorial pacific pelagic clays, *Earth Planet. Sci. Lett.*, *339-340*, 151–163, doi:10.1016/j.epsl.2012.05.030.

Trommsdorff, V., and B. W. Evans (1974), Alpine metamorphism of peridotitic rocks, *Schweizerische Mineral. und Petrogr. Mitteilungen, 54*, 333–354.

Trümpy, R. (1975), Penninic-Austroalpine boundary in the Swiss Alps: A presumed former continental margin and its problems, *Am. J. Sci.*, *275-A*, 209–238.

Tucholke, B. E., and J. Lin (1994), A geological model for the structure of ridge segments in slow spreading ocean crust, *J. Geophys. Res.*, *99*(B6), 11937, doi:10.1029/94JB00338.

Whitmarsh, R. B., M. O. Beslier, P. J. Wallace, et al., (1998), Editors, *Proc. ODP, Initial Reports, 173,* College Station, TX (Ocean Drilling Program), doi: 10.2973/odp.proc.ir.173.1998

Whitney, D. L., C. Teyssier, P. Rey, and W. R. Buck (2012), Continental and oceanic core complexes, *Geol. Soc. Am. Bull.*, doi:10.1130/B30754.1.

ARTICLE 2

LINKING TECTONIC AND FLUID HISTORY DURING THE FORMATION OF HYPEREXTENDED DOMAINS:

the examples of Tasna in the Alps, Mauléon in the Pyrenees and Hobby High at deep Iberian Margin

Victor Hugo G. Pinto[1,2], Gianreto Manatschal[1], Anne Marie Karpoff[1], Emmanuel Masini[1] and Adriano Viana[2]

[1]Institut de Physique du Globe de Strasbourg, CNRS UMR7516, Université de Strasbourg

1 rue Blessig, 67084 Strasbourg Cedex, France

[2]Exploration & Production, Petrobras S.A., Av. República do Chile, 330, Rio de Janeiro, Brazil

ABSTRACT

Late-stage of extension in magma-poor rifted systems is characterized by extreme crustal thinning and mantle exhumation resulting in hyperextended domains. During these stages, extensional detachment fault systems cut through a thinned continental crust and reach the mantle allowing seawater to percolate resulting in the saussuritization of continental crust and the serpentinization of the mantle. These processes lead to losses of elements in both mantle and continental crust.

We present geological observations and geochemistry data from present-day Iberia-Newfoundland conjugated rifted margins, the fossil Alpine Tethyan margins and the West Pyrenees hyperextended system to show evidences for large-scale fluid flow and the conditions they were developed. The results points to two types of fluids, one dominated by the interaction of seawater and continental crustal rocks producing Si-Ca-enriched fluids, and another characterized by seawater-mantle interaction leading to serpentinization and major losses in Si, Mg, Fe, Mn, Ca, Ni and Cr. Fluids formed by serpentinization can be traced using Ni-Cr-V and Fe-Mn along fault zones related to extensional detachment faults and in the overlying sedimentary rocks. The data set from these three hyperextended domains allowed us to date the relative age of fluid formation and migration. Because similar observations can be made at different extensional systems, we conclude that fluid percolation is an important and characteristic process during the evolution of hyperextended domains. Serpentinization associated with mantle exhumation is observed at many rifted margins worldwide, and may have been formed when basins and seaways were not fully connected to oceans. In basins that remain isolated and/or restricted during late stages of rifting, these fluids can have a significant importance for changing the composition of seawater and the chemistry of sediments.

TABLE OF CONTENTS

1. INTRODUCTION

Fluid-flow along extensional detachment faults are often described in magma-poor rifted margins [*Manatschal*, 1999; *Manatschal et al*., 2000; *Pinto et al*., 2014b, in prep.], in continental metamorphic core complexes [*Hayman*, 2006] and ocean core complexes [*McCaig et al*., 2007]. While in metamorphic core complexes meteoric water interacts with continental crustal rocks leading to saussuritization, in oceanic core complexes the interaction between seawater and mantle leads to serpentinization [*Boschi et al*., 2006; *McCaig et al*., 2007; *Castelain et al*., 2014]. At magma-poor rifted margins, seawater interaction with continental crust also leads to the saussuritization along extensional detachment systems [*Manatschal*, 1999; *Pinto et al*., 2014b, in prep.]. Some of these faults are also responsible to mantle exhumation and consequently for triggering serpentinization [*Pinto et al*., 2014b, in prep.].

Fluids formed by serpentinization have been pointed as an important source of elements that may be linked with the origin of life [*Kelley et al*., 2005; *Russell*, 2007; *Müntener*, 2010]. They can be collected in active ultramafic-hosted hydrothermal vents and their chemical composition is described [*Kelley et al*., 2001; *Shanks*, 2001; *Fouquet et al*., 2010]. When expelled through hydrothermal systems, they eventually oxidize precipitating on the ocean floor [*Fouquet et al*., 2010] with sediments [*Dias and Barriga*, 2006; *Dias et al*., 2011] allowing a chemical comparison between fluids and their resulting oxides.

Serpentinization is also a common process at distal parts of magma-poor rifted margins [*Boillot et al*., 1988; *Manatschal and Bernoulli*, 1998; *Péron-Pinvidic and Manatschal*, 2009] in zones known as Ocean-Continent Transition (OCT). Many examples show that these zones can extend through hundreds of kilometers [*Dean and Minshull*, 2000; *Sutra et al*., 2013] in a dip section and over large areas transversely to the margin. Serpentinization may occur down to 5-6 km, as indicated by seismic velocity data in the Iberia and Newfoundland margins [*Dean and Minshull*, 2000; *Hopper et al*., 2007; *Afilhado et al*., 2008; *Minshull et al*., 2014]. Therefore, the serpentinization of the mantle has to be related with a considerable quantity of fluids enriched in elements from the mantle [*Pinto et al*., 2014a, in prep.]. *Pinto et al*., [2014b, in prep.] showed that the serpentinization starts beneath thinned continental crust prior to exhumation of the mantle at the seafloor and that these fluids can migrate through extensional detachment systems toward supradetachment basins affecting the syn-tectonic sediments. In a second stage, extension of the future distal margin leads to development of basins that can be restricted and isolated from the global oceans. At this stage, fluids could *pollute* the seawater and interact with the post-rift sedi-

ments. The element losses due to serpentinization and saussuritization can have a strong impact on seawater composition and the nature of pre-rift and syn-exhumation sediments. Large amount of SiO_2+MgO+CaO+FeO+MnO, that corresponds to about 10% to 30% of the original mass of peridotites, can be lost during serpentinization [*Pinto et al*., 2014a, in prep.]. This may lead to considerable changes in the chemistry of seawater. Considering that many margins worldwide went on mantle exhumation during Cretaceous time, it may also have a more global impact. Therefore, the study of the role of mantle-related fluids in distal margins are extremely important for understanding the changes in the seawater chemistry, changes on syn- to post-diagenetic process in distal margins and in the rheology of the lithosphere. In this work we present evidence that continental crust- and mantle-related fluids migrate through extensional detachment faults, and also affect the sedimentary section during the formation of hyperextended domains and mantle exhumation at late stage of rifting. The imprint of these fluids occur in syn- to post-tectonic sediments affecting them during eodiagenetic processes, which allow us to define the age of the fluids percolation in the sedimentary basin.

2. EXAMPLES OF HYPEREXTENDED DOMAINS FROM MAGMA-POOR RIFT SYSTEMS

Hyperextended domains in magma-poor rifted systems are characterized by thinned continental crust, commonly less than 10 km thick. In these domains, extensional detachment systems usually cut through the thinned continental crust rooting in the mantle leading to serpentinization (Figure 1A) [*Pinto et al*., 2014b, in prep.]. Eventually, they result in mantle exhumation to the seafloor along extensional detachment systems. Hyperextended domains can evolve leading to the formation of a zone of exhumed subcontinental mantle (ZECM) that can be progressively affected by rare to moderate magmatic addition (Figure 1B), which can develop sea-floor spreading in between conjugate margins (Figure 1C). In magma-poor rifted margins, part of the thinned continental crust and the ZECM affected by incipient magmatism characterizes the Ocean-Continent Transition (OCT) [*Desmurs et al*., 2001; *Bronner et al*., 2011; *Manatschal et al*., 2011].

In the studied systems, the hyperextended domains exhibit some particularities related to their formation and evolution. Some of them are more evolved resulting in extensive zones of exhumed mantle and posterior embryonic oceanic crust formation (e.g, Iberian Margin), while others present similar characteristic but less evolved and occurs in a smaller scale (e.g, Alpine Tethys) or even do not present expressive mantle exhumation (e.g., West Pyrenees). Despite some local differences, those magma-poor systems share characteristics and processes that include hyper-

extension, serpentinization and mantle exhumation occurring in restricted basins, which enable us to study the link between their formation and the role of fluids (Figure 2 A-B).

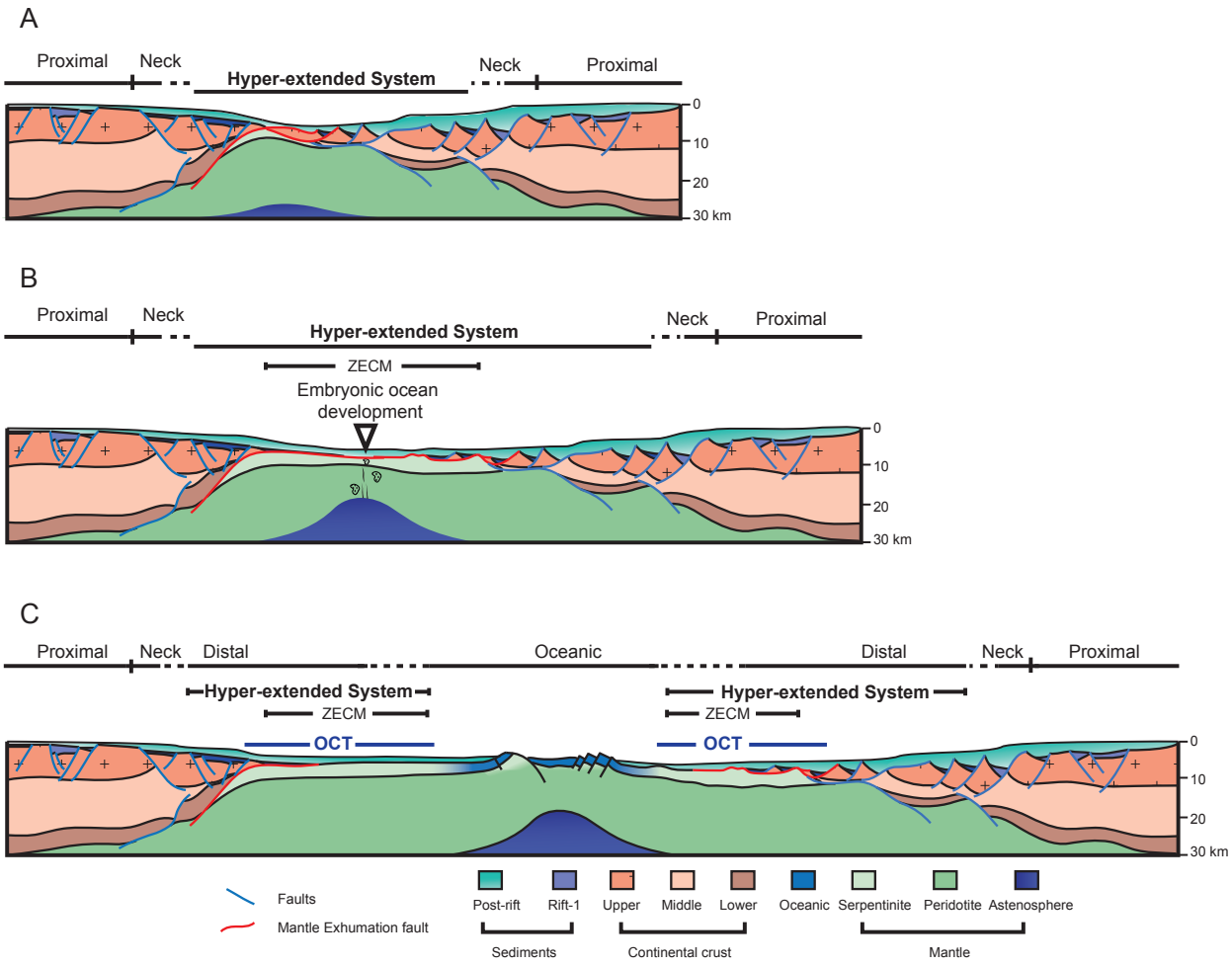

Figure 1. Evolution of hyperextended system and magma-poor rifted margin formation. (A) The deformation is focused in a narrow zone forming a hyperextended domain where detachment faults root in the mantle. (B) Mantle rocks are exhumed at the seafloor along extensional detachment faults, creating a narrow Zone of Exhumed Continental Mantle (ZECM) between two continental blocks. Incipient magmatism is expressed in forms of local occurrence of basalt layer and gabbros leading to the formation of a Embryonic Ocean. (C) Formation of a mid-ocean ridge and conjugated margins. The final architecture of the hyperextended domain in the Pyrenees are between (A) and (B). The Alps are best depicted by (B) and the Iberian-Newfoundland by (C). Figure modified after [*Sutra et al.*, 2013].

2.1. The Tasna OCT in the Alps

The Tasna OCT [*Florineth and Froitzheim*, 1994] exposed in the Swiss Alps are an unique field example preserving the primary structure of an OCT over 6 km including up to 600 meter of vertical section [*Manatschal*, 2006] (Figure 3A). The top of the continental basement is characterized by an extensional detachment fault (Upper Tasna Detachment, UTD) made of cataclasites and gouges that are overlain by tectono-sedimentary breccias. These breccias are composed by clasts of the granitic-gneissic and migmatitic basement rocks impregnated by silica. At the bottom of the continental basement, an extensional detachment fault (Lower Tasna Detachment, LTD)

is characterized by brittle deformation in the mantle, where cataclasites, foliated cataclasites and ophicalcites make most part of the fault zone [*Manatschal et al*., 2006]. Cretaceous sedimentary sequences, thin basalts and pillow lavas (about 35 m thick) overlie this exhumed mantle.

Manatschal et al. [*2006*] presented Ar/Ar ages of phlogopite from spinel websterite, which show 169.1±0.4 and 170.5±0.4 Ma. They interpreted them as cooling ages related to the exhumation of the mantle rocks in the footwall of the LTD through temperatures about 400 ^{0}C. This corresponds to temperatures at which serpentinization may initiate. In another nappe 20 km to the east of Tasna unit, small veins of K-rich and Ca-poor alkaline magmatic have been found containing phlogopite and zircons. U-Pb data of these zircons gives crystallization ages of 167.3±2.7 Ma, while Ar-Ar on phlogopite shows cooling ages of about 161 Ma [*Hauser and Müntener*, 2011]. Therefore, the age of serpentinization and mantle exhumation that is followed by the incipient magmatism in Alpine Tethys occurs from Middle to Late Jurassic times [*Manatschal et al*., 2006; *Hauser and Müntener*, 2011].

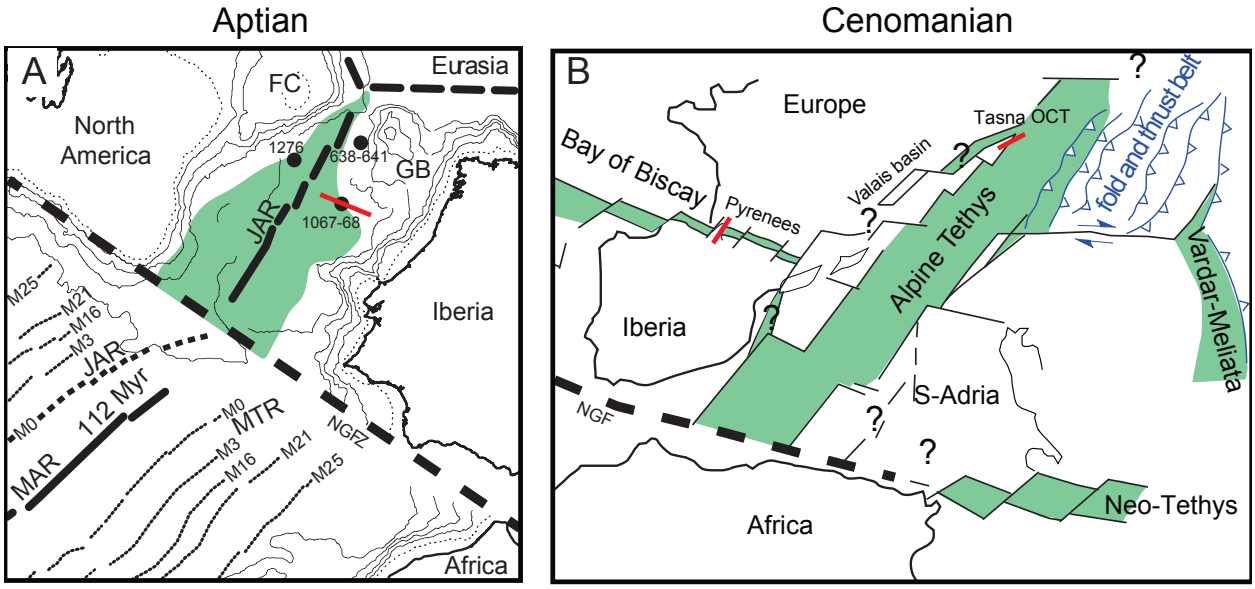

Figure 2. Paleogeographic maps. The maps show that the basins were not completely connected to the oceans. Green polygons mark the hyperextended domains where mantle were exhumed to the seafloor. (A) Paleogeographic map of Newfound and Iberia at Aptian times, modified from [*Tucholke and Sibuet*, 2012]. FC: Flemish Cap, GB: Galicia Bank , JAR: J-Anomaly Ridge; NGFZ: Newfoundland–Gibraltar Fracture Zone (NGFZ). The dots are ODP Sites used in this study and the red lines are seismic sections presented in Figure 3. (B) Paleogeographic map of the Alpine Tethys and the Pyrenees *sea* between Iberia and Europe. Red lines are the section from Mauléon Basin and Tasna OCT presented in Figure 3. Map modified from *Manatschal and Müntener* [2009].

2.2. The Hobby High along the deep Western Iberian Margin

The Hobby High (Figure 3B) is an oceanward termination of the thinned continental crust at the Iberian Margin and corresponds to the first exhumation of continental mantle at the sea-floor within an E-W section. Extensional detachment faults are recognized and interpreted to be responsible for mantle exhumation [*Manatschal et al*., 2001; *Sutra et al*., 2013].

The hyperextended domain of the Iberian Margin is made of a thinned continental crust and exhumed continental mantle (ZECM) with overlying extensional continental allochthons. Oceanwards, the ZECM becomes progressively more influenced by magmatism leading to the formation of an embryonic oceanic crust. This is evidenced by the strong magnetic J-anomaly [*Russell and Whitmarsh*, 2003; *Bronner et al*., 2011], seismic velocity pattern [*Dean and Minshull*, 2000; *Minshull et al*., 2014] and by the ages of magmatic rocks from the ODP Site 1070 [*Jagoutz et al*., 2007]. This zone can extend across 240 km and along more than 200 km in the Central West Iberia margin [*Sutra and Manatschal*, 2012; *Pinto et al*., 2014a, in prep.].

The age of the mantle exhumation and OCT formation can be constrained by dating the overlying sediments and using radiogenic methods. Microfossils in the matrix of the ultramafic-bearing debris deposited over the exhumed mantle are dated as Valanginian to Barremian [*Wilson et al*., 2001], where the Valanginian microfossils are thought to be reworked. Emplacement of gabbros in the previously serpentinized mantle from ODP Site 1070 is dated with U-Pb on zircon as 127 ± 4 Ma [*Jagoutz et al*., 2007]. Younger alkaline magmatic veins dated by U/Pb on zircons show ages of 113 ±2 Ma [*Jagoutz et al*., 2007]. This Aptian age coincides with the J-magnetic anomaly, which may mark the transition of the embryonic oceanic crust formation and the seafloor spreading [*Dean and Minshull*, 2000; *Bronner et al*., 2011; *Minshull et al*., 2014]. Therefore, the ages of the mantle exhumation, the incipient magmatism and the formation of the OCT are interpreted to occur between Barremian and Aptian/Albian, a time interval of approximately 18 Myr.

2.3. The Mauléon Basin in the West Pyrenees

The hyperextended system in the West Pyrenees preserves remnants of an incipient mantle exhumed system (Figure 3C) that did not develop much compared to the examples of the Iberian Margin and the Alps. Serpentinized mantle outcrops occur in few places in the axis of the hyperextended basin [*Jammes et al*., 2009] as rounded shapes with less than 1.5 km and they are usually covered by a thick sedimentary layers. An extensional detachment fault, the North Mauléon Detachment (NMD), is associated with upper and middle crustal rocks, and has been interpreted

to be responsible for the exhumation of the subcontinental mantle in the Mauléon basin [*Jammes et al*., 2009; *Masini et al*., 2014]. Exhumation along extensional detachment systems becomes more obvious eastward of the Pyrenean chain, where fault rocks along the exhumed mantle and the overlying sedimentary breccias are better exposed [*Lagabrielle et al*., 2010; *Clerc et al*., 2012]. Cooling ages on phlogopite from a gabbroic dike intruded in the mantle rocks are about 108-105 Ma [*Masini et al*., 2014]. The exhumed mantle is sealed by Cenomanian sediments, which gives a minimum age for the exhumation. Therefore the hyper-extension and incipient mantle exhumation in the Pyrenees are interpreted to be between 108-94 Ma, what gives an 14 Myr time span.

3. GEOLOGICAL DATA AND OBSERVATION

3.1. Continental basement rocks prior to brittle deformation

The continental basement rocks are different at the three studied sites. In the Tasna OCT, they are made of granitic-gneissic-migmatitic rocks, and partly mylonitized and strongly hydrated meta-gabbros, the first belonging to the pre-rift upper crust, the later to the former middle to lower crust [*Manatschal et al*., 2006].

At the Hobby High at the Iberia margin, the continental basement drilled at ODP Sites 1067 and 900 is characterized by amphibolites, meta-gabbros and tonalites that represent pre-rift middle to lower crust [*Hébert et al*., 2008]. The tonalite gneisses often present coarse plagioclase and the amphibolites usually present lenses of anorthosite that sometimes show sharp and diffuse contacts with the amphibolites [*Whitmarsh et al*., 1998; *Manatschal et al*., 2001]. Diffuse contacts suggest that anorthosites spread throughout the basement, and therefore, plagioclase minerals would be an important component of basement rocks around the Hobby High area. Calcite, epidote and chlorite veins often cut the amphibolites.

The basement rocks associated with the North Mauléon Detachment in the West Pyrenees are composed of two main groups. The first one is made of upper crustal rocks, which are mainly Ordovician and Silurian quartzites and schists. The second one is composed of middle to lower crustal rocks and encompasses pre-Cambrian paragneisses in amphibolite and granulite facies. These two groups are separated by the W-E Louhossoa lineament [*Jammes et al*., 2009] where paragneisses with semi-brittle structures are often observed.

3.2. Fault rocks in the continental basement

The rift-related fault rocks from all studied areas are characterized by brittle fault rocks that

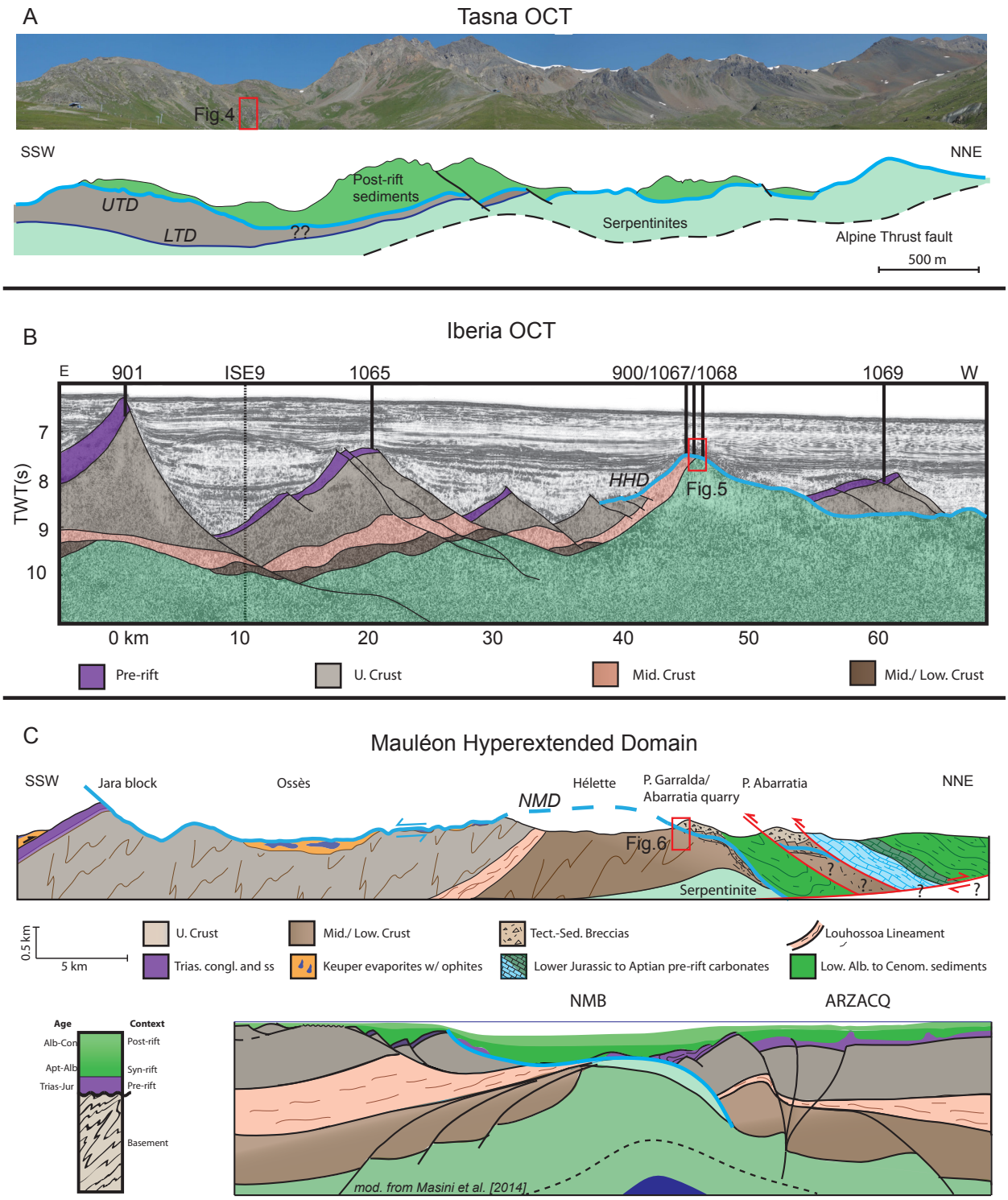

Figure 3. Hyperextended domains. (A) The photo at the top shows the Tasna OCT and the figure at the bottom shows the interpretation. UTD: Upper Tasna Detachment; LTD: Lower Tasna Detachment. After *Florineth and Froitzheim* [1994] and *Manatschal et al.* [2006]. Location is 46.82^{0}N/10.25^{0}E. (B) Reflection seismic Section Lusigal-12 in the Iberia margin. HHD: Hobby High Detachment. The numbers at the top are ODP Sites. (C) The figure at the top is the geological section from the breakaway fault (Jara) to the most distal segment of the North Mauléon Detachment (NMD). Red lines are thrust faults formed during Pyrenean compression. Although in this section, the serpentinites are not exposed, they outcrop 5 km more to the west. The figure at the bottom shows the reconstruction of this hyperextended system, modified from *Masini et al.* [2014]. Location: Jara block (43.19^{0}N/ 1.29^{0}W) and Pic Garralda (43.34^{0}N/1.24^{0}W).

usually exhibit a gradual increase of deformation toward the top of the footwall. In the Tasna OCT (Figure 4A), the Upper Tasna Detachment (UTD) is made of up to 100 m of cataclasites with locally centimetric gouges and up to 0.5 meters of gouges (Figure 4C) at the top of the UTD. When the cataclasitic structures start to become more evident, it can be observed that the new and weak cataclastic foliation overprints the older gneissic foliation. In this zone, jigsaw structures are often observed. Towards the core zone the cataclasites become more foliated (Figure 4D) and are followed by the increase of deformation and saussuritization. The saussuritization is responsible for the (i) breaking-down of feldspars resulting in albitization, (ii) chloritization of biotites (more rare) and plagioclases, and (iii) alteration of feldspar to sericite and illite. Most of these reactions are responsible for losses of Si and Ca that are evidenced by quartz and calcite veins. The SEM analyses show that the breakdown of plagioclase is often accompanied by veins of quartz and calcite. Chloritization is evidenced by Fe-rich veins, which cut the plagioclase leading to the formation of chamosite (Figure A2, Annexes). The gouges are characterized by a well-developed foliation, defined by chlorite-illite-sericite-rich matrix, by clasts of quartz veins and cataclasites. In both cataclasites and gouges Fe-oxides often occur in the syn-tectonic foliation.

At Hobby High along the Iberian Margin (Figure 5A-C), the extensional detachment fault (HHD) is made of cataclasites, foliated cataclasites, gouges and fault breccias showing different proportions of matrix (ODP Site 1067) [*Manatschal et al*., 2001]. The fault zone of the ODP Site 1067 has more than 50 meters. In general, from bottom to top, the fault zone is made of cataclasites and gouges that grades to fault breccias. Cataclasites show clasts surrounded by a chlorite-rich matrix as well as veins of chlorite, epidote and rarely calcite. Locally observed, foliated cataclasites exhibit millimetric to centimetric clasts of amphibolite and quartz-feldspatic rock in a foliated matrix heavily composed of chlorite, epidote and calcite veins. Gouges are strongly foliated and exhibit rounded clasts in a matrix of chlorite and recrystallized micro-calcite. Some of these gouges have calcite-rich matrices and usually occur close to tonalite-amphibolite fault breccias. In this section, late stage of calcite veins (up to 2 mm) usually cut the epidote and chlorite veins. Fault breccias are found above this section and they usually present centimetric clasts of amphibolite (up to 20 cm). Fault breccias tend to change from clast-supported to more matrix-supported up section. Fe-oxyhydroxide banding is often observed in the matrix of these fault rocks.

In the North Mauléon Detachment (NMD) in the West Pyrenees, the fault zones are usually up to 30 meters thick. They are composed of cataclasites, foliated cataclasites and rarely gouges (Figure 6A-C). In this detachment fault system, low-angle detachment fault is locally exposed in the Abarratia query and Pic Garralda (Figure 6B), where foliated cataclasites dips about 40°

toward NW. At microstructural scale, the foliated cataclasites of Pic Garralda are made of clasts of quartz, sericitized feldspars and rounded agglomerates of quartz. The matrix of this rock type is composed by syn-tectonic curve-shaped sericite/illite and chlorite (minor) as well as Fe-oxyhydroxides, which made up to 50% of the zone of cataclastic flow.

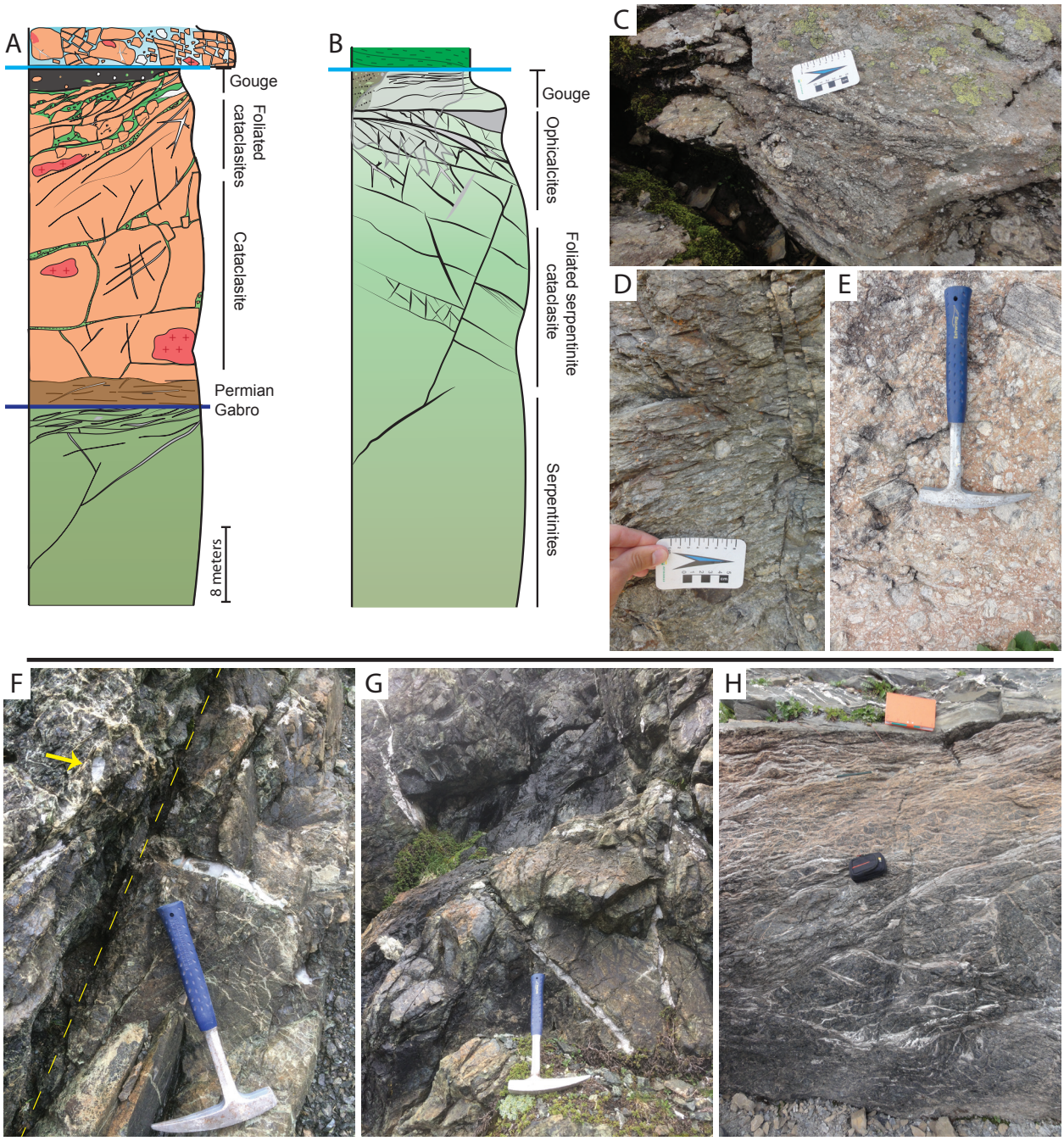

Figure 4. Fault rocks from the Upper and Lower Tasna detachment. (A) Fault rock profile showing the UTD in light blue and LTD in dark blue. (B) The UTD profile in the exhumed mantle. (C) Gouge layer at the top of the UTD. (D) Foliated cataclasite with lenses of centimetric gouges. (E) Tectono-sedimentary breccia with silicified matrix. (F) Foliated cataclasite and calcite veins in the mantle of the LTD. The brittle shear zone forms a foliated cataclasite and cuts the previous foliation and calcite veins (bellow dash line). Elongated clast of calcite showing that the veining can also be syn-deformation. (G) Large calcite veins cutting the serpentinites in the LTD. The outcrop is 5 meter bellow the one from photo F. (H) Increase of deformation from bottom to top of the UTD evidenced by more penetrative foliation between the field book and the camera case. The field book is above the shales that overlie the top of the horizontal UTD.

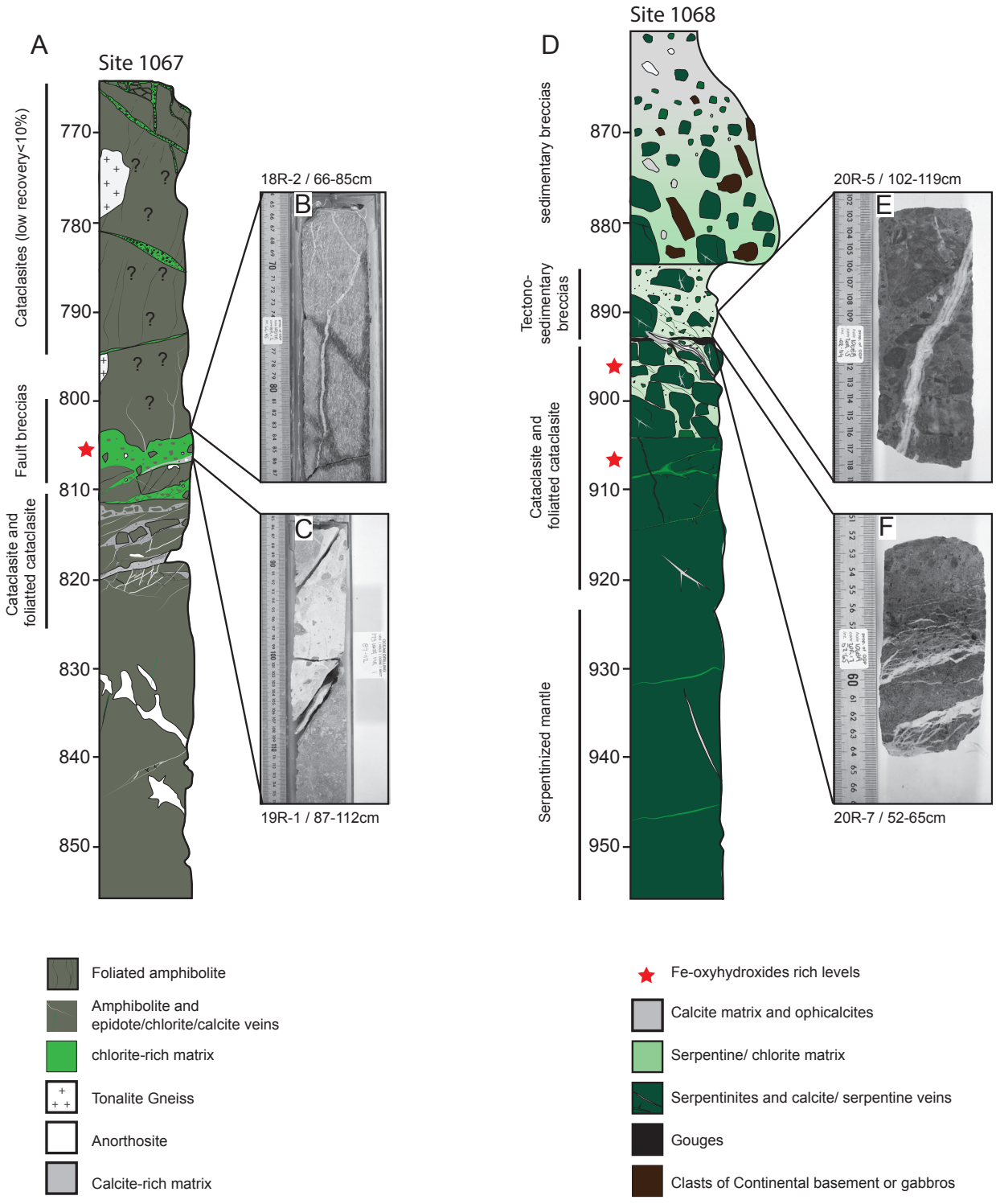

Figure 5. Fault rocks from the Hobby High Detachment (HHD). The description at the left side of the profiles represents the predominance of lithotypes but is not restrict to it. (A) Fault zone profile of the ODP Site 1067. (B) Calcite veins cutting the amphibolite weakly brecciated (C) Cataclasite at the base of the dipping normal fault and gouge with calcite-rich matrix (white rocks). (D) Fault zone profile in the mantle (ODP Site 1068). (E) Tectono-sedimentary breccia cut by calcite veins. (F) Fault breccia heavily cut by calcite veins.

Another characteristic feature of the NMD system is a series of sub-vertical normal faults that are associated with the extensional detachment. In the Abarratia quarry, these normal faults show small to moderate displacement (up to 1 m) where black and reddish foliated cataclasites (Figure 6C) with centimetric lenses of gouges are observed. The matrix of these faults exhibit disseminated Fe-oxides. The sub-vertical normal faults in Pic Garralda are characterized by cataclasites exhibiting typical jigsaw fractures that are often filled by Fe-oxides in a matrix of syn-tectonic sericite and minor chlorite. These faults present small displacements and usually cut through leucocratic bands of granulite composed of about 10% of plagioclase and 90% of inequigranular and polygonal aggregates of quartz.

In other segments of the NMD (between Ossès and Jara, see Figure 3C) the cataclasites developed in the Devonian-Ordovician quartzites and schists. In these places the feldspar are strongly sericitized and Fe-oxides and dark pink matrix of Mn-oxides are frequently observed in centimetric cataclastic corridors. Along the NMD abnormal concentrations of Fe-oxides can be found in the foliation and matrix of the cataclasites. These oxides can be followed along 19 km from the endmost segment of the NMD until the breakaway fault where Fe-oxides are also observed in the Triassic pre-rift sediments.

3.3. **Serpentinites**

The mantle exposed in the studied sites is made of serpentinized lherzolites, and local harzburgites, pyroxenites and dunites that locally preserve their original igneous fabric. In all studied sites, the serpentinized peridotites are heavily composed by micro to millimetric chrysotile/ lizardite veins.

The mantle in Tasna OCT is composed of hydrated spinel-lherzolites and spinel websterites layers [*Manatschal et al*., 2006]. Major and trace element data from whole rock and minerals indicate a fertile composition, e.g., incompatible elements such as sodium in clinopyroxenes [*Manatschal et al*., 2006]. The serpentinized peridotite often exhibits a well-developed high temperature spinel foliation in the bottom of the section. Although the mantle rocks are more than 90% serpentinized, original igneous textures are locally preserved. Olivine is replaced by chrysotile/lizardite, spinel is rimmed by opaque magnetite, and pyroxene is commonly serpentinized or chloritized. Ti-hornblende and phlogopite are locally preserved in pyroxenite levels. Up section, olivine and pyroxenes are completely altered to serpentines and the spinel foliation gives place to a serpentinite foliation. This foliation is usually cut by multi-stage veins of chrysotile/ lizardite and locally by calcite veins.

In the Iberian example, serpentinite mesh structures, after olivine, contain submicroscopic fibers of lizardite and brucite. *Beard and Hopkinson* [2000] highlighted the occurrence of andradite and hydroandradite (silicate and hydrated silicate of Ca and Fe) in the matrix intergrowing with the serpentines. They are also common in serpentine veins where they are often accompanied by Fe-Ni alloys and Ni-sulfides. Calcite veins containing Fe, Mn and Mg in forms of oxyhydroxides and carbonate where described at ODP Sites 897 and 899 [*Milliken and Morgan*, 1996]. They are a common feature in the upper parts of the exhumed serpentinites of the Iberian serpentinites and usually cut this previous lizardite/ chrysotile veins [*Morgan and Milliken*, 1996].

In the Western Pyrenees (e.g., Col d'Urdach, see map in Figure A8) the mantle is characterized by serpentinized peridotite and minor harzburgites, with degree of serpentinization to up to 80%. In thin section, relicts of pyroxenes rimmed by serpentine and chlorite are locally preserved. Serpentines after olivine are largely observed. Chrysotile/ lizardite veins usually cut the rock in several directions and Fe-oxides are usually associated. Bodies of Fe-oxides of about 0.5 meter wide occur in the serpentines (e.g., Col d'Urdach). In thin section, intergrowth contacts between quartz with the Fe-oxides (Figure A7) and veins of Fe-oxides can be observed. The presence of SiO_2 and Fe-oxides is interpreted to be related to serpentinization of more Fe-rich olivine (fayalite). Ophicalcites are common and they are usually cut by centimetric grayish calcite veins that clearly show creak-seal processes. In thin section, these veins often display syntaxial and asymmetrical growth and they are accompanied by micrometric Fe-oxides. At latest stages, brownish micritic and sparry calcites clearly grew over the serpentinites and the previously described calcite veins.

3.4. **Fault rocks in the mantle**

The fault zones in the exhumed serpentinized mantle of all studied examples share many similarities regarding to the protoliths, fault rocks, evolution of veining, temperature formation and geochemical composition. The fault rocks are characterized by cataclasites, foliated cataclasites, fault breccias and gouges. They were developed under low temperature brittle deformation and greenschist facies, as evidenced by new-formed low temperature minerals in the "brittle" foliation (e.g., chrysotile, lizardite and chlorite) suggesting that the extensional detachment faults may have rooted at shallow levels (<12 km).

In Iberian Margin, the fault rocks have been sampled along the exhumed mantle at many ODP Sites, e.g., 1068, 1070, 897 and 899. The thickness of the fault zone is higher than 50 m as indicated by drilled wells that did not penetrate into undeformed serpentinites (e.g., Site 1068). From

bottom to top, the fault rocks from these wells are made of cataclasites, foliated cataclasites, fault breccias and gouges (Figure 5D-F). Cataclasites show typical jigsaw fractures where the matrix is made of millimetric clasts of serpentinite and veins of chrysotile/lizardite. Foliated cataclasites are characterized by chlorite- and serpentine-rich matrix, sometimes also calcite-rich. Fault breccias tend to change from clast-supported to be more matrix-supported up section. They are composed by millimetric to centimetric clasts of serpentinites and locally pyroxenites, as well as by matrices of chlorite, serpentine, Fe-oxyhydroxides and usually pervasive sparitic calcite. Fault breccias are heavily cut by calcite veins and exhibit locally jigsaw structures. The clasts of some fault breccias tend to "float" in the calcite matrix, suggesting they formed as a result of high-pressure fluids (e.g., Site 1070A-8R-1). In these zones, quartz veins sometimes are filling fractures (e.g., Site 1070A-8R-3). Gouge layers are characterized by rounded clasts as well as by serpentine and calcite veins that accompanied the tectonic foliation. These gouges are usually cut by late stage calcite veins. All those veins contain the same previously described elements observed in the serpentinites. Up-section, tectono-sedimentary breccias and matrix-supported sedimentary breccias often overlie the top of the fault zone (Figure 5D).

In the exhumed mantle from Tasna, the UTD (Figure 4B and 4H) is characterized from bottom to top by (i) cataclasites showing jigsaw fractures filled by serpentine veins, (ii) foliated cataclasites with centimetric to decimetric angular clasts of serpentinites cut by chrysotile/lizardite/chlorite veins, (iii) matrix-supported tectonic breccias heavily cut by serpentine/chlorite/calcite veins, (iv) local millimetric to centimetric gouges with chlorite/serpentine matrix and millimetric rounded clasts. Serpentine veins are always present in the fault zone and they are commonly cut by Fe-oxides bearing calcite veins. The frequency of calcite veins increases from bottom to top of the UTD fault zone. The types of fault rocks of the LTD (Figure 4F-G) are quite similar to those of UTD, but with two main exceptions. The first is the occurrence of layers composed by chlorite and serpentinites that show a strong foliation locally observed close to the contact with the altered metagabbros from the continental crust. The second is the relationship between serpentine and calcite veins in the cataclastic foliation. These calcite veins are cut by a brittle shear zone and clasts of calcite can be found in the foliation associated with this structure (Figure 4F).

The fault zone in the exhumed mantle in the Mauléon Basin is only locally exposed (Figure 6D). However, cataclasites similar to the ones from Tasna are observed. They are affected by late millimetric to centimetric calcite veins (Figure 6E) comprising Fe-oxides. Close to the fault zones, Fe-oxides are observed within the serpentinites (Figure 6F).

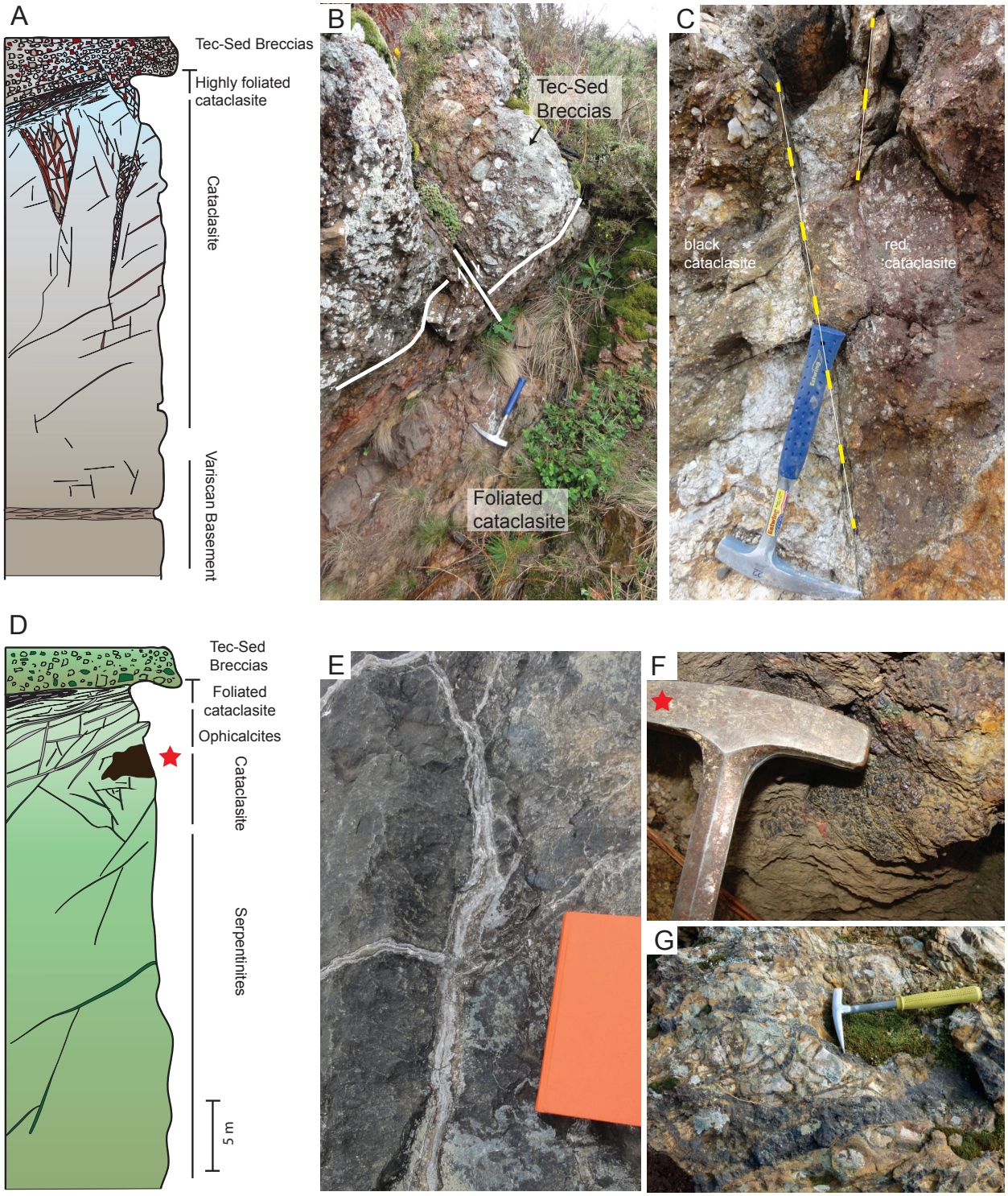

Figure 6. Fault zone from the North Mauléon Detachment (NMD). (A) Fault zone profile of NMD. The more reddish color highlights the presence of Fe-oxides and the bluish color the silicification at the top of the fault zone. (B) Outcrop at the Pic Garralda showing the low-angle contact of foliated cataclasites and the tectono-sedimentary breccias. (C) Fault zone made of cataclasites affected by secondary sub-vertical normal faults (dash lines) at the Abarratia query. (D) Fault zone profile of the mantle. Note the Fe-oxide layer at the serpentinites. (E) Calcite veins cutting the serpentinites. (F) Fe-oxides crust formed in the serpentinites. (G) Veins of Fe-oxyhydroxides in the Triassic sediments from the breakaway of NMD.

3.5. **Sediments from the hyperextended domain**

In order to investigate the presence of fluids that can affect the sedimentary basins in the hyperextended domain, we choose the ODP Sites 638 and 641 (Leg 103) from the Iberian distal margin. The Leg 103 represents a unique available dataset, once they drilled through the sedimentary rocks from a distal supradetachment basin.

The sedimentary sequence is characterized by syn-tectonic sediments deposited from Valanginian to latest Aptian and post-tectonic sediments deposited from lowermost Albian time [*Boillot et al*., 1987]. The Valanginian sediments are composed of sandstone interbedded with claystones. The Hauterivian is made of claystones at the base grading to marlstones originated from slump deposits. The Barremian section mainly shows marlstones. The Aptian is composed of sedimentary breccia alternated with limestone/marlstone and calcarenite beds. The Albian is mainly made of shales and black shales, characterizing the post-rift sequence.

Additionally, we used ODP Site 1276 (Leg 210) located in the OCT of the Newfoundland margin in order to compare the results with those from ODP Sites 638 and 641. At the ODP Site 1276, the Late Aptian-Early Albian is characterized by thick graded gravity-flow deposits of disorganized beds of sandstone, siltstone, grainstone, and calcareous mudrock that often is interrupted by thin turbidites [*Shipboard Scientific Party*, 2004b]. Nevertheless most part of the section is made of mudrocks. The XRD analyses show they are mainly formed by chlorite, kaolinite, smectite, feldspar and quartz. The exception is at depths (below seafloor) between 1613 m and 1622 m, where olivine and pyroxene are locally observed [*Shipboard Scientific Party*, 2004b]. In the Late Aptian-Early Albian sediments, diagenetic nodules and concretionary bands of siderite and dolomite as well as pyrite are occasionally observed. Similar sedimentary rocks from those of Aptian/Albian are observed until the Cenomanian. From Turonian onwards, the sedimentary sequence changes and it is best depicted by mud-dominated deposition where hemipelagic sediments are often interbedded with thin turbidites.

Although ODP Site 1067 drilled through the extensional detachment and overlaying sediments, this site does not enable us to get insights of the fluid flow activity during the rift evolution, since the sediments that overlie the Hobby High were deposited much later, after the fault activity (Figure 3B).

The Tasna OCT (Figure 3A) shows a similar situation from that observed at the Hobby High [*Manatschal et al*., 2006]. The sediments related to exhumation is, apart from cemented tec-

tono-sedimentary breccias, not observed and the whole structure is passively onlapped by younger, post-rift sediments. The cause of such a late sedimentation is interpreted as these areas represent structural highs. However, the occurrence of tectono-sedimentary breccias (Figure 4E) that are clearly related to the detachment fault activity let us assume that this has a Jurassic age, even though no fossil is observed in their matrix. These tectonic-sedimentary breccias are characterized by *in situ* deformation but also show evidence for a sedimentary origin, e.g. they contain millimetric layers of very thin sandstones and locally centimetric graded beds. But it is clear that if they were deposited, their source is local and the sedimentary transport is negligible. The tectonic-sedimentary breccias overlying the UTD are replete of SiO_2 that is observed not only in the matrix but also involving the clasts as new crystallized quartz.

In the Mauléon Basin, tectono-sedimentary breccias are also observed overlying the NMD (Figure 6B). They are cemented by SiO_2 and also contain Fe-oxides in their matrix. Fe-oxyhydroxides are also a common feature in the Triassic pre-rift sandstones overlying the NMD. They are expressed as series of Fe-veins (±5 cm thick) composed by hematite and goethite. Field observations show that these Fe-veins are limited to the areas where the Triassic sequence is cut by the NMD, responsible for mantle exhumation (Figure 6G).

4. GEOCHEMICAL DATA

4.1. Mantle rocks

We used ICP-MS/AES and XRF data of serpentinites from the Alpine Tethys with different degrees of serpentinization [*Müntener et al*., 2010; *Pinto et al*., 2014b, in prep.] in order to show losses that took place during serpentinization as well as evidence that this process occurred associated with hydrothermal activity.

Pinto et al. [2014b, in prep.] grouped these data in 3 groups: (1) samples with ≤10% of serpentinization; (2) samples between <10 and ≤60% of serpentinization; (3) samples with > 60% of serpentinization. They show that elements are lost during the entire serpentinization processes. In the Figure 7A the total gain and loss is presented considering the alteration from group 1 to group 3. Si, Mg, Ca, Fe, Mn and the trace elements Ni, Cr and V are some of the main elements lost by serpentinization. In fact, these losses occurred at mineral-scale, as it can be observed by major losses of elements such as Si, Mg, Fe and Mn in olivine and pyroxene of these samples (Figure 8). This is supported by laboratory experiments where these minerals are subjected to hydration resulting in losses of these elements [*Daval et al*., 2011; *Ogasawara et al*., 2013].

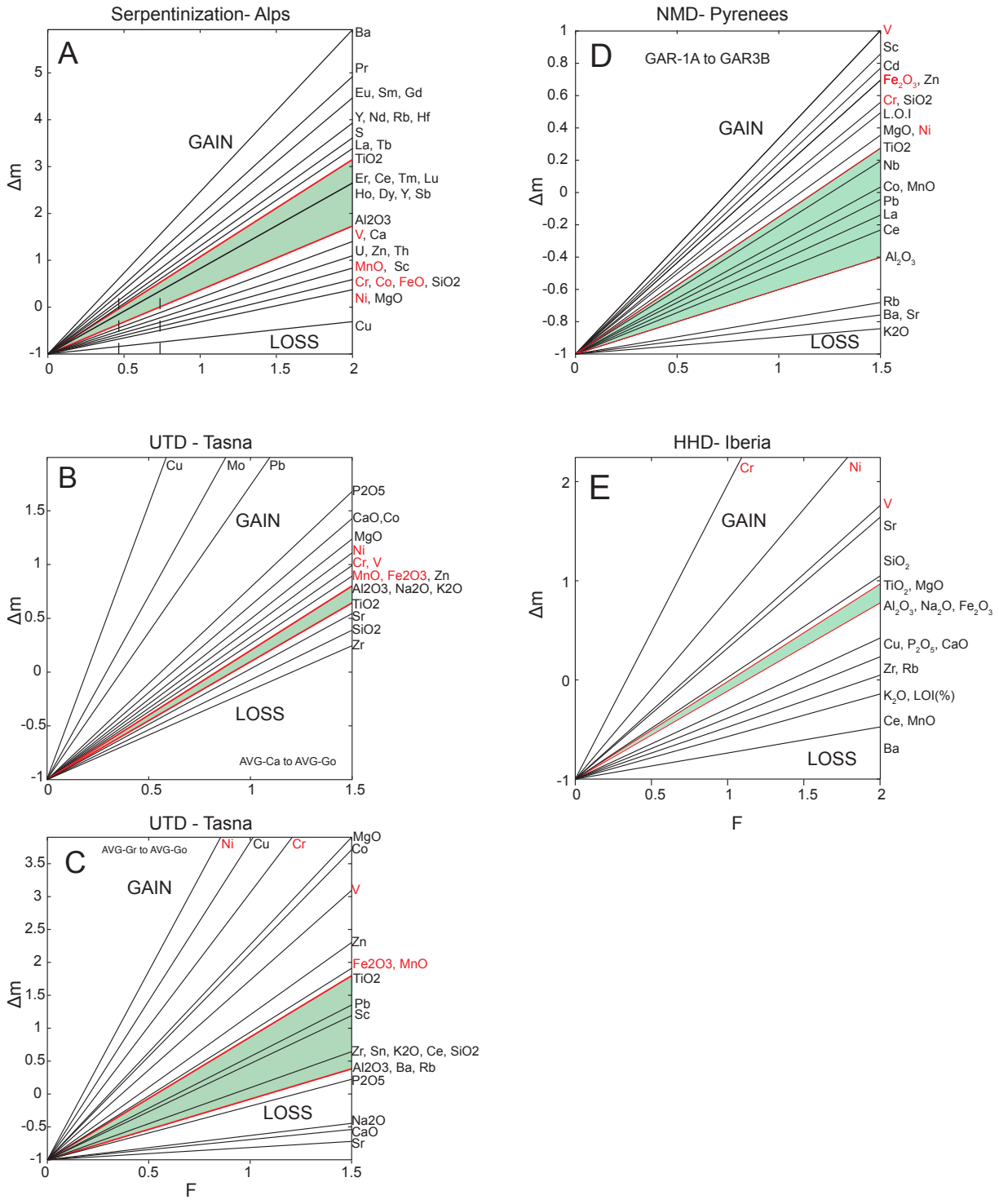

Figure 7. Gain and loss of elements. The figures shows the transformation between two lithotypes. Therefore the comparison between them highlight the gains and losses of elements. (A) Gain and losses from less serpentinized peridotites (Group 1) to more serpentinized peridotites (Group 3). Note the losses of elements, such as Ni, Cr, V, Si, Mg, Fe and Mn. In the figures from (B) to (E), note that Ni, Cr and V are always gain in the fault rocks of the extensional detachment systems. Data from Table 1. (B) Transformation from average values of cataclasites to gouges in the UTD at Tasna OCT. (C) Transformation from average values of granite to gouges in the UTD at Tasna OCT. The data from granites are the average of a reference Albula granite [*Pinto et al.*, 2014, in prep.]. (D) Transformation from GAR-1A (Gneiss) to GAR-3B (red cataclasite) from Pic Garralda (Mauléon Basin). (E) Transformation from cataclasites (18R-1, 91-93 cm) to fault breccia/gouges (19R-2, 114-119 cm) in the HHD at Iberia OCT. The elements in red were used as proxies for tracing mantle-related fluids. Note that the element lost during serpentinization are the same enriching (gain) the fault rocks from extensional detachment system in the continental crust.

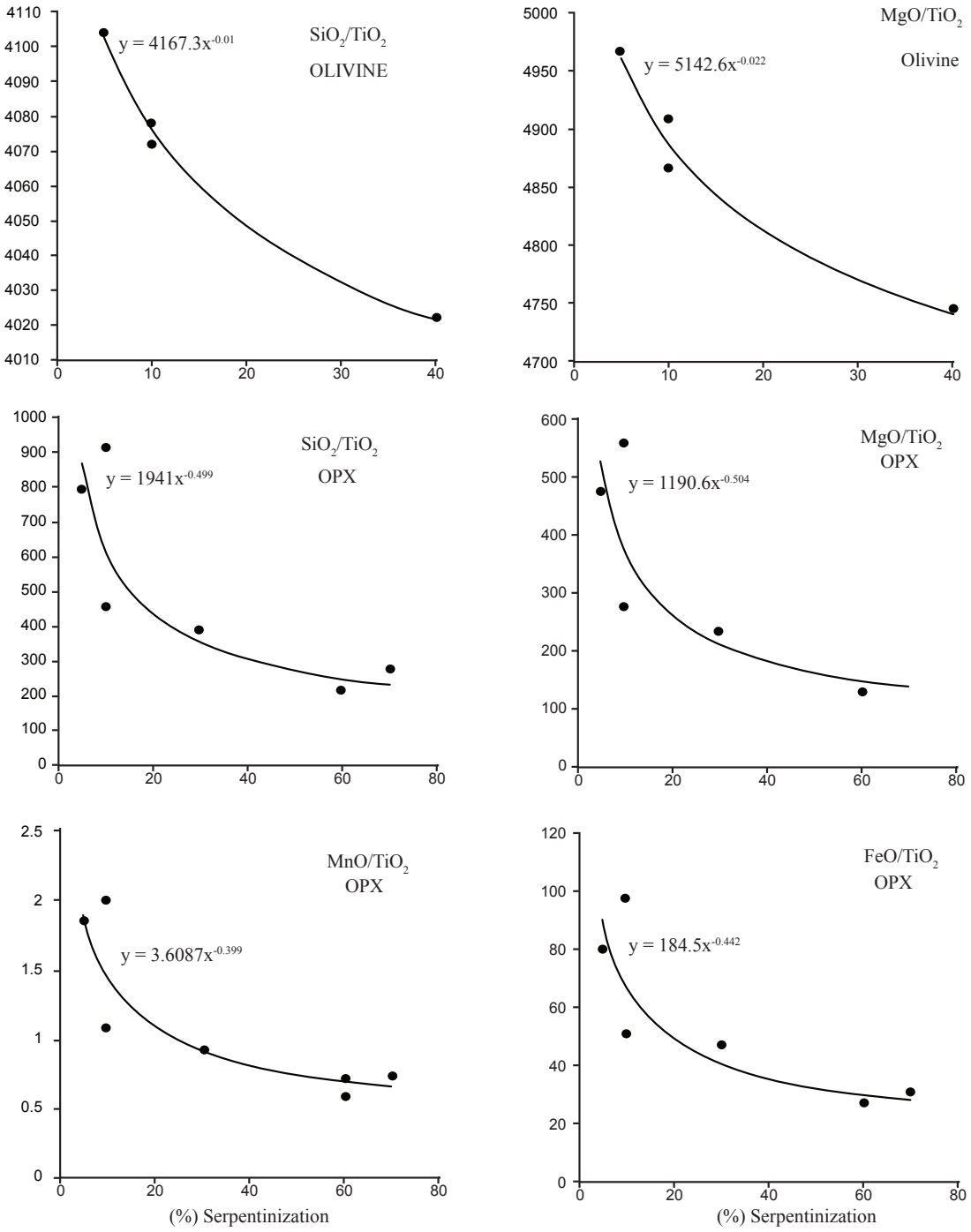

Figure 8. Loss of elements in olivine and pyroxene from serpentinized peridotites of the Platta nappe. The figures show that the more the samples are serpentinized the lower the values of Si, Mg, Fe and Mn are, assuming Ti as an immobile element. Chemical analyses from *Müntener et al.* [2010].

In the Iberian Margin the peridotites are more than 90% serpentinized and their major and trace element have the main chemical characteristic [e.g., *Hebert et al*., 2001] of the serpentinites from the Alps, i.e., depleted in Ni, Cr, V, Si, Mg, Ca, Fe and Mn. Chemical analyses performed on veins of chrysotile, lizardite and calcite from the fault rocks of the Iberian OCT (ODP Site 1068) exhibit an elevated content of metal, e.g., Ni, Fe and in less extent Cr and Co [*Beard and Hopkinson*, 2000]. The serpentinites from the Mauléon Basin show a wide range of serpentinization.

Like the serpentinites from the Alps, the less serpentinized peridotites are rich in elements such as Ni, Fe and Mg and the highly serpentinized peridotites are more depleted in these elements [e.g., *Fabribs et al*., 1998].

Oxygen isotopic studies performed on chrysotile/lizardite in the serpentinites, calcite veins and carbonate matrix in ophicalcites points to different temperatures and condition of formation (Figure 9). The $^{18}O_{serp}$ (SMOW) measured in chrysotile/lizardite from Tasna serpentinites are between 9-14‰ and the modeled temperatures are between 67-109 ^{0}C [*Engström et al*., 2007]. At Iberia, the $^{18}O_{serp}$ from chrysotile/lizardite in the serpentinites are between 4-9‰ with estimated temperatures between 100-175 ^{0}C. In the core zone of the detachment (e.g, ODP Site 1068), $^{18}O_{serp}$ are between 5-13‰ showing they are formed between 70-150 ^{0}C [*Skelton and Valley*, 2000].

The isotopic analyses were also performed on veins and they represent an important tool to evaluate the temperature of fluids in different stages. Calcite veins in Tasna show $^{18}O_{calcite}$ (SMOW) around 17-20‰ with estimated temperatures between 50-100 ^{0}C [*Engström et al*., 2007]. In other Penninic nappes, calcite veins have $^{18}O_{calcite}$ between 14-18‰ showing temperatures around 100 ^{0}C [*Früh-Green et al*., 1990]. The calcite veins and carbonate matrix of ophicalcites from the ODP Sites 637, 897 and 899 show high $^{18}O_{calcite}$ between 25-32‰ [*Evans and Baltuck*, 1988; *Milliken and Morgan*, 1996]. The data suggest that the temperature should be relatively low, however *Milliken and Morgan* [1996] argument that due to uncertainties about the exhumation history, the ^{18}O data allow a wide range for interpretation and values lower than 100 ^{0}C is completely possible. In addition, the majority of calcite veins and calcite matrix measured from Iberia sites corresponds to

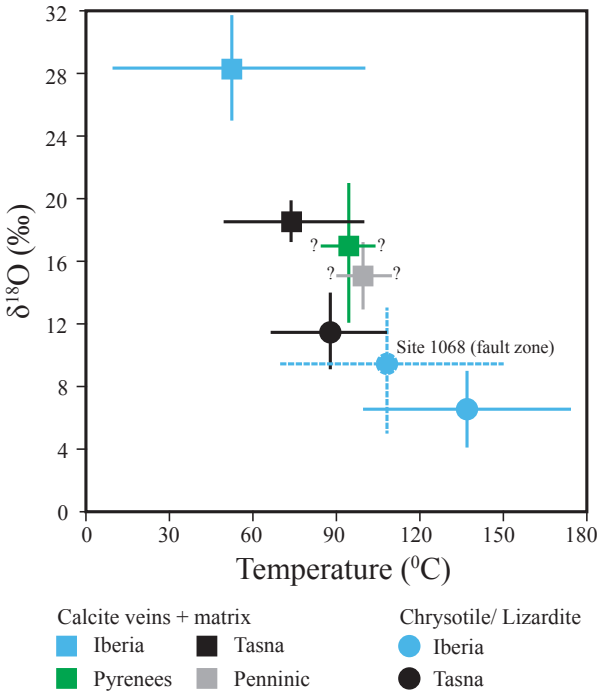

Figure 9. Range of oxygen isotopes. The figure shows the approximately range of oxygen isotopes and temperature from chrysotile/ lizardite and calcite veins. In general the serpentine veins show higher temperatures than the calcite veins. Data from the serpentinites of the Iberia distal margin, Tasna OCT, the West Pyrenees and other Penninic nappes in the Alps. Data from [*Evans and Baltuck*, 1988; *Früh-Green et al*., 1990; *Milliken and Morgan*, 1996; *Skelton and Valley*, 2000; *Engström et al*., 2007; *Clerc et al*., 2013], see text for details.

the one related to post-exhumation [*Bernoulli and Weissert*, 1985; *Clerc et al*., 2013]. In the *hydrothermal* [*Clerc et al*., 2013] calcite veins from the West Pyrenees, the $^{18}O_{calcite}$ present wide rage of 12-22‰. Based on the equivalence of the same tectonic setting in the Iberia and in the Alps, a temperatures of the order of 100 ^{0}C can be estimated for the calcite veins of the Pyrenees.

4.2. **Continental fault rocks**

The bulk composition of the fault rocks of extensional detachment faults from Iberian Margin, Tasna OCT and the Mauléon Basin were analyzed with ICP-AES/MS and XRF methods (Table 1). They allowed us to understand the relationship between fault activity, deformation, fluid-rock interaction and fluid migration along detachment systems. We used the Gresen-type plot proposed by *Potdevin and Marquer* [1987] to quantify the elements that entered in fault zone (gains) and elements that left the fault zone (losses) using Al and Ti as immobile elements (Figure A1). *Pinto et al*. [2014b, in prep.] showed that many of these elements, especially Ni-Cr-V, are retained in the phyllosilicate minerals that compose the matrix of the fault rocks.

In the studied fault rocks of the extensional detachment faults at the Hobby High (ODP Site 1067), UTD from Tasna and NMD from Pyrenees, a systematic and elevated gain of elements such Ni, Cr, V can be observed (Figure 7 B-E). These gains are in agreement with results from other extensional detachment systems in hyperextended domains of the Alpine Tethyan margins that are responsible for mantle exhumation [*Manatschal et al*., 2000; *Pinto et al*., 2014b, in prep.]. Such gains are not observed in more continentalwards extensional detachment systems and therefore, they were used as fingerprints for tracing mantle-related fluids in the distal margin [*Pinto et al*., 2014b, in prep.].

4.3. **Sedimentary rocks**

The chemical analyses of sediments of the ODP Sites 638B and 641C [*Clauser et al*., 1988] were used to track the signature of fluids in the sediments associated with hyperextended domains and exhumation of mantle rocks. Part of the chemical analyses available for ODP Site 638 and 641 is shown in the Figure 10. The data were used to verify if the enrichment of specific elements is due to normal diagenesis or if they have an external source. Therefore, the following paragraph synthesize the main points about the application of the element variation or elemental ratio.

In these sites we used the $CaCO_3$ profile in order to distinguish carbonate- from clastic-bearing rocks. Usually, Mg variation points to the presence of clay minerals, therefore, they are

higher in clastic rocks. Fe also tends to be higher in clay-bearing rocks, once that Fe makes part of clay minerals (e.g., chlorite). Most of the time, Mn is a minor element in clay and carbonate minerals and is not considered to be high in normal depositional settings. Normal Mn/Fe ratio values ranges from 0.5 to 1. Sr is higher in clay stones than in carbonates, because some clay minerals are formed from the alteration of feldspar that is a sink for Sr. In deep marine carbonates (biogenic calcite) the Sr/Ca and Mg/Sr ratios tend to have a given behavior even considering diagenetic al-

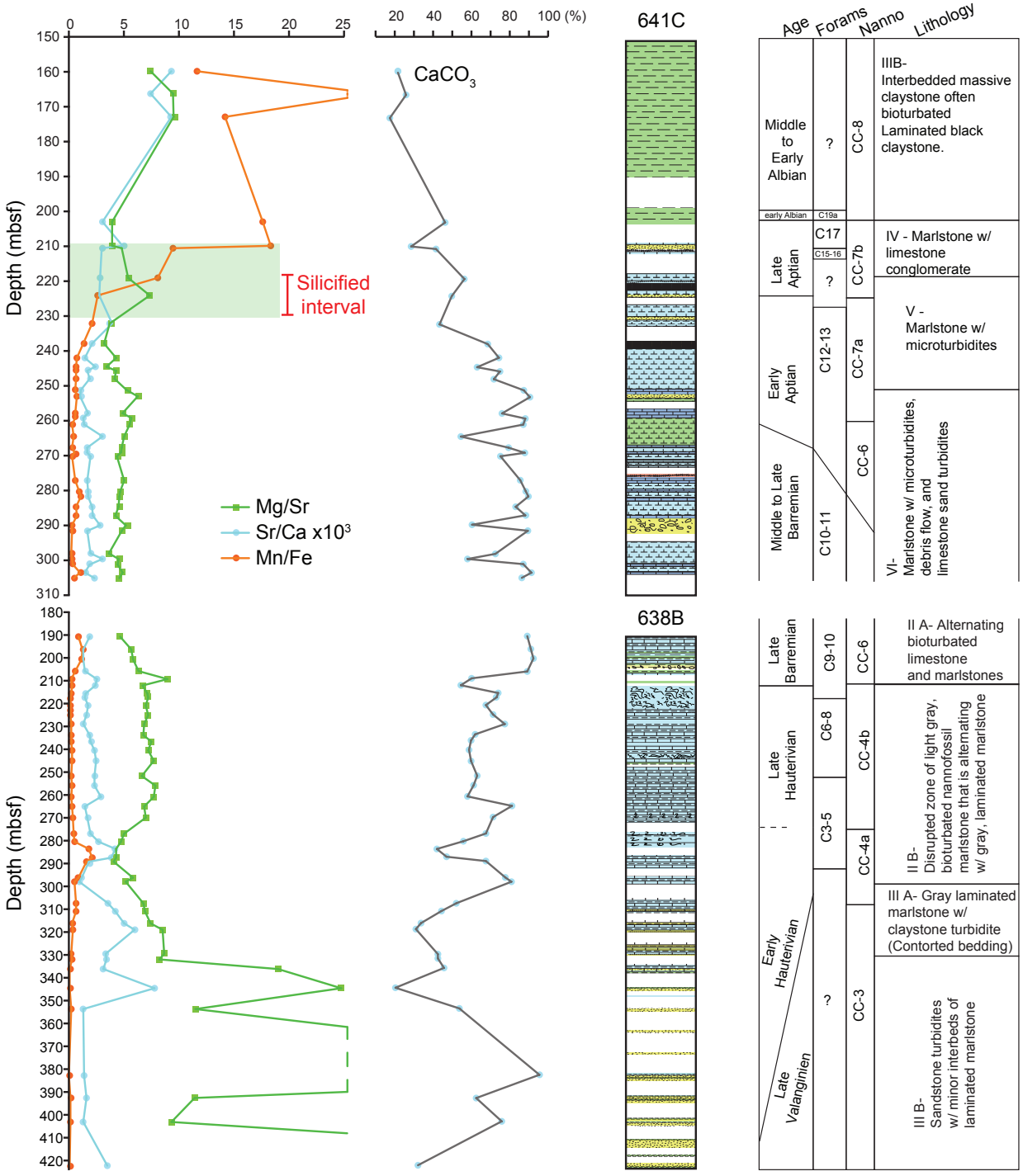

Figure 10. Geochemical variation from the ODP Site 638B and 641C. Note the enrichment of Mn, Mg and Si in rocks of Late Aptian age. This enrichment is interpreted to be caused by the progressive serpentinization accompanied by mantle exhumationData from [Clauser et al., 1988].

teration (release of trace elements to the seawater) [*Baker et al*., 1982; *Graham et al*., 1982; *Ando et al*., 2006].

At ODP Sites 638B the changes in $CaCO_3$ reflect the variation of lithologies, specially in Late Valanginian to Early Hauterivian section where there is a frequent intercalation of thin sandy turbidites and marlstones. The variation of Mg/Sr usually follows the changes of $CaCO_3$. The exception is the increase of Mg/Sr due to the clay-bearing facies (e.g., ~345 m). However, the increase of Mg/Sr at depth about 210 m is not due to changes in the lithology, once it is composed by marlstone. In this site, the Mn/Fe does not change much and the ratio keeps around 0.7-1.

At ODP Site 641C, from Barremian to Early Aptian, there is not much change between Sr/Ca, Mg/Sr and $CaCO_3$. Likewise, the Mn/Fe ratio change very little. Only from Early Aptian to Late Aptian-Early Albian is there an increase of Mg/Sr ratio while $CaCO_3$ is lowering. This is accompanied by an increase in Mn/Fe. The observed increase in Mg and Mn is not related to facies variations, once the sedimentary sequence of Aptian age is mainly composed of carbonate-bearing rocks (marlstone/thin limestone). Therefore, in order to explain these enrichments it is necessary an external source for these elements.

Additionally, we use the chemical analyses from ODP Site 1276 [*Robertson*, 2007] in order to observe the behavior of Fe-Mn and other metals (Cr, Ni, V) during the same period (Upper Aptian-Lower Albian), as well as to compare the results with those from the ODP Sites 638B and 641C from the conjugate margin. In the Figure 11, these metals are plotted in relation to Al content, once they are often present in the phylosillicate structure (e.g., Fe in chlorite and illite). If they are in excess, it is probably due to an enrichment of these elements rather than an increase in the amount of phyllosilicate minerals. Indeed, this is constrained by the fact that the Si/Al ratio (not plotted) is constant through the section with only local exception in sediments younger than Cenomanian. Once ODP Site 1276 data refers to a claystone-rich section, an increase of these elements can also be attributed to the formation of oxides. It is possible to observe an increasing of Fe+Mn values from Upper Aptian to Lower Albian sequences, specially at depths about 1580 m and 1638 m (Figure 11). In fact, Fe+Mn contents in the Upper Aptian-Lower Albian are higher than values of the Albian sequence and only increase again in the Upper Cenomanian. In addition, the high Mn/Fe ratio is observed in Upper Aptian-Lower Albian sediments (e.g., about 1667 m). This can point to an excess of Mn rather than a lack in Fe, once Mn is less frequent in phyllosilicate. However, Mn enrichment can also reflect the presence of oxides. The Upper Aptian-Lower Albian sediments are also marked by high values of Ni+Cr+V contents at depth about 1537 m and 1667 m.

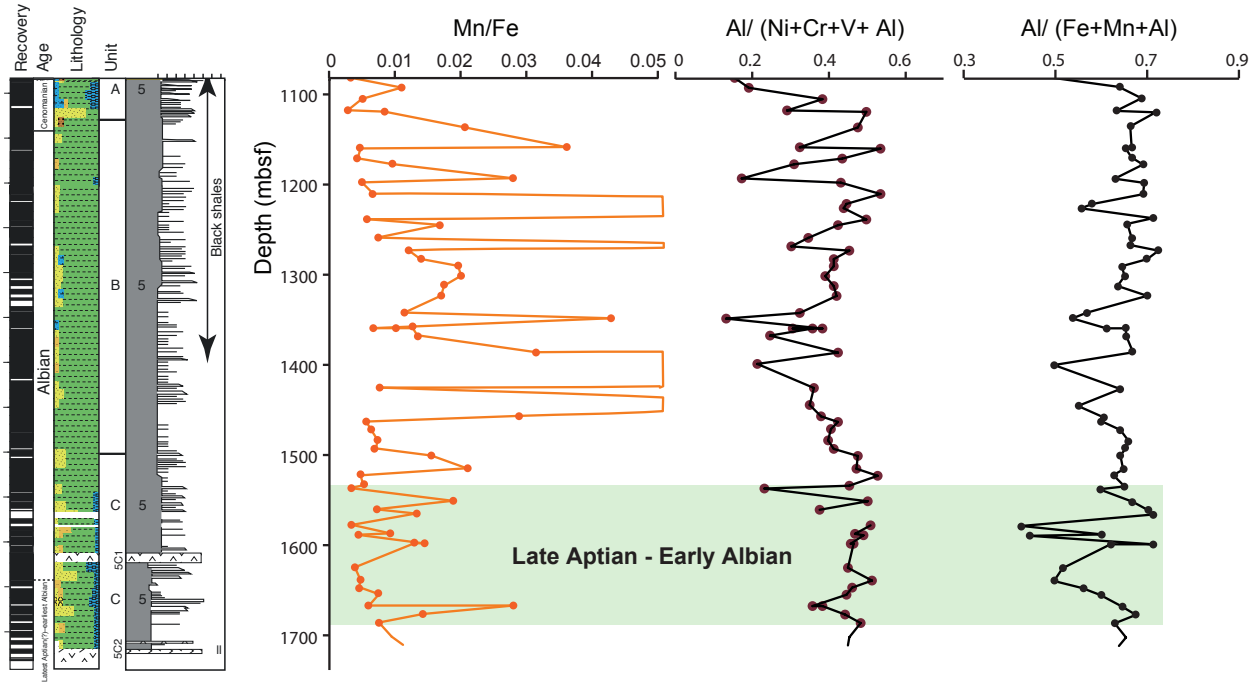

Figure 11. Geochemical variation from the ODP Site 1276. The Mn/Fe graphic shows the Mn/Fe increases to the right. The Al/(Ni+Cr+V+Al) and Al/(Fe+Mn+Al) graphic shows that the Ni+Cr+V and Fe+Mn increases to the left. Note that the Late Aptian-Early Albian is marked by an enrichment of Fe+Mn and Ni+Cr+V, interpreted to be caused by the progressive serpentinization accompanied by mantle exhumation Apart of this section, the enrichment in metals in latest Albian to Cenomanian may be caused by the progressive magmatism and the onset of the mid-ocean ridge. Data from [Robertson, 2007].

5. DISCUSSION

5.1. Fluids in Hyperextended Systems

5.1.1. Continental crust- vs. mantle-related fluids

The previous observations show that the brittle deformation accompanied by fluid-rock interaction leads to the formation of two types of fluid in hyperextended domains, one that points to a signature of the continental crust and another to that of the mantle. A possible compositional overlap observed in the continental crust is mainly caused by Si and Ca that are abundant elements in both mantle and continental sources. While in some cases Si and Ca are undoubtedly the products of saussuritization in the continental fault rocks (e.g., when it is observed at SEM that calcite and quartz veins "left" plagioclases due to albitization), in others we cannot ensure (e.g., some centimetric veins of quartz cutting through the fault zone). However, an important observation is that even far from zones of exhumed mantle, fault zones of extensional detachment described more continentalwards are heavily cut by quartz and calcite veins [*Pinto et al.*, 2014b, in prep.].

As shown in Figure 7A and 8 serpentinization also leads to major losses of Si and Ca.

While the presence of Ca is strongly evidenced by calcite veins in the serpentinites and fault zones in the exhumed mantle, quartz veins (Si) are rarely observed in exhumed mantle at rifted margin. Nevertheless, fluids formed by serpentinization processes can be distinguished from those due to saussuritization, using trace elements such as Ni, Cr and V [*Pinto et al*., 2014b, in prep.]. In this study we use the term "mantle-related fluids" for fluids that are related to high values of e.g., Ni, Cr, V, Fe and Mn. However, since in all examples the mantle rocks show evidence for syn- to post exhumation magmatic activity [*Schaltegger et al*., 2002; *Bronner et al*., 2011; *Manatschal et al*., 2011; *Pinto et al*., 2014a, in prep.], we do not ignore the possibility of some water-rock interaction with mafic rocks, although they are very few compared to the volume of serpentinized peridotites.

An important point is that the overlying sediments may also register the composition of both fluids, once they lie above extensional detachment systems in the continent or on the exhumed mantle. In the following section we discuss the evidence for these types of fluids in the mantle, fault zones and in the sediments.

5.1.2. **Evidence for fluid flow in the mantle and the composition of mantle-related fluids**

First-order evidence for fluid flow during serpentinization can be shown by the formation of hydrated minerals such as serpentine, chlorite and brucite as well as by the intensely multi-stage veining (e.g., chrysotile, lizardite and calcite). As shown in Figures 7A and 8, serpentinization is also responsible for leaching major and trace elements. As seawater percolates through the porous space (including fractures) these element losses can enrich the fluid in dissolved elements such as Si, Mg, Ca, Fe, Mn, Ni, Cr and V. This has been demonstrated at ultramafic-hosted hydrothermal systems at MAR [e.g., *Shanks*, 2001] and by laboratory experiments [e.g., *Ogasawara et al*., 2013].

The composition of the fluids can be constrained by the formation of minerals that resulted of fluid flow in the mantle as previously described in the serpentinites and in the fault zone in the mantle. Macro evidence for these mineralizations are better exemplified by spots of Fe-oxide crusts in the serpentinites from the Pyrenees (Figure 6F), what has been also described in the Alpine Tethyan serpentinites [*Pinto et al.,* 2014b, in prep.]. Fe-oxides are also often observed in veins of serpentine and calcite showing an important circulation of Ca- and Fe-enriched fluid. The occurrence of andradite and hydroandradite in serpentine veins from the ODP Site 1068 [*Beard and Hopkinson,* 2000] is an evidence for percolation of fluids enriched in Si and Fe. In the same site the presence of awaruite and pentlandite (Ni-Fe alloys and sulfide) in veins is also an evidence for

Ni- and Fe-enriched fluids.

5.1.3. The record of fluids in the fault rocks from continental extensional detachment systems

Major evidence for fluid migration in the extensional detachment systems is depicted by syn-tectonic phyllosilicates in the matrix of fault rocks that are product of water-assisted saussuritization reactions. This process is responsible for losses in Si and Ca that can be observed along the fault zone in form of quartz and calcite veins. Many of these veins are parallel to the cataclastic foliation showing that fluids were focused along the fault. Fe-oxides and Fe-rich chlorite forming a rim around plagioclase (Figure A2) are also often observed following the matrix of the foliated cataclasite (Figure 4A) suggesting that Fe was a component of this fluid. We interpreted that the imprint of a fluid enriched in Si and Ca in continental extensional detachment systems is originated in the continental crust during deformation and detachment activity. This is supported by high-resolution SEM-BSE data of quartz and calcite veins formed by albitization and sericitization reactions (e.g., Figure A6). Moreover, quartz and calcite veins also occur in other detachment fault systems, away from hyperextended domains, therefore without a direct relationship with mantle exhumation [*Pinto et al*., 2014b, in prep.].

The origin of Fe in the continental fault zone is hard to prove as it is a major element in the continental crust rocks. However, in the studied sites Fe-rich secondary phases are usually found in extensional detachment system in hyperextended domains and rarely in more proximal domains of magma-poor rifted margin. In addition, as shown in Figure 7B-D, Fe is gained along fault zones of those detachment systems, indicating that its origin is external to the continental system.

Apart from the physical evidence, the percolation of fluid is also shown by the gains of trace elements registered in the syn-tectonic phyllosilicate in the fault rocks. They are best depicted by Ni, Cr, and V. *Pinto et al*. [2014b, in prep.] interpreted these trace metals as proxies for mantle-related fluids in the distal margin, mainly based on the observation that (i) they are hundreds of time higher in mantle than in continental rocks, (ii) these elements are lost during serpentinization and they were retained (gained) (See Figure 7A and 8) in the fault rocks along extensional detachment systems (See Figure 7B-E) responsible for mantle exhumation in hyperextended domains, and (iii) they are not observed in extensional detachment systems in the more proximal parts of the margin. This leads to the conclusion that they must be channelized along detachment systems that are responsible for mantle exhumation.

5.1.4. **"Formation" of mantle-related fluids and their migration along detachment fault zones**

The characterization of losses of elements caused by serpentinization, the isotopic signature, the mineral reactions and mineralizations previously described, led us to suggest that mantle-related fluids are formed under hydrothermal conditions. The best estimation under what thermal conditions the serpentinization occurred may be given by mineral stability field and ^{18}O data (Figure 9). The ^{18}O from chrysotile and lizardite veins in the serpentinites show temperatures between 70-175ºC. In the fault zone of the ODP Site 1068, the stability of marcasite points to temperature even higher that could reach up to 240ºC [*Beard and Hopkinson*, 2000]. Late calcite veining in these hydrothermal system also seems to record the decrease of the hydrothermal activity. This is shown by ^{18}O, which points to temperatures lower than 100ºC. The evidence for hydrothermal activity is in agreement with previous studies in some of the investigated domains. *Pinto et al*. [2014b, in prep.] described in the Alpine Tethyan serpentinites Fe-oxide crusts associated with high content of barite (Ba=9%) and hydrothermally formed chlorite. *Perseil and Latouche* [1989] also described ultramafic-bearing mineralization in the cherts overlying the Alpine Tethys serpentinites that were formed by hydrothermal activity. In the Iberian Margin, *Beard and Hopkinson* [2000] concluded that the ODP Site 1068 represents a fossil ultramafic-hydrothermal vent, mainly based on the chemistry and studies of mineral stability in serpentinites and fault rocks, discussed in previous sections. Moreover, the evolution of hyperextended domains is probably affected by a high thermal gradient that resulted from the lithospheric thinning as well as by exothermic serpentinization reaction [*Schuiling*, 1964], similar to what has been suggested for Lost City hydrothermal system at MAR [e.g., *Kelley et al*., 2001].

An important point is that the hydrothermal activity is concomitant with the development of the hyperextended domains. It is mainly triggered by extensional detachment faults that cut through the thinned continental crust rooting in the underling mantle allowing downward migration of seawater into the deforming and very permeable mantle, facilitating the serpentinization. These detachment faults control the progressive mantle exhumation, the increase of serpentinized zone and the degree of serpentinization resulting in the leaching of elements and the formation of mantle-related fluids. Mantle-related fluids, created by this hydrothermal system, posteriorly migrate upward through extensional detachment fault systems. The upward migration of fluids occurred during the upwarping of detachment faults when they were active, what enhanced the permeability in the fault zone [*Tenthorey and Fitzgerald*, 2006]. This fluid can posteriorly scape to the seawater and/or interact with the overlying sediments.

5.1.5. **A fluid signature in sediments from hyperextended domains**

The observation that in the Late Aptian carbonate-bearing section (ODP Site 641), Mg content increases while Ca stay constant and that this is accompanied by an increase of Mn, suggests that this is not merely related to normal variation during diagenesis and that it must exist an external and additional source for Mg. Apart of the previously mentioned metal, silicified levels in OPD Site 641 (Figure 10) occurs in the Upper Aptian sediments [*Haggerty and Germann*, 1988]. These occurrence recorded at ODP Sites 638 and 641 can be correlated with the enrichment of Ni+Cr+V and Fe+Mn in a shaly section of Late Aptian/Early Albian at ODP Site 1276 at the Newfoundland margin (Figure 11). It is important to highlight that the observed enrichment of these elements coincides with the age of mantle exhumation to the seafloor [*Tucholke and Sibuet*, 2007].

At the hyperextended domain in the Mauléon Basin, the veins of Fe-oxide/hydroxide (hematite and goethite) that cut through the Triassic pre-rift sediments evidenced the imprint of Fe-enriched fluids (Figure 6G). This happens in the breakaway of the extensional detachment fault system (NMD), which is responsible for mantle exhumation [*Jammes et al*., 2009; *Masini et al*., 2014] and where Fe-oxides are usually observed along the fault zone.

All these observations points to an enrichment in Fe, Mn, Ni, Cr, V, observed in the sediments from Iberian-Newfoundland margins and in the Mauléon Basin that can be traced along fault zones of hyperextended domains. As shown before, serpentinization leads to major losses of Fe, Mn, Ni, Cr, V. Therefore, we attribute the enrichment of these elements in the sediments to the mantle-related fluids. One can argue that the incipient magmatism observed in some of the studied domains could influence this composition. However, this influence may be of minor importance or even negligible by the following observations: (i) in the studied segment of the Iberia-Newfoundland margin, the Late Aptian is dominated by serpentinization rather than magmatic processes [*Shipboard Scientific Party*, 2004a]. This is supported by well and refraction seismic data [*Dean and Minshull*, 2000] as well as by magnetic anomalies [*Bronner et al*., 2011; *Minshull et al*., 2014]; (ii) the occurrence of these metals is also observed in fault zone from Tasna where magmatism is restricted to thin basaltic layers; (iii) these metals occurs in the West Pyrenees where magmatism is not observed in the studied section of the NMD and even the post-mantle exhumation magmatism are extremely rare; (iv) serpentinization is a major processes leading to elevated losses of these elements in hyperextended domains of magma-poor rifted margins [*Pinto et al*., 2014a, in prep.]. In addition, the observed content increases are not due to sedimentary processes, once clasts of mantle rock and its related minerals are not observed in the studied sections

[*Tucholke et al*., 2004].

Apart from the occurrence of these metal, silicification is a common process that affects the sediments in hyperextended domains. The occurrence of silicification in post-rift (i.e., post-tectonic) sediments in supradetachment basins cannot be related to saussuritization in the continental crust, once the deformation and fault activity is ceased at the time of the deposition of the Aptian sequence. Therefore, this may be also originated by major losses and subsequent transfer of Si during serpentinization (i.e., from mantle-related fluids).

The imprint of Si-rich fluids is also found in the tectono-sedimentary breccias from the Mauléon Basin and the Tasna OCT. In this case, Si is probably associated with continental crust-related fluids. This is mainly supported by the observation that detachment fault systems were active (i.e., leading to saussuritization) during the formation of these breccias, and also that Si (i.e., quart veins) can be followed from the fault zone to these breccias, which overlie the UTD and the NMD (Figure 4E and 6B).

5.1.6. **Model for fluid-flow in hyperextended domains**

Three major points need to be taken into account from the previous discussion in order to link the evolution of hyperextended domains and the fluid history in magma-poor rift systems: (i) continental crust-related fluids are observed along the detachments and tectono-sedimentary breccias over exhumed continental crust; (ii) mantle-related fluids were observed along extensional detachments over the mantle and in continental crust as well as in pre- and post-rift sediments; (iii) fluid migration ceased in segment of extensional detachment system that are no longer active moving further to the active segment of the hyperextended domain [*Pinto et al*., 2014b, in prep.] (Figure 12A-D).

Therefore, when detachment faults are active, continental crust-related fluids migrate along the fault zone interacting with the tectono-sedimentary breccias. This can happen before the detachment faults reach the mantle or even at the same time (Figure 12A). When detachments root in the mantle triggering serpentinization, mantle-related fluids migrate along the fault zones of detachment systems affecting the pre-rift section as observed in the Pyrenees (Figure 12A-B). Although with the available data we did not show that these fluids affect the syn-tectonic sediments, *Pinto et al*. [2014b, in prep.] present data from supradetachment basin in a hyperextended domain of a Alpine Tethyan margin, where syn-tectonic sediments are affect by direct migration of mantle-related fluids through extensional detachment faults.

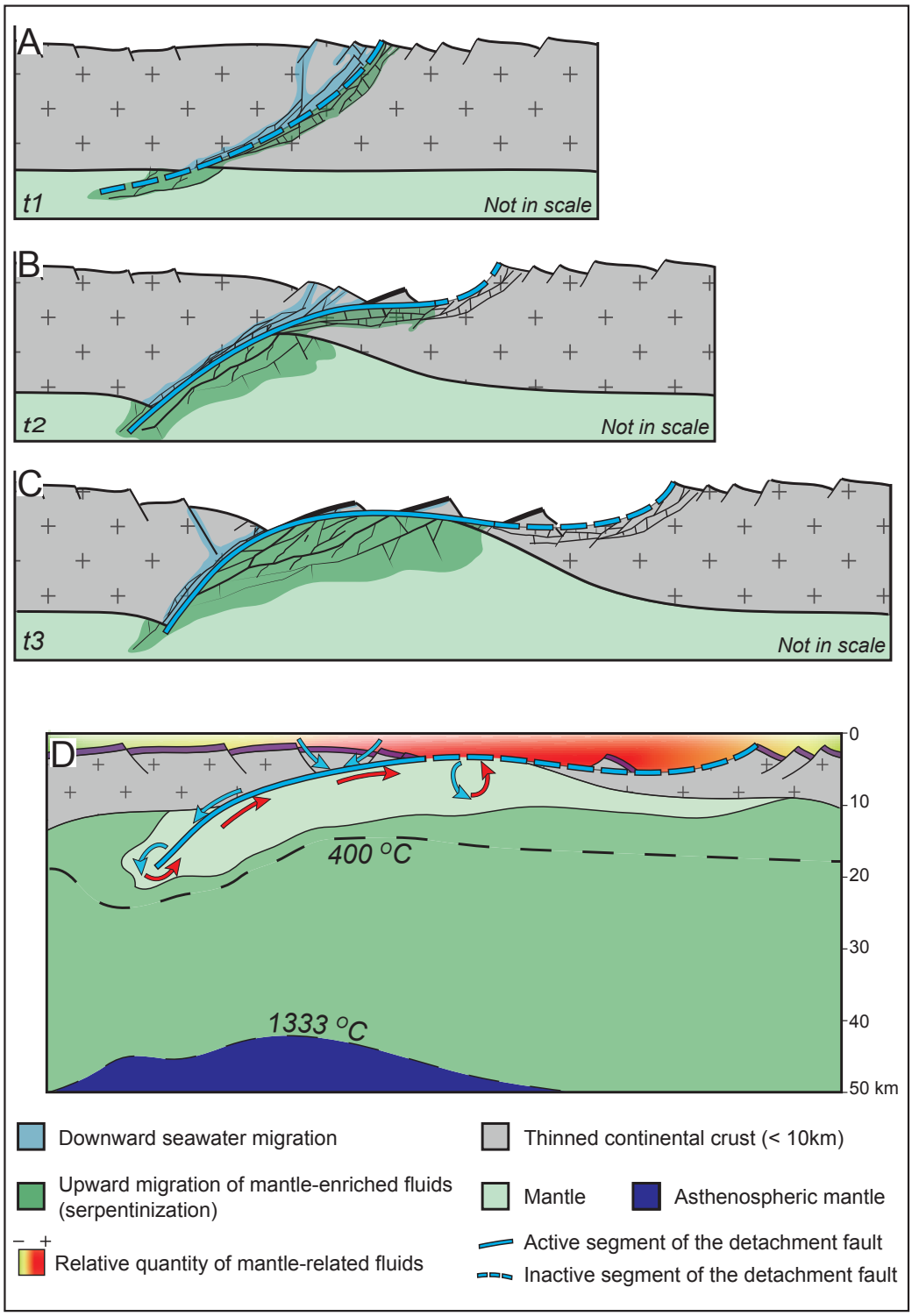

Figure 12. Formation and migration of mantle- and continental crust-related fluids. (A) Seawater percolates downward through extensional detachment systems during their activity. That results in the saussuritization of the continental crust and the serpentinization of the mantle. These processes form the continental crust- and mantle-related fluids that migrate through the detachment systems. Note that at this stage serpentinization starts bellow the thinned continental crust. (B) The evolving deformation in the hyperextended domain increases both saussuritization and serpentinization. (C) The segment of the fault is inactive close to the breakaway and deformation and fluid flow is focused in the ZECM (the upwarping segment of the detachment). (D) When mantle is exhumed at the seafloor, the mantle-related fluids pollute the seawater and affect the post-rift sediments.

When the segment of the extensional detachment fault over the continental crust are no longer active, these fluids scape in the area where the mantle is about to be exhumed (Figure 12B-C). This leads to a diffusive hydrothermal flow of mantle-related fluids, which form a plume *polluting* the seawater and interacts with the post-rift sediments (Figure 12D). The coeval deposition of sediments in the Late Aptian/Early Albian in Iberia-Newfoundland "captured" the modified-seawater signature. This process was also identified in post-tectonic sediments in the Alpine Tethyan margin [*Pinto et al*., 2014b, in prep.] and similarly in the present-day South Atlantic Ocean, where a plume of Mn-Fe extends over huge distance [*Saito et al*., 2013].

5.2. **Geochemical and sedimentological implications**

The serpentinization and mantle exhumation associated with OCT formation occurs over short time spans leading to relatively narrow and poorly connected basins (e.g., Red Sea). This system can evolve in a relative short time (about 15 Myr) and can develop later a magma-poor rifted margin during breakup. Exhumed mantle domains, such as the Iberia margin are formed by a serpentinized crust (layer) up to 5-6 km thick [*Dean and Minshull*, 2000; *Hopper et al*., 2007; *Minshull et al*., 2014] that covers more than 40,000 km^2 [*Sutra and Manatschal*, 2012; *Pinto et al*., 2014a, in prep.]. Such high volumes of serpentinized mantle lead to considerable losses of Si, Mg, Ca, Fe, Mn, Ni and Cr that can escape to the seawater or the overlying sediments [*Pinto et al*., 2014a, in prep.].

An important characteristic of these systems is that major losses of elements during serpentinization happen when the seawater of these basins is not fully connected to the global ocean (see Figure 2). Therefore, the influence of the mantle-related fluids, especially in more restricted sedimentary basins, can be enhanced leading to changes in the seawater chemistry and affecting the nature of sediments as well as syn- to post-diagenetic processes (e.g., silicification).

The observation that the transfer of elements from mantle during serpentinization can spread out in the seawater and be registered in the post-tectonic sediments, let us use it as proxy for dating serpentinization and eventually mantle exhumation in hyperextended rifted systems. This can be a useful analysis, especially in rifted margins where refraction seismic data do not exist and direct sampling of mantle rocks is not possible, but where the post-rift sedimentary rocks are usually available.

6. CONCLUSIONS

In hyperextended systems, two distinctive types of fluids are recognized, the continental crust- and mantle-related fluids. The first one is formed by saussuritization that occurs during detachment fault activity, and the second one is formed by serpentinization when these faults cut the crust and root in the mantle. The composition of continental crust-related fluids is best depicted by Ca and Si, which can be observed from their imprints along extensional detachment faults and the overlying tectono-sedimentary breccias. The mantle-related fluids are characterized by Si, Ca, Mg, Fe, Mn, Ni, Cr and V. Their imprint can also be observed along extensional detachment systems and within pre- to post-rift sediments.

As these fluids occur in all studied sites, they seem to be an important element highlighting a characteristic process in hyperextended domains, which may evolve to magma-poor rifted margins.

The evolution of hyperextended domains coincides with the formation of restrict basins, not fully connected to ocean waters. Therefore, the observed fluid flow can enhance the impact in the marine waters and sedimentary processes, affecting early diagenetic evolution in such basins.

As the mantle-related fluids are often observed in post-rift sediments, they can be used as proxies for understanding the time of serpentinization and mantle exhumation in present day magma-poor rifted margins.

Table 1. Bulk rock geochemistry of fault rocks.

Sample	*	VA-T3-07	VA-T3-20	T-7-rt	VA-T2-09	**AVG-Go**	VA-T2-08	VA-T3-18
Lithologie	*	go	go	go	go	go	ca	chl-sch-cat
Unit	*	Tasna	Tasna	Tasna	Tasna	Tasna	Tasna	Tasna
Place	*	Mot de Ri	Mot de Ri	Mot de Ri	Mot de Ri	Mot de Ri	Mot de Ri	Mot de Ri
Lab	*	Acme	Acme	SARM	SARM	*	SARM	Acme
Al_2O_3	%	15.52	15.45	17.00	16.20	16.04	16.56	10.86
CaO	%	1.00	0.88	0.98	0.87	0.93	0.67	0.51
Fe_2O_3	%	6.40	7.25	7.28	6.36	6.82	6.24	4.85
K2O	%	3.14	3.53	3.53	4.70	3.73	4.36	2.51
MgO	%	2.95	4.13	3.69	4.19	3.74	3.18	1.94
MnO	%	0.07	0.10	0.11	0.09	0.09	0.09	0.06
Na_2O	%	2.33	1.26	1.27	0.84	1.43	1.50	0.99
P_2O_5	%	0.17	0.16	0.16	0.14	0.16	0.12	0.06
SiO_2	%	64.33	62.35	61.80	61.97	62.61	63.13	74.79
TiO_2	%	0.51	0.92	1.01	0.79	0.81	0.75	0.75
As	ppm	7.70	8.00	-	4.83	6.84	3.44	6.70
Ba	ppm	380.00	654.00	828.70	671.10	633.45	731.90	489.00
Be	ppm	3.00	3.00	*	3.36	3.12	1.82	2.00
Bi	ppm	0.20	<0.1	*	< L.D.	0.20	0.13	0.10
Cd	ppm	1.00	<0.1	1.00	0.33	0.78	0.14	<0.1
Ce	ppm	45.70	67.50	134.00	70.49	79.42	84.99	80.50
Co	ppm	21.80	13.00	20.20	17.97	18.24	10.89	12.40
Cr	ppm	41.05	68.42	126.60	130.00	91.52	79.12	61.58
Cs	ppm	5.00	2.00	2.61	3.74	3.34	2.98	2.10
Cu	ppm	195.70	25.10	41.90	31.79	73.62	12.90	16.50
Dy	ppm	8.43	4.78	6.60	4.45	6.06	3.47	3.89
Er	ppm	4.92	2.57	3.74	2.36	3.40	1.86	2.23
Eu	ppm	1.70	1.36	1.96	1.19	1.55	1.28	1.13
Ga	ppm	18.90	19.40	*	22.21	20.17	24.25	14.10
Gd	ppm	8.30	5.92	9.30	5.21	7.18	4.78	5.17
Hf	ppm	4.10	6.10	10.63	5.39	6.56	6.82	8.60
Ho	ppm	1.61	0.97	1.41	0.85	1.21	0.64	0.76
La	ppm	30.40	34.80	67.52	35.89	42.15	41.46	38.50
Lu	ppm	0.51	0.37	0.54	0.36	0.44	0.30	0.34
Mo	ppm	<0.1	0.60	1.80	< L.D.	1.20	0.52	0.20
Nb	ppm	9.80	12.90	18.68	12.26	13.41	13.32	12.10
Nd	ppm	30.90	31.40	57.46	31.67	37.86	35.59	35.30
Ni	ppm	50.60	35.10	46.00	48.15	44.96	34.98	30.30
Pb	ppm	17.60	18.80	50.80	22.07	27.32	9.67	10.70
Pr	ppm	7.39	8.26	15.40	8.37	9.85	9.82	9.39
Rb	ppm	115.90	105.00	122.10	127.50	117.63	120.60	81.70
Sb	ppm	<0.1	<0.1	0.40	< L.D.	0.40	< L.D.	<0.1
Sc	ppm	8.00	15.00	15.60	16.37	13.74	15.28	10.00
Sm	ppm	7.46	6.29	11.01	6.20	7.74	6.72	6.44
Sn	ppm	3.00	3.00	3.70	1.61	2.83	1.55	<1
Sr	ppm	73.60	28.10	40.00	41.80	45.88	52.36	38.60
Ta	ppm	0.70	0.80	1.72	0.94	1.04	0.97	0.60
Tb	ppm	1.37	0.90	1.26	0.77	1.08	0.66	0.72
Th	ppm	8.50	10.60	21.90	11.47	13.12	17.01	14.50
Tm	ppm	0.68	0.38	0.55	0.34	0.49	0.28	0.33
U	ppm	30.60	2.30	2.05	1.57	9.13	1.61	1.70
V	ppm	91.00	119.00	127.20	108.50	111.43	102.10	71.00
W	ppm	0.60	0.90	1.30	1.64	1.11	0.82	<0.5
Y	ppm	45.00	28.10	37.70	25.73	34.13	18.05	20.20
Yb	ppm	3.84	2.52	3.54	2.27	3.04	1.89	2.32
Zn	ppm	155.00	88.00	83.00	115.50	110.38	118.50	65.00
Zr	ppm	164.40	230.10	349.40	201.10	236.25	253.80	327.00

Table 1. Bulk

Sample	**AVG-Ca**	VA-L-9a	VA-L-9b	VA-BI3-1	**AVG-Gr**	VP-GAR-01.A	VP-GAR-03.B
Lithologie	ca	Granite	Granite	Granite	Granite	Paragneiss	ca
Unit	Tasna	Middle Err	Middle Err	Middle Err	Middle Err	G-1a	G-3B
Place	Mot de Ri	Laviner	Laviner	Val Bever	-	Leuco proto	red catac
Lab	*	SARM	LHyGeS	ACME	*	SARM	SARM
Al_2O_3	13.71	15.84	15.80	20.59	17.41	2.97	1.16
CaO	0.59	1.53	1.64	6.13	3.10	< L.D.	< L.D.
Fe_2O_3	5.55	2.70	3.14	4.89	3.58	2.03	2.26
K2O	3.44	3.88	3.82	2.35	3.35	0.51	0.05
MgO	2.56	1.05	1.04	1.41	1.17	0.57	0.51
MnO	0.07	0.04	0.05	0.06	0.05	0.01	0.00
Na_2O	1.25	4.03	3.83	3.96	3.94	0.07	< L.D.
P_2O_5	0.09	0.17	0.23	0.18	0.19	< L.D.	< L.D.
SiO_2	68.96	67.45	67.60	56.87	63.97	92.02	93.84
TiO_2	0.75	0.32	0.38	0.62	0.44	0.26	0.22
As	5.07	2.13	*	<0.5	2.13	2.14	3.19
Ba	610.45	724.80	820.90	602.00	715.90	85.02	13.46
Be	1.91	2.77	*	2.00	2.39	< L.D.	< L.D.
Bi	0.11	< L.D.	*	<0.1	<L.D.	0.18	< L.D.
Cd	0.14	< L.D.	0.30	<0.1	0.30	0.22	0.25
Ce	82.75	77.35	118.00	16.60	70.65	29.45	14.79
Co	11.65	3.95	7.00	6.80	5.92	4.02	2.72
Cr	70.35	15.00	31.70	20.53	22.41	21.76	22.30
Cs	2.54	1.79	1.81	3.80	2.47	0.25	< L.D.
Cu	14.70	< L.D.	24.70	5.60	15.15	< L.D.	5.54
Dy	3.68	3.08	4.08	3.70	3.62	1.52	2.71
Er	2.04	1.34	1.92	2.10	1.79	0.89	1.66
Eu	1.21	1.20	1.48	1.65	1.44	0.35	0.44
Ga	19.18	20.07	-	24.80	22.44	4.05	2.54
Gd	4.98	4.29	6.38	3.65	4.77	1.60	2.09
Hf	7.71	3.71	5.01	7.50	5.41	6.32	9.76
Ho	0.70	0.51	0.77	0.77	0.69	0.32	0.61
La	39.98	40.00	62.61	7.60	36.74	14.06	7.92
Lu	0.32	0.17	0.23	0.33	0.24	0.16	0.29
Mo	0.36	< L.D.	*	0.20	0.20	< L.D.	< L.D.
Nb	12.71	11.01	16.03	9.40	12.15	4.51	3.59
Nd	35.45	31.19	47.27	11.90	30.12	11.43	8.31
Ni	32.64	9.78	10.00	3.60	7.79	9.13	7.75
Pb	10.19	17.86	30.20	5.20	17.75	4.29	2.65
Pr	9.60	8.61	13.10	2.42	8.04	3.16	2.08
Rb	101.15	115.70	133.60	141.00	130.10	16.59	3.46
Sb	< L.D.	< L.D.	0.50	<0.1	0.50	< L.D.	< L.D.
Sc	12.64	7.30	8.46	13.00	9.59	2.04	2.48
Sm	6.58	5.63	8.20	3.26	5.70	2.02	1.97
Sn	1.55	1.19	2.70	4.00	2.63	1.37	< L.D.
Sr	45.48	204.50	207.30	340.50	250.77	51.21	6.84
Ta	0.79	1.27	1.87	1.00	1.38	0.39	0.36
Tb	0.69	0.59	0.77	0.64	0.67	0.25	0.39
Th	15.76	14.19	19.80	3.10	12.36	5.45	4.26
Tm	0.30	0.18	0.26	0.34	0.26	0.14	0.25
U	1.66	2.04	2.64	4.40	3.03	0.90	0.86
V	86.55	28.25	37.50	59.00	41.58	17.79	23.32
W	0.82	0.70	*	0.90	0.80	0.59	0.91
Y	19.13	15.36	20.60	19.60	18.52	8.50	18.53
Yb	2.10	1.15	1.57	2.07	1.60	0.96	1.74
Zn	91.75	44.32	47.90	61.00	51.07	16.79	18.07
Zr	290.40	145.80	159.70	347.20	217.57	253.10	403.50

7. REFERENCES

Afilhado, A., L. Matias, H. Shiobara, A. Hirn, L. Mendes-Victor, and H. Shimamura (2008), From unthinned continent to ocean: The deep structure of the West Iberia passive continental margin at 38°N, *Tectonophysics*, *458*(1-4), 9–50, doi:10.1016/j.tecto.2008.03.002.

Ando, A., H. Kawahata, and T. Kakegawa (2006), Sr/Ca ratios as indicators of varying modes of pelagic carbonate diagenesis in the ooze, chalk and limestone realms, *Sediment. Geol.*, *191*(1-2), 37–53, doi:10.1016/j.sedgeo.2006.01.003.

Baker, P. A., J. M. Gieskes, and H. Elderfield (1982), Diagenesis of Carbonates in Deep-Sea Sediments--Evidence From SR/CA Ratios and Interstitial Dissolved SR2+ Data, *SEPM J. Sediment. Res.*, *Vol. 52*(1), 71–82, doi:10.1306/212F7EE1-2B24-11D7-8648000102C1865D.

Beard, J. S., and L. Hopkinson (2000), A fossil, serpentinization-related hydrothermal vent, Ocean Drilling Program Leg 173, Site 1068 (Iberia Abyssal Plain): Some aspects of mineral and fluid chemistry, *J. Geophys. Res.*, *105*(B7), 16527, doi:10.1029/2000JB900073.

Bernoulli, D., and H. Weissert (1985), Sedimentary fabrics in Alpine ophicalcites, south Pennine Arosa zone, Switzerland, *Geology*, doi:10.1130/0091-7613(1985)13<755.

Boillot, G., E. L. Winterer, and A. W. Meyer (1987), *Proceedings of the Ocean Drilling Program, 103 Initial Reports*, Proceedings of the Ocean Drilling Program, edited by G. Boillot, E. L. Winterer, and A. W. Meyer, Ocean Drilling Program.

Boillot, G., J. Girardeau, and J. Kornprobst (1988), The rifting of the Galicia margin: crustal thinning and emplacement of mantle rocks on the seafloor, *Proc. Ocean Drill. Program, …*, *103*, 741–756.

Boschi, C., G. L. Früh-Green, A. Delacour, J. A. Karson, and D. S. Kelley (2006), Mass transfer and fluid flow during detachment faulting and development of an oceanic core complex, Atlantis Massif (MAR 30°N), *Geochemistry, Geophys. Geosystems*, *7*(1), n/a–n/a, doi:10.1029/2005GC001074.

Bronner, A., D. Sauter, G. Manatschal, G. Péron-Pinvidic, and M. Munschy (2011), Magmatic breakup as an explanation for magnetic anomalies at magma-poor rifted margins, *Nat. Geosci.*, *4*(8), 549–553.

Castelain, T., A. M. McCaig, and R. A. Cliff (2014), Fluid evolution in an Oceanic Core Complex: A fluid inclusion study from IODP hole U1309 D-Atlantis Massif, 30°N, Mid-Atlantic Ridge, *Geochemistry, Geophys. Geosystems*, *15*(4), 1193–1214, doi:10.1002/2013GC004975.

Clauser, S., M. Renard, and G. Richebois (1988), Contents and Isotopic Compositions of Lower Cretaceous carbonates from the Galicia Margin (ODP Leg 103): Reconstruction of the paleochemistry of the Early Cretaceous Ocean, *Proc. Ocean Drill. Program, Sci. Results*, *103*, 115–117.

Clerc, C., Y. Lagabrielle, M. Neumaier, J.-Y. Reynaud, and M. de Saint Blanquat (2012), Exhumation of subcontinental mantle rocks: evidence from ultramafic-bearing clastic deposits nearby the Lherz peridotite body, French Pyrenees, *Bull. la Soc. Geol. Fr.*, *183*(5), 443–459, doi:10.2113/gssgfbull.183.5.443.

Clerc, C., P. Boulvais, Y. Lagabrielle, and M. de Saint Blanquat (2013), Ophicalcites from the northern Pyrenean belt: a field, petrographic and stable isotope study, *Int. J. Earth Sci.*, *103*(1), 141–163, doi:10.1007/s00531-013-0927-z.

Daval, D. et al. (2011), Influence of amorphous silica layer formation on the dissolution rate of olivine at 90°C and elevated pCO2, *Chem. Geol.*, *284*(1-2), 193–209, doi:10.1016/j.chemgeo.2011.02.021.

Dean, S., and T. Minshull (2000), Deep structure of the ocean-continent transition in the southern Iberia Abyssal Plain from seismic refraction profiles: The IAM-9 transect at 40°20' N, *J. Geophys. Res.*, *105*, 5859–5885.

Desmurs, L., G. Manatschal, and D. Bernoulli (2001), The Steinmann Trinity revisited: mantle exhumation and magmatism along an ocean-continent transition: the Platta nappe, eastern Switzerland, *Geol. Soc. London, Spec. Publ.*, *187*(1), 235–266, doi:10.1144/GSL.SP.2001.187.01.12.

Dias, Á. S., and F. J. A. S. Barriga (2006), Mineralogy and geochemistry of hydrothermal sediments from the serpentinite-hosted Saldanha hydrothermal field (36°34′N; 33°26′W) at MAR, *Mar. Geol.*, *225*(1–4), 157–175, doi:http://dx.doi.org/10.1016/j.margeo.2005.07.013.

Dias, Á. S., G. L. Früh-Green, S. M. Bernasconi, and F. J. A. S. Barriga (2011), Geochemistry and stable isotope constraints on high-temperature activity from sediment cores of the Saldanha hydrothermal field, *Mar. Geol.*, *279*(1–4), 128–140, doi:http://dx.doi.org/10.1016/j.margeo.2010.10.017.

Engström, A., A. Skelton, and N. Grassineau (2007), Isotopic and petrological evidence of fluid-rock interaction at a Tethyan ocean-continent transition in the Alps: implications for tectonic processes and carbon transfer during early ocean formation, *Geofluids*, *7*(4), 401–414, doi:10.1111/j.1468-8123.2007.00194.x.

Evans, C. A., and M. Baltuck (1988), Low-temperature alteration of peridotite, Hole 637A, in *Proceedings of the Ocean Drilling Program, Scientific Results, Vol. 103*, vol. 103, pp. 235–239.

Fabriès, J., J.-P. Lorand, and J.-L. Bodinier (1998), Petrogenetic evolution of orogenic lherzolite massifs in the central and western Pyrenees, *Tectonophysics*, *292*, 145–167.

Florineth, D., and N. Froitzheim (1994), Transition from continental to oceanic basement in the Tasna nappe (Engadine window, Graubünden, Switzerland): evidence for Early Cretaceous opening of the Valais ocean, *Schweizerische Mineral. und Petrogr. Mitteilungen*, *74*(3), 437–448.

Fouquet, Y. et al. (2010), Geodiversity of hydrothermal processes along the Mid-Atlantic Ridge and ultramafic-hosted mineralization: A new type of oceanic Cu-Zn-Co-Au volcanogenic massive sulfide deposit, in *Diversity of Hydrothermal Systems on Slow Spreading Ocean Ridges*, vol. 188, pp. 321–367, AGU, Washington, DC.

Früh-Green, G. L., H. Weissert, and D. Bernoulli (1990), A multiple fluid history recorded in Alpine ophiolites, *J. Geol. Soc. London.*, *147*, 959–970.

Graham, D. W., M. L. Bender, D. F. Williams, and L. D. Keigwin (1982), Strontium-calcium ratios in Cenozoic planktonic foraminifera, *Geochim. Cosmochim. Acta*, *46*(7), 1281–1292, doi:10.1016/0016-7037(82)90012-6.

Haggerty, J. A., and S. H. Germann (1988), Resedimentation and diagenesis, including silicification, of Barremian-Aptian shallow-water carbonates from the Galicia Margin, Eastern North Atlantic, at Ocean Drilling Program Site 641, in *Proc. ODP, Sci. Results, 103*, vol. 103, edited by G. Boillot, E. L. Winterer, A. W. Meyer, and J. Applegate, pp. 513–530, College Station, TX (Ocean Drilling Program).

Hauser, A.-C., and O. Müntener (2011), New age constraints on the opening of the Piemont-Ligurian Ocean (Tasna-Nauders area, CH-A), in *9th Swiss Geoscience Meeting*, Zurich.

Hayman, N. W. (2006), Shallow crustal fault rocks from the Black Mountain detachments, Death Valley, CA, *J. Struct. Geol.*, *28*(10), 1767–1784, doi:10.1016/j.jsg.2006.06.017.

Hebert, R., K. Gueddari, M. R. LaFleche, M.-O. Beslier, and V. Gardien (2001), Petrology and geochemistry of exhumed peridotites and gabbros at non-volcanic margins: ODP Leg 173 West Iberia ocena-continent transition zone, *Geol. Soc. London, Spec. Publ.*, *187*(1), 161–189, doi:10.1144/GSL.SP.2001.187.01.09.

Hébert, R., G. Beaudoin, M. Rochon, and V. Gardien (2008), Metamorphic evolution and oxygen isotope geochemistry of rift-precursor amphibolites from Hole 1067A ODP Leg 173 off West Iberian Galicia Bank rifted margin, *Lithos*, *101*(1-2), 162–176, doi:10.1016/j.lithos.2007.07.017.

Hopper, J. R., T. Funck, and B. E. Tucholke (2007), Structure of the Flemish Cap margin, Newfoundland: insights into mantle and crustal processes during continental breakup, *Geol. Soc. London, Spec. Publ.*, *282*(1), 47–61, doi:10.1144/SP282.3.

Jagoutz, O., O. Müntener, G. Manatschal, D. Rubatto, G. Péron-Pinvidic, B. D. Turrin, and I. M. Villa (2007), The rift-to-drift transition in the North Atlantic: A stuttering start of the MORB machine?, *Geology*, *35*(12), 1087, doi:10.1130/G23613A.1.

Jammes, S., G. Manatschal, L. Lavier, and E. Masini (2009), Tectonosedimentary evolution related to extreme crustal thinning ahead of a propagating ocean: Example of the western Pyrenees, *Tectonics*, *28*(4).

Kelley, D. S. et al. (2001), An off-axis hydrothermal vent field near the Mid-Atlantic Ridge at 30 degrees N., *Nature*, *412*(6843), 145–9, doi:10.1038/35084000.

Kelley, D. S. et al. (2005), A serpentinite-hosted ecosystem: the Lost City hydrothermal field., *Science*, *307*(5714), 1428–34, doi:10.1126/science.1102556.

Lagabrielle, Y., P. Labaume, and M. de Saint Blanquat (2010), Mantle exhumation, crustal denudation, and gravity tectonics during Cretaceous rifting in the Pyrenean realm (SW Europe): Insights from the geological setting of the lherzolite bodies, *Tectonics*, *29*(4).

Manatschal, G. (1999), Fluid-and reaction-assisted low-angle normal faulting: evidence from rift-related brittle fault rocks in the Alps (Err Nappe, eastern Switzerland), *J. Struct. Geol.*, *21*(7), 777–793.

Manatschal, G. (2006), Remnants of the Ancient Tethys Margins preserved in the Ortler and Tasna units in the Alps (SE-Switzerland/N-Italy), , 1–51.

Manatschal, G., and D. Bernoulli (1998), Rifting and early evolution of ancient ocean basins: the record of the Mesozoic Tethys and of the Galicia-Newfoundland margins, *Mar. Geophys. Res.*, 371–381.

Manatschal, G., D. Marquer, and G. L. Früh-Green (2000), Channelized fluid flow and mass transfer along a rift-related detachment fault (Eastern Alps, southeast Switzerland), *Geol. Soc. Am. Bull.*, *112*(1), 21.

Manatschal, G., N. Froitzheim, M. Rubenach, and B. D. Turrin (2001), The role of detachment faulting in the formation of an ocean-continent transition: insights from the Iberia Abyssal Plain, *Geol. Soc. London, Spec. Publ.*, *187*(1), 405–428.

Manatschal, G., A. Engström, L. Desmurs, U. Schaltegger, M. Cosca, O. Müntener, and D. Bernoulli (2006), What is the tectono-metamorphic evolution of continental break-up: The example of the Tasna Ocean–Continent Transition, *J. Struct. Geol.*, *28*(10), 1849–1869.

Manatschal, G., D. Sauter, A. M. Karpoff, E. Masini, G. Mohn, and Y. Lagabrielle (2011), The Chenaillet Ophiolite in the French/Italian Alps: An ancient analogue for an Oceanic Core Complex?, *Lithos*, *124*(3-4), 169–184, doi:10.1016/j.lithos.2010.10.017.

Masini, E., G. Manatschal, J. Tugend, G. Mohn, and J.-M. Flament (2014), The tectono-sedimentary evolution of a hyperextended rift basin: the example of the Arzacq–Mauléon rift system (Western Pyrenees, SW France), *Int. J. Earth Sci.*, doi:10.1007/s00531-014-1023-8.

McCaig, A. M., R. a. Cliff, J. Escartin, A. E. Fallick, and C. J. MacLeod (2007), Oceanic detachment faults focus very large volumes of black smoker fluids, *Geology*, *35*(10), 935, doi:10.1130/G23657A.1.

Milliken, K., and J. Morgan (1996), Chemical evidence for near-seafloor precipitation of calcite in serpentinites (site 897) and serpentinite breccias (site 899), Iberia Abyssal Plain, in *Proceedings of the Ocean Drilling Program, Scientific Results, Vol. 149*, vol. 149, edited by R. B. Whitmarsh, D. S. Sawyer, and D. G. Klaus, A., and Masson, pp. 553–558.

Minshull, T. A., S. M. Dean, and R. B. Whitmarsh (2014), The peridotite ridge province in the southern Iberia Abyssal Plain: Seismic constraints revisited, *J. Geophys. Res. Solid Earth*, *119*(3), 1580–1598, doi:10.1002/2014JB011011.

Morgan, J. K., and K. L. Milliken (1996), Petrography of calcite veins in serpentinized peridotite basement rocks from the Iberia Abyssal Plain, Sites 897 and 899: kinematic and environmental implications, in *Proceedings of the Ocean Drilling Program, Scientific Results*, vol. 149, edited by R. B. Whitmarsh, D. S. Sawyer, A. Klaus, and D. G. Masson, pp. 559–569.

Müntener, O. (2010), Serpentine and serpentinization: A link between planet formation and life, *Geology*, *38*(10), 959–960, doi:10.2747/0020.

Müntener, O., G. Manatschal, L. Desmurs, and T. Pettke (2010), Plagioclase Peridotites in Ocean-Continent Transitions: Refertilized Mantle Domains Generated by Melt Stagnation in the Shallow Mantle Lithosphere, *J. Petrol.*, *51*(1-2), 255–294, doi:10.1093/petrology/egp087.

Ogasawara, Y., A. Okamoto, N. Hirano, and N. Tsuchiya (2013), Coupled reactions and silica diffusion during serpentinization, *Geochim. Cosmochim. Acta*, *119*, 212–230, doi:10.1016/j.gca.2013.06.001.

Péron-Pinvidic, G., and G. Manatschal (2009), The final rifting evolution at deep magma-poor passive margins from Iberia-Newfoundland: a new point of view, *Int. J. Earth Sci.*, *98*(7), 1581–1597.

Perseil, E. A., and L. Latouche (1989), Découverte de microstructures de nodules polymétaliques dans les minéralisations manganésifères métamorphiques de Falotta et de Parsettens (Grisons-Suisse), *Miner. Depos.*, *24*, 111–116.

Pinto, V. H., G. Manatschal, A. M. Karpoff, E. Masini, and A. Viana (2014a), Implication of element loss and mantle hydration during serpentinization in rifted margins,

Pinto, V. H., G. Manatschal, A. M. Karpoff, and A. Viana (2014b), Tracing mantle-related fluids in magma-poor rifted margins: the example of Alpine Tethyan rifted margins,

Potdevin, J. L., and D. Marquer (1987), Quantitative Methods for the Estimation of Mass Transfers by Fluids in Deformed Metamorphic Rocks, *Geodin. Acta*, *1*(3), 193–206.

Robertson, A. H. F. (2007), Geochemical evidence for the sedimentary and diagenetic development of the Mesozoic–early Cenozoic Newfoundland rifted margin, northwest Atlantic (Ocean Drilling Program Leg 210, Site 1276)., in *Proceedings of the Ocean Drilling Program, Scientific Results*, vol. 210, edited by B. E. Tucholke, J.-C. Sibuet, and A. Klaus, Ocean Drilling Program, College Station, TX (Ocean Drilling Program).

Russell, M. J. (2007), The alkaline solution to the emergence of life: energy, entropy and early evolution., *Acta Biotheor.*, *55*(2), 133–79, doi:10.1007/s10441-007-9018-5.

Russell, S. M., and R. B. Whitmarsh (2003), Magmatism at the west Iberia non-volcanic rifted continental margin: evidence from analyses of magnetic anomalies, *Geophys. J. Int.*, *154*(3), 706–730, doi:10.1046/j.1365-246X.2003.01999.x.

Saito, M. a., A. E. Noble, A. Tagliabue, T. J. Goepfert, C. H. Lamborg, and W. J. Jenkins (2013), Slow-spreading submarine ridges in the South Atlantic as a significant oceanic iron source, *Nat. Geosci.*, *6*(9), 775–779, doi:10.1038/ngeo1893.

Schaltegger, U., L. Desmurs, G. Manatschal, O. Muntener, M. Meier, M. Frank, and D. Bernoulli (2002), The transition from rifting to sea-floor spreading within a magma-poor rifted margin: field and isotopic constraints, *Terra Nov.*, *14*, 156–162.

Schuiling, R. D. (1964), Serpentinization as a Possible Cause of High Heat-flow Values in and near the Oceanic Ridges, *Nature*, *201*(4921), 807–808, doi:10.1038/201807b0.

Shanks, W. C. (2001), Stable Isotopes in Seafloor Hydrothermal Systems: Vent fluids, hydrothermal deposits, hydrothermal alteration, and microbial processes, *Rev. Mineral. Geochemistry*.

Shipboard Scientific Party (2004a), Leg 210 summary, in *Proc. ODP, Init. Repts., 210*, vol. 210, edited by B. E. Tucholke, J.-C. Sibuet, and A. Klaus, pp. 1–78, Ocean Drilling Program, College Station, TX (Ocean Drilling Program).

Shipboard Scientific Party (2004b), Site 1276, in *ODP, Init. Repts., 210*, vol. 210, edited by B. E. Tucholke, J.-C. Sibuet, and A. Klaus, pp. 1–358, Ocean Drilling Program, College Station, TX (Ocean Drilling Program).

Skelton, A. D. ., and J. W. Valley (2000), The relative timing of serpentinisation and mantle exhumation at the ocean–continent transition, Iberia: constraints from oxygen isotopes, *Earth Planet. Sci. Lett.*, *178*(3-4), 327–338, doi:10.1016/S0012-821X(00)00087-X.

Sutra, E., and G. Manatschal (2012), How does the continental crust thin in a hyperextended rifted margin? Insights from the Iberia margin, *Geology*, *40*(2), 139–142, doi:10.1130/G32786.1.

Sutra, E., G. Manatschal, G. Mohn, and P. Unternehr (2013), Quantification and restoration of extensional deformation along the Western Iberia and Newfoundland rifted margins, *Geochemistry, Geophys. Geosystems*, *14*(8), 2575–2597, doi:10.1002/ggge.20135.

Tenthorey, E., and J. Fitzgerald (2006), Feedbacks between deformation, hydrothermal reaction and permeability evolution in the crust: Experimental insights, *Earth Planet. Sci. Lett.*, *247*(1-2), 117–129, doi:10.1016/j.epsl.2006.05.005.

Tucholke, B. E., and J. Sibuet (2007), Leg 210 synthesis: tectonic, magmatic, and sedimentary evolution of the Newfoundland-Iberia rift, in *Proc. ODP, Sci. Results, 210*, vol. 210, edited by B. E. Tucholke, J.-C. Sibuet, and A. Klaus, pp. 1–56, Ocean Drilling Program, College Station, TX (Ocean Drilling Program).

Tucholke, B. E., J.-C. Sibuet, and A. Klaus (2004), Site 1276, in *Proceedings of the Ocean Drilling Program, Initial Reports Volume 210*, vol. 210.

Whitmarsh, R. B., M. O. Beslier, and P. J. Wallace (1998), *Proceedings of the Ocean Drilling Program, Initial Reports, 173*.

Wilson, R. C. L., G. Manatschal, and S. Wise (2001), Rifting along non-volcanic passive margins: stratigraphic and seismic evidence from the Mesozoic successions of the Alps and western Iberia, *Geol. Soc. London, Spec. Publ.*, *187*(1), 429–452, doi:10.1144/GSL.SP.2001.187.01.21.

ARTICLE 3

IMPLICATIONS OF ELEMENT LOSS AND MANTLE HYDRATION DURING SERPENTINIZATION IN RIFTED MARGINS

Victor Hugo G. Pinto[1,2], Gianreto Manatschal[1], Anne Marie Karpoff[1] and Adriano Viana[2]

[1]Institut de Physique du Globe de Strasbourg, CNRS UMR7516, Université de Strasbourg, 1 rue Blessig, 67084 Strasbourg Cedex, France.

[2]Exploration & Production, Petrobras S.A., Av. República do Chile, 330, Rio de Janeiro, Brazil.

ABSTRACT

Serpentinization along exhumed mantle domain may have contributed to the evolution of early life, the change of the seawater chemistry and the physical properties of the lithosphere. At Ocean-Continent Transitions (OCT) of magma-poor rifted margins serpentinization is a major process. Nonetheless, neither the quantification of the amount of serpentinization nor the associated water absorption and element losses have ever been attempted. Here we present a first-order quantification based on geological observation and new available data derived from present-day and fossil rifted margins. We use geophysical and petrological data to quantify the amount of water absorbed and element losses during serpentinization along the OCT of the Central Western Iberian Margin. The results show that approximately 17,142 km^3 of water can be absorbed in the mantle accompanying significant loss of Si, Mg, Fe, Mn, Ca, Ni and Cr of the order of 10^{14} tons that are caused by serpentinization. We conclude that water absorption may have important implications for rheological changes, lithospheric strength, and eventual subsequent reactivation and subduction. In addition, the losses of elements may play an important role on the geochemical budget of seawater as well as on the nature of sediments and diagenesis during mantle exhumation that predates breakup and early seafloor spreading.

TABLE OF CONTENTS

1. INTRODUCTION

It is well known that serpentinization can absorb large volumes of water. Serpentinites sampled on both OCT and oceans by ocean drilling or dredging as well as from exposed ophiolites have allowed the characterization of many reactions [*Ogasawara et al*., 2013] and processes linked to serpentinization and mantle exhumation. In the last 15 years, fluids have been directly sampled from active ultramafic-hosted hydrothermal vents associated with oceanic core complexes (OCC) at slow to ultraslow spreading Mid-Ocean Ridges (MOR) showing that serpentinization is responsible for a significant mass transfer [*Boschi et al*., 2006; *McCaig et al*., 2007; *MacLeod et al*., 2009]. The composition of these fluids is best depicted by H_2 and CH_4 gases and dissolved Si, Mg, Ca, Fe, Mn, Ni and Co [*Kelley et al*., 2001; *Fouquet et al*., 2010; *Seyfried et al*., 2011]. In the fossil rifted margins exposed in the Alps, large amount of hydrothermal cherts (SiO_2) presenting botryoidal Mn minerals and Fe-Ni alloys are found covering the exhumed subcontinental mantle [*Perseil and Latouche*, 1989], where serpentinization is responsible for the formation of Si-enriched fluids [*Pinto et al*., 2014a, in prep.]. This is supported by recent laboratory results where a SiO_2 layer is formed at the edges of the apparatus when olivine minerals are subjected to water injection [*Daval et al*., 2011], and by dissolved SiO_2 in the aqueous solution after hydration of pyroxene and olivine [*Ogasawara et al*., 2013]. Element losses as Ca, Mg and Si produced by serpentinization were also described by small scale studies from ODP sites at rifted margins [*Gibson et al*., 1996; *Morgan and Milliken*, 1996]. Although, it is known that serpentinization leads to major element loss, there are neither studies that discuss the amount of elements losses and water absorption nor their importance for the global seawater and sedimentary chemistry during hyperextension and mantle exhumation that result in the formation of OCT. This is mainly due to the fact that only 5 wells sampled the exhumed mantle and related sediments at OCT, to the fact that hydrothermal systems at OCT are no long active and also because many processes related to the formation of OCT are still not well understood. Nevertheless, field observation and recent petrological studies of remnants of exhumed continental mantle from the Alpine Tethyan margins, together with refraction velocity and reflection seismic data from the Iberian Margin allowed us to make a first-order quantification of the volume of water absorbed and elements lost in the OCT of magma-poor rifted margin. Using density, velocity, LOI/H_2O and petrological data we established a linear equation that predicts the amount of water absorbed by serpentinites when seismic velocities in the mantle are known. Analyses of losses of elements using the Gresens-type method [*Potdevin and Marquer*, 1987] enabled us to estimate the amount of elements that can be leached during serpentinization. The overall results and observations related to serpentinization processes

at OCT point to important implications for the chemistry of seawater and sedimentary rocks during the formation of oceans. Considering that exhumed mantle occurs at more than 50% of the global distal rifted margins [*Reston and McDermott*, 2011], these processes may be of major importance for the recycling of elements, transport of water in subduction zones and may therefore have a considerable impact on the chemistry evolution of oceans and mantle reservoirs throughout the Earth's history.

2. DOMAINS AND LIMITS OF THE IBERIA MARGIN

Domains of the magma-poor Iberia rifted margins have been defined considering the thickness of the continental crust and the nature of the OCT [*Péron-Pinvidic and Manatschal*, 2009]. In a dip section, the OCT of the Iberian Margin is made of more than 160 km of serpentinized mantle that grades oceanwards to an embryonic oceanic crust and finally a Penrose type oceanic crust [*Tucholke and Sibuet*, 2007; *Péron-Pinvidic and Manatschal*, 2009]. The nature and transition of these embryonic to "truly" oceanic crust has been a matter of debate over the last two decades. Seismic velocity data, gravity and magnetic anomalies have been the main methods to improve the working hypothesis. In the Iberia-Newfoundland conjugated margins, a prominent magnetic anomaly, the J-anomaly, which encompasses M3 to M0, seems to mark an important transition between the zone of exhumed mantle to an embryonic oceanic crust. *Bronner et al*. [2011] showed in these margins that the J-anomaly can be caused by intrusive and extrusive mafic rocks in a previously serpentinized mantle and may mark the location of breakup and onset of seafloor spreading. Recently, *Minshull et al*. [2014] repositioned these anomalies in relation to the refraction data from *Dean and Minshull* [2000], which allow these data to be constrained with reflection seismic and geological observations.

Figure 1 synthetizes some major geological observations, seismic velocity and the reinterpreted IAM-9 seismic reflection section. The continental basement, between 240 and 270 km, is characterized by hyperextended continental crust that lies above a serpentinized mantle. Oceanwards, the Zone of Exhumed Continental Mantle (ZECM) is made of 5-6 km thick serpentinized mantle (240-100 km) that progressively grades to an embryonic oceanic crust (100-30 km) along the J-anomaly zone [*Russell and Whitmarsh*, 2003]. In this zone, detachment fault systems were identified [*Reston and McDermott*, 2011] and they cut the previous main detachment fault responsible for exhuming mantle rocks to the seafloor. This later detachment may also play a role in the serpentinization.

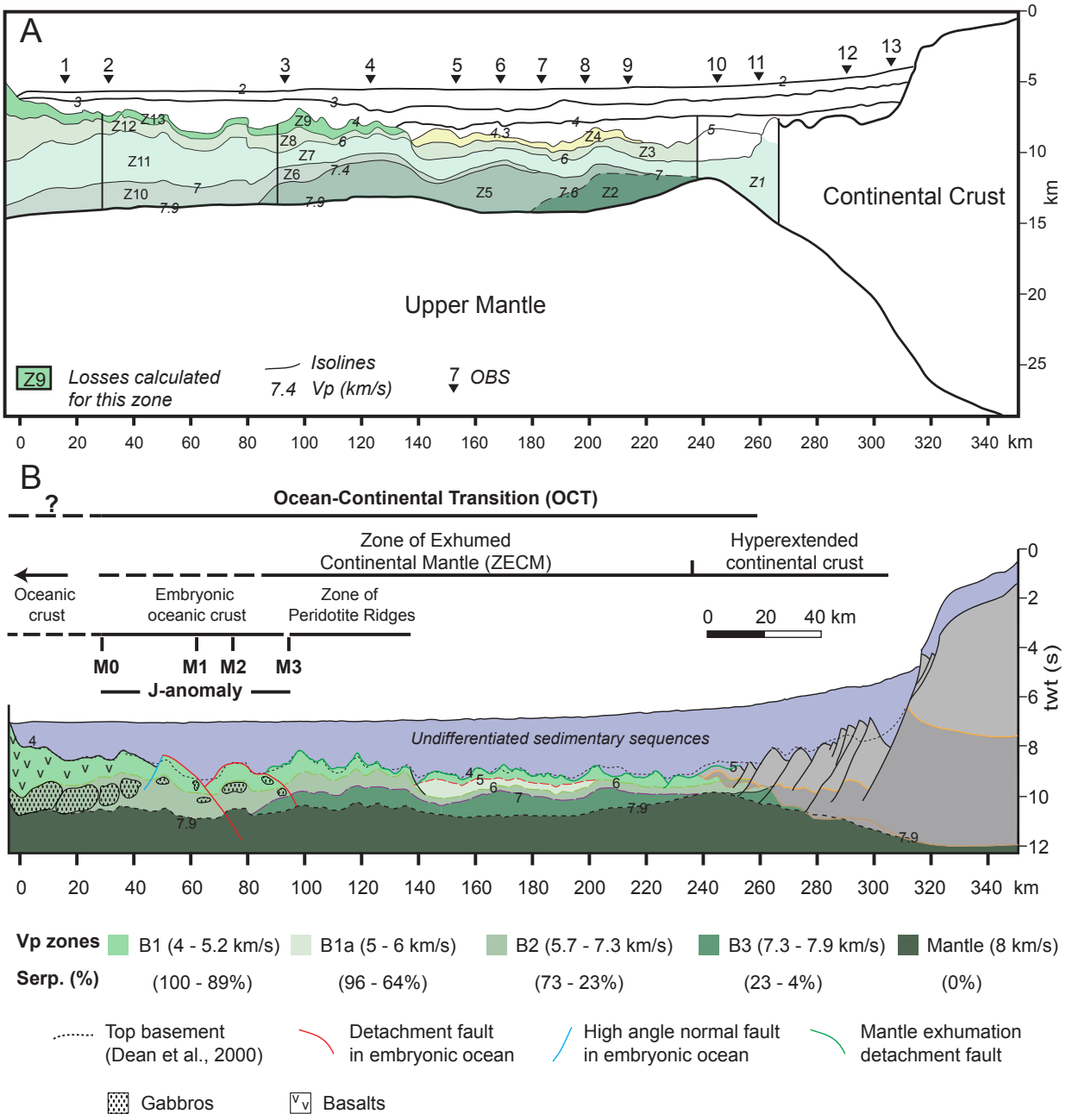

Figure 1. Seismic data from IAM-9 section. (A) Refraction data showing the velocities and the zones used to estimate the amount of water absorbed during serpentinization. Note the zones (Z1, Z2, etc.) used in the calculation. Data from *Dean and Minshull* [2000]. (B) Interpreted reflection seismic section used to define the domains and limits of the rifted margin.

3. RELATION BETWEEN VP, DENSITY, GEOCHEMISTRY AND SERPENTINIZATION

A correlation between seismic velocity (Vp), density and serpentinized peridotites (Figure 2 A-B) is described by *Miller and Christensen* [1997]. It is known that low temperature serpentine minerals (e.g., chrysotile and lizardite) have 13 %wt of water. Thus, a serpentinite composed by 100% of serpentine (i.e., 100% serpentinization) also contains 13 %wt of water. Using a data set of serpentinized peridotites [*Müntener et al*., 2010] where the degree of serpentinization was defined

by petrological criteria (e.g., presence of olivine/serpentine), we correlate the degree of serpentinization with the percentage of hydration (Figure 2C) that also corresponds to the Loss on Ignition (LOI). Taking into account all these results, it is possible to construct one model that predicts the behavior of density, Vp, hydration with the progressive serpentinization (Figure 2D).

The correlation between Vp and serpentinization was used to transform the velocity isolines in serpentinite isolines through the IAM-9 seismic section [*Dean and Minshull*, 2000] (Figure 1). The density values were used to calculate the loss of elements as explained below. The correlation between the volume of serpentinites and amount of hydration was used to calculate the mass balance in the IAM-9 section, as presented in Figure 1 and Tables 1, A1-A3, see appendix for details.

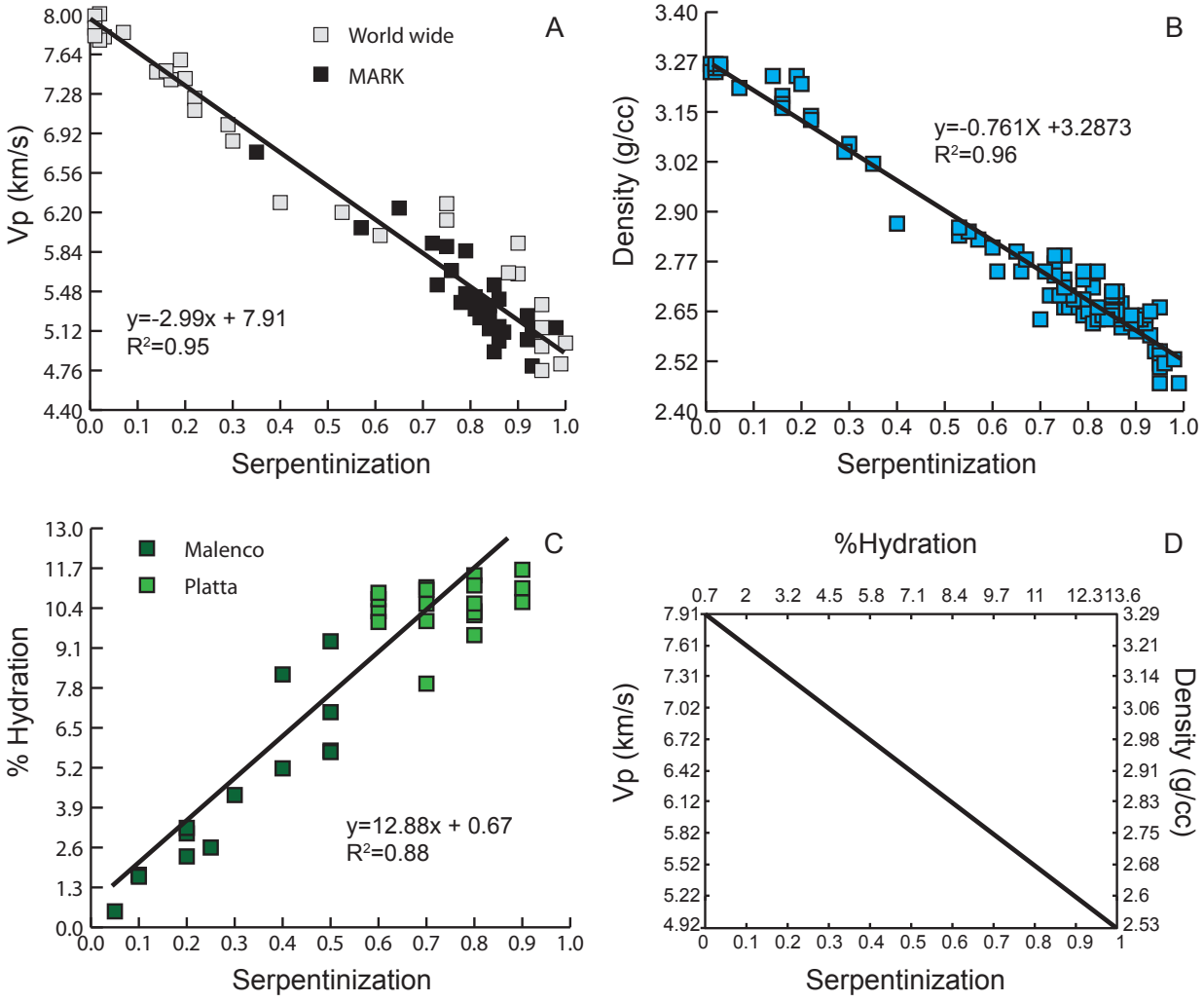

Figure 2. Petrological and petrophysical data. (A) Seismic velocity (Vp) vs. degree of serpentinization, data from *Miller and Christensen* [1997]. (B) Density vs. degree of serpentinization, data from *Miller and Christensen* [1997]. (C) Percentage of hydration vs. degree of serpentinization. The hydration corresponds to the loss on ignition (LOI) caused by the presence of water in serpentines, data from *Müntener et al.* [2010]. (D) is the proposed model that included all previous ones. This model was used to estimate the amount of water absorbed and elements lost in each zone from Figure 1A. See appendix for detailed explanation.

4. AMOUNT OF WATER ABSORBED IN THE OCT

The interpreted IAM-9 reflection and refraction seismic data (Figure 1) were used to estimate the amount of hydration and element loss through the different domains in the ZECM. Because the J-anomaly marks the onset of first embryonic oceanic crust, we assume that the zone of serpentinization extends until the end of the J-anomaly, dated as Aptian [*Shipboard Scientific Party*, 2004]. Although the embryonic oceanic crust is partially composed of magmatic rocks, the ODP Site 1070 shows that the magma was emplaced in the previously serpentinized mantle. This enables us to suggest that this zone was entirely made of serpentinites before the magmatic event that led to breakup and onset of seafloor spreading. Therefore, in our interpretation we start the serpentinization at the position 270 km and we extend it to the position 30 km, i.e., from the mantle underlying the hyperextended crust to the end of J-anomaly, which corresponds to the M0 anomaly. In addition, the choice of the M0 as a limit for our estimation is based on the fact that this anomaly is relatively easy to correlate in the southern and central part of the Iberian Margin. In order to propose a volumetric calculation of the serpentinite for the central part of Iberia margin (Table A3) we extended the map of the distribution of exhumed mantle [*Sutra and Manatschal*, 2012] to the location of the IAM-9 line (Figure 3).

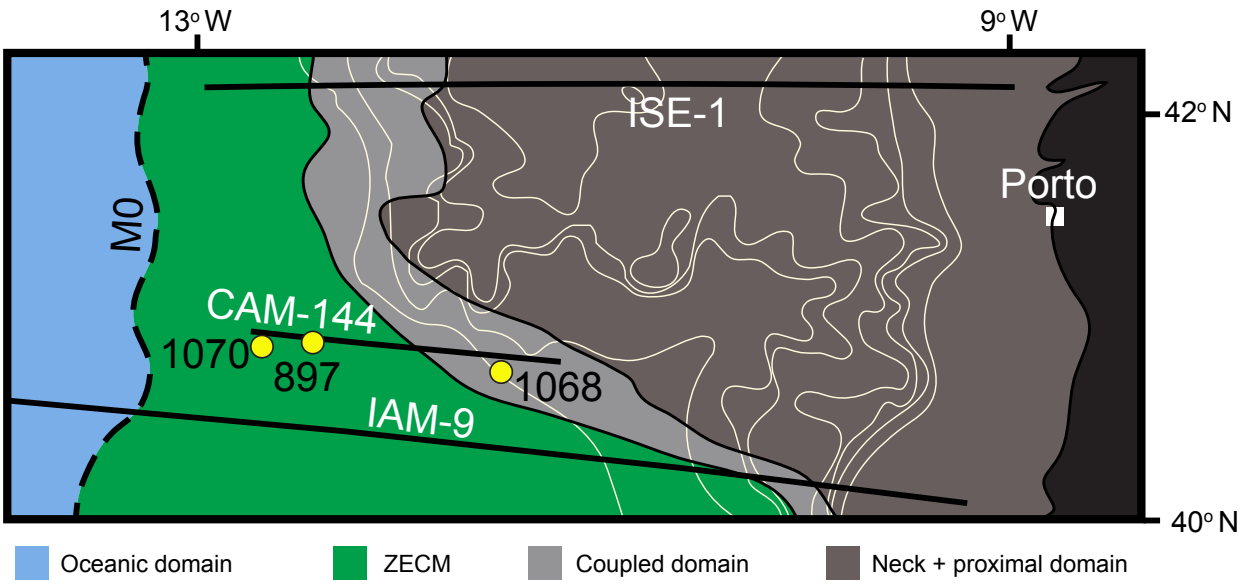

Figure 3. Map of domains from the Central Western Iberian Margin. The map was modified from *Sutra and Manatschal* [2012] and expanded to the south where is localized the IAM-9 section. Yellow circles are ODP Sites close to the IAM-9. The other reflection seismic lines (CAM-144 and ISE-1) were used for controlling the limits of the domains. This map was used to estimate the volume of water absorbed and the losses of elements in the Central Western Iberian Margin.

Based on refraction seismic data, *Minshull et al*. [2014] showed that the thickness of the serpentinized mantle is about 5-6 km (Figure 1A). Although the gradient of serpentinized peridotites changes along the ZECM, the first 3 km below the top of the exhumed serpentinized basement (until 6.4 km/s) correspond to a degree of serpentinization of up to 50%. But a detailed calculation, based on Figure 1A, coupled with the result from the model (Figure 2D) allowed us to better quantify the amount of absorbed water and the element losses in the ZECM (see appendix for calculation). The results presented in Table A2 show that there are 3,511 Gt of serpentinized rocks, which 205 Gt (205 km^3) correspond to H_2O. Using the average values calculated to the exhumed domain and coupled domain (Figure 1) we predicted that 17,142 km^3 of H_2O is absorbed in the central part of the Iberian Margin (Figure 3) which is 7% of the Red Sea water volume. As the area of serpentinized mantle at the Central Iberia Margin is 45,006 km^2 and the volume of absorbed water is 17,142 km^3, the estimated drop of water depth would be approximately 380 m, if serpentinization occurred in a closed system (i.e., without the progressive input of seawater due to the opening of the ocean).

Nevertheless, these first-order results can be influenced by seismic velocity models, since velocities can change between OBS stations [*Dean and Minshull*, 2000], and by the observation that hydration of peridotites, not only forms serpentine but also chlorite. The presence of chlorite in the serpentinites may affect the results lowering the estimated volume of water once the water content of chamosite is 8% and of clinochlore is 12%. However, chlorite is not widely present in rocks from the OCT and most of the chlorites described are clinochlore [*Beard and Hopkinson*, 2000], which show similar percentage of water as the serpentines, hence they may not strongly influence our results.

5. AMOUNT OF ELEMENT LOSSES IN OCT

Based on a dataset from the fossil OCT in the Alps, which includes samples from weak to completely serpentinized rocks [*Müntener et al*., 2010], it was possible to calculate the elemental losses during serpentinization. The major and trace elements of these serpentinites were analyzed with ICP-AES/MS and XRF [*Müntener et al*., 2010]. Using the Gresens-type method [*Potdevin and Marquer*, 1987], we were able to calculate the percentage of element losses compared to the peridotites (protolith) which is represented by mean values of the less serpentinized peridotites (i.e., samples ≤10% of serpentinization). We divided the data set in 3 groups based on petrological criteria (e.g., olivine/serpentine ratio) that share a correlation with the loss on ignition (LOI).

Therefore, the group 1 encompasses the peridotites ≤10% of serpentinization; group 2 is composed of samples between <10 and ≤60% of serpentinization; group 3 is made of samples with > 60% of serpentinization.

In order to simplify the calculations, we assumed that the zones less than 60% serpentinized (velocities>6 km/s) (see Figure 1) correspond to losses of elements related to the transformation from group 1 to group 2, which means moderate serpentinization. The zones higher than 60% serpentinized (velocities<6 km/s) correspond to losses of elements related to the transformation from group 1 to group 3, which means highly serpentinized peridotites (for a more detailed description see appendix).

The results from the IAM-9 section show that the percentages of losses compared to the peridotite protolith are between 8% and 18% for SiO_2, 10% to 19% for MgO, 1% to 3% for FeO, and about 0.1% for Ni and 0.1% for Cr (see Table 1 and Table A2 in the appendix for averages and standard deviation). The lower percentage values resulted from the consideration that the aluminum behaves as an immobile element, while the higher values consider that titanium behaves as immobile element (see Figure A1 in the Annexes of the thesis). Thus, the result strongly depends on the behavior of element immobility, which makes it difficult to determine more precise values. However, independently of the calculation, it can be shown that the results obtained in our study are similar to what has been measured over active hydrothermal system related to serpentinization [*Kelley et al*., 2001; *Edmonds*, 2010] in Mid-Ocean Ridges (MOR), as well as by laboratory serpentinization experiments [*Daval et al*., 2011; *Ogasawara et al*., 2013].

Using the seismic data (Figure 1), our serpentinization model (Figure 2D) and the mapped area of serpentinization (Figure 3) integrated with our calculated loss of elements (Table A1), it is possible to estimate the amount of element lost from the mantle into the seawater or the overlying sediments in the Iberian Margin as summarized in the Table 1 and Table A3.

6. IMPLICATIONS OF MASSIVE SERPENTINIZATION IN THE OCT

The amount of water absorbed and elements losses caused by serpentinization processes during the formation of OCT can have many implications for mantle rheology, for the chemistry of seawater and sediments as well as for economical appraisal. An important characteristic regarding the evolution of OCT is that they often develop in restricted basins where the seawater is not fully connected to the global ocean water. Therefore, our results can enhance the previously mentioned implications.

One important consequence is related to the rheological changes caused by hydration on the evolving hyperextended system and OCT formation. As our results show, a considerable volume of water of about 17142 km^3, may have been absorbed in the Central Iberia margin when the mantle was exhumed between Newfoundland and Iberia [*Tucholke and Sibuet*, 2007]. Thus, serpentinization weakens the uppermost part of the mantle [*Reston and Manatschal*, 2011] where the yield strength of 250 MPa in peridotites is reduced to about 130 MPa in serpentinite, a reduction of about 52% [*Reston and Manatschal*, 2011]. This may exert a control in the emplacement of the magmatic addition during the Aptian/ Early Abian [*Tucholke and Sibuet*, 2007; *Bronner et al*., 2011] that is followed by the emplacement of a seafloor spreading system, which is developed exactly in the domain previously weakened by hydration/serpentinization.

Serpentinization is also responsible for large amounts of elements that may be lost to this restricted basin *enriching* [*Pinto et al*., 2014a, in prep.] the seawater in elements such as Si, Mg, Ca, Fe and Mn, which can account together to up to 19% and 40% of the original unaltered peridotites, considering respectively Al and Ti as immobile (Table A2, this appendix). This is strongly supported by the losses observed at ultramafic-hosted hydrothermal systems in mid-ocean ridges (MOR) [*Kelley et al*., 2001; *Douville et al*., 2002; *Boschi et al*., 2006; *Kelley and Shank*, 2010], by laboratory experiments with olivine and pyroxenes [*Daval et al*., 2011; *Ogasawara et al*., 2013] as well as by density decrease of serpentinites [*Miller and Christensen*, 1997]. An important point is that with the areal extent and the 5-6 km thick serpentinized mantle observed in refraction data [*Dean and Minshull*, 2000; *Hopper et al*., 2007; *Afilhado et al*., 2008; *Minshull et al*., 2014] and verified by wells [*Beard and Hopkinson*, 2000; *Skelton and Valley*, 2000; *Shipboard Scientific Party*, 2004; *Jagoutz et al*., 2007] in the Iberia-Newfoundland OCT, the amounts of losses of these elements are enormous (Table 1). Although the stage of mantle exhumation occurs in a restricted setting, the fact that many margins went to mantle exhumation and serpentinization during the Cretaceous [*Dias*, 2005; *Tucholke and Sibuet*, 2007; *Unternehr et al*., 2010; *Reston and Manatschal*, 2011; *Zalan et al*., 2011] and that the same process occurred along ocean core complexes [*MacLeod et al*., 2009; *Reston and Ranero*, 2011] at MOR, the fluids produced by serpentinization may affect globally the chemistry of the oceanic waters at this period. Indeed, recent studies [*Cannat et al*., 2013; *Ligi et al*., 2013; *Saito et al*., 2013] at MOR, that attempted to quantify the volume of elements/molecules that escape through hydrothermal systems, have been pointed to large losses of gases such as CH_4 and H_2 as well as elements such as Si, Mg, Fe, Mn and Ca.

The amount of Mg, and to a lesser extent Ca, released into seas and oceans along rifted margins and MOR, should be taken into account for paleotemperature correction [*Evans and Müller*, 2012; *O'Brien et al*., 2014] since Mg/Ca ratios are used in paleoclimate studies. The results from Table 1 show that the amount of Mg losses can be about 17 times higher than Ca pointing that Mg/Ca ratio from Early to Middle Cretaceous are higher than Cenozoic as largely observed [*Ligi et al*., 2013]. Following these losses, considerable amount of CH_4 released during serpentinization [*Cannat et al*., 2013] at OCT of the rifted margins and at off-axis oceanic ridges may account for an important temperature increase during Cretaceous, once methane is 20 times more heating-trap than carbon dioxide [*Beerling et al*., 2009].

This amount of element lost by serpentinization also affects sedimentary basins in the distal margins [*Pinto et al*., 2014a, 2014b, in prep.]. Indeed, fluids are enriched in mantle elements by serpentinization before mantle exhumation at the seafloor below the thinned continental crust and consequently they are channelized through extensional detachment faults affecting the syntectonic sediments [*Pinto et al*., 2014a, in prep]. With the progressive mantle exhumation [*Pinto et al*., 2014b, in prep.] fluids escape to the seawater and interact with post-rift sediments [*Haggerty and Germann*, 1988; *Pinto et al*., 2014a, 2014b, in prep.]. The resulted interaction between these fluids and sediments is expressed by strong silicification and enrichment of oxyhydroxides and/or carbonates of Fe, Mn, Mg and Ca [*Haggerty and Germann*, 1988; *Pinto et al*., 2014a, 2014b, in prep.] during eodiagenesis [*Pinto et al*., 2014a, in prep]. These results have important economic impact for petroleum exploration activities, once they can destroy the porosity of reservoirs by silicification and quartz veining.

It is worthwhile to mention that the serpentinized crust, about 5-6 km thick, is depleted in many elements (Table 1) but saturated in water. It can eventually be consumed on subduction zones impacting not only on the early evolution of orogens [*Reston and Manatschal*, 2011] but also on the magmatism along orogenic arcs. The H_2O retained is not only an important fluid source triggering arc melting [*John et al*., 2011; *Deschamps et al*., 2013] but is also an efficient transport-agent to recycle the chemical components [*Manning*, 2004; *Deschamps et al*., 2013] in the upper crust and deeper in the mantle [*Rupke et al*., 2004].

The cyclic mantle exhumation accompanied by serpentinization, water absorption, element losses and its later subduction, must had a substantial impact on changing the geochemistry of major Earth reservoirs during the evolution of the planet.

Table 1. Porcentage and mass of gain and loss

	IAM-9 seismic Section			Central Iberia Margin	
	Avg. Gain and Loss (%)	STDEV Gain and Loss (%)	Total Mass gained and lost (ton)	Minimum mass gained or lost (ton)	Maximum mass gained or lost (ton)
Water	7.88%	4.43%	2.05E+11	-	1.71E+13
SiO2	-16.10%	8.09%	-4.49E+11	-6.74E+13	-1.26E+14
MgO	-17.67%	8.14%	-4.98E+11	-7.94E+13	-1.33E+14
CaO	-0.38%	0.28%	-1.07E+10	-8.08E+11	-3.72E+12
FeO	-2.77%	1.49%	-7.62E+10	-1.10E+13	-2.22E+13
MnO	-0.03%	0.02%	-8.48E+08	-1.06E+11	-2.88E+11
Ni	-0.09%	0.04%	-2.57E+09	-4.01E+11	-6.81E+11
Cr	-0.10%	0.04%	-2.98E+09	-4.28E+11	-7.94E+11

7. REFERENCES

Afilhado, A., L. Matias, H. Shiobara, A. Hirn, L. Mendes-Victor, and H. Shimamura (2008), From unthinned continent to ocean: The deep structure of the West Iberia passive continental margin at 38°N, *Tectonophysics*, *458*(1-4), 9–50, doi:10.1016/j.tecto.2008.03.002.

Beard, J. S., and L. Hopkinson (2000), A fossil, serpentinization-related hydrothermal vent, Ocean Drilling Program Leg 173, Site 1068 (Iberia Abyssal Plain): Some aspects of mineral and fluid chemistry, *J. Geophys. Res.*, *105*(B7), 16527, doi:10.1029/2000JB900073.

Beerling, D., R. a. Berner, F. T. Mackenzie, M. B. Harfoot, and J. a. Pyle (2009), Methane and the CH4 related greenhouse effect over the past 400 million years, *Am. J. Sci.*, *309*(2), 97–113, doi:10.2475/02.2009.01.

Boschi, C., G. L. Früh-Green, A. Delacour, J. A. Karson, and D. S. Kelley (2006), Mass transfer and fluid flow during detachment faulting and development of an oceanic core complex, Atlantis Massif (MAR 30°N), *Geochemistry, Geophys. Geosystems*, *7*(1), n/a–n/a, doi:10.1029/2005GC001074.

Bronner, A., D. Sauter, G. Manatschal, G. Péron-Pinvidic, and M. Munschy (2011), Magmatic breakup as an explanation for magnetic anomalies at magma-poor rifted margins, *Nat. Geosci.*, *4*(8), 549–553.

Cannat, M., F. Fontaine, and J. Escartín (2013), Serpentinization and Associated Hydrogen And Methane Fluxes at Slow Spreading Ridges, in *Diversity Of Hydrothermal Systems On Slow Spreading Ocean Ridges*, pp. 241–264, American Geophysical Union.

Daval, D. et al. (2011), Influence of amorphous silica layer formation on the dissolution rate of olivine at 90°C and elevated pCO2, *Chem. Geol.*, *284*(1-2), 193–209, doi:10.1016/j.chemgeo.2011.02.021.

Dean, S., and T. Minshull (2000), Deep structure of the ocean-continent transition in the southern Iberia Abyssal Plain from seismic refraction profiles: The IAM-9 transect at 40°20’ N, *J.*

Geophys. Res., *105*, 5859–5885.

Deschamps, F., M. Godard, S. Guillot, and K. Hattori (2013), Geochemistry of subduction zone serpentinites: A review, *Lithos*, *178*, 96–127, doi:10.1016/j.lithos.2013.05.019.

Dias, J. L. (2005), Tectônica, estratigrafia e sedimentação no Andar Aptiano da margem leste brasileira, *Bol. Geociências da PETROBRAS*, *13*, 7–25.

Douville, E., J. . Charlou, E. . Oelkers, P. Bienvenu, C. . Jove Colon, J. . Donval, Y. Fouquet, D. Prieur, and P. Appriou (2002), The rainbow vent fluids (36°14′N, MAR): the influence of ultramafic rocks and phase separation on trace metal content in Mid-Atlantic Ridge hydrothermal fluids, *Chem. Geol.*, *184*(1-2), 37–48, doi:10.1016/S0009-2541(01)00351-5.

Edmonds, H. N. (2010), Chemical signatures from hydrothermal venting on slow spreading ridges, in *Diversity of Hydrothermal Systems on Slow Spreading Ocean Ridges*, vol. 188, pp. 27–42, AGU, Washington, DC.

Evans, D., and W. Müller (2012), Deep time foraminifera Mg/Ca paleothermometry: Nonlinear correction for secular change in seawater Mg/Ca, *Paleoceanography*, *27*(4), n/a–n/a, doi:10.1029/2012PA002315.

Fouquet, Y. et al. (2010), Geodiversity of hydrothermal processes along the Mid-Atlantic Ridge and ultramafic-hosted mineralization: A new type of oceanic Cu-Zn-Co-Au volcanogenic massive sulfide deposit, in *Diversity of Hydrothermal Systems on Slow Spreading Ocean Ridges*, vol. 188, pp. 321–367, AGU, Washington, DC.

Gibson, I. L., M.-O. Beslier, G. Cornen, K. L. Milliken, and K. E. Seifert (1996), Major- and trace-element seawater alteration profiles in serpentinite formed during the development of the Iberia Margin, site 897, , *149*(May), 519–527.

Haggerty, J. A., and S. H. Germann (1988), Resedimentation and diagenesis, including silicification, of Barremian-Aptian shallow-water carbonates from the Galicia Margin, Eastern North Atlantic, at Ocean Drilling Program Site 641, in *Proc. ODP, Sci. Results, 103*, vol. 103, edited by G. Boillot, E. L. Winterer, A. W. Meyer, and J. Applegate, pp. 513–530, College Station, TX (Ocean Drilling Program).

Hopper, J. R., T. Funck, and B. E. Tucholke (2007), Structure of the Flemish Cap margin, Newfoundland: insights into mantle and crustal processes during continental breakup, *Geol. Soc. London, Spec. Publ.*, *282*(1), 47–61, doi:10.1144/SP282.3.

Jagoutz, O., O. Müntener, G. Manatschal, D. Rubatto, G. Péron-Pinvidic, B. D. Turrin, and I. M. Villa (2007), The rift-to-drift transition in the North Atlantic: A stuttering start of the MORB machine?, *Geology*, *35*(12), 1087, doi:10.1130/G23613A.1.

John, T., M. Scambelluri, M. Frische, J. D. Barnes, and W. Bach (2011), Dehydration of subduct-

ing serpentinite: Implications for halogen mobility in subduction zones and the deep halogen cycle, *Earth Planet. Sci. Lett.*, *308*(1-2), 65–76, doi:10.1016/j.epsl.2011.05.038.

Kelley, D. S., and T. M. Shank (2010), Hydrothermal systems: A decade of discovery in slow spreading environments, in *Diversity of Hydrothermal Systems on Slow Spreading Ocean Ridges*, vol. 188, pp. 369–407, AGU, Washington, DC.

Kelley, D. S. et al. (2001), An off-axis hydrothermal vent field near the Mid-Atlantic Ridge at 30 degrees N., *Nature*, *412*(6843), 145–9, doi:10.1038/35084000.

Ligi, M., E. Bonatti, M. Cuffaro, and D. Brunelli (2013), Post-mesozoic rapid increase of seawater Mg/Ca due to enhanced mantle-seawater interaction., *Sci. Rep.*, *3*, 2752, doi:10.1038/srep02752.

MacLeod, C. J., R. C. Searle, B. J. Murton, J. F. Casey, C. Mallows, S. C. Unsworth, K. L. Achenbach, and M. Harris (2009), Life cycle of oceanic core complexes, *Earth Planet. Sci. Lett.*, *287*(3-4), 333–344, doi:10.1016/j.epsl.2009.08.016.

Manning, C. E. (2004), The chemistry of subduction-zone fluids, *Earth Planet. Sci. Lett.*, *223*(1-2), 1–16, doi:10.1016/j.epsl.2004.04.030.

McCaig, A. M., R. a. Cliff, J. Escartin, A. E. Fallick, and C. J. MacLeod (2007), Oceanic detachment faults focus very large volumes of black smoker fluids, *Geology*, *35*(10), 935, doi:10.1130/G23657A.1.

Miller, D. J., and N. I. Christensen (1997), Seismic velocities of lower crustal and upper mantle rocks from the slow-spreading Mid-Atlantic Ridge south of the Kane Transform Zone (MARK), in *Proceedings of the Ocean Drilling Program, Scientific Results*, vol. 153, edited by J. A. Karson, M. Cannat, D. J. Miller, and D. Elthon, pp. 437–454, Texas.

Minshull, T. A., S. M. Dean, and R. B. Whitmarsh (2014), The peridotite ridge province in the southern Iberia Abyssal Plain: Seismic constraints revisited, *J. Geophys. Res. Solid Earth*, *119*(3), 1580–1598, doi:10.1002/2014JB011011.

Morgan, J. K., and K. L. Milliken (1996), Petrography of calcite veins in serpentinized peridotite basement rocks from the Iberia Abyssal Plain, Sites 897 and 899: kinematic and environmental implications, in *Proceedings of the Ocean Drilling Program, Scientific Results*, vol. 149, edited by R. B. Whitmarsh, D. S. Sawyer, A. Klaus, and D. G. Masson, pp. 559–569.

Müntener, O., G. Manatschal, L. Desmurs, and T. Pettke (2010), Plagioclase Peridotites in Ocean-Continent Transitions: Refertilized Mantle Domains Generated by Melt Stagnation in the Shallow Mantle Lithosphere, *J. Petrol.*, *51*(1-2), 255–294, doi:10.1093/petrology/egp087.

O'Brien, C. L., G. L. Foster, M. A. Martínez-Botí, R. Abell, J. W. B. Rae, and R. D. Pancost

(2014), High sea surface temperatures in tropical warm pools during the Pliocene, *Nat. Geosci.*, *7*(8), 606–611, doi:10.1038/ngeo2194.

Ogasawara, Y., A. Okamoto, N. Hirano, and N. Tsuchiya (2013), Coupled reactions and silica diffusion during serpentinization, *Geochim. Cosmochim. Acta*, *119*, 212–230, doi:10.1016/j.gca.2013.06.001.

Péron-Pinvidic, G., and G. Manatschal (2009), The final rifting evolution at deep magma-poor passive margins from Iberia-Newfoundland: a new point of view, *Int. J. Earth Sci.*, *98*(7), 1581–1597.

Perseil, E. A., and L. Latouche (1989), Découverte de microstructures de nodules polymétaliques dans les minéralisations manganésifères métamorphiques de Falotta et de Parsettens (Grisons-Suisse), *Miner. Depos.*, *24*, 111–116.

Pinto, V. H., G. Manatschal, A. M. Karpoff, and A. Viana (2014a), Tracing mantle-related fluids in magma-poor rifted margins: the example of Alpine Tethyan rifted margins, *Geochemistry, Geophys. Geosystems*.

Pinto, V. H. G., G. Manatschal, A. M. Karpoff, E. Masini, and A. Viana (2014b), Linking tectonic evolution and fluid history during the formation of the hyperextended domains: the example of Tasna in the Alps, Mauléon in the Pyrenees and Hobby High in Iberia, *Geochemistry Geophys. Geosystems*.

Potdevin, J. L., and D. Marquer (1987), Quantitative Methods for the Estimation of Mass Transfers by Fluids in Deformed Metamorphic Rocks, *Geodin. Acta*, *1*(3), 193–206.

Reston, T., and G. Manatschal (2011), Rifted Margins: Building Blocks of Later Collision, in *Arc-Continent Collision SE - 1*, pp. 3–21, Springer Berlin Heidelberg.

Reston, T. J., and K. G. McDermott (2011), Successive detachment faults and mantle unroofing at magma-poor rifted margins, *Geology*, *39*(11), 1071–1074, doi:10.1130/G32428.1.

Reston, T. J., and C. R. Ranero (2011), The 3-D geometry of detachment faulting at mid-ocean ridges, *Geochemistry, Geophys. Geosystems*, *12*(7), 1–19, doi:10.1029/2011GC003666.

Rupke, L. H., J. P. Morgan, M. Hort, and J. A. D. Connolly (2004), Serpentine and the subduction zone water cycle, *Earth Planet. Sci. Lett.*, *223*(1-2), 17–34, doi:10.1016/j.epsl.2004.04.018.

Russell, S. M., and R. B. Whitmarsh (2003), Magmatism at the west Iberia non-volcanic rifted continental margin: evidence from analyses of magnetic anomalies, *Geophys. J. Int.*, *154*(3), 706–730, doi:10.1046/j.1365-246X.2003.01999.x.

Saito, M. a., A. E. Noble, A. Tagliabue, T. J. Goepfert, C. H. Lamborg, and W. J. Jenkins (2013), Slow-spreading submarine ridges in the South Atlantic as a significant oceanic iron source,

Nat. Geosci., *6*(9), 775–779, doi:10.1038/ngeo1893.

Seyfried, W. E., N. J. Pester, K. Ding, and M. Rough (2011), Vent fluid chemistry of the Rainbow hydrothermal system (36°N, MAR): Phase equilibria and in situ pH controls on subsea-floor alteration processes, *Geochim. Cosmochim. Acta*, *75*(6), 1574–1593, doi:10.1016/j.gca.2011.01.001.

Shipboard Scientific Party (2004), Leg 210 summary, in *Proc. ODP, Init. Repts., 210*, vol. 210, edited by B. E. Tucholke, J.-C. Sibuet, and A. Klaus, pp. 1–78, Ocean Drilling Program, College Station, TX (Ocean Drilling Program).

Skelton, A. D. ., and J. W. Valley (2000), The relative timing of serpentinisation and mantle exhumation at the ocean–continent transition, Iberia: constraints from oxygen isotopes, *Earth Planet. Sci. Lett.*, *178*(3-4), 327–338, doi:10.1016/S0012-821X(00)00087-X.

Sutra, E., and G. Manatschal (2012), How does the continental crust thin in a hyperextended rifted margin? Insights from the Iberia margin, *Geology*, *40*(2), 139–142, doi:10.1130/G32786.1.

Tucholke, B. E., and J. Sibuet (2007), Leg 210 synthesis: tectonic, magmatic, and sedimentary evolution of the Newfoundland-Iberia rift, in *Proc. ODP, Sci. Results, 210*, vol. 210, edited by B. E. Tucholke, J.-C. Sibuet, and A. Klaus, pp. 1–56, Ocean Drilling Program, College Station, TX (Ocean Drilling Program).

Unternehr, P., G. Peron-Pinvidic, G. Manatschal, and E. Sutra (2010), Hyperextended crust in the South Atlantic: in search of a model, *Pet. Geosci.*, *16*(3), 207–215, doi:10.1144/1354-079309-904.

Zalán, P. V, M. Severino, C. A. Rigoti, L. P. Magnavita, Jab. Oliveira, and A. R. Vianna (2011), An Entirely New 3D-View of the Crustal and Mantle Structure of a South Atlantic Passive Margin – Santos, Campos and Espírito Santo Basins, Brazil, #30177 (2011), , 1–12.

8. APPENDIX

Calculations

Table A1.

The Table A1 presents the calculated median values from serpentinized peridotites and serpentinites of the Lower Penninic nappes (Malenco and Platta nappes) from the Alps (Müntener et al., 2010). Samples are grouped by open and closed intervals of degree of serpentinization. Samples with degree of serpentinization ≤10%, samples between]10 60%] and samples more than 60% serpentinized (>60%). Some of these samples are plotted in the Figure 2C.

Afterwards, we calculated the gain and losses following the rules:

- We use the group weakly serpentinized (≤10%) as the protolith.

- We calculated the alteration (serpentinization) from ≤10% to]10 60%], which characterizes the samples weakly and moderately serpentinized (§).

- We calculated the serpentinization from]10 60%] to >60% which characterizes the samples highly serpentinized (§).

Considering Al and Ti as immobile elements, we calculate the *f*-factor for Al and Ti according to the equation 1, for details see *Potdevin and Marquer* [1987].

Eq. 1. $$\frac{\Delta m}{m_0} = \frac{m_a}{m_0}.f.\frac{\rho_a}{\rho_o} - 1$$

This equation gives the mass variation relative to the initial concentration of elements or chemical compounds, where the correct mass lost or gained is a function of the density and the *f*-factor. This factor was estimated using the immobile elements Al and Ti (see Figure A1 in the Annexes of the thesis), it means there are no mass variations of Al and Ti ($\Delta m/m_0=0$). Once the element mass (i.e., concentration) is known from the chemical analyses and density is calculated using the Figure 2B, the *f*-factor can be easily found. Once *f* is known, we use it to calculate the mass variation for the other elements. Because, the calculated mass variation is different assuming the *f*-factor for Ti or for Al, the calculated range gives an idea of maximum and minimum amount that can be lost or gained during serpentinization. Multiplying the mass variation values (§) by the initial values of the protolith (≤10%), we estimate the percentage or the mass of gain/ losses (#).

Note: Check the superscript symbols (§ and #) in the header of Table A1.

Table A2.

The Table A2 gives all the information necessary to calculate the losses of elements and the amount of absorbed water that occurs during serpentinization. At the very top of the table we present the zones identified in the IAM-9 seismic section. Therefore, the coupled zone is Z1, the Zone of Exhumed Continental Mantle encompasses Z2 to Z9, and the embryonic oceanic zone is Z10 to Z13. A summation, average and STDEV were calculated in order to give an idea of masses of water and elements involved in each zone. The volume field (superscript symbol †) is in fact a calculated area of these zones with a lateral continuity of 1 km used in order to have a volumetric calculation. The serpentinization field in the Table A2 came from the association with the velocities from refraction seismic data (Figure 1A) and the equation plotted in Figure 2A. The density field are calculated using the equation from Figure 2B and considering average values for seismic velocities (Vp) intervals in the Figure 1A.

The mass (ton) and the percentage of loss (%) of elements were calculated for each zone (Z1, Z2, etc.) using the Ti and Al as references. To do this we use the results from Table A1, following the criteria:

- If the degree of serpentinization is higher than 60%, we chose the results of Al and Ti (Table A1) that correspond to the alteration from the group <10% to the group >60%. On the other hand, if the degree of serpentinization is lower than 60% it was used the values that correspond to the alteration from group <10% to the group]10 60%].

For example, in order to calculate the zone Z1, which the average value of serpentinization degree is 34%, we multiply the percentage of SiO_2 lost that is 5.12% and 18.81%, respectively for Al and Ti references, by $2.55x10^{11}$ tons of serpentinized rock. This is equal to $1.31x10^{10}$ and $3.88x10^{10}$ tons of silica lost respectively. We plotted the percentage of losses of elements below the calculated mass, as we also consider the average percentage for estimation of the loss along the central Iberia margin, using the map of the Figure 3.

Table A3.

Table A3 presents the results of absorbed water and element losses for the central area of Iberia Margin. The area of the Coupled Domain and the Zone of Exhumed Continental Mantle (ZECM) is measured using the map presented in Figure 3. The average thicknesses, given by the IAM-9 section, and the average densities of these domains allowed an estimation of the volume of serpentinized peridotites. The volume of absorbed water was assessed using the average values of the hydration factor multiplied by the volume of serpentinized rock in each domain. In order to estimate the overall element losses in the central Iberia Margin, the percentage of losses from Table A2 is multiplied by the volume of serpentinized peridotites. The results considering both Al and Ti as references for immobility give a range that can be possible maximum and minimum values of losses caused by serpentinization.

Table A1. Gain and Loss estimation

Elements	Median values <10	Median values]10-60]	Median values >60	Ref. Al2O3]10-60][§]	Ref. TiO2]10-60][§]	ref. Al2O3 %wt (ou g)[#]	ref. TiO2 %wt (ou g)[#]	Ref. Al2O3 >60[§]	Ref. TiO2 >60[§]	ref. Al2O3 %wt (ou g)[#]	ref. TiO2 %wt (ou g)[#]
SiO_2	43.44	41.72	40.10	-0.12	-0.35	-5.12	-15.22	-0.43	-0.63	-18.81	-27.23
TiO_2	0.05	0.07	0.12	0.36	0.00	0.02	0.00	0.52	0.00	0.03	0.00
Al_2O_3	2.11	2.29	3.43	0.00	-0.26	0.00	-0.55	0.00	-0.34	0.00	-0.72
FeO	7.94	7.83	7.70	-0.09	-0.33	-0.75	-2.64	-0.40	-0.61	-3.21	-4.83
MnO	0.12	0.13	0.13	-0.01	-0.27	0.00	-0.03	-0.33	-0.56	-0.04	-0.07
MgO	42.75	39.27	34.97	-0.16	-0.38	-6.68	-16.18	-0.50	-0.67	-21.27	-28.62
CaO	1.72	1.84	2.36	-0.02	-0.27	-0.03	-0.47	-0.16	-0.45	-0.27	-0.77
Na_2O	0.04	0.00	0.00	-1.00	-1.00	-0.04	-0.04	-1.00	-1.00	-0.04	-0.04
K_2O	0.02	0.00	0.00	-1.00	-1.00	-0.02	-0.02	-1.00	-1.00	-0.02	-0.02
P_2O_5	0.01	0.01	0.10	-0.10	-0.34	0.00	0.00	5.10	3.01	0.05	0.03
Cr_2O_3	0.38	0.34	0.40	-0.20	-0.41	-0.08	-0.16	-0.36	-0.58	-0.14	-0.22
NiO	0.35	0.32	0.26	-0.17	-0.39	-0.06	-0.14	-0.55	-0.70	-0.19	-0.25
LOI	1.65	5.82	10.21	2.24	1.38	3.70	2.29	2.80	1.50	4.62	2.48
Ba	1.03	0.22	4.26	-0.81	-0.86	-8.34E-05	-8.86E-05	1.54	0.67	1.58E-04	6.89E-05
Ce	0.22	0.30	0.53	0.26	-0.07	5.82E-06	-1.53E-06	0.46	-0.04	1.02E-05	-8.43E-07
Co	105.00	96.00	99.50	-0.16	-0.38	-1.68E-03	-4.01E-03	-0.42	-0.62	-4.39E-03	-6.48E-03
Cr	2712.00	2496.00	2687.00	-0.15	-0.38	-4.19E-02	-1.02E-01	-0.39	-0.60	-1.06E-01	-1.63E-01
Cs	0.01	1.24	0.78	161.38	118.60	1.13E-04	8.30E-05	67.35	43.97	4.71E-05	3.08E-05
Cu	51.00	22.50	21.00	-0.59	-0.70	-3.03E-03	-3.58E-03	-0.75	-0.83	-3.81E-03	-4.25E-03
Dy	0.20	0.23	0.47	0.02	-0.25	4.50E-07	-5.04E-06	0.43	-0.06	8.71E-06	-1.24E-06
Er	0.13	0.16	0.29	0.13	-0.17	1.64E-06	-2.11E-06	0.40	-0.08	5.09E-06	-9.61E-07
Eu	0.03	0.05	0.11	0.30	-0.04	9.75E-07	-1.38E-07	1.04	0.34	3.38E-06	1.11E-06
Gd	0.12	0.17	0.38	0.29	-0.05	3.52E-06	-5.67E-07	0.95	0.28	1.14E-05	3.40E-06
Hf	0.07	0.06	0.20	-0.24	-0.44	-1.68E-06	-3.11E-06	0.75	0.15	5.31E-06	1.06E-06
Ho	0.05	0.06	0.11	0.06	-0.22	3.02E-07	-1.03E-06	0.41	-0.07	1.94E-06	-3.45E-07
La	0.06	0.09	0.16	0.37	0.01	2.18E-06	5.34E-08	0.61	0.06	3.62E-06	3.64E-07
Lu	0.02	0.02	0.05	0.00	-0.26	4.39E-09	-5.76E-07	0.42	-0.06	9.32E-07	-1.39E-07
Nb	0.06	0.03	3.10	-0.63	-0.73	-4.06E-06	-4.67E-06	28.75	18.57	1.84E-04	1.19E-04
Nd	0.19	0.29	0.57	0.39	0.02	7.32E-06	3.99E-07	0.83	0.21	1.58E-05	3.92E-06
Ni	2205.00	2011.50	1887.00	-0.16	-0.38	-3.57E-02	-8.44E-02	-0.47	-0.65	-1.05E-01	-1.44E-01
Pb	0.05	-	0.45	-	-	-	-	4.58	2.67	2.27E-05	1.32E-05
Pr	0.03	0.06	0.11	0.58	0.16	1.85E-06	5.21E-07	1.17	0.43	3.74E-06	1.37E-06
Rb	0.14	0.24	0.41	0.58	0.16	7.97E-06	2.23E-06	0.80	0.19	1.11E-05	2.59E-06
S	200.00	550.00	550.00	1.53	0.86	3.05E-02	1.72E-02	0.69	0.11	1.38E-02	2.23E-03
Sc	10.00	9.00	11.00	-0.17	-0.39	-1.73E-04	-3.91E-04	-0.32	-0.56	-3.24E-04	-5.55E-04
Sm	0.07	0.11	0.23	0.39	0.02	2.77E-06	1.56E-07	1.00	0.32	7.16E-06	2.27E-06
Sr	3.03	5.05	6.60	0.53	0.13	1.61E-04	3.85E-05	0.34	-0.12	1.02E-04	-3.66E-05
Ta	0.01	0.00	0.05	-0.85	-0.89	-1.02E-06	-1.06E-06	1.69	0.77	2.02E-06	9.22E-07
Tb	0.03	0.03	0.06	0.18	-0.13	4.39E-07	-3.35E-07	0.57	0.03	1.43E-06	8.63E-08
Th	0.00	0.01	0.00	0.52	0.12	2.06E-07	4.65E-08	-0.31	-0.55	-1.24E-07	-2.18E-07
Tm	0.02	0.02	0.05	0.03	-0.24	5.44E-08	-5.26E-07	0.43	-0.06	9.21E-07	-1.29E-07
U	0.00	0.00	0.01	-0.75	-0.81	-2.99E-07	-3.26E-07	-0.23	-0.49	-9.29E-08	-1.98E-07
V	51.00	51.50	73.00	-0.07	-0.32	-3.70E-04	-1.62E-03	-0.12	-0.42	-6.16E-04	-2.15E-03
Y	1.11	1.36	3.26	0.12	-0.18	1.31E-05	-1.97E-05	0.80	0.18	8.90E-05	2.04E-05
Yb	0.14	0.14	0.30	-0.11	-0.35	-1.60E-06	-4.87E-06	0.34	-0.12	4.70E-06	-1.69E-06
Zn	41.00	44.50	49.50	0.00	-0.27	-1.27E-05	-1.09E-03	-0.26	-0.51	-1.06E-03	-2.10E-03
Zr	1.26	1.45	6.30	0.06	-0.22	7.00E-06	-2.80E-05	2.07	1.02	2.61E-04	1.29E-04
% Alteration	0.10	0.50	0.80								
Rho (g/cc) median	3.21	2.91	2.68								
References				Al2O3	TiO			Al2O3	TiO		
f-factor				1.015	0.747			0.736	0.484		

Table A2. General calculations

	EMBRYONIC OCEANIC ZONE						EXHUMED ZONE										COUPLED			
	Z13	Z12	Z11	Z10	*AVE*	*SUM*	Z9	Z8	Z7	Z6	Z5	Z4	Z3	Z2	*AVE*	*SUM*	*Z1*	**TOTAL**	**AVE**	**STDEV**
Vp TOPO	4	5	6	7			4	5	6	7	7.4	4.3	5	7.6			6	-	-	-
Vp BASE	5	6	7	7.9			5	6	7	7.4	7.9	5	6	7.9			7.9	-	-	-
Volume (km3)†	27.27	56.7	179.61	98.91		362.49	32.98	28.02	174.35	47.77	241.52	45.55	82.24	84.75		737.18	84.18	1183.85	-	-
Serpentinization	0.98	0.80	0.48	0.18			*0.98*	*0.80*	*0.48*	*0.26*	*0.12*	*0.98*	*0.80*	*0.08*			*0.34*	-	-	-
H2O factor	0.13	0.11	0.07	0.03	0.09		0.13	0.11	0.07	0.04	0.02	0.13	0.11	0.02	0.08		0.05	-	-	-
Rho (g/cc)	2.54	2.68	2.92	3.15	2.82		2.54	2.68	2.92	3.09	3.20	2.54	2.68	3.22	2.86		3.03	-	-	-
Massa Rocha (ton)	6.93E+10	1.52E+11	5.25E+11	3.12E+11		1.06E+12	8.38E+10	7.51E+10	5.09E+11	1.48E+11	7.73E+11	1.16E+11	2.20E+11	2.73E+11		2.20E+12	2.55E+11	3.51E+12	-	-
Massa Seawater (ton)	9.22E+09	1.66E+10	3.60E+10	9.29E+09		7.12E+10	1.12E+10	8.22E+09	3.50E+10	5.91E+09	1.67E+10	1.54E+10	2.41E+10	4.79E+09		1.21E+11	1.28E+10	2.05E+11	-	-
Volume Water (km3)	9.22	16.64	36.01	9.29		71.15	11.15	8.22	34.95	5.91	16.71	15.40	24.13	4.79		121.27	12.81	205.24	-	-
Mass(ton) SiO2 - Ref. Al	-1.30E+10	-2.86E+10	-2.69E+10	-1.60E+10		-8.45E+10	-1.58E+10	-1.41E+10	-2.61E+10	-7.56E+09	-3.96E+10	-2.18E+10	-4.15E+10	-1.40E+10		-1.80E+11	-1.31E+10	-2.78E+11	-	-
Loss (%) of SiO2 - Ref. Al	-18.81%	-18.81%	-5.12%	-5.12%	-11.97%		-18.81%	-18.81%	-5.12%	-5.12%	-5.12%	-18.81%	-18.81%	-5.12%	-11.97%		-5.12%	-	-9.69%	7.10%
Mass (ton) SiO2 - Ref. Ti	-1.89E+10	-4.14E+10	-7.99E+10	-4.74E+10		-1.88E+11	-2.28E+10	-2.05E+10	-7.75E+10	-2.25E+10	-1.18E+11	-3.15E+10	-6.00E+10	-4.16E+10		-3.94E+11	-3.88E+10	-6.20E+11	-	-
Loss of SiO2 - Ref. Ti	-27.23%	-27.23%	-15.22%	-15.22%	-21.23%		-27.23%	-27.23%	-15.22%	-15.22%	-15.22%	-27.23%	-27.23%	-15.22%	-21.23%		-15.22%	-	-19.22%	6.24%
Mass (ton) ref. Al to FeO	-2.23E+09	-4.88E+09	-3.93E+09	-2.33E+09		-1.34E+10	-2.69E+09	-2.41E+09	-3.82E+09	-1.11E+09	-5.79E+09	-3.72E+09	-7.08E+09	-2.05E+09		-2.87E+10	-1.91E+09	-4.39E+10	-	-
Loss of FeO - Ref. Al	-3.21%	-3.21%	-0.75%	-0.75%	-1.98%		-3.21%	-3.21%	-0.75%	-0.75%	-0.75%	-3.21%	-3.21%	-0.75%	-1.98%		-0.75%	-	-1.57%	1.28%
Mass (ton) ref. Ti to FeO	-3.35E+09	-7.34E+09	-1.39E+10	-8.24E+09		-3.28E+10	-4.05E+09	-3.63E+09	-1.35E+10	-3.90E+09	-2.04E+10	-5.59E+09	-1.06E+10	-7.22E+09		-6.89E+10	-6.75E+09	-1.09E+11	-	-
Loss of FeO - Ref. Ti	-4.83%	-4.83%	-2.64%	-2.64%	-3.74%		-4.83%	-4.83%	-2.64%	-2.64%	-2.64%	-4.83%	-4.83%	-2.64%	-3.74%		-2.64%	-	-3.37%	1.13%
Mass (ton) ref. Al to MnO	-2.69E+07	-5.89E+07	-8.25E+06	-4.90E+06		-9.89E+07	-3.25E+07	-2.91E+07	-8.00E+06	-2.32E+06	-1.21E+07	-4.49E+07	-8.55E+07	-4.29E+06		-2.19E+08	-4.01E+06	-3.22E+08	-	-
Loss of MnO - Ref. Al	-0.04%	-0.04%	0.00%	0.00%	-0.02%		-0.04%	-0.04%	0.00%	0.00%	0.00%	-0.04%	-0.04%	0.00%	-0.02%		0.00%	-	-0.01%	0.02%
Mass (ton) ref. Ti to MnO	-4.57E+07	-1.00E+08	-1.69E+08	-1.01E+08		-4.16E+08	-5.52E+07	-4.95E+07	-1.64E+08	-4.76E+07	-2.49E+08	-7.63E+07	-1.45E+08	-8.81E+07		-8.76E+08	-8.23E+07	-1.37E+09	-	-
Loss of MnO - Ref. Ti	-0.07%	-0.07%	-0.03%	-0.03%	-0.05%		-0.07%	-0.07%	-0.03%	-0.03%	-0.03%	-0.07%	-0.07%	-0.03%	-0.05%		-0.03%	-	-0.04%	0.02%
Mass (ton) ref. Al to MgO	-1.47E+10	-3.23E+10	-3.51E+10	-2.08E+10		-1.03E+11	-1.78E+10	-1.60E+10	-3.40E+10	-9.87E+09	-5.16E+10	-2.46E+10	-4.69E+10	-1.83E+10		-2.19E+11	-1.70E+10	-3.39E+11	-	-
Loss of MgO - Ref. Al	-21.27%	-21.27%	-6.68%	-6.68%	-13.98%		-21.27%	-21.27%	-6.68%	-6.68%	-6.68%	-21.27%	-21.27%	-6.68%	-13.98%		-6.68%	-	-11.55%	7.57%
Mass (ton) ref. Ti to MgO	-1.98E+10	-4.35E+10	-8.49E+10	-5.04E+10		-1.99E+11	-2.40E+10	-2.15E+10	-8.25E+10	-2.39E+10	-1.25E+11	-3.31E+10	-6.31E+10	-4.42E+10		-4.17E+11	-4.13E+10	-6.57E+11	-	-
Loss of MgO - Ref. Ti	-28.62%	-28.62%	-16.18%	-16.18%	-22.40%		-28.62%	-28.62%	-16.18%	-16.18%	-16.18%	-28.62%	-28.62%	-16.18%	-22.40%		-16.18%	-	-20.33%	6.45%
Mass (ton) ref. Al to CaO	-1.90E+08	-4.17E+08	-1.40E+08	-8.34E+07		-8.31E+08	-2.30E+08	-2.06E+08	-1.36E+08	-3.95E+07	-2.07E+08	-3.18E+08	-6.05E+08	-7.31E+07		-1.82E+09	-6.83E+07	-2.71E+09	-	-
Loss of CaO - Ref. Al	-0.27%	-0.27%	-0.03%	-0.03%	-0.15%		-0.27%	-0.27%	-0.03%	-0.03%	-0.03%	-0.27%	-0.27%	-0.03%	-0.15%		-0.03%	-	-0.11%	0.13%
Mass (ton) ref. Ti to CaO	-5.33E+08	-1.17E+09	-2.48E+09	-1.47E+09		-5.66E+09	-6.45E+08	-5.78E+08	-2.41E+09	-6.99E+08	-3.66E+09	-8.91E+08	-1.70E+09	-1.29E+09		-1.19E+10	-1.21E+09	-1.87E+10	-	-
Loss of CaO - Ref. Ti	-0.77%	-0.77%	-0.47%	-0.47%	-0.62%		-0.77%	-0.77%	-0.47%	-0.47%	-0.47%	-0.77%	-0.77%	-0.47%	-0.62%		-0.47%	-	-0.57%	0.15%
Mass (ton) ref. Al to Ni	-7.25E+07	-1.59E+08	-1.88E+08	-1.11E+08		-5.31E+08	-8.77E+07	-7.86E+07	-1.82E+08	-5.28E+07	-2.76E+08	-1.21E+08	-2.31E+08	-9.77E+07		-1.13E+09	-9.12E+07	-1.75E+09	-	-
Loss of Ni - Ref. Al	-0.10%	-0.10%	-0.04%	-0.04%	-0.07%		-0.10%	-0.10%	-0.04%	-0.04%	-0.04%	-0.10%	-0.10%	-0.04%	-0.07%		-0.04%	-	-0.06%	0.04%
Mass (ton) ref. Ti to Ni	-1.00E+08	-2.19E+08	-4.43E+08	-2.63E+08		-1.03E+09	-1.21E+08	-1.08E+08	-4.30E+08	-1.25E+08	-6.52E+08	-1.67E+08	-3.18E+08	-2.31E+08		-2.15E+09	-2.15E+08	-3.39E+09	-	-
Loss of Ni - Ref. Ti	-0.14%	-0.14%	-0.08%	-0.08%	-0.11%		-0.14%	-0.14%	-0.08%	-0.08%	-0.08%	-0.14%	-0.14%	-0.08%	-0.11%		-0.08%	-	-0.10%	0.03%
Mass (ton) ref. Al to Cr	-7.36E+07	-1.61E+08	-2.20E+08	-1.31E+08		-5.86E+08	-8.90E+07	-7.97E+07	-2.14E+08	-6.19E+07	-3.24E+08	-1.23E+08	-2.34E+08	-1.15E+08		-1.24E+09	-1.07E+08	-1.93E+09	-	-
Loss of Cr - Ref. Al	-0.11%	-0.11%	-0.04%	-0.04%	-0.07%		-0.11%	-0.11%	-0.04%	-0.04%	-0.04%	-0.11%	-0.11%	-0.04%	-0.07%		-0.04%	-	-0.06%	0.03%
Mass (ton) ref. Ti to Cr	-1.13E+08	-2.47E+08	-5.37E+08	-3.19E+08		-1.22E+09	-1.36E+08	-1.22E+08	-5.21E+08	-1.51E+08	-7.91E+08	-1.88E+08	-3.59E+08	-2.80E+08		-2.55E+09	-2.61E+08	-4.03E+09	-	-
Loss of Cr - Ref. Ti	-0.16%	-0.16%	-0.10%	-0.10%	-0.13%		-0.16%	-0.16%	-0.10%	-0.10%	-0.10%	-0.16%	-0.16%	-0.10%	-0.13%		-0.10%	-	-	-

Table A3. Volume of absorbed water and mass of lost element

	Coupled Domain	Exhumed + Embryonic Domain	TOTAL
Area Iberia (km^2)	11872	33134	
Ave-Thick (km)	2.96	5.46	
Vol (km^3)	35141.12	180911.64	216052.76
Vol H2O (km^3)	1764.84	15377.49	17142.33
Mass Serpentinite (ton)	1.07E+14	5.17E+14	6.24E+14
SiO_2 Ref Al (ton)	-5.46E+12	-6.19E+13	-6.74E+13
SiO_2 Ref TiO	-1.62E+13	-1.10E+14	-1.26E+14
FeO Ref Al	-7.98E+11	-1.02E+13	-1.10E+13
FeO Ref TiO	-2.82E+12	-1.93E+13	-2.22E+13
MnO Ref Al	-1.67E+09	-1.04E+11	-1.06E+11
MnO Ref TiO	-3.44E+10	-2.54E+11	-2.88E+11
MgO Ref Al	-7.12E+12	-7.23E+13	-7.94E+13
MgO Ref TiO	-1.72E+13	-1.16E+14	-1.33E+14
CaO Ref Al	-2.85E+10	-7.80E+11	-8.08E+11
CaO Ref TiO	-5.04E+11	-3.21E+12	-3.72E+12
Ni Ref Al	-3.81E+10	-3.63E+11	-4.01E+11
Ni Ref TiO	-8.99E+10	-5.92E+11	-6.81E+11
Cr Ref Al	-4.47E+10	-3.83E+11	-4.28E+11
Cr Ref TiO	-1.09E+11	-6.85E+11	-7.94E+11

FINAL PART

4. GENERAL DISCUSSIONS

4.1. Evidence for fluids in distal rifted margins (hyperextended systems)

One of the first questions in this thesis was about the evidence for the fluid flow in the distal rifted margins and hyperextended rift systems. As the investigated sites are fossil rift systems exposed in orogens, the fluid in water or gas phase is not observed on the surface. They may still be trapped in the deep sedimentary section (e.g., gas pools) within the Mauléon Basin, however, there are not directly accessible. The available data from the Iberian Margin are usually from wells drilled on highs where structural traps are usually opened what preventing the accumulation of fluids. Therefore, the investigation was restricted to the imprint of fluids in the rocks.

As addressed in the Articles 1 and 2, the evidence for fluids flow is best depicted by neoformed syn-kinematic phyllosilicates from the fault rocks in the continental crust and mantle as well as by the syn- to post-kinematic veins along the detachment faults. Fluid-rock interactions in the fault rocks from the mantle led to the formation of (i) chrysotile, lizardite, and chlorite in the syn-kinematic foliation of the fault rocks; (ii) Fe and Ni oxides, hydroxides and sulfide of e.g., Fe, Mg and Ni; and (iii) calcite veins and rare quartz veins.

The fault rocks of extensional detachment systems on continental crust also show strong fluid-rock interaction, leading to intense saussuritization. The saussuritization processes resulted in the following transformations.

a) Strong chloritization of feldspars and biotites (when present). In the fault zone from the Alps, the formed chlorites are mainly chamosite (Fe-rich). Chloritization of feldspar needs an external source for Fe and this reaction is often observed when Fe-rich veins (i.e., fluids) cut plagioclases leading to the formation of chlorite at the rim of these plagioclases (Figure A2).

b) Albitization of plagioclases. This reaction leads to loss/depletion of Ca from plagioclases resulting in the formation of Na-rich plagioclases (albite). The by-product of this reaction is the formation of calcite and quartz veins, which can be observed in SEM analyses.

c) Sericitization and illitization. These processes result in the alteration of K-feldspars and plagioclase and are more evident in granitic/gneissic rocks.

d) Formation of veins. In the fault zone, the veins are mainly quartz and calcite. Although quartz and calcite veins are usually product of albitization, it is known that all the other processes are responsible for losses in Si. In addition, in the HHD (ODP Site 1067) epidote veins are often observed and are interpreted to be the result of retrograde metamorphism of hornblendes accompanied by deformation of detachment faults.

These processes are of first order in the fault zone. They can be easily observed and are mainly characterized by a greenish color resulting from chloritization, and by centimetric quartz veins. Moreover, weak saussuritization is also observed in the undeformed basement, e.g., the Albula granite in the Err nappe. I think that hydration can also extend to areas outside of the fault zones, where fluids can use microfractures or the permoporosity of the rock, a parameter which is, however, low in granites.

4.2. **Understanding the nature of the fluids**

As discussed in the Articles 1 and 2 fluid flow occurred in the fault zone of extensional detachment systems over continental crust and in the exhumed mantle. The fluid flow in the fault zone occurred influenced by hydrothermal activity, where seawater interacted with mantle and continental crustal rocks. This was evidenced by neoformed minerals and also by oxygen isotopic analyses which points to a fluid temperature lower than 180 ºC.

The serpentinization of mantle rocks leads to losses and leaching of elements (e.g., Si, Mg, Fe, Ca, Ni, Cr, V) that enriched the original seawater in these elements forming a *mantle-related fluids*. The fluid flow and the enrichment of fluids is recorded in the fault zone on the mantle as neoformed minerals parageneses (e.g., FeNi alloys, Fe-oxyhydroxides, phyllosilicates).

During deformation, saussuritization of the continental crust accompanied by seawater percolation resulted in losses of Si and Ca that enriched the original seawater with these elements forming a *continental crust-related fluid*. The imprint of these fluids is observed as quartz and calcite veins in the fault zone from extensional detachment systems not only in hyperextended domains but also in more proximal parts of rifted margins (e.g., Necking zone). As observed at outcrop and micro-scale, the losses of Si and Ca increases with deformation. This is also observed evidenced by strontium isotopic data (Figure 8), which shows an increase of the radioactive Sr from the granite to the cataclasites and gouges. They show that the deformation and saussuritization result in the “destruction” of feldspars, which release this isotope that is subsequently retained in the neoformed phyllosilicates.

Important results about the nature of fluids came from the geochemical analyses of the fault rocks of extensional detachment faults on the continental crust that are related to mantle exhumation in hyperextended domains. The data show systematic gains of Ni, Cr and V, and sometimes Fe and Mn, what is oppositely observed in extensional detachment faults from more proximal parts of the margins (see Figure 8 Article 1 and Figure 7 Article 2). The geochemical analyses of the clay fraction of the fault rocks show that many of these elements (e.g., Ni, Cr, V) are retained in the neoformed phyllosilicates (see Figure 9 and Table 3 Article 1). In the Err detachment system from the Alps, an increase of these elements toward the distal segments of this detachment system is described (see Figure 10 Article 1). These observations allowed the demonstration that the mantle-related fluids were not only restricted to the exhumed mantle domain, but that they were also focused through extensional detachment faults.

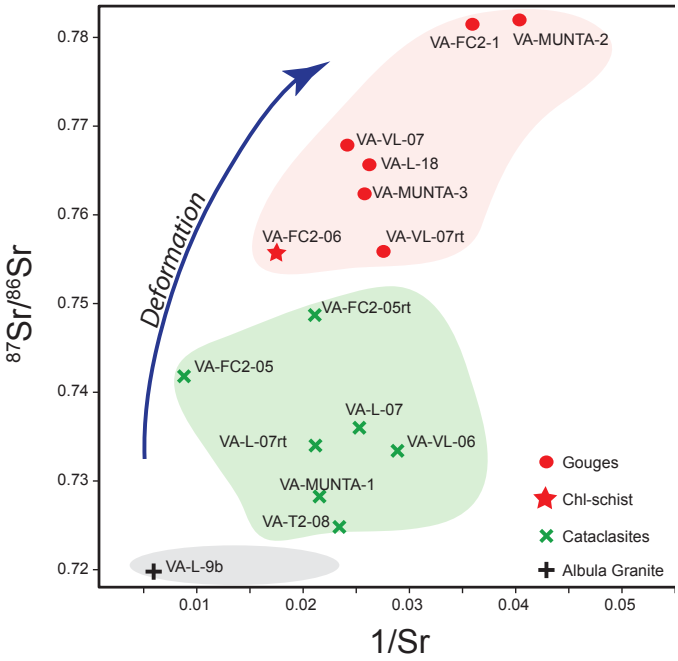

Figure 8. Strontium isotopes of the clay fraction. The figure shows the Sr isotopic results of the clay fraction from the Albula granite (V.A-L-9b) and fault rocks from the Err detachment. Note that ^{87}Sr (usually high in feldspars) increases with deformation. See text for explanation. For comparison purpose, Sr isotopic ratio of Jurassic water (185 Ma) is $^{87}Sr/^{86}Sr$~7072 (Jones and Jenkyns, 2001). The sample sites are shown in the Article 1 and the geographic coordinates are in the annexes (Table A1).

4.3. **Understanding the migration pathways**

The observation that continental crust- and mantle-related fluids migrated through extensional detachment systems led me to propose a model to explain the pathways and the conditions of fluid migration. As discussed in the Articles 1 and 2, the hyperextended domain prior to detachment faulting was previously thinned to about 10 km. This explains why the detachment systems observed in the hyperextended domains affect only the brittle continental crust and root in the underlying mantle that was already at a shallow level. This allows the percolation of seawater through detachment systems triggering serpentinization reactions and the subsequent losses of elements that enriched the seawater and thus forming a mantle-related fluid. These processes can be contemporaneous to the saussuritization of the continental crust and the enrichment of fluids with elements from the continental crust (continental crust-related fluids).

It is important to note, that active detachment systems may be a prerequisite to have a fluid system. Active faulting can keep high permeability along the fault zone, which is necessary to build a hydrothermal cell. Without tectonic activity, the permeability may decrease due to water-rock reactions (alteration) that subsequently lead to mineral precipitations when the equilibrium of fluids is reached. This process causes the shutting down of the fluid circulation. These are important observations because when the deformation migrates further in the direction of the future distal margin, the segment of the detachment fault close to the breakaway becomes inactive preventing fluid migration in this part of the fault (see Figure 15, Article 1).

4.4. **The sink of fluids**

The fluid flow in the rifted margins can have different sinks. As discussed in the Article 3 the seawater can be "absorbed" in the mantle leading to the formation of thick serpentinite sections. The observed hydration of the continental crust in the hyperextended domains also absorbs a considerable amount of seawater, although it was not calculated (see the Section 2.4).

Fluid enriched in mantle and crustal elements can also migrate upward *contaminating* the overlying syn- to post-tectonic sediments and the seawater. The results from the analyses of the sedimentary sequence enabled me to propose the control of the tectonic evolution of rift systems for each of these occurrences. As the detachment fault cuts the brittle continental crust rooting in the mantle, the upward migration of fluids through the extensional detachment system reaches the basin floor and interacts with the syn-tectonic sediments (see Articles 1 and 2). The syn-tectonic sedimentary breccias and turbidites record the signature of mantle-related fluids (enriched in Ni, Cr, V, Fe and Mn) and the tectono-sedimentary breccias (see Article 2) are affected by continental-related fluids (Si-rich). In fact, quartz veins (hence Si) can also be found in the sedimentary breccias and the turbidites. They are often observed concordant to the bedding and also cutting it. I think that this is not a product of pressure/dissolution caused by the sedimentary overburden, since the sedimentary thickness in that basin is less than 600 m. However, it is extremely difficult to point in this case if the Si is associated with mantle- or continental crust-related fluids.

The direct migration through extensional detachment systems is ceased when the segment of detachment fault under the sedimentary basin is no longer active. This led to the interpretation that the enrichment observed in the post-tectonic sediments (see Article 1 and 2) must be explained by other processes. The deposition of the post-tectonic sediments is time-equivalent to the mantle exhumation at the seafloor further in the future distal margin. At this time, the losses of elements are intensified (see Figure 6C and 16, Article 1) due to the increase of the degree and area of

serpentinization. Therefore, the mantle-related fluids *pollute* the seawater in a narrow basin (see Article 3) and the post-tectonic sediments (clay-bearing sediments) capture this signature (e.g., Ni, Cr, V). These observation shows that the mantle, the continental crust and the sea can be sinks, but also the source for fluids. Moreover, the sedimentary basin acts as the sink for these fluids.

4.5. When does fluid migration take place during the evolution of hyperextended systems

The discussion about the age of the migration of fluids along the extensional detachment systems and in the sedimentary section is addressed in the Article 1 and 2. In the following section only the key points are addressed.

In the Eastern Swiss Alps, the Jurassic fault rocks exposed in the Err nappe are often observed as reworked clasts in the Middle-Upper Jurassic sediments. These clasts show the same characteristics such as structures, mineralogical (including new-formed hydrated phyllosilicates) and geochemical composition of the fault rocks exposed along the detachment faults [*Manatschal*, 1995]. This is one of the major evidence to show that detachment activity and fluid percolation occurred around Middle-Upper Jurassic (see discussion in Article 1). Serpentinization also occurred during Middle/Late Jurassic accompanied by the activity of extensional detachment systems. This led me to show that percolation and imprint of both types of fluids along extensional detachment system occurred at Middle to Late Jurassic times and that this percolation is intimately linked to the evolution of a hyperextended system.

Similar observations were also made at the Mauléon Basin and at the Iberia Margin. A detailed description of how to date (relatively) the migration of fluids along extensional detachment faults is addressed in the Article 1, where fluid percolation in other domains of hyperextended systems were used as comparison.

The age of fluid migration is also constrained by the analyses of the sedimentary section, which the main results are discussed in the Articles 1 and 2. Enrichment of Ni, Cr, V, Fe and Mn as well as silicification in these sediments allowed us to understand when the two types of fluids migrated to the sedimentary section and also understand in what domains they can be found. Usually the post-rift (post-tectonic) sediments over the continental crust that are contemporaneous to the mantle exhumation are more enriched in Ni, Cr, V, Fe and Mn compared to the syn-rift (syn-tectonic) sediments. This is mainly caused by the increase of the area and the degree of serpentinization during this stage.

4.6. **The volume of fluids involved in the evolution of hyperextended systems**

Estimate the amount of fluids involved in the evolution of hyperextended domains can be difficult. In Article 3, I quantified the volume of seawater absorbed in the mantle and the mass of elements lost by serpentinization during mantle exhumation that can be carried by fluid. This was possible due to the assembly of petrophysical, geophysical, and geochemical data from the studied zones of exhumed mantle. However, to quantify the amount of fluids absorbed in the crust is even more difficult due to the lack of data and the resolution of the existent ones (see Section 2.4).

The results from Article 3, point to a huge volume of seawater that can be absorbed in the mantle. In the central part of the Western Iberia margin about $1.71x10^{13}$ ton of water was absorbed in the mantle leading to the formation of 5-6 km of thick serpentinite crust (see Figure 1 Article 3). Considering that the basins were restrict to major ocean water circulation, the water absorption in this area would result in water depth decrease of ~380 m. Our results point to an important mass of element losses, which the sum of SiO_2, MgO, FeO, MnO, CaO, Ni and Cr is of the order of 10^{14} ton. This element loss happens at the same period of the hydration of the mantle.

Therefore, these volumetric result may explain why we observe a systematic high enrichment not only in the fault zone but also in the sediments, specially in the post-rift (post-tectonic) sediments, which deposition is contemporaneous to mantle exhumation.

4.7. **Economical implication**

The percolation of fluids through the sedimentary basin can have implication for the quality of petroleum reservoirs. Although detailed studies regarded to the diagenetic processes of the sediments were not performed, I question to what extent these fluids can affect petroleum reservoirs located in hyperextended domains (Figure 9). Fluids enriched in Si and Ca can crystallize as quartz and calcite phases in the pore of sandstones or carbonate rocks, leading to reduction of the primary porosity. Silicification is a major process that affects the syn to post-tectonic sediments. The two types of fluids are enriched in Si and a distinction between them is sometimes only possible considering the relationship between structural evolution and sedimentation.

It is also important to note that the oils from the southeastern Brazilian margins show a signature of Ni, Cr, V and Fe that could be associated with serpentinization [*Szatmari*, 1989; *Szatmari et al*., 2011]. However, it does not necessarily mean that the hydrocarbons (petroleum) were generated by serpentinization, but they are more likely formed by organic maturation

during burial. But the occurrence of these metals may be intimately related to serpentinization. A possible explanation is based on the results that mantle-related fluids percolates through the sedimentary section resulting in the precipitation of elements such as Ni, Cr, V, Fe and Mn as different mineralogical phases (e.g., NiFe alloy and Fe-oxyhydroxides). Our results show high concentration of these elements especially in post-tectonic (or post-rift) sediments, usually mud-bearing (e.g., shales). Therefore, when these shales with sufficient carbon content reach the oil window, petroleum is expulsed caring these metals, which are posteriorly accumulated in the reservoirs. Another possible explanation is that mantle related-fluids migrate direct to the petroleum reservoirs. However, these seems highly improbable once these petroleum reservoirs are much younger (Cenozoic) compared to mantle exhumation that occurred in Early to Middle Cretaceous time [*Zalan et al*., 2011].

Another economical implication is related to mineralization especially when serpentinization processes in involved. The described mineralization along the fault zone and in the serpentinites from the distal margins and mid-ocean ridges [*Fouquet et al*., 2010] suggest that this process can be important to mineralization of e.g., Fe, Ni, Cr and Co.

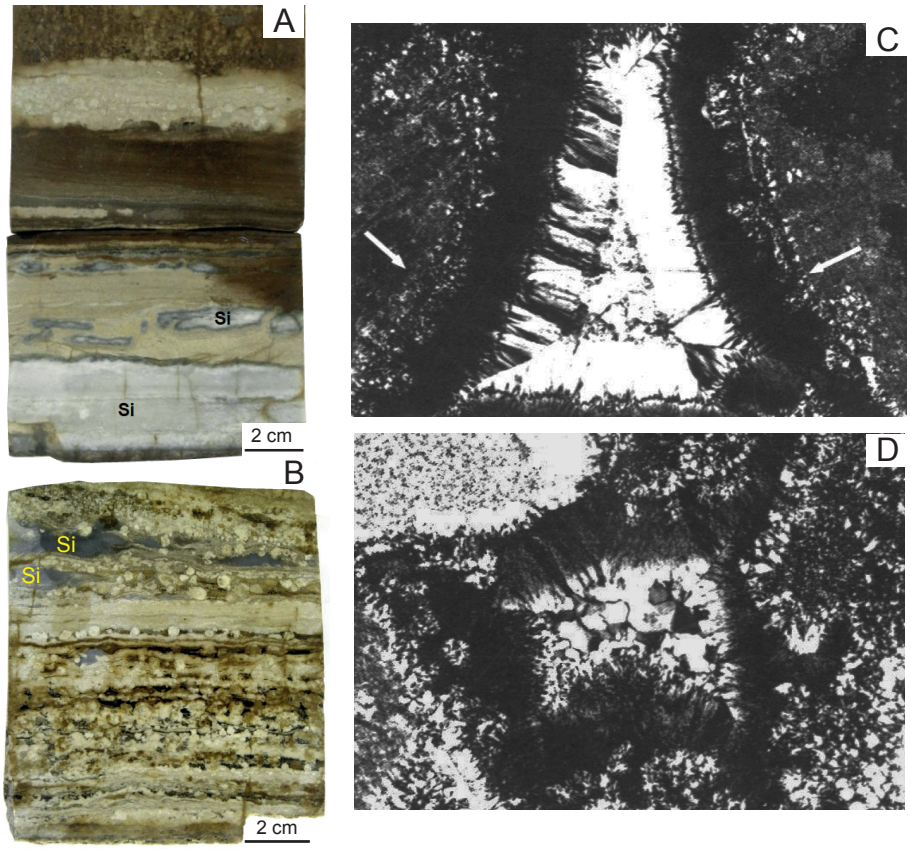

Figure 9. Silicification of sedimentary rocks. A laminated calcilutite with quartz parallel to lamination (bedding). (B) Microbiolite level with quartz nodules. (C) Silicified rudstones (D) Pore-filling cement in form of chalcedony and mega-quartz. Figures A and B from the Aptian section of Brazilian distal margin [*Petersohn et al.*, 2013]. Figure B and C from the Late Aptian section of the Iberia distal margin (Site ODP 103-8R-CC 13-15cm) [*Haggerty and Germann*, 1988].

4.8. **Implication of fluids for the evolution of hyperextended domains**

Important mineralogical changes caused by hydration of the mantle and crust can have major implications for the evolution of the hyperextended systems and future breakup processes. The mineralogical changes from a quartz-feldspatic to phyllosilicate-rich crust in the hyperextended domain can lead to the weakening of the continental crust especially along extensional detachment systems that cut the crust and root in the mantle. This is accompanied by the transformation from an olivine-pyroxene to serpentine mantle that underlie the thinned continental crust (Figure 10). Therefore, fluid can play an important role in the weakening and focalization of deformation that leads to the break up of the crust followed by mantle exhumation.

When mantle is exhumed at the seafloor (see Figure 1 Article 3) the hydration of the mantle can create a serpentinized crust (5-6 km thick), which was strongly weakened. In addition, in this zone new extensional detachment systems developed in the already exhumed serpentinized mantle (e.g., zone of the J-anomaly in distal Iberian Margin). These detachment systems could act as important structures that allowed the emplacement of the magmatic addition observed in the *embryonic ocean crust* and also the posterior lithospheric breakup fallowed by the formation of a seafloor spreading systems.

4.9. **Implication of fluids for the evolution of orogens and changes in the reservoirs of the Earth.**

Remnants of distal rifted margins and hyperextended domains are often observed in orogens, e.g., Eastern Swiss Alps and the West Pyrenees. These domains can be made of large serpentinized crust depleted in elements and saturated in water such as the ones observed in the Iberia margin (5-6 km thick). They can be eventually consumed on subduction zones impacting not only on the early evolution of orogens but also on the magmatism along orogenic arcs. The retained H_2O is not only an important fluid source to trigger melting but it is also an efficient transport-agent to recycle the chemical composition in the upper crust and deep in the mantle.

The cyclic mantle exhumation accompanied by serpentinization, water absorption, element losses and its later subduction, must have substantial impact on changing the geochemistry of major Earth reservoir during the evolution of the planet.

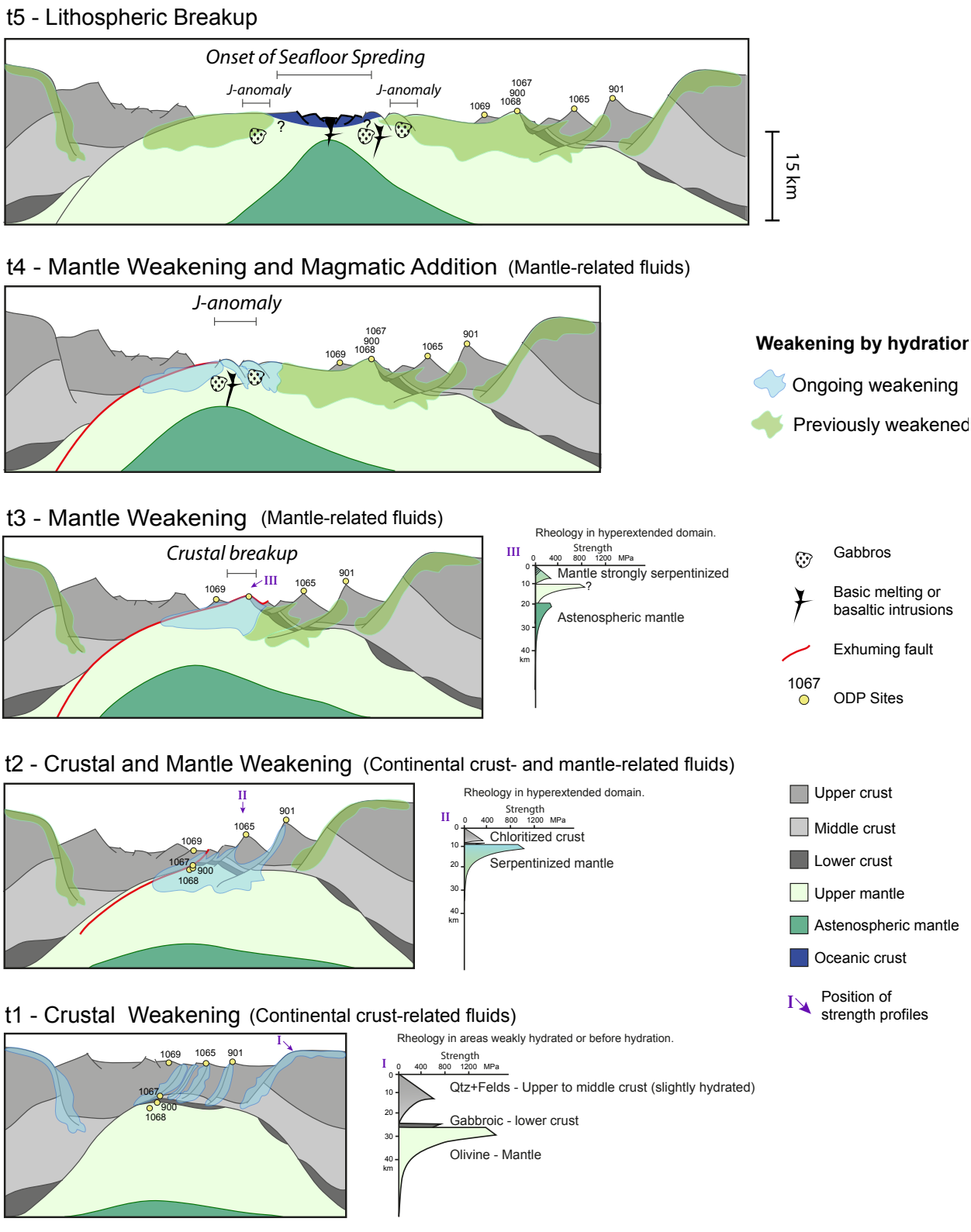
t5 - Lithospheric Breakup
Onset of Seafloor Spreding
J-anomaly
J-anomaly
1069
1067
900
1068
1065
901
15 km
t4 - Mantle Weakening and Magmatic Addition (Mantle-related fluids)
J-anomaly
1069
1067
900
1068
1065
901
Weakening by hydratior
Ongoing weakening
Previously weakened
t3 - Mantle Weakening (Mantle-related fluids)
Crustal breakup
1069
III
1065
901
Rheology in hyperextended domain.
III
Strength
0 400 800 1200 MPa
Mantle strongly serpentinized
?
Astenospheric mantle
0
10
20
30
40
km
Gabbros
Basic melting or basaltic intrusions
Exhuming fault
1067
ODP Sites
t2 - Crustal and Mantle Weakening (Continental crust- and mantle-related fluids)
II
901
1065
1069
1067
900
1068
Rheology in hyperextended domain.
II
Strength
0 400 800 1200 MPa
Chloritized crust
Serpentinized mantle
0
10
20
30
40
km
Upper crust
Middle crust
Lower crust
Upper mantle
Astenospheric mantle
Oceanic crust
I
Position of strength profiles
t1 - Crustal Weakening (Continental crust-related fluids)
I
1069
1065
901
1067
900
1068
Rheology in areas weakly hydrated or before hydration.
I
Strength
0 400 800 1200 MPa
Qtz+Felds - Upper to middle crust (slightly hydrated)
Gabbroic - lower crust
Olivine - Mantle
0
10
20
30
40
km

Figure 10.

Figure 10. Rheological changes. The figures show from bottom to top the rheological changes in the hyperextended domain caused by hydration of the continental crust and the upper mantle. Note that the chemical evolution of the fluids takes place at the same time as the rheological changes. The weakening of the hyperextended domains is evidenced by the strongly altered basement in the crustal rocks (e.g., chloritization) and in the mantle (e.g., serpentinization). In stage t1, high angle normal faults cut the thinned continental crust allowing seawater percolation during deformation, which leads to the weakening of the crust in this area. The weakening of the crust facilitates the fault systems penetrating the upper mantle resulting in the serpentinization at t2. In stage t3, deformation is localized along one detachment system (red line), which plays an important role in fracturing the upper mantle allowing the increase of serpentinization. The weakening caused by strong serpentinization facilitates the emplacement of magmatic addition, observed at t4. Moreover, late extensional detachment systems developed over the exhumed mantle may play an important role in the development of distal margins enhancing the weakening of the upper mantle and allowing the emplacement of magma (e.g., the J-anomaly zone). At this stage the local magmatic addition can have an impact on the composition of the mantle-related fluids. At t5, the seafloor spreading system is developed in the previously weakened zone. At this stage hydrothermal systems similar to those described in the MAR (see Article 1) can take place.

5. GENERAL CONCLUSIONS

Two types of fluids were described. The first is a fluid enriched in Si and Ca results from the interaction between seawater and continental crust rocks (*continental crust-related fluids*). The second is a fluid enriched in Si, Mg, Fe, Mn, Ca, Ni, Cr and V results from the interaction between seawater and mantle rocks (*mantle-related fluids*). These interactions are manly triggered by the activity of extensional detachment system.

The imprint of continental crust-related fluids is observed in all domains where detachment fault systems are major structures. The imprint of mantle-related fluids is only observed in detachment systems associated with mantle exhumation in hyperextended domains.

The sedimentary rocks also recorded the percolation of both types of fluids. Tectono-sedimentary breccias record the circulation of continental crust-relates fluids that is mainly evidenced by silicification. The rift and post-rift sedimentary rocks in hyperextended domains records the imprint of mantle-related fluid circulation, which is evidenced by the enrichment of Ni, Cr, V, Fe and Mn. Because both types of fluids are enriched in Si, it is not clear if the silicification of some syn-tectonic sediment in hyperextended domains is related to mantle- or continental crust-related fluids. However, the silicification and the impregnation of Ni, Cr, V, Fe and Mn in post-tectonic sediments that are contemporaneous with serpentinization and mantle exhumation are associated with mantle-related fluids. This is supported by the impregnations on sediments overlying the continental crust and mantle.

As the mantle-related fluids are often observed in post-rift sediments, they can be used as proxies for understanding the time of serpentinization and mantle exhumation in present day magma-poor rifted margins.

The distribution of these types of fluids is depicted by two processes. The first is the focused migration through extensional detachment fault systems that are able to carry these fluids towards the sedimentary basin over the continental crust. The second one is the spreading and enrichment of these fluids in the seawater that can interact with the post-rift sedimentation. The evolution of hyperextended domains is marked by an important fluid circulation of crustal and upper mantle scale, which develops in narrow zone of extensional systems. These systems can evolve to large zone of exhumed mantle, and eventually, culminate in seafloor spreading and the formation of rifted margins.

The hydration of mantle and crustal rocks in these hyperextended domains can have

large impact in rheological changes. Basically, these changes are resulted from the formation of phyllosilicate minerals in both mantle and crustal rocks (e.g., chlorite, illite and serpentines). In a first moment, these changes can lead to the focalization of deformation along extensional detachment systems, which are responsible for mantle exhumation and continental breakup. This is accompanied by weakening of the ZECM that is often enhanced by the formation of new extensional detachment system that develops in this domain. The weakened ZECM can control magmatic addition that can be followed by the development of a seafloor spreading system.

Serpentinization in hyperextended system is responsible for significant losses of elements that start to occur in basins with more restrict condition. This narrow environment can enhance the fluid-rock interaction not only in the basement but also in the sediments.

Although the stage of mantle exhumation occurs in more restricted settings, the fact that many present-day margins and MOR went to mantle exhumation along detachment systems during the Cretaceous, the fluids produced by serpentinization may affect globally the chemistry of the ocean waters at this period.

Comparative studies with MOR show that losses of CH_4 and H_2 as well as Mg, and Ca through hydrothermal systems are strongly related to serpentinization. The amount of Mg, and at a less extent of Ca, released into the seawater along rifted margins and MOR, should be taking into account for paleotemperature correction when Mg/Ca ratios are used in paleoclimate studies. Moreover, these gases may account for an important temperature increase during Cretaceous, once CH_4 is 20 times more heating-trap than CO_2.

The hydrated and depleted mantle can eventually be consumed on subduction zones impacting not only on the early evolution of orogens but also on the magmatism along orogenic arcs.

The cyclic mantle exhumation accompanied by serpentinization, water absorption, element losses and its later subduction, must have substantial impact on changing the geochemistry of major Earth reservoirs during the evolution of the planet.

6. PERSPECTIVE FOR FUTURE STUDIES

Future studies on the subject of fluids can have different branches. They include the investigation of fluid-rock interaction in continental crust, mantle rocks and sedimentary rocks. Therefore detailed geochemical studies such as fluid inclusions and phase modeling, not addressed in this thesis, is fully recommended. They can reveal detailed condition of fluid flow in the studied systems.

Another subject that can be developed concerns to the migration pathways, not only along the fault zones but also in the sedimentary basins. This may include numerical basin modelling that can be constrained by the natural laboratory addressed in this thesis. However, numerical modelling that couples sedimentary basin and continental crust as well as mantle seems to be far to be achieved. Thus, a wide and new branch of research is open for future geoscientists.

The ability for upscaling petrophysical parameters to the scale of the margin is necessary to quantify rheological changes of the lithosphere caused by fluid flow in hyperextended domains. In this sense, numerical modeling can be a useful tool to test eventual future hypotheses.

The examples of hyperextended domains addressed in this work are related to magma-poor rift systems. Therefore, studies of domains where magma plays an important role for the evolution of rifted systems need to be investigated. It includes the examples of the South Atlantic Margins where magmatism was active during major extensional events (e.g., Santos and Campos Basins). This system can show a very complex history of fluid-rock interactions, once fluids could interacted with mantle rocks while magmatism was strongly active.

7. REFERENCES

Afilhado, A., L. Matias, H. Shiobara, A. Hirn, L. Mendes-Victor, and H. Shimamura (2008), From unthinned continent to ocean: The deep structure of the West Iberia passive continental margin at 38°N, *Tectonophysics*, *458*(1-4), 9–50, doi:10.1016/j.tecto.2008.03.002.

Ague, J. J. (2003), Fluid Flow in the Deep Crust, *Treatise on geochemistry*, *5*, 195–228.

Anping, H., D. Jinxing, Y. Chun, Z. Qinghua, and N. Yunyan (2009), Geochemical characteristics and distribution of CO2 gas fields in Bohai Bay Basin, *Pet. Explor. Dev.*, *36*(2), 181–189, doi:10.1016/S1876-3804(09)60118-X.

Beard, J. S., and L. Hopkinson (2000), A fossil, serpentinization-related hydrothermal vent, Ocean Drilling Program Leg 173, Site 1068 (Iberia Abyssal Plain): Some aspects of min-

eral and fluid chemistry, *J. Geophys. Res.*, *105*(B7), 16527, doi:10.1029/2000JB900073.

Beaumont, C., C. E. Keen, and R. Boutilier (1982), On the evolution of rifted continental margins: comparison of models and observations for the Nova Scotian margin, *Geophys. J. R. astr. Soc*, *70*, 667–715.

Benedicto, A., V. Plagnes, P. Vergely, N. Flotte, and R. A. Schultz (2008), Fault and fluid interaction in a rifted margin: integrated study of calcite-sealed fault-related structures (southern Corinth margin), *Geol. Soc. London, Spec. Publ.*, *299*(1), 257–275, doi:10.1144/SP299.16.

Bernoulli, D., G. Manatschal, L. Desmurs, and O. Müntener (2003), *Where did Gustav Steinmann see the trinity? Back to the roots of an Alpine ophiolite concept. In: Special Paper 373: Ophiolite concept and the evolution of geological thought.*, edited by Y. Dilek and S. Newcomb, Geological Society of America.

Block, L., and L. H. Royden (1990), Core complex geometries and regional scale flow in the lower crust, *Tectonics*, *9*(4), 557–567, doi:10.1029/TC009i004p00557.

Boillot, G., J. Girardeau, and J. Kornprobst (1988), The rifting of the Galicia margin: crustal thinning and emplacement of mantle rocks on the seafloor, *Proc. Ocean Drill. Program*, *103*, 741–756.

Boschi, C., G. L. Früh-Green, A. Delacour, J. A. Karson, and D. S. Kelley (2006), Mass transfer and fluid flow during detachment faulting and development of an oceanic core complex, Atlantis Massif (MAR 30°N), *Geochemistry, Geophys. Geosystems*, *7*(1), n/a–n/a, doi:10.1029/2005GC001074.

Bourquin, S., A. Bercovici, J. López-Gómez, J. B. Diez, J. Broutin, A. Ronchi, M. Durand, A. Arché, B. Linol, and F. Amour (2011), The Permian–Triassic transition and the onset of Mesozoic sedimentation at the northwestern peri-Tethyan domain scale: Palaeogeographic maps and geodynamic implications, *Palaeogeogr. Palaeoclimatol. Palaeoecol.*, *299*(1-2), 265–280, doi:10.1016/j.palaeo.2010.11.007.

Buck, W. R. (1988), Flexural Rotation of Normal Faults, *Tectonics*, *7*(5), 959–973, doi:Doi 10.1029/Tc007i005p00959.

Caine, J. S., J. P. Evans, and C. B. Forster (1996), Fault zone architecture and permeability structure, *Geology*, *24*(11), 1025–1028.

Clerc, C. (2012), Évolution du domaine nord pyrénéen au Crétacé. Amincissement crustal extrême et thermicité élevée: un analogue pour les marges passives, 249 pp., Universite Pierre et Marie Curie.

Coney, P. J., and T. A. Harms (1984), Cordilleran metamorphic core complexes: Cenozoic ex-

tensional relics of Mesozoic compression, *Geology*, *12*, 550–554.

Dick, H. J. B. et al. (2000), A long in situ section of the lower ocean crust: results of ODP Leg 176 drilling at the Southwest Indian Ridge, *Earth Planet. Sci. Lett.*, *179*(1), 31–51, doi:10.1016/S0012-821X(00)00102-3.

Driscoll, N. W., J. R. Hogg, N. Christie-Blick, and G. D. Karner (1995), Extensional tectonics in the Jeanne d'Arc Basin, offshore Newfoundland: implications for the timing of break-up between Grand Banks and Iberia, *Geol. Soc. London, Spec. Publ.*, *90*(1), 1–28, doi:10.1144/GSL.SP.1995.090.01.01.

Edmonds, H. N. (2010), Chemical signatures from hydrothermal venting on slow spreading ridges, in *Diversity of Hydrothermal Systems on Slow Spreading Ocean Ridges*, vol. 188, pp. 27–42, AGU, Washington, DC.

Evam, P., M. Chester, and S. Louis (1995), Fluid-rock interaction in faults of the San Andreas system : Inferences from San Gabriel fault rock geochemistry and microstructures depths fault at Pacoima and associated, , *100*(94), 7–13.

Evans, J. P., C. B. Forster, and J. V. Goddard (1997), Permeability of fault-related rocks, and implications for hydraulic structure of fault zones, *J. Struct. Geol.*, *19*(11), 1393–1404, doi:10.1016/S0191-8141(97)00057-6.

Finlow-Bates, T., and E. F. Stumpfl (1981), The behaviour of so-called immobile elements in hydrothermally altered rocks associated with volcanogenic submarine-exhalative ore deposits, *Miner. Depos.*, *16*(2), doi:10.1007/BF00202743.

Florineth, D., and N. Froitzheim (1994), Transition from continental to oceanic basement in the Tasna nappe (Engadine window, Graubünden, Switzerland): evidence for Early Cretaceous opening of the Valais ocean, *Schweizerische Mineral. und Petrogr. Mitteilungen*, *74*(3), 437–448.

Fodor, R. V., E. H. McKee, and H. E. Asmus (1983), K-Ar ages and the opening of the South Atlantic Ocean: Basaltic rock from the Brazilian margin, *Mar. Geol.*, *54*(1-2), M1–M8, doi:10.1016/0025-3227(83)90002-6.

Fouquet, Y. et al. (2010), Geodiversity of hydrothermal processes along the Mid-Atlantic Ridge and ultramafic-hosted mineralization: A new type of oceanic Cu-Zn-Co-Au volcanogenic massive sulfide deposit, in *Diversity of Hydrothermal Systems on Slow Spreading Ocean Ridges*, vol. 188, pp. 321–367, AGU, Washington, DC.

Franke, D. (2013), Rifting, lithosphere breakup and volcanism: Comparison of magma-poor and volcanic rifted margins, *Mar. Pet. Geol.*, *43*, 63–87, doi:10.1016/j.marpetgeo.2012.11.003.

Froitzheim, N., and G. Manatschal (1996), Kinematics of Jurassic rifting, mantle exhumation, and passive-margin formation in the Austroalpine and Penninic nappes (eastern Switzerland), *Geol*. *Soc*. *Am*. *Bull*., *108*(9), 1120–1133.

Froitzheim, N., S. M. Schmid, and P. Conti (1994), Repeated change from crustal shortening to orogen-parallel extension in the Austroalpine units of Graubünden, *Eclogae Geol*. *Helv*., *87*(2), 559–612.

Früh-Green, G. L., H. Weissert, and D. Bernoulli (1990), A multiple fluid history recorded in Alpine ophiolites, *J*. *Geol*. *Soc*. *London*., *147*, 959–970.

Geoffroy, L. (2005), Volcanic passive margins, *Comptes Rendus Geosci*., *337*(16), 1395–1408.

Gresens, R. (1967), Composition-volume relationships of metasomatism, *Chem*. *Geol*., *2*, 47–65.

Haggerty, J.A., Germann, S.H., 1988. Resedimentation and diagenesis, including silicification, of Barremian-Aptian shallow-water carbonates from the Galicia Margin, Eastern North Atlantic, at Ocean Drilling Program Site 641, in: Boillot, G., Winterer, E.L., Meyer, A.W., Applegate, J. (Eds.), Proc. ODP, Sci. Results, 103. College Station, TX (Ocean Drilling Program), pp. 513–530.

Hauser, A.-C., and O. Müntener (2011), New age constraints on the opening of the Piemont-Ligurian Ocean (Tasna-Nauders area, CH-A), in *9th Swiss Geoscience Meeting*, Zurich.

Hayman, N. W. (2006), Shallow crustal fault rocks from the Black Mountain detachments, Death Valley, CA, *J*. *Struct*. *Geol*., *28*(10), 1767–1784, doi:10.1016/j.jsg.2006.06.017.

Hellinger, S., and J. Sclater (1983), Some comments on two-layer extensional models for the evolution of sedimentary basins, *J*. *Geophys*. *Res*., *88*(B.10), 8251–8269.

Hippertt, J. F., and A. J. Massucatto (1998), Phyllonitization and development of kilometer-size extension gashes in a continental-scale strike-slip shear zone, north Goiás, central Brazil, *J*. *Struct*. *Geol*., *20*(4), 433–445, doi:10.1016/S0191-8141(97)00106-5.

Hopkinson, L., J. . Beard, and C. A. Boulter (2004), The hydrothermal plumbing of a serpentinite-hosted detachment: evidence from the West Iberia non-volcanic rifted continental margin, *Mar*. *Geol*., *204*(3-4), 301–315, doi:10.1016/S0025-3227(03)00374-8.

Hussein, R. A. M., and Z. Xiaomin (2014), Deformational Mechanism and Tectonic Evolution of Mesozoic-Cenozoic Nonmarine Basins from Bohai Bay Basin - China, *SUST J*. *Eng*. *Comput*. *Sci*., *15*(2), 8–25.

Jammes, S., G. Manatschal, L. Lavier, and E. Masini (2009), Tectonosedimentary evolution related to extreme crustal thinning ahead of a propagating ocean: Example of the western Pyrenees, *Tectonics*, *28*(4).

Jones, C.E., Jenkyns, H.C., 2001. Seawater strontium isotopes, ocean anoxic events, and sea-floor hydrothermal activity in the Jurassic and Cretaceous. Am. J. Sci. 301, 112–149.

Kelley, D. S., and T. M. Shank (2010), Hydrothermal systems: A decade of discovery in slow spreading environments, in *Diversity of Hydrothermal Systems on Slow Spreading Ocean Ridges*, vol. 188, pp. 369–407, AGU, Washington, DC.

Kelley, D. S. et al. (2001), An off-axis hydrothermal vent field near the Mid-Atlantic Ridge at 30 degrees N., *Nature*, *412*(6843), 145–9, doi:10.1038/35084000.

Kharaka, Y. K., and J. S. Hanor (2003), Deep fluids in the continents: I. Sedimentary basins, *Treatise on geochemistry*, *5*, 1–48.

Kusznir, N., and G. Karner (2007), Continental lithospheric thinning and breakup in response to upwelling divergent mantle flow: application to the Woodlark, Newfoundland and Iberia margins, *Geol. Soc. London, Spec. Publ.*, *282*(1), 389–419.

Kusznir, N. J., G. Marsden, and S. S. Egan (1991), A flexural-cantilever simple-shear/pure-shear model of continental lithosphere extension: applications to the Jeanne d'Arc Basin, Grand Banks and Viking Graben, North Sea, *Geol. Soc. London, Spec. Publ.*, *56*(1), 41–60, doi:10.1144/GSL.SP.1991.056.01.04.

Lagabrielle, Y., P. Labaume, and M. de Saint Blanquat (2010), Mantle exhumation, crustal denudation, and gravity tectonics during Cretaceous rifting in the Pyrenean realm (SW Europe): Insights from the geological setting of the lherzolite bodies, *Tectonics*, *29*(4).

Lavier, L., W. Roger Buck, and A. N. B. Poliakov (1999), Self-consistent rolling-hinge model for the evolution of large-offset low-angle normal faults, *Geology*, *27*(12), 1127, doi:10.1130/0091-7613(1999)027<1127:SCRHMF>2.3.CO;2.

Lemoine, M., T. Bas, M. Bourbon, P.-C. Graciansky, J.-L. Rudkiewicz, J. Megard-Galli, and P. Tricart (1986), The continental margin of the Mesozoic Tethys in the Western Alps, *Mar. Pet. Geol.*, *3*, 179–199.

Lemoine, M., P. Tricart, and G. Boillot (1987), Ultramafic and gabbroic ocean floor of the Ligurian Tethys (Alps, Corsica, Apennines): In search of a genetic imodel, *Geology*, *15*(7), 622.

Lister, G., and G. Davis (1989), The origin of metamorphic core complexes and detachment faults formed during Tertiary continental extension in the northern Colorado River region, USA, *J. Struct. Geol.*, *11*(1-2), 65–94.

Lister, G., M. Etheridge, and P. Symonds (1986), Detachment faulting and the evolution of passive continental margins, *Geology*, *14*(3), 246.

Lister, G. S., M. A. Etheridge, and P. A. Symonds (1991), Detachment models for the forma-

tion of passive continental margins, *Tectonics*, *10*(5), 1038, doi:10.1029/90TC01007.

Loprieno, A., R. Bousquet, S. Bucher, S. Ceriani, F. H. Dalla Torre, B. Fügenschuh, and S. M. Schmid (2010), The Valais units in Savoy (France): a key area for understanding the palaeogeography and the tectonic evolution of the Western Alps, *Int*. *J*. *Earth Sci*., *100*(5), 963–992, doi:10.1007/s00531-010-0595-1.

MacLean, W. H., and T. J. Barrett (1993), Lithogeochemical techniques using immobile elements, *J*. *Geochemical Explor*., *48*(2), 109–133, doi:10.1016/0375-6742(93)90002-4.

MacLeod, C. J. et al. (2002), Direct geological evidence for oceanic detachment faulting: The Mid-Atlantic Ridge, 15°45′ N, *Geology*, *30*(10), 879–882, doi:10.1130/0091-7613(2002)030.

MacLeod, C. J., R. C. Searle, B. J. Murton, J. F. Casey, C. Mallows, S. C. Unsworth, K. L. Achenbach, and M. Harris (2009), Life cycle of oceanic core complexes, *Earth Planet*. *Sci*. *Lett*., *287*(3-4), 333–344, doi:10.1016/j.epsl.2009.08.016.

MacLeod, C. J., J. Carlut, J. Escartín, H. Horen, and A. Morris (2011), Quantitative constraint on footwall rotations at the 15°45′N oceanic core complex, Mid-Atlantic Ridge: Implications for oceanic detachment fault processes, *Geochemistry*, *Geophys*. *Geosystems*, *12*(5), n/a–n/a, doi:10.1029/2011GC003503.

Magoon, L., and W. Dow (1994), The petroleum system, in *The Petroleum System--from source to trap*, vol. 60, edited by L. B. Magoon and W. G. Dow, AAPG Memoir.

Manatschal, G. (1995), *Jurassic rifting and formation of a passive continental margin (Platta and Err nappes*, *Eastern Switzerland): geometry*, *kinematics and geochemestry of fault rocks and a comparision with the Galicia margin*., Zurich.

Manatschal, G. (1999), Fluid-and reaction-assisted low-angle normal faulting: evidence from rift-related brittle fault rocks in the Alps (Err Nappe, eastern Switzerland), *J*. *Struct*. *Geol*., *21*(7), 777–793.

Manatschal, G., and D. Bernoulli (1998), Rifting and early evolution of ancient ocean basins: the record of the Mesozoic Tethys and of the Galicia-Newfoundland margins, *Mar*. *Geophys*. *Res*., 371–381.

Manatschal, G., D. Marquer, and G. L. Früh-Green (2000), Channelized fluid flow and mass transfer along a rift-related detachment fault (Eastern Alps, southeast Switzerland), *Geol*. *Soc*. *Am*. *Bull*., *112*(1), 21.

Manatschal, G., N. Froitzheim, M. Rubenach, and B. D. Turrin (2001), The role of detachment faulting in the formation of an ocean-continent transition: insights from the Iberia Abyssal Plain, *Geol*. *Soc*. *London*, *Spec*. *Publ*., *187*(1), 405–428.

Manatschal, G., A. Engström, L. Desmurs, U. Schaltegger, M. Cosca, O. Müntener, and D. Bernoulli (2006), What is the tectono-metamorphic evolution of continental break-up: The example of the Tasna Ocean–Continent Transition, *J. Struct. Geol.*, *28*(10), 1849–1869.

Masini, E., 2011. L'évolution tectono-sédimentaire syn-rift des bassinsde marge passive profonde : Exemples du bassin de Samedan (Alpes centrales, Suisse)et du bassin de Mauléon (Pyrénées basques françaises). PhD 1–223.

Masini, E., Manatschal, G., Mohn, G., Ghienne, J., Lafont, F., 2011. The tectono-sedimentary evolution of a supra-detachment rift basin at a deep-water magma-poor rifted margin: the example of the Samedan Basin preserved in the Err nappe in SE Switzerland. Basin Res.

Masini, E., G. Manatschal, and G. Mohn (2013), The Alpine Tethys rifted margins: Reconciling old and new ideas to understand the stratigraphic architecture of magma-poor rifted margins, edited by H. Weissert, *Sedimentology*, *60*(1), 174–196, doi:10.1111/sed.12017.

Masini, E., G. Manatschal, J. Tugend, G. Mohn, and J.-M. Flament (2014), The tectono-sedimentary evolution of a hyperextended rift basin: the example of the Arzacq–Mauléon rift system (Western Pyrenees, SW France), *Int. J. Earth Sci.*, doi:10.1007/s00531-014-1023-8.

McCaig, A. M., R. a. Cliff, J. Escartin, A. E. Fallick, and C. J. MacLeod (2007), Oceanic detachment faults focus very large volumes of black smoker fluids, *Geology*, *35*(10), 935, doi:10.1130/G23657A.1.

McKenzie, D. (1978), Some remarks on the development of sedimentary basins, *Earth Planet. Sci. Lett.*, *40*(1), 25–32.

McKenzie, D., and M. J. Bickle (1988), The volume and composition of melt generated by extension of the lithosphere, *J. Petrol.*, *29*(3), 625–679.

Mohn, G., G. Manatschal, M. Beltrando, E. Masini, and N. Kusznir (2012), Necking of continental crust in magma-poor rifted margins: Evidence from the fossil Alpine Tethys margins, *Tectonics*, *31*(1), n/a–n/a, doi:10.1029/2011TC002961.

Morgan, J. K., and K. L. Milliken (1996), Petrography of calcite veins in serpentinized peridotite basement rocks from the Iberia Abyssal Plain, Sites 897 and 899: kinematic and environmental implications, in *Proceedings of the Ocean Drilling Program*, *Scientific Results*, vol. 149, edited by R. B. Whitmarsh, D. S. Sawyer, A. Klaus, and D. G. Masson, pp. 559–569.

Passchier, C. W., and R. A. J. Trouw (2005), *Microtectonics*, Springer.

Peate, D. (1997), The Paraná-Etendeka Province, *Geophisical Monogr. Ser.*, *100*(Large igneous provinces: Continental, oceanic, and Planetary Flood Volcanism), 217–245.

Péron-Pinvidic, G., and G. Manatschal (2009), The final rifting evolution at deep magma-poor passive margins from Iberia-Newfoundland: a new point of view, *Int. J. Earth Sci.*, *98*(7), 1581–1597.

Péron-Pinvidic, G., G. Manatschal, T. Minshull, and D. Sawyer (2007), Tectonosedimentary evolution of the deep Iberia-Newfoundland margins: Evidence for a complex breakup history, *Tectonics*, *26*(2), TC2011.

Potdevin, J. L., and D. Marquer (1987), Quantitative Methods for the Estimation of Mass Transfers by Fluids in Deformed Metamorphic Rocks, *Geodin. Acta*, *1*(3), 193–206.

Petersohn, E., Abelha, M., Pedrosa, L., 2013. Brasil pre-salt 1: Libra, in: 1° Licitação de Partilha de Produção. ANP, Rio de Janeiro.

Rehrig, W. A., and S. J. Reynolds (1980), *Cordilleran Metamorphic Core Complexes*, Geological Society of America Memoirs, Geological Society of America.

Reston, T., C. Krawczyk, and D. Klaeschen (1996), The S reflector west of Galicia (Spain): Evidence from prestack depth migration for detachment faulting during continental breakup, *J. Geophys. Res.*, *101*, 8075–8091.

Royden, L., and C. Keen (1980), Rifting process and thermal evolution of the continental margin of eastern Canada determined from subsidence curves, *Earth Planet. Sci. Lett.*, *51*(2), 343–361.

Santos Neto, E. V, J. R. Cerqueira, and A. Prinzhofer (2011), Natural gas geochemistry of the southern offshore Brazilian Basins, in *International Meeting on Organic Geochemistry*, p. 264.

Schaltegger, U., Desmurs, L., Manatschal, G., Muntener, O., Meier, M., Frank, M., Bernoulli, D., 2002. The transition from rifting to sea-floor spreading within a magma-poor rifted margin: field and isotopic constraints. Terra Nov. 14, 156–162.

Schmid, S. . M., and M. R. Handy (1991), Towards a Genetic Classiftcation of Fault Rocks : Geological Usage and Tectonophysical lmplications, *Press. London*, 339–361.

Schmid, S. M., B. F Genschuh, E. Kissling, R. Schuster, and B. Fugenschuh (2004), Tectonic map and overall architecture of the Alpine orogen, *Eclogae Geol. Helv.*, *97*(1), 93–117.

Schroeder, T., and B. E. John (2004), Strain localization on an oceanic detachment fault system, Atlantis Massif, 30°N, Mid-Atlantic Ridge, *Geochemistry, Geophys. Geosystems*, *5*(11), n/a–n/a, doi:10.1029/2004GC000728.

Scott, R. J., and G. S. Lister (1992), Detachment faults:Evidence for a low-angle origin, *Geology*, *20*(9), 833–836, doi:10.1130/0091-7613(1992)020<0833:DFEFAL>2.3.CO;2.

Shipboard Scientific Party (1987), Site 639, in *Proc*. *ODP*, *Init*. *Repts*., *103*, edited by G. Boillot, E. L. Winterer, and A. W. Meyer, pp. 409–532, College Station, TX (Ocean Drilling Program).

Shipboard Scientific Party (1998), Site 1068, in *Proc*. *ODP*, *Init*. *Repts*., *173*, vol. 173, edited by R. B. Whitmarsh, M.-O. Beslier, and P. J. Wallace, pp. 163–218, Ocean Drilling Program, College Station, TX (Ocean Drilling Program).

Sibson, R. (1977), Fault rocks and fault mechanisms, *J*. *Geol*. *Soc*. *London*., *I*(1935), 191–213.

Sibson, R. H. (1994), Crustal stress, faulting and fluid flow, *Geol*. *Soc*. *London*, *Spec*. *Publ*., *78*(1), 69–84, doi:10.1144/GSL.SP.1994.078.01.07.

Sibuet, J.-C. (2004), Pyrenean orogeny and plate kinematics, *J*. *Geophys*. *Res*., *109*(B8), 1–18, doi:10.1029/2003JB002514.

Stampfli, G. M. (1993), Le Briançonnais, terrain exotique dans les Alpes?, *Eclogae Geol*. *Helv*., *86*(1), 1–45.

Stipp, M., H. Stünitz, R. Heilbronner, and S. Schmid (2002), The eastern Tonale fault zone: a "natural laboratory" for crystal plastic deformation of quartz over a temperature range from 250 to 700 °C, *J*. *Struct*. *Geol*., *24*(12), 1861–1884.

Sutra, E., G. Manatschal, G. Mohn, and P. Unternehr (2013), Quantification and restoration of extensional deformation along the Western Iberia and Newfoundland rifted margins, *Geochemistry*, *Geophys*. *Geosystems*, *14*(8), 2575–2597, doi:10.1002/ggge.20135.

Szatmari, P. (1989), Petroleum Formation by Fischer-Tropsch Synthesis in Plate Tectonics, *Am*. *Assoc*. *Pet*. *Geol*. *Bull*., *73*(8), 989–998.

Szatmari, P., T. C. O. Fonseca, and N. F. Miekeley (2011), Mantle-like Trace Element Composition of Petroleum – Contributions from Serpentinizing Peridotites, in *Tectonics*, edited by D. Closson, pp. 1–28, InTech.

Thomaz Filho, A., A. M. P. Mizusaki, E. J. Milani, and P. Cesero (2000), Rifting and magmatism associated with the South America and Africa break up, *Brazilian J*. *Geosci*., *30*(1), 17–19.

Trumpy, R. (1975), Penninic-Austroalpine boundary in the Swiss Alps: A presumed former continental margin and its problems, *Am*. *J*. *Sci*., *275-A*, 209–238.

Tucholke, B. E., and J. Sibuet (2007), Leg 210 synthesis: tectonic, magmatic, and sedimen-

tary evolution of the Newfoundland-Iberia rift, in *Proc*. *ODP*, *Sci*. *Results*, *210*, vol. 210, edited by B. E. Tucholke, J.-C. Sibuet, and A. Klaus, pp. 1–56, Ocean Drilling Program, College Station, TX (Ocean Drilling Program).

Tugend, J., Manatschal, G., Kusznir, N.., Masini, E., MOHN, G., Thinon, I., 2014. Formation and deformation of hyperextended rift systems: Insights from rift domain mapping in the Bay of Biscay-Pyrenees. Tectonics 33, 1–38.

Vergés, J., M. Fernàndez, and A. Martínez (2002), The Pyrenean orogen: pre-, syn-, and post-collisional evolution, *J*. *Virtual Explor*., 55–74.

Wernicke, B. (1985a), Uniform-sense normal simple shear of the continental lithosphere, *Can*. *J*. *Earth Sci*., *22*(1), 108–125, doi:10.1139/e85-009.

Wernicke, B. (1985b), Uniform-sense normal simple shear of the continental lithosphere, *Can*. *J*. *Earth Sci*.

Wernicke, B., and G. Axen (1988), On the role of isostasy in the evolution of normal fault systems, *Geology*, *16*, 848–851, doi:10.1130/0091-7613(1988)016<0848.

Wilson, R. C. L., G. Manatschal, and S. Wise (2001), Rifting along non-volcanic passive margins: stratigraphic and seismic evidence from the Mesozoic successions of the Alps and western Iberia, *Geol*. *Soc*. *London*, *Spec*. *Publ*., *187*(1), 429–452, doi:10.1144/GSL.SP.2001.187.01.21.

Wise, D., D. Dunn, and J. Engelder (1984), Fault-related rocks: Suggestions for terminology, *Geology*.

Zalán, P. V, M. Severino, C. A. Rigoti, L. P. Magnavita, J.A.B. Oliveira, and A. R. Viana (2011), An Entirely New 3D-View of the Crustal and Mantle Structure of a South Atlantic Passive Margin – Santos, Campos and Espírito Santo Basins, Brazil, AAPG, 1–12.

ANNEXES

8. ANNEXES

8.1. Sample preparation and analytical procedures

The analytical procedures related to ICP-MS, ICP-AES and X-Ray diffraction analyses were carried by me under the supervision of the technicians and professors from the Laboratoire d'Hydrologie et de Geochimie de Strasbourg (LHyGeS). Some ICP analyses were also performed in others laboratories as described below.

A) Samples preparation for mineralogy (XRD) and geochemical analyses (ICP).

1 – cut the rock using the saw to select non-weathered parts.

2 – break the samples in pieces of about 20 mm using a hammer

3 – reduce the grain size up to about 2-5 mm using a crusher lab.

4 – crush with an agate mortar and pestle eventual pieces which has not possible to reduce with a crusher lab.

5 – reduce the grain size to about 80 μm (powder) using an electrical agate mill

6 – sub-sampling by the coning and quartering technique

After the quartering of powders the samples were prepared for the specific analyses (XRD and ICP)

B) Mineralogy: X-ray diffraction analyses (XRD)

The X-ray diffraction (XRD) patterns from non-oriented powder of bulk samples are obtained using Bruker® D5000 diffractometer with Ni-filtered CuKα radiation at a scan speed of 1°/min, 40 kV/30 mA, 0.1°-1° slits, with a Brucker® DIFFRACplus-EVA determination program.

Oriented aggregates of the extracted fine fractions (<2 μm) collected on glass slide were sequentially air-dried, ethylene-glycol treated, hydrazine treated, and heated at 490°C. Diffractometer parameters: q-2q mode, CuKα radiation, scan speed 0.02°/s, 40kV/30 mA, 0.2°-1° slits.

After the steps of samples preparation, it was performed the:

1 – acidification of the carbonate-bearing samples

2 – clay size separation (<2 μm) using a centrifuge

3 – lamina preparation of the bulk rock and the clay fraction

4 – bulk rock and clay size analyses using the Bruker® D5000 diffractometer

Four analyses of the clay fraction were performed. The first was a (1) normal analysis where the samples were dried at room conditions. For the second analyses, the samples were treated with (2) Ethylene glycol in order to inflate the smectites and make the distinction with other clays. For the third, the samples were treated with hydrazine in order to inflate the kaolinite minerals and make the distinction with other clays. For the forth analyses, the samples were heated at 490 ^{0}C during 4h in order to dehydrate the smectites and recheck their presence.

Note: a detailed analytical procedure can be see in the CD-ROM.

C) ICP-MS and ICP-AES

The Geochemical analyses were performed in the Laboratoire d'Hydrologie et de Geochimie de Strasbourg (LHyGeS)/ UMR 7517. It was used the ISA Jobin Yvon - JY 124 for the Inductively Coupled Plasma - Atomic Emission Spectrometry (ICP-AES) analyses of major elements, and the Thermo scientific X series II for the Inductively Coupled Plasma - Mass Spectrometry (ICP-MS) for the trace elements analyses.

After the samples preparation procedures listed in (A), the following steps were performed.

1 – put 4 g of the sample in a ceramic crucible

2 – put a set of ceramic crucibles in the furnace at 110 ^{0}C in order to evaporate the water (humidity) absorbed in the powder

3 – re-weight the sample

4 – put a set of ceramic crucibles in the furnace at 1000 ^{0}C in order to measure the lost on ignition (LOI)

5 - mix 100 mg of the sample with 750 mg of lithium tetraborate ($Li_2B_4O_7$) in carbon crucibles

6 – put it in the furnace with a controlled atmosphere at 1000 ^{0}C during 20 min in order to melt the samples

7 – put the melt in a solution of glycerol, HNO_3 and water

8 – put the solution in the ICP-AES and ICP-MS

Major and minor elements were measured with an ICP-AES have a relative error of ±10%. Rare earth elements (REE) and other trace elements measured with ICP-MS have a relative error of ±5% at the 1σ level. The samples are calibrated with international standards.

The international standard used in the ICP analyses are those from the CRPG Nancy (K. Govindaradju, Geostandards Newsletter, 1995, vol. 19). They are the BE-N (basalt), UB-N (serpentinite), AN-G (anorthosite), GS-N (granite), WS-E (dolerite) and DR-N (diorite).

Note: a detailed analytical procedure can be see in the CD-ROM.

The analytical procedures of the samples analyzed in the SARM laboratories are quite similar from those used in the LHyGeS. For additional information I recommend access their website (http://helium.crpg.cnrs-nancy.fr/SARM/index.html).

The analytical procedures of the samples analyzed in the ACME laboratories are similar from those used in the LHyGeS. For additional information I recommend access their website (http://acmelab.com).

D) Thin section

The thin section was performed in the laboratory of the EOST-IPGS at Strasbourg University and in private companies, Thin Section Lab (http://thinsectionlab.online.fr/fr/index.html) and Vancouver GeoTech Labs (http://www.thinsection.com/HOME.htm).

The preparation of the samples consisted in:

1 – cut the samples in a standard tablet with a saw. This procedure was performed by me in order to use the same criteria and make a standard choice for the geochemical analyses

2 – the thin section (27 mm x 46 mm) was prepared by the technicians from the companies listed in the Table A1

3 – some thin sections were polished in order to analyze the microstructures and elemental

composition with the Scanning Electron Microscope (SEM) coupled with an Energy-Dispersive X-ray Spectroscopy (EDS).

E) SEM-EDS analyses

Au-coated freshly broken surfaces of bulk samples were examined with a Tescan®Vega II XMU scanning electron microscope (SEM) coupled with an energy dispersive X-ray analysis system (EDAX-XM4) for spot chemical analysis. All the analyses were performed in the LHyGeS.

8.2. **Sample description and applied methods**

The following tables shows a general description and identification of the samples. It includes their geographic position and the applied methods with the respective laboratory.

The following nomenclature was used:

- V.A to designates my samples from the Alps

- V.P to designates my samples from the Pyrenees

These abbreviations was suppressed in the tables from the articles 1, 2 and 3, in order to save space. Therefore, only the abbreviation related to the geological site was used in the articles.

I recommend use the name of the geological site or the geographic coordinates for find the location of the samples from the Alps and the Pyrenees.

Also in the Sample information table, we can find the name of the regions where rocks were sampled, e.g., Graubünden in the Swiss Alps, Piemonte in Italian Alps, Provence-Alpes-Côte d'Azur in French Alps and Aquitaine in the French Pyrenees.

Coordinate systems are: in Suisse grid (CH1903), italic font; UTM (32T) for the Alps and UTM (30T) for the Pyrenees, both with normal font.

Sample information

Sample	Rock	Macroscopic Description	E	N	Geological site	Region	X-Ray	Thin Sections	Major and trace elements. Bulk rock	Major and trace elements. Clay fraction.	Sr isotope. Bulk rock	Sr isotope. Clay fraction
V.A VL-01	Black Gouge	Black gouge rock with very fine matrix with millimetric to some centimetric rounded clasts of feldspar . Peace of 4cm of Triassic carbonate within the gouge.	554287	5159922	Piz Val Lunga	Graubünden						
V.A VL-02	Black Gouge	Black gouge rock with very fine matrix with millimetric to few centimetric clasts. The clasts are composed by green cataclasite and feldspars.	554287	5159922	Piz Val Lunga	Graubünden						
V.A_VL-03	Dolomitic Carbonate	Dark gray rock, high density, with very fine matrix. Millimetric white veins and amorphous milky color calcite.	554188	5159467	Piz Val Lunga	Graubünden						
V.A_VL-04	Dolomitic Carbonate	Dark gray rock, high density, with very fine matrix. Full of millimetric white veins.	554188	5159467	Piz Val Lunga	Graubünden						
V.A_VL-05	Green Cataclasite w/ quartz veins	Green rock composed by quartz, feldspar and chlorite. Veins of quartz and jigsaw clasts of quartz and feldspar make 80% of the sample and 20% is made by chlorite. The green mineral has a fine granulometry. In a small scale it is possible to see a lot of small veins.	554287	5159922	Piz Val Lunga	Graubünden		Strasbourg				
V.A_VL-06	Gouge	Green rock composed by quartz, feldspar and chlorite. Veins of quartz and jigsaw clasts of quartz and feldspar makes 40% of the sample and 60 % is made by chlorite. The green mineral has a fine granulometry. In a small scale it is possible to see a lot of small veins.	554287	5159922	Piz Val Lunga	Graubünden	LHyGeS-Strasbourg	Strasbourg	SARM	SARM		SARM

Table A1. Sample informations. The table shows the concise macroscopic description of the most used samples in this thesis. It was prioritized the samples that are used in the three articles.

Sample	Rock	Macroscopic Description	E	N	Geological site	Region	X-Ray	Thin Sections	Major and trace elements. Bulk rock	Major and trace elements. Clay fraction.	Sr isotope. Bulk rock	Sr isotope. Clay fraction
V.A_VL-07	Black Gouge	Black rock with very fine matrix with millimetric clast (sometimes rounded) cut by calcite veins. Rounded peace of 5cm of quartz within the gouge. Low density.	554287	5159922	Piz Val Lunga	Graubünden	LHyGeS-Strasbourg	Thin Section Lab	SARM	SARM	SARM	SARM
V.A_VL-07a	Black Gouge	Black rock with very fine matrix with millimetric clast (sometimes rounded) cut by calcite veins. Rounded peace of 5cm of quartz within the gouge. Low density.	554287	5159922	Piz Val Lunga	Graubünden			SARM			
V.A_VL-08	Dolomitic Carbonate	Dark gray rock, high density, with very fine matrix. Full of millimetric white veins of calcite.	554287	5159922	Piz Val Lunga	Graubünden		Strasbourg	LHyGeS-Strasbourg			
V.A_VL-09	Gouge	Black rock with very fine matrix with millimetric and centimetric clasts of green cataclasite.	554287	5159922	Piz Val Lunga	Graubünden		Thin Section Lab				
V.A_VL-10	Gouge	Black rock with very fine matrix with millimetric to centimetric clasts of qartz/feldspathic rock.	554287	5159922	Piz Val Lunga	Graubünden						
V.A_P-01	Shale	Dark gray shale, very foliated.	552321	5156843	Parsettens	Graubünden						
V.A_P-02	Quartz Vein	White quartz vein with fractures. Apparently there are sericite and a green mineral.	552321	5156843	Parsettens	Graubünden	LHyGeS-Strasbourg		LHyGeS-Strasbourg			
V.A_P-03	Sed-Breccia (Saluver A) in contact with gouge	Dark gray rock with argillaceous matrix full of millimetric to centimetric clasts. It is possible to see a foliation that can be originated by the activity of the detachment. At the top of the sample it looks like a syn-tectonic sedimentary breccia. It is possible to see a gradual change from a gouge with clasts to a sedimentary rock.	552321	5156843	Parsettens	Graubünden	LHyGeS-Strasbourg		LHyGeS-Strasbourg			

Sample	Rock	Macroscopic Description	E	N	Geological site	Region	X-Ray	Thin Sections	Major and trace elements. Bulk rock	Major and trace elements. Clay fraction.	Sr isotope. Bulk rock	Sr isotope. Clay fraction
V.A_P-04	Tec-Sed Breccia (Fm. Bardela/ Saluver A)	White gray clast-supported rock composed by centimetric angular clasts of Triassic dolomite, plagioclase, quartz and apparently by pieces of green cataclasite.	552321	5156843	Parsettens	Graubünden						
V.A_P-05	Sed-Breccia (Saluver A)	Dar gray rock given by matrix, Moderate schistosity, fine matrix-supported with centimetric angular clasts of feldspar and quartz.	552321	5156843	Parsettens	Graubünden	LHyGeS-Strasbourg		LHyGeS-Strasbourg			
V.A_P-06	Sed-Breccia (Saluver A)	Green rock composed by millimetric to centimetric clasts of feldspar and quartz. Apparently clast-supported with chloritic matrix.	552321	5156843	Parsettens	Graubünden	LHyGeS-Strasbourg		LHyGeS-Strasbourg			
V.A_P-07	Serpentinite/ Qtz veins/ chl-rich	Dark green rock, high density, composed by fibrous green mineral. The rock is cut by 4 cm quartz vein. There is a thin black massive crust at the top of the sample that seem to be a chl-rich.	552039	5157025	Parsettens	Graubünden	LHyGeS-Strasbourg	Strasbourg	LHyGeS-Strasbourg			
V.A_L-06	Cataclasite w/qtz veins	Green rock with white quartz-feldspathic clasts. The green mineral has a fine granulometry.	555515	5155276	Piz Laviner	Graubünden						
V.A_L-07	Green Cataclasite	Light green rock with quartz-feldspathic vein. The green mineral has a fine granulometry. Absence of schistosity. This samples seems to be less cataclasitic than the above	555515	5155276	Piz Laviner	Graubünden	LHyGeS-Strasbourg	Thin Section Lab	SARM	SARM	SARM	SARM

Sample	Rock	Macroscopic Description	E	N	Geological site	Region	X-Ray	Thin Sections	Major and trace elements. Bulk rock	Major and trace elements. Clay fraction.	Sr isotope. Bulk rock	Sr isotope. Clay fraction
V.A_L-7a	Green Cataclasite	Light green rock with quartz-feldspathic vein. The green mineral has a fine granulometry. Absence of schistosity. This samples seems to be less cataclasitic than the above	555515	5155276	Piz Laviner	Graubünden			SARM			
V.A_L-08	Green Cataclasite to gouge	Green and black rock. The samples is a contact between a gouge and a cataclasite. The gouge has millimetric to centimetric clasts of quartz-feldspathic rock and a fine matrix that composed 50% of the rock. The cataclasite as a fine green mineral probably chlorite and clasts of quartz-feldspathic rock. It is possible to see a weak lineation in the rock.	556013	5155371	Piz Laviner	Graubünden						
V.A_L-9a	Albula Granite	Light green granite with some part composed by biotite weakly altered to chlorite. Feldspar is weakly altered with some very small veins of clay minerals.	556286	5155780	Piz Laviner	Graubünden			SARM	SARM		
V.A_L-9b	Albula Granite	Light green granite with some part composed by biotite weakly altered to chlorite. Feldspar is weakly altered with some very small veins of clay minerals.	556280	5155787	Piz Laviner	Graubünden	LHyGeS-Strasbourg	Strasbourg	LHyGeS-Strasbourg	SARM		SARM
V.A_L-10	Gouge w/ big quartz clasts	Black rock with very fine matrix with millimetric to centimetric clasts of quartz and feldspar as well as the green cataclasite rock.	555515	5155276	Piz Laviner	Graubünden						
V.A_L-11	Ultracataclasite to Gouge	Black rock, very fine matrix with millimetric to centimetric clasts of quartz/feldspathic of the green cataclasite. Moderate foliation.	557193	5156080	Piz Laviner	Graubünden						

Sample	Rock	Macroscopic Description	E	N	Geological site	Region	X-Ray	Thin Sections	Major and trace elements. Bulk rock	Major and trace elements. Clay fraction.	Sr isotope. Bulk rock	Sr isotope. Clay fraction
V.A_L-12	Ultracataclasite to Gouge	Black rock, very fine matrix with millimetric to centimetric clasts of quartz/feldspar from the green cataclasite. Weak to moderate foliation.	557193	5156080	Piz Laviner	Graubünden						
V.A_L-13	Ultracataclasite to Gouge	Green and black rock covered by a white crust of altered feldspar.	557193	5156080	Piz Laviner	Graubünden						
V.A_L-14	Green Cataclasite	Green cataclasite rock composed by millimetric to centimetric clasts of feldspar and quartz. Apparently clast-supported with chloritic matrix.	557193	5156080	Piz Laviner	Graubünden	LHyGeS-Strasbourg	Strasbourg	LHyGeS-Strasbourg			
V.A_L-15	Ultracataclasite to Gouge	Black rock with fine matrix with millimetric to centimetric clasts of quartz and feldspar, and centimetric pieces of the green cataclasite.	557193	5156080	Piz Laviner	Graubünden						
V.A_L-16	Gouge/ Ultracataclasite	Black rock with very fine matrix with millimetric clast of feldspar, cataclasite and granite. Moderate to strong foliation	557193	5156080	Piz Laviner	Graubünden	LHyGeS-Strasbourg		LHyGeS-Strasbourg			
V.A_L-17	Contact Cataclasite/ ?gouge?	The sample has two different rock types. A cataclasite composed manly by quart and feldspar, and a cataclasite/ ?gouge? composed by centimetric to millimetric clast of cataclasite and clasts of feldspar. The clasts are elongated and few clasts are rounded.	557193	5156080	Piz Laviner	Graubünden		Thin Section Lab				

Sample	Rock	Macroscopic Description	E	N	Geological site	Region	X-Ray	Thin Sections	Major and trace elements. Bulk rock	Major and trace elements. Clay fraction.	Sr isotope. Bulk rock	Sr isotope. Clay fraction
V.A_L-18	Gouges	Gouge composed by a black fine matrix and centimetric clasts of manly cataclasite and few quartz and feldspar. Clasts are elongated and some few clasts are moderated rounded. Some times it is possible to see a layering of green cataclasite within the gouge. Moderate foliation.	557193	5156080	Piz Laviner	Graubünden	LHyGeS-Strasbourg	Thin Section Lab	SARM	SARM		SARM
V.A_L-19	Ultracataclasite to Gouge	Black rock with fine matrix with millimetric to centimetric clasts of quartz and feldspar, and centimetric pieces of the green cataclasite.	557193	5156080	Piz Laviner	Graubünden						
V.A_FC-01	Sandstone (Saluver B?)	Black sandstone made of a black fine layered bands with grains probably from the green cataclasite. The matrix is probably composed by the gouge material.	556048	5148595	Fuorcla Cotschna	Graubünden						
V.A_FC-02	Sandstone (Saluver B?)	Black sandstone rock made by a black fine layered with grains probably composed by green cataclasite.	556048	5148595	Fuorcla Cotschna	Graubünden						
V.A_FC-03	Thin sandstone to silt (Saluver B?)	Black rock composed by a black fine matrix and millimetric quartz-feldspathic grains. Moderate cohesion.	556048	5148595	Fuorcla Cotschna	Graubünden						
V.A_FC-04	Shale	Black shale.	556089	5148860	Fuorcla Cotschna	Graubünden	LHyGeS-Strasbourg					
V.A_FC-05	Sed-Breccia (Bardela+Saluver A)	Sedimentary breccia composed by Triassic dolomites with superficial iron oxidation	556048	5148595	Fuorcla Cotschna	Graubünden						

Sample	Rock	Macroscopic Description	E	N	Geological site	Region	X-Ray	Thin Sections	Major and trace elements. Bulk rock	Major and trace elements. Clay fraction.	Sr isotope. Bulk rock	Sr isotope. Clay fraction
V.A_FC-06	Triassic Carbonate	Carbonates took in the gouge layer. The rock has a middle gray color and is made mainly by dolomite and carbonate veins.	556048	5148595	Fuorcla Cotschna	Graubünden						
V.A_FC-07	Sandstone (Saluver A)	Chlorite-rich thin sandstone with black colour and very fine matrix. No clasts.The rock has high cohesion.	556048	5148595	Fuorcla Cotschna	Graubünden	LHyGeS-Strasbourg	Strasbourg	LHyGeS-Strasbourg			
V.A_FC-8C	Cataclasite	Green to gray rock with millimetric to centimetric white quartz-feldspathic clasts rarely rounded. Sometimes it's possible to observe a weak layering with the green foliated matrix and quartz, what gives to the rock a weak foliation. Some Clasts are fractured.	556048	5148595	Fuorcla Cotschna	Graubünden	LHyGeS-Strasbourg		LHyGeS-Strasbourg			
V.A_FC-8M	Cataclasite	Green to gray rock with millimetric to centimetric white quartz-feldspathic clasts rarely rounded. This samples is similar to the FC-8C, however more matrix-rich.	556048	5148595	Fuorcla Cotschna	Graubünden	LHyGeS-Strasbourg		LHyGeS-Strasbourg			
V.A_FC-09	Sed-Breccia (Saluver A)	The rock has a middle gray color. It is a clast-supported rock composed by centimetric to millimetric quartz-feldspathic fragments in a weak foliated matrix.	556048	5148595	Fuorcla Cotschna	Graubünden						
V.A_FC-10	Sed-Breccia (Bardela+Saluver A?)	The rock has a brown color. It is a clast-supported rock composed by centimetric clasts of Triassic carbonate, few quartz-feldspathic clasts, and lasts of green cataclasite.	556048	5148595	Fuorcla Cotschna	Graubünden						

Sample	Rock	Macroscopic Description	E	N	Geological site	Region	X-Ray	Thin Sections	Major and trace elements. Bulk rock	Major and trace elements. Clay fraction.	Sr isotope. Bulk rock	Sr isotope. Clay fraction
V.A_FC-11	Sed-Breccia (Bardela+Saluver A?)	The rock has a brown color. It is a clast-supported rock composed by centimetric clasts of Triassic carbonate, quartz-feldspathic rock and pieces of green cataclasite. The matrix seem to be composed of green cataclasite.	556048	5148595	Fuorcla Cotschna	Graubünden						
V.A_FC-12	Sed-Breccia (Bardela)	The rock has a brown color. It is a clast-supported rock composed by centimetric clasts of Triassic carbonate.	556048	5148595	Fuorcla Cotschna	Graubünden						
V.A_FC2-01	Gouge	Black rock with very thin black matrix and clasts of quartz and triassic carbonate	556048	5148595	Fuorcla Cotschna	Graubünden	LHyGeS-Strasbourg		SARM	SARM		SARM
V.A_FC2-05	Cataclasite	Greenish rock composed by chlorite and clasts of quartz and feldspar	556048	5148595	Fuorcla Cotschna	Graubünden	LHyGeS-Strasbourg		SARM		SARM	SARM
V.A_FC2-5a	Cataclasite	Greenish rock composed by chlorite and clasts of quartz and feldspar	556048	5148595	Fuorcla Cotschna	Graubünden			SARM	SARM		
V.A_FC2-6	Clast-rich chl-schist	Schist with high amount of clasts of quartz and matrix made by chlorite and muscovite.	556048	5148595	Fuorcla Cotschna	Graubünden	LHyGeS-Strasbourg	Strasbourg	SARM	SARM		SARM
V.A_T-01	Altered gabbro (hydrated)	Fine grained green rock apparently composed by plagioclase and a green mineral. High density rock.	595409	5186646	Tasna	Graubünden	LHyGeS-Strasbourg	Strasbourg	LHyGeS-Strasbourg			
V.A_T-02	Gouge	Black rock composed by a black fine matrix and millimetric quartz-feldspathic clasts. Strong foliation.	595278	5186206	Tasna	Graubünden						

Sample	Rock	Macroscopic Description	E	N	Geological site	Region	X-Ray	Thin Sections	Major and trace elements. Bulk rock	Major and trace elements. Clay fraction.	Sr isotope. Bulk rock	Sr isotope. Clay fraction
V.A_T-03	Contact Cataclasite/ Gouge	Contact between a black rock and a yellowish one. The black rock is made of a fine matrix, millimetric quartz-feldspathic clasts. The yellowish rock is a composed by quartz-feldspathic clasts.	595278	5186206	Tasna	Graubünden						
V.A_T-04	Gouge	Black gouge composed by a black fine matrix and millimetric to centimetric clasts of quartz-feldspathic rock and green cataclasite?. The clast sometimes is elongated. Moderate foliation.	595278	5186206	Tasna	Graubünden		Strasbourg				
V.A_T-05	Shale (Tonschiefer)	Middle gray shale.	595169	5186238	Tasna	Graubünden						
V.A_T-06	Shale (Tonschiefer)	Middle gray shale.	595169	5186238	Tasna	Graubünden	LHyGeS-Strasbourg		LHyGeS-Strasbourg			
V.A_T-07 (rt)	Gouge	Black to dark brown gouge composed by fine foliated matrix, millimetric to centimetric clasts (40%) of quartz-feldspathic rock and millimetric veins of quartz. Some of the clasts are elongated.	595278	5186206	Tasna	Graubünden	LHyGeS-Strasbourg		LHyGeS-Strasbourg			
V.A_T-08	Ultramylonite	Fine-grained black to dark green rock with a mylonitic structure.	595255	5186777	Tasna	Graubünden						
V.A_T-09	Mylonite	Fine-grained black to dark green rock with a mylonitic structure. In this samples it possible to see some millimetric elongated clasts.	595245	5186807	Tasna	Graubünden						
V.A_T-10	Mylonite	Mid-grained dark green mylonite consisting of quartz-feldspathic elongated bands and millimetric rounded clasts.	595245	5186807	Tasna	Graubünden						
V.A_T-11	Mylonite	Mid-grained and middle green mylonite consisting of quartz-feldspathic elongated clasts and quartz veins.	595245	5186807	Tasna	Graubünden		Vancouver GeoTech Labs	ACME			

Sample	Rock	Macroscopic Description	E	N	Geological site	Region	X-Ray	Thin Sections	Major and trace elements. Bulk rock	Major and trace elements. Clay fraction.	Sr isotope. Bulk rock	Sr isotope. Clay fraction
V.A_T-13	Serpentinite	Rock with a dark green colour given by green minerals like serpentine and probably minor olivine and pyroxenes. The rocks is cut by calcite veins.	595310	5186786	Tasna	Graubünden	LHyGeS-Strasbourg					
V.A_T-14	Tectonic Sedimentary Breccia	Middle green color tectonic-sedimentary breccia composed by a phyllosilicate matrix (chlorite?) and millimetric quartz-feldspathic clasts.	595186	5186225	Tasna	Graubünden	LHyGeS-Strasbourg		SARM			
V.A_T2-08	Cataclasite	Greenish rock made of chloritic matrix, millimetric quartz-feldspathic clasts.	595278	5186206	Tasna	Graubünden	LHyGeS-Strasbourg	Strasbourg	LHyGeS-Strasbourg		SARM	
V.A_T2-09	Gouge	Black to dark brown gouge composed by fine foliated matrix, millimetric to centimetric clasts of quartz and feldspar.	595278	5186206	Tasna	Graubünden	LHyGeS-Strasbourg	Strasbourg	SARM		SARM	
V.A_T3-07	Gouge	Black to dark brown gouge composed by fine foliated matrix, millimetric to centimetric clasts of quartz and feldspar.	595278	5186206	Tasna	Graubünden		Vancouver GeoTech Labs	ACME			
V.A_T3-18	Chl-Schist cataclasite	The rock shows high content of chlorite and presents clasts of quartz/feldspar. Although the rock presents a schistosity due to the high content of chlorite and advanced deformation, they keep a cataclasite structure marked by the brecciated quartz and feldspar.	595278	5186206	Tasna	Graubünden		Vancouver GeoTech Labs	ACME			
V.A_T3-20	Gouge	Black to dark brown gouge composed by fine foliated matrix, millimetric to centimetric clasts of quartz and feldspar.	595278	5186206	Tasna	Graubünden		Vancouver GeoTech Labs	ACME			
V.A-Munta-1	Cataclasite	Green cataclasite with locally preserved fabric of the Albula granite.	*786112*	*157406*	Alp Muntatsch	Graubünden	LHyGeS-Strasbourg		SARM			SARM

Sample	Rock	Macroscopic Description	E	N	Geological site	Region	X-Ray	Thin Sections	Major and trace elements. Bulk rock	Major and trace elements. Clay fraction.	Sr isotope. Bulk rock	Sr isotope. Clay fraction
V.A-Munta-2	Gouge	Gouge with moderate foliation composed by thin matrix of chlorite and clasts of feldspar and quartz.	*786112*	*157406*	Alp Muntatsch	Graubünden	LHyGeS-Strasbourg	Strasbourg	SARM	SARM		SARM
V.A-Munta-3	Gouge	Gouge with moderate foliation composed by thin matrix of chlorite and clasts of feldspar and quartz.	*786112*	*157406*	Alp Muntatsch	Graubünden	LHyGeS-Strasbourg		SARM	SARM		SARM
V.A.BI3-1	Albula Granite	Granite with very well preserved igneous fabric. The rocks is composed mainly by feldspar and quartz with few biotites and rarely hornblende.	*778535*	*157789*	Piz Bial	Graubünden		Vancouver GeoTech Labs	ACME			
V.A-BERN3-6	Gneiss	The rock shows gneissic structure and is composed mainly by quartz and feldspar. This rock is the protolith of the Bernina detachment.	*795158*	*148805*	Val da Fain	Graubünden		Vancouver GeoTech Labs	ACME			
V.A-BERN3-9	Ultracataclasite	The rock show a greenish colour and is composed by mainly by clasts of quartz and feldspar within a matrix of chlorite/sericite that makes less than 15% of the rock.	*794958*	*149110*	Val da Fain	Graubünden		Vancouver GeoTech Labs	ACME			
V.A-GROS3-05	Mylonite	Mylonite composed mainly by thin matrix of recrystallised quartz and feldspar. This rock is one of the protolith of the Grosina detachment.	591148	5134116	Grosina	Lombardia		Vancouver GeoTech Labs	ACME			
V.A-GROS3-07	Ultracataclasite	The rock show a greenish to greyish colour and is composed by very thin matrix of quartz and feldspar and chlorite, and clasts of quartz and feldspar.	591326	5134309	Grosina	Lombardia		Vancouver GeoTech Labs	ACME			

Sample	Rock	Macroscopic Description	E	N	Geological site	Region	X-Ray	Thin Sections	Major and trace elements. Bulk rock	Major and trace elements. Clay fraction.	Sr isotope. Bulk rock	Sr isotope. Clay fraction
V.A-CHAB-2	Gouge	Black gouge, very similar from those of the Err nappe. It is composed by a phyllosilicate-rich matrix (chlorite) and rounded clasts of quartz. (France)	320226	4980774	Mont Chaberton	Provence-Alpes-Côte d'Azur		Vancouver GeoTech Labs	ACME			
V.A-Lan-1	Peridotite	Lherzolite Peridotite from Lanzo (Italy)	374022	5003857	Lanzo	Piemonte		Strasbourg	ACME			
V.A.F3-01	Serpentinite	Highly serpentinite peridotite composed mainly of serpentines.	*771058*	*157588*	Platta	Graubünden		Vancouver GeoTech Labs	ACME			
V.A.F3-02	Serpentinite	Highly serpentinite peridotite composed mainly of serpentines.	*771058*	*157588*	Platta	Graubünden		Vancouver GeoTech Labs	ACME			
V.P-GAR-01.A	Leucocratic paragneiss (Amphibolite to Greenshiste Facies)	Gray to orangish medium-grained psammitic rock. The rocks is characterized by coarse to middle grained mineral of feldspar and quartz. Some few biotite and amphiboles are dispersed in the rock. There are quartz veins parallel to the very weak schistosity. Sampled out of the fault zone.	642291	4800058	Garalda	Aquitaine		Thin Section Lab	ACME			
V.P-GAR-03.B	Red Cataclasite	Reddish matrix-supported cataclasite. The rock presents similar mineralogy from those of the sample GAR-01.A, however feldspar are sericitized. The rock is well-defined by jigsaw structures. It is composed by millimetric clasts of quartz-feldspathic rock and a characteristic reddish matrix that makes more than 30% of the sample.	642291	4800058	Garalda	Aquitaine		Thin Section Lab	ACME			

8.3. **Geochemistry and Mineralogy**

The next images and data are related to the geochemical studies performed in the thesis. They additionally support the topics discussed in the three articles. Some of these data represent the methods used this study. Indeed, dozens of XRD analyses were performed and they were recorded in the CD attached.

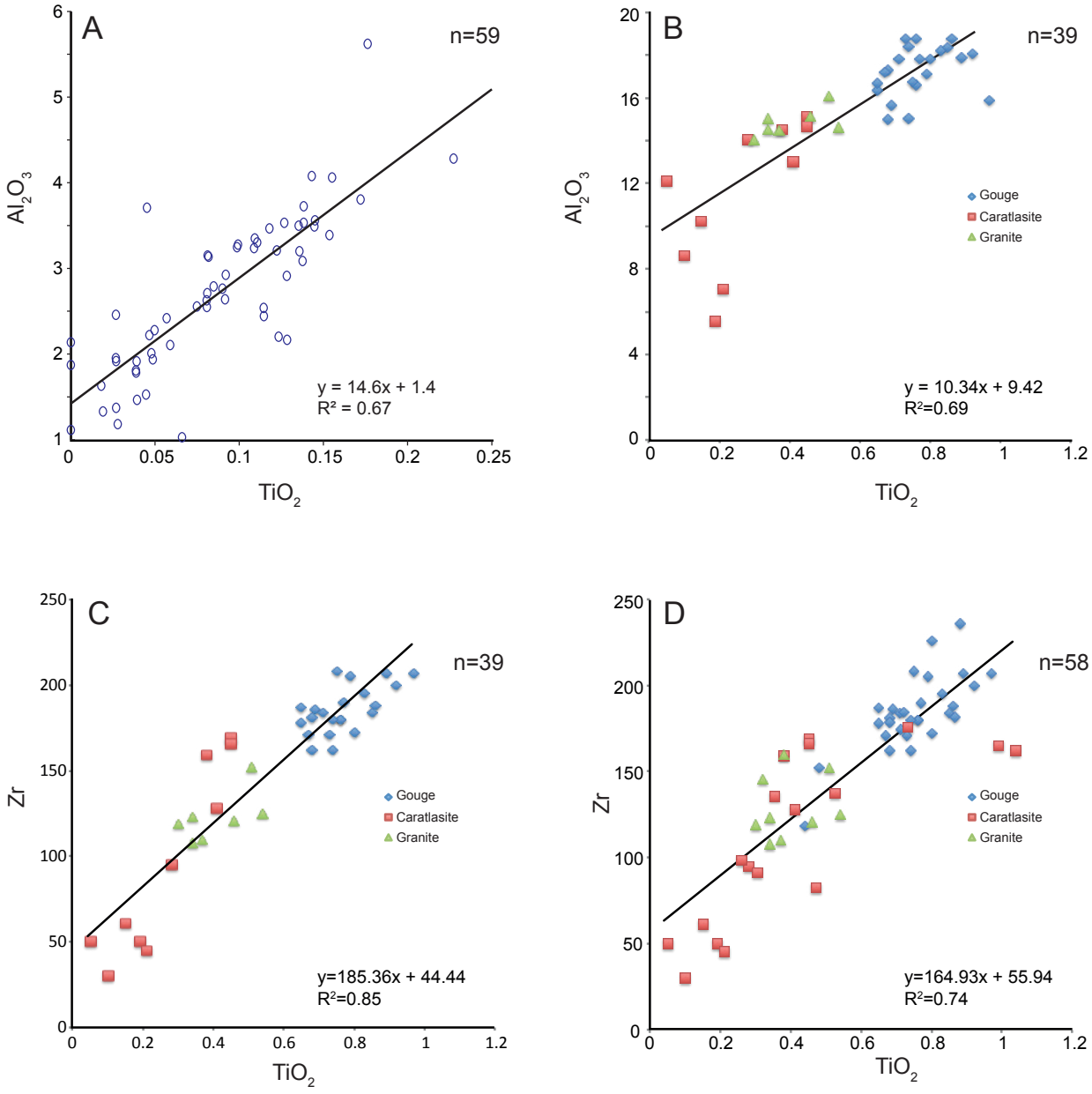

Figure A1. Immobile elements. The graphs show the relationship between Al_2O_3, TiO_2 and Zr of the samples from Platta, Malenco and Err nappes in the Swiss Alps. The linear relationship between these elements evidences their immobile behavior. (A) Al_2O_3 vs. TiO_2 in the serpentinized peridotites that varies from 5 to 95% of serpentinization. The good linear correlation is only displaced because of 3 samples that are positioned at the extremities. Data from *Müntener et al.* [2010]. (B) Al_2O_3 vs. TiO_2 from fault rocks. (C) Zr vs. TiO_2 from fault rocks. Data in B and C are from the Albula granite and the fault rocks from the Err detachment [*Manatschal et al.*, 2000]. (D) Zr vs. TiO_2 from the same data in Figure C and own data (see Table 2 from Article 1 data from Err unit).

Sr isotopes

Sample	Type	Sr (ppm)	87Sr/86Sr	err (2σ) of 87Sr/86Sr
VA-T2-10	Clay	64.57	0.718735	0.000010
VA-T2-08	Clay	42.72	0.724820	0.000011
VA-T2-09	Clay	36.62	0.726637	0.000017
VA-L-18	Clay	38.12	0.765646	0.000018
VA-MUNTA-2	Clay	24.78	0.781964	0.000014
VA-MUNTA-3	Clay	38.79	0.762368	0.000013
VA-VL-07	Clay	41.4	0.767858	0.000014
VA-VL-07	Bulk	36.29	0.755887	0.000015
VA-FC2-1	Clay	27.83	0.781482	0.000022
VA-F2-12	Clay	2.17	0.708317	0.000012
VA-T2-06	Clay	2.77	0.711144	0.000008
VA-L-9b	Clay	168.5	0.719767	0.000013
VA-MUNTA-1	Clay	46.43	0.728256	0.000011
VA-VL-06	Clay	34.63	0.733401	0.000017
VA-L-07	Clay	39.54	0.736007	0.000013
VA-L-07	Bulk	47.2	0.733997	0.000016
VA-F2-11	Clay	< L.D.	0.710879	0.000040
VA-FC2-06	Clay	56.18	0.755608	0.000024
VA-FC2-05	Clay	113.8	0.741810	0.000008
VA-FC2-05	Bulk	47.4	0.748705	0.000022

Table A2. Strontium isotopes measured in bulk and clay fraction from fault rocks, serpentinites and tectonic sedimentary breccias. See Table A1 for sample description.

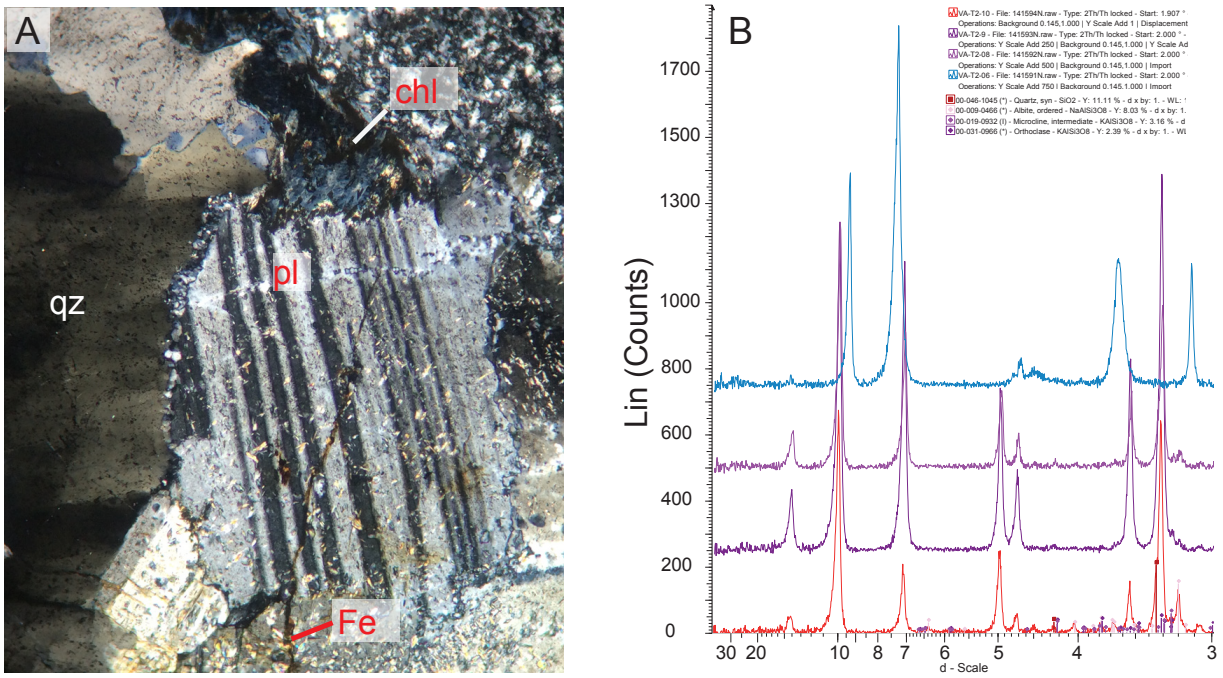

Figure A2. Chloritization of plagioclase. As plagioclases do not have Fe in their structures, it must come from other source. According to the usual gain of Fe observed in the fault rocks from the extensional detachments systems in the continental crust, this Fe is interpreted to come from the mantle-related fluids. (A) Note that the Fe-vein cuts through the plagioclase. Sample from the Tasna OCT. (B) XRD data showing the main composition of the clay fraction of the fault rocks from Tasna.

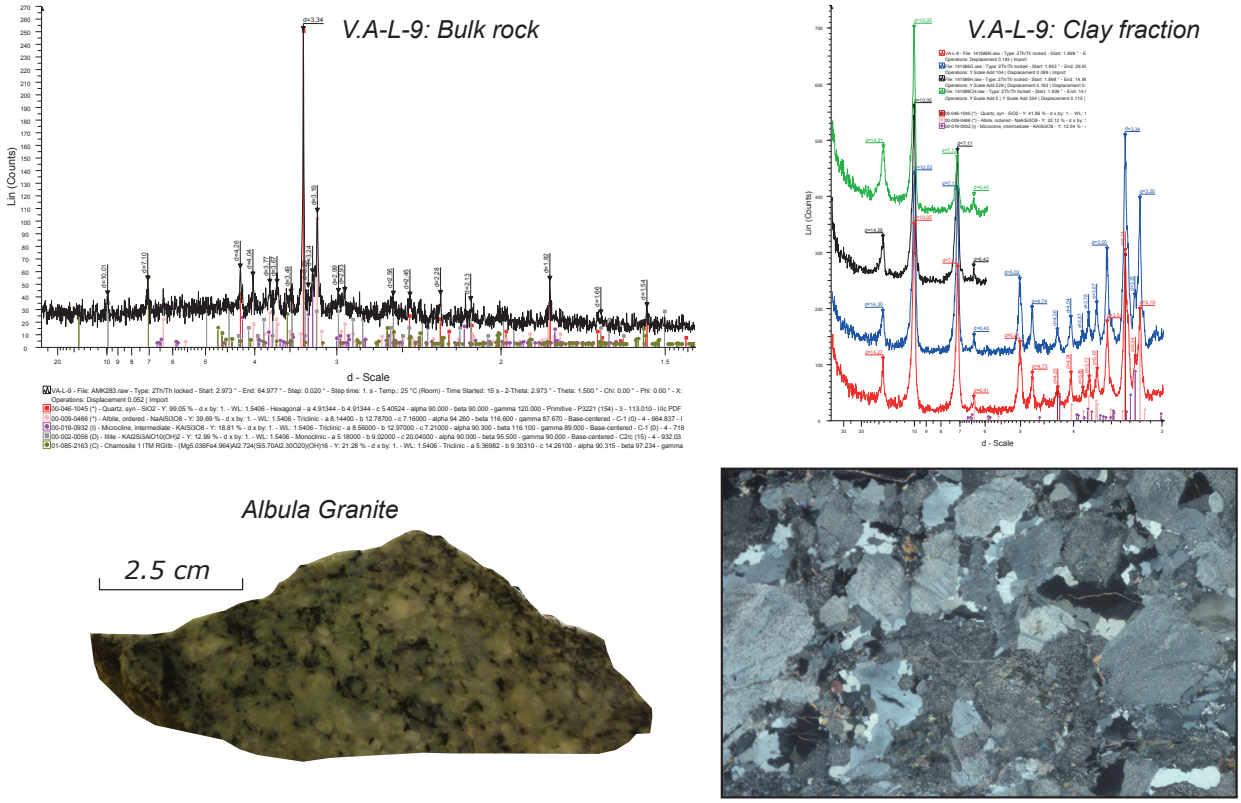

Figure A3. Mineralogical study of fault rocks from extensional detachment. Mineralogical recognition was done using optical microscopy and XRD of bulk rock and clay fraction (<2 micrometers). The sample is the Albula granite outside the fault zone of the Err detachment. It is little affected by fluid-rock interactions.

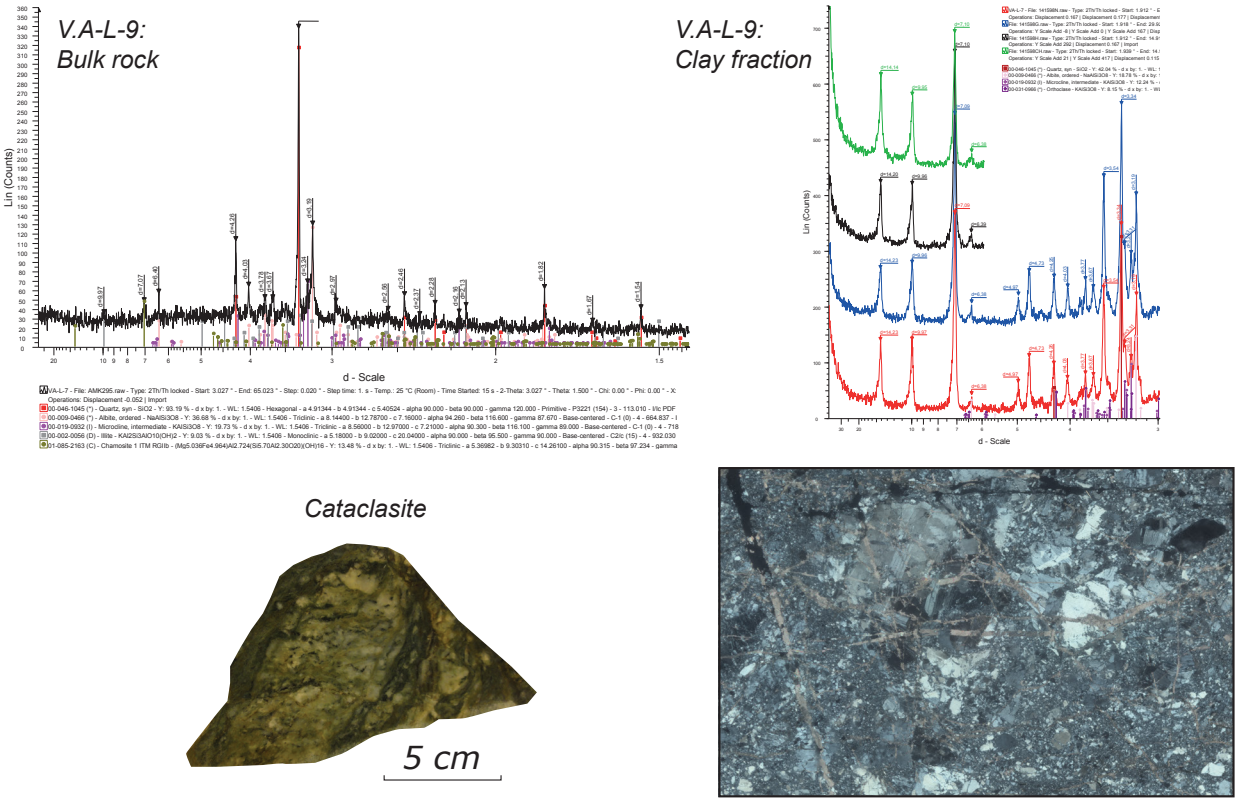

Figure A4. Mineralogical study of fault rocks from extensional detachment. Same methods from the previous figure. Cataclasite sampled in the fault zone of the Err detachment. Note the increase of neoformed phyllosilicates.

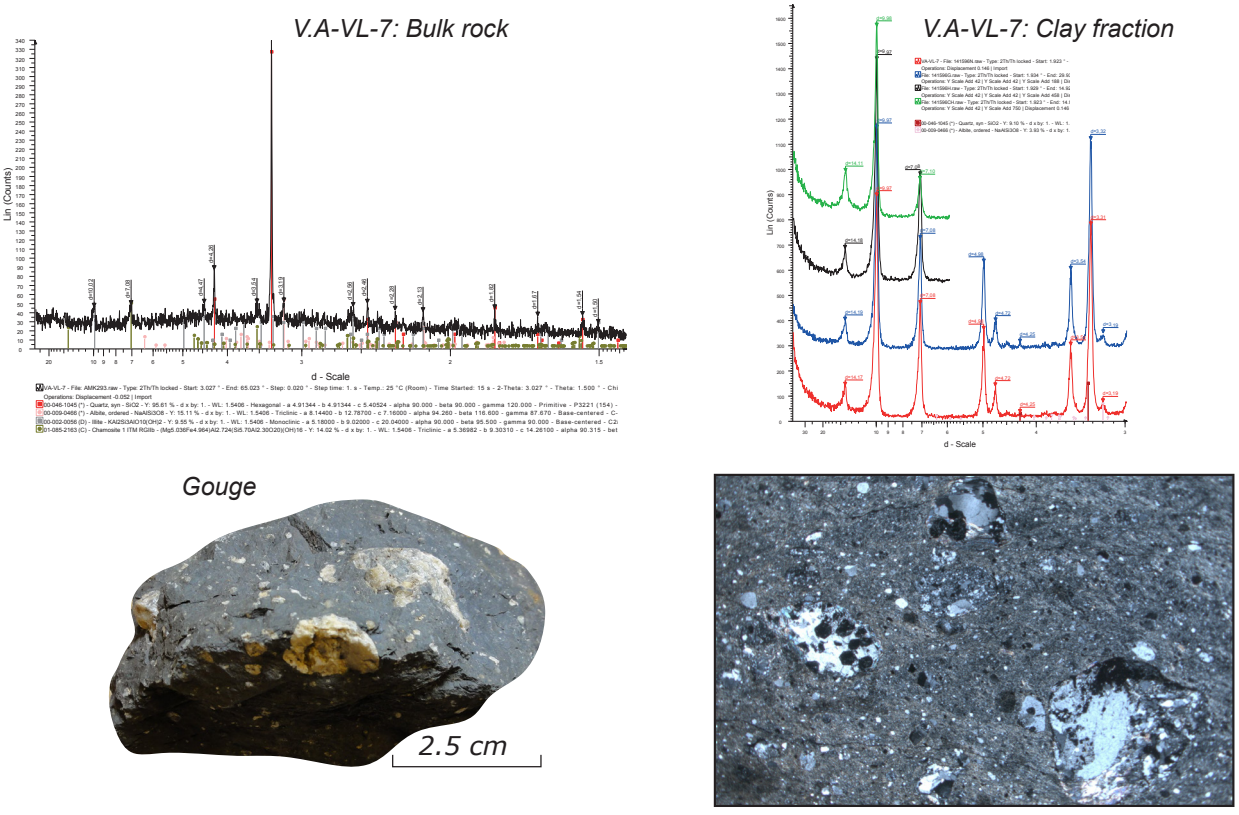

Figure A5. Mineralogical study of fault rocks from extensional detachment. Same methods from the previous figure. Gouge sampled at the top of the footwall of the Err detachment. Note the increase of neoformed phyllosilicates which makes more than 70% of the rock.

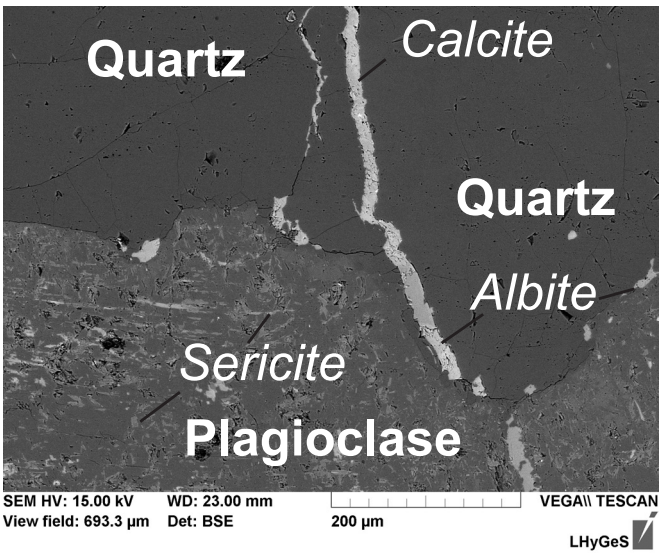

Figure A6. Scanning electron microscope with back-scattered electrons (SEM-BSE) image. Note that the alteration (hydration) of plagioclase led to sericitization and albitization at the rim of the plagioclase. Albitization of plagioclase resulted in losses of Ca that is evidenced by calcite vein. The elemental composition of the minerals were analysed with a coupled EDS (energy dispersive X-ray analysis system).

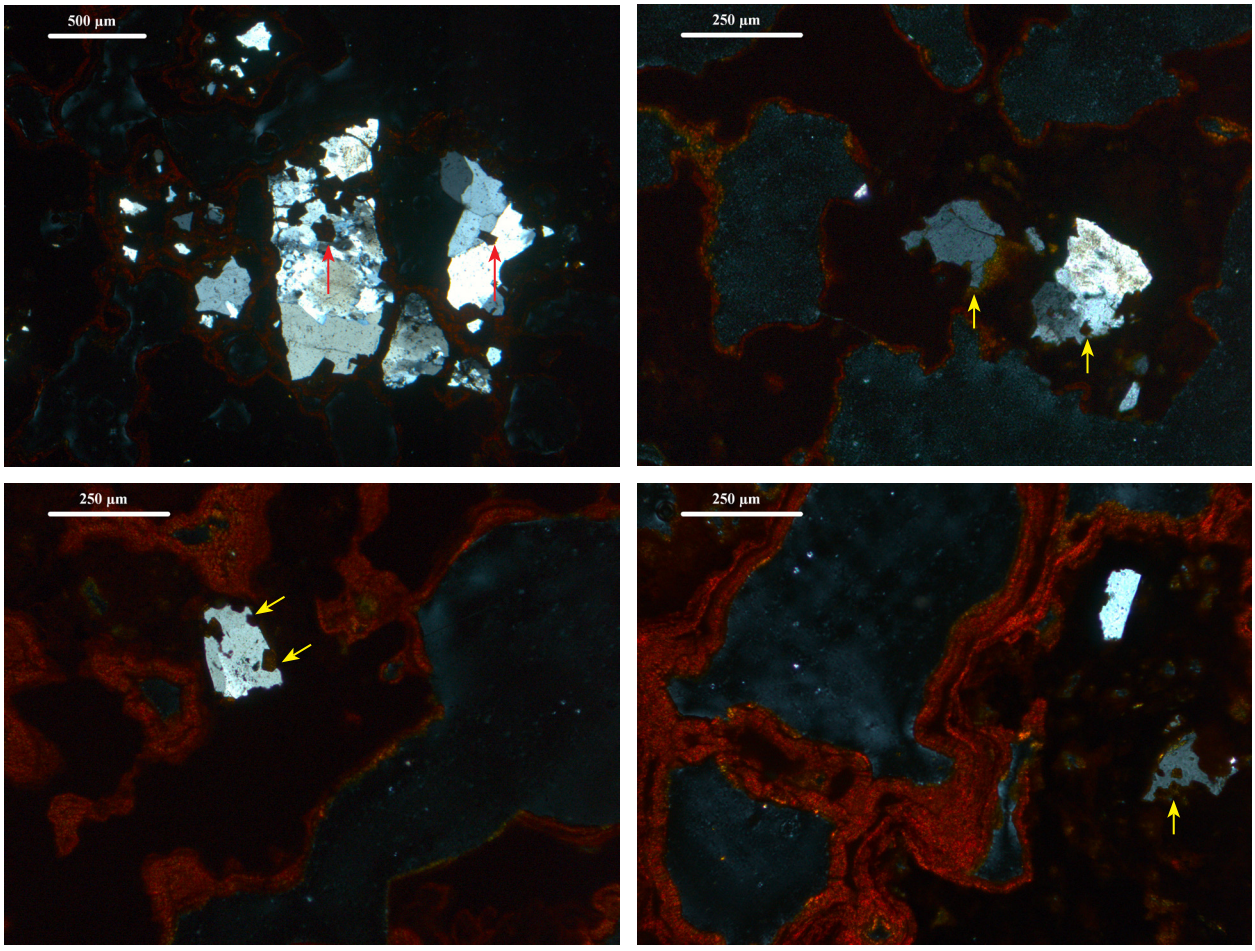

Figure A7. Optical microscopic images of Fe-oxides from Col d'Urdach, Pyrenees. See Figure A8 for location. This image is from a thin section made on the Fe-oxides spot in the Mauléon basin (see Figure 6F in the Article 2). Note that quartz crystals seem to intergrow with the Fe-oxides (some example pointed by the red and yellow arrows). This observation together with the results of element losses (Figure 7A and 8, from Article 2) shows that of Fe and Si are cogenetic by-products of fluid-rock interaction during serpentinization (mantle-related fluids).

Bulk Rock (XRD analyses)

							Clay minerals				
							Serpentines				
Sample	**Quartz**	**Feldspar Na**	**Feldspar K**	**Hematite**	**Magnetite**	**Calcite**	**Amesite**	**Chrysotile**	**Lizardite**	**Chlorite**	**Illite**
VA-F2-11						X		XX	XX		
VA-F2-12				X	X	XX		X	X		
VA-FC2-1	XX									X	X
VA-FC2-5	XX						X				X
VA-FC2-6	XX									X	X
VA-L-7	XX	X	X							X	X
VA-L-9	XX	X	X							X	X
VA-L-18	XX	X	X							X	X
VA-Munta-1	XX	X	X							X	X
VA-Munta-2	XX	X	X							X	X
VA-Munta-3	XX	X	X							X	X
VA-T2-06					X	XX		X	X		
VA-T2-08	XX	X	X							X	X
VA-T2-9	XX	X	X							X	X
VA-T2-10	XX	X	X							X	X
VA-VL-6	XX	X								X	X
VA-VL-7	XX	X								X	X

Clay fraction <2 microns (XRD analyses)

Samples	**Chlorite**	**Illite**	**Talc**	**Amesite**	**Chrysotile**	**Lizardite**	**Amphibole**	**Quartz**	**Feldspar Na**	**Feldspar K**
VA-F2-11					XX	XX				
VA-F2-12			X		XX	XX	XX			
VA-FC2-1	XX	XX							X	
VA-FC2-5		XX		XX					X	X
VA-FC2-6	XX	XX						X	X	
VA-L-7	XX	XX						XX	XX	XX
VA-L-9	XX	XX						XX	XX	XX
VA-L-18	XX	XX							X	
VA-Munta-1	XX	XX						XX	XX	
VA-Munta-2	XX	XX						XX	XX	XX
VA-Munta-3	XX	XX						XX	X	
VA-T2-06	X		XX		XX	XX				
VA-T2-08	XX	XX						XX	XX	XX
VA-T2-9	XX	XX						XX	XX	XX
VA-T2-10	XX	XX						XX	XX	XX
VA-VL-6	XX	XX						XX	XX	XX
VA-VL-7	XX	XX						XX	XX	

Obs.

XX Major Phase

X Minor Phase

Table A3. XRD analyses of bulk and clay fraction. The tables exemplify the analytical method concerned to the mineralogical identification. New mineralogical phases from serpentinites, crustal, sedimentary and fault rocks were studied using XRD. The result of other samples are recorded in the CD disk.

Relative amount (%)

Mirerals	d (obs max) A	VA-F2-11	VA-F2-12	VA-FC2-1	VA-FC2-5	VA-FC2-6	VA-L-7	VA-L-9	VA-L-18	VA-Munta-1	VA-Munta-2	VA-Munta-3	VA-T2-06	VA-T2-08	VA-T2-9	VA-T2-10	VA-VL-6	VA-VL-7	VA-FC-4	VA-FC-7	VA-FC-8c
Illite	9.86	-	-	25	18	35	traces	11	9	traces	8	12	-	13	16	12	traces	16	14	15	12
Glaucophane	8.17	-	-	-	-	-	-	-	-	-	-	-	-	-	-	-	-	-	-	-	-
Serpentine	7.29	89	22	-	-	-	-	-	-	-	-	-	31	-	-	-	-	-	-	-	-
Chamosite	7.07	-	-	20	-	23	7	10	8	10	6	6	-	12	16	7	6	9	8	39	6
Amésite	7.06	-	-	-	8	-	-	-	-	-	-	-	-	-	-	-	-	-	-	-	-
Barite	3.44	-	-	-	-	-	-	-	-	-	-	-	-	-	-	-	-	-	-	-	-
Quartz	3.34	-	-	55	74	42	49	43	38	67	53	54	-	44	34	41	42	68	78	46	82
Orthoclase	3.31	-	-	-	-	-	-	-	-	traces	10	13	-	15	15	16	-	-	-	-	-
Microcline	3.24	-	-	-	-	-	23	19	25	traces	16	10	-	8	16	traces	52	-	-	-	-
Anorthite	3.21	-	-	-	-	-	-	-	-	-	-	-	-	8	3	24	-	-	-	-	-
Albite	3.19	-	-	-	-	-	21	17	20	23	7	5	-	-	-	-	-	7	-	-	-
Calcite	3.03	11	66	-	-	-	-	-	-	-	-	-	66	-	-	-	-	-	-	-	-
Epidote	2.9	-	-	-	-	-	-	-	-	-	-	-	-	-	-	-	-	-	-	-	-
Hématite	2.7	-	12	-	-	-	-	-	-	-	-	-	-	-	-	-	-	-	-	-	-
Magnétite	2.53	-	traces	-	-	-	-	-	-	-	-	-	3	-	-	-	-	-	-	-	-
TOTAL		100	100	100	100	100	100	100	100	100	100	100	100	100	100	100	100	100	100	100	100

Table A4. Semi-quantitative analysis of the mineralogical composition of basement, sedimentary and fault rocks. The values were calculated based on the intensity of the XRD analyses from bulk rocks. Most of the samples are reported in the Article 1 and 2.

Relative amount (‘

Mirerals	d (obs max) A	VA-FC-8m	VA-L-14	VA-L-16	VA-P-2	VA-P-3	VA-P-5	VA-P-6	VA-P-7	VA-T-1	VA-T-6	VA-T-7	VA-T-13	VA-T-14	PN 5 a	PN 5 b	PN5 c	PN5 d	PN5 e
Illite	9.86	17	8	11	2	28	37	17	11	-	30	18	14	13	5		10	3	11
Glaucophane	8.17	-	-	-	-	-	-	-	-	-	-	-	7	-	-	-	-	-	-
Serpentine	7.29	-	-	-	-	-	-	-	-	-	-	-	-	-	-	-	-	-	-
Chamosite	7.07	6	5	10	3	13	14	12	57	20	22	31	37	15	3		10	9	28
Amésite	7.06	-	-	-	-	-	-	-	-	-	-	-	-	-	-	-	-	-	-
Barite	3.44	-	-	-	-	-	-	-	5	-	-	-	-	-	-	-	-	-	-
Quartz	3.34	77	72	49	83	53	46	51	13	-	32	33	8	32	77	100	71	88	56
Orthoclase	3.31	-	-	-	-	-	-	-	-	8	traces	traces	13	-	-	-	-	-	-
Microcline	3.24	-	-	20	-	-	-	-	-	9	8	13	13	-	-	-	-	-	-
Anorthite	3.21	-	-	-	-	-	-	-	-	14	8	-	-	-	-	-	-	-	-
Albite	3.19	-	15	10	11	6	3	20	14	2	traces	5	8	40	15		9		5
Calcite	3.03	-	-	-	1	-	-	-	-	-	-	-	-	-	-	-	-	-	-
Epidote	2.9	-	-	-	-	-	-	-	-	47									
Hématite	2.7	-	-	-	-	-	-	-	-	-	-	-	-	-	-	-	-	-	-
Magnétite	2.53	-	-	-	-	-	-	-	-	-	-	-	-	-	-	-	-	-	-
TOTAL		100	100	100	100	100	100	100	100	100	100	100	100	100	100	100	100	100	100

CONT. OF PREVIOUS TABLE

8.4. **Fault zone description from Mauléon Basin**

The next images and data are related to some of the geological observation from the Mauléon Basin. They concern to a more detailed description observed in the North and South Mauléon Detachments (NMD and SMD). The images show evidence for structures not only related to low angle normal faults but also to a system associated with the evolution of extensional detachments. These descriptions are complementary to the Article 2.

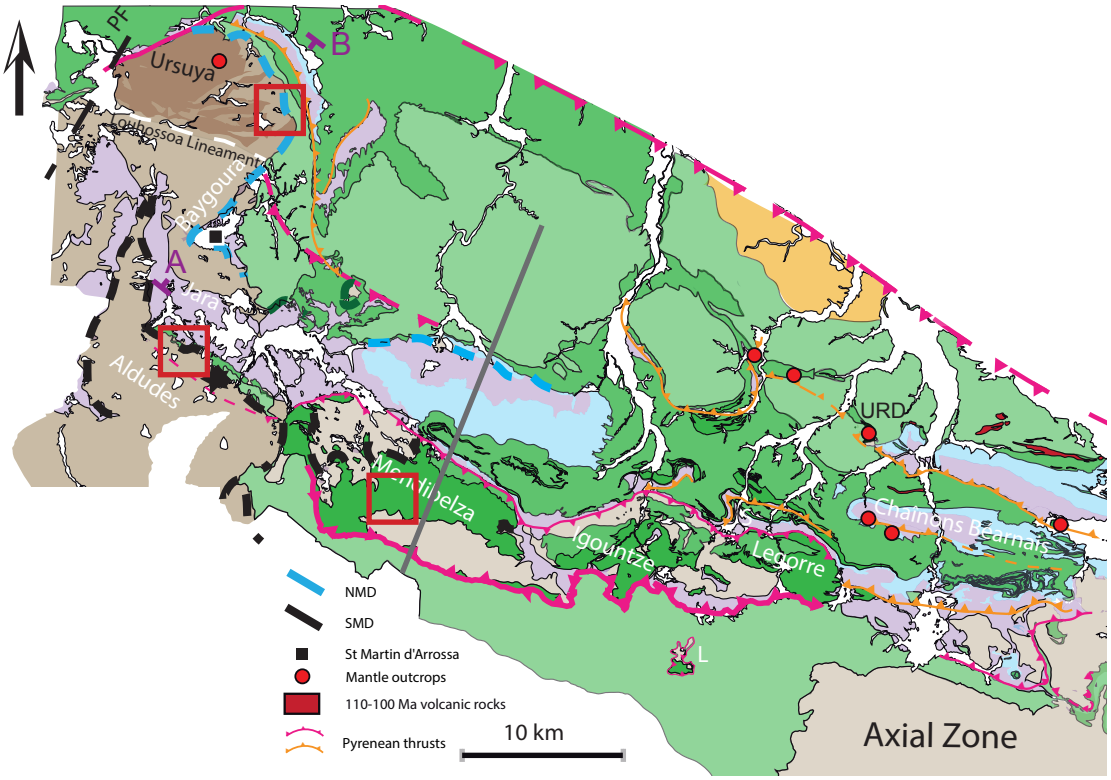

Figure A8. Geological map of the Mauléon Basin (mod. from *Masini* 2011). The red circles are the mantle outcrop. The Col d'Urdach (URD) is indicated in the map. The red squares show the location of the following figures from Aldudes, Garralda and Mendibelza.

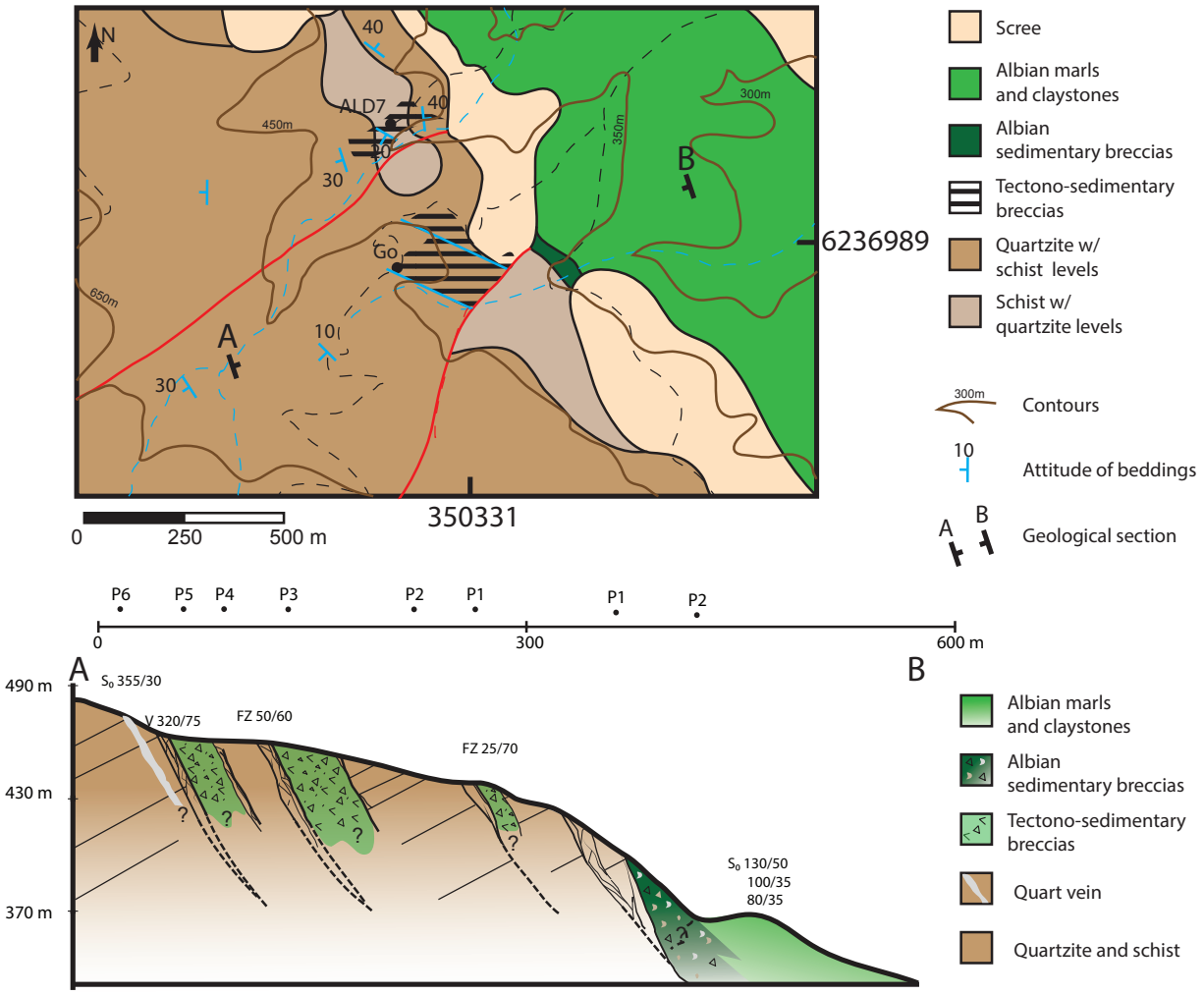

Figure A9. Detailed map and geological section of Aldudes, SMD from Mauléon Basin (see Figure A8 for location). Note the secondary normal faults bounding small and local basins with tectono-sedimentary breccias. The low-angle normal fault (blue line in Figure A11) of the detachment system is only locally preserved (some tens of meter to the north of the map above). Therefore, the extensional detachment systems in the South Mauléon Basin are composed by a main extensional detachment fault (i.e., low-angle normal fault) and high angle normal faults bounding tectono-sedimentary breccias. This is contrasting with NMD and the examples from the Alps where the tectono-sedimentary breccias overlies the low-angle extensional normal faults.

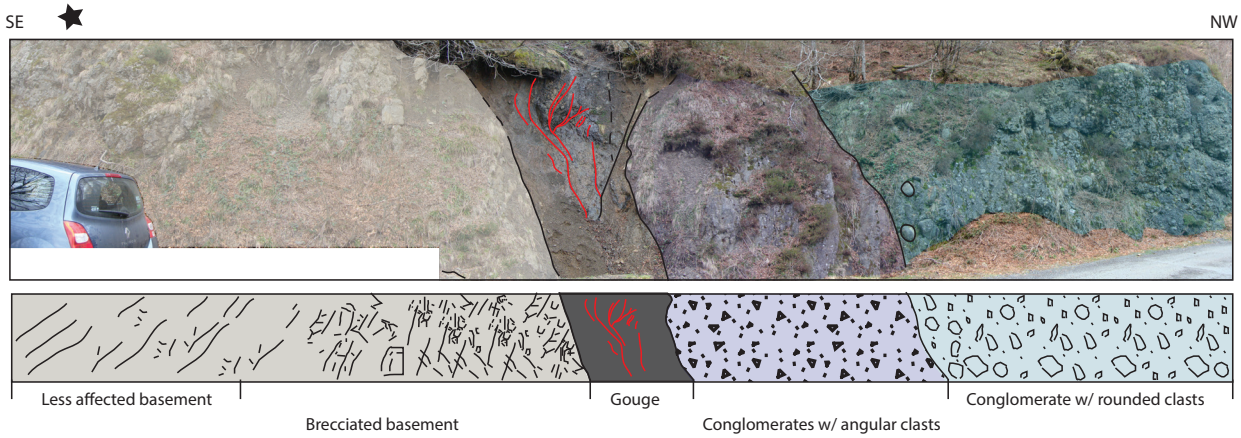

Figure A10. Fault zone in Mendibelza (see regional map for location). This structure is interpreted as a continuation of the extensional detachment system from the Aldude area. They show characteristic fault rocks similar to those observed in the former Adriatic distal margin, exposed in the Alps (e.g., gouges).

Aldudes (SMD)
Detachment
Low to medium-grade
(300<T<500ºC)

Tectono-sedimentary breccia completely silicified.

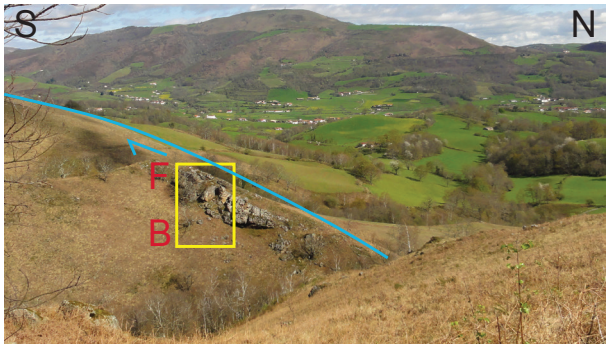

South Mauléon Detachment (blue line). The picture shows the footwall, the Cretaceous basin in the valley and the hanging wall (the mountain in the back of the valley).

This outcrop is located outside the fault zone. Note that the sedimentary bedding is still preserved (i.e., not deformed by SMD).

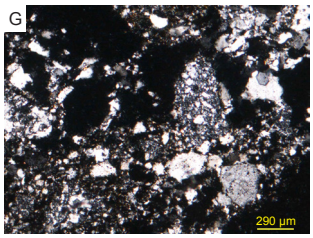

Tectono-sedimentary breccias observed in the SMD often exhibit cataclastic flow. The formation of this rock probably occurred at the sea bottom.
Sample: ALD-5

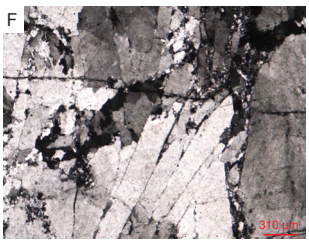

Transgranular fracturing. Some of them showing healing feature caused by the percolation of Si-rich fluids leading to quartz precipitation. Bulging in these fractures show that quartz formed under the influence of deformation in very low-grade condition (<300 ºC).
Sample: ALD-7f

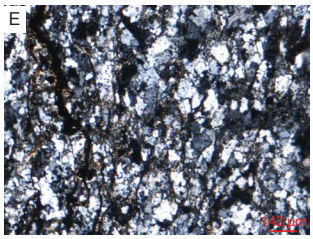

Weak elongation of quartzes. Neoformed sericites/illites in the weak cataclastic foliation showing evidence for percolation of fluids.
Sample: ALD-7d2

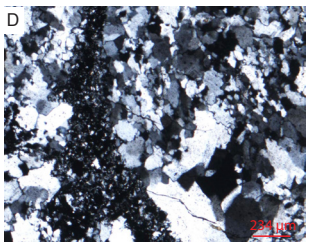

Weak-developed cataclastic structure cutting the earlier GBR (Grain Boundary Rotation) fabric. The GBR shows that the rock was deformed at temperatures a little bit higher and after was affect by a more brittle deformation.
Sample: ALD-7c

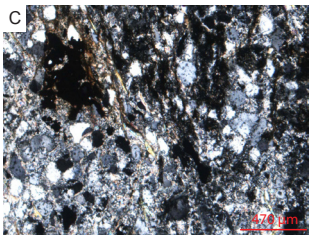

Sericitization in greywacke rock led to the formation of clay minerals developed in the cataclastic foliation. It is possible to see the fault rocks starts to become foliated.
Sampled: ALD-7b

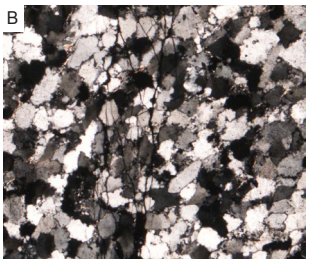

Low grade processes show by weak undulose extinction, bulging and locally GBR. It is possible that water decrease the strength facilitating dislocation creep in the quartz. The fractures cut the bulging and GBR fabric. It shows that the rock was deformed at temperatures a little bit higher and after was affect by brittle deformation.
Sample: ALD-7a

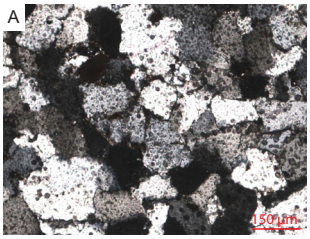

Very weak or absent undulose extinction. Undeformed rock. It has never reached low greenschist facies (T<300 ºC).
Sampled: ALD-6

Figure A11. Structures and microstructures of the fault rocks from the SMD system. These figures show the gradual deformation caused by SMD system. On the left, from bottom to top: the unaffected Paleozoic basement, the fault zone of SMD and the tectono-sedimentary breccias. On the right, from bottom to top the gradual deformations observed in thin sections. The temperature ranges is based on recovery and low-T recrystallization processes of quartz.

Pic Garralda (NMD) Detachment Very Low-grade (T<300ºC)

The hammer lies in the foliated cataclasite and just above we observe tectono-sedimentary breccias. These rocks are characteristic of detachment fault systems.

Vertical brittle shear zone related to the North Mauléon Detachment system. The brittle structures cut the old variscan schistosity developing cataclastic structures.

Variscan basement out of the fault zone. The rocks are mainly composed by quartzites and less frequent by metapelites both in amphibolite facies.

L

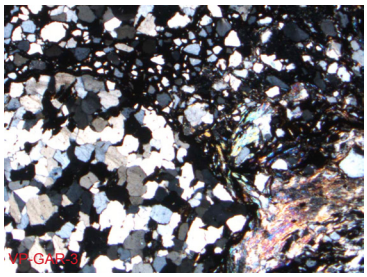

Note that the syn-kinematic muscovite grew in the cataclastic foliation showing a fluid flow and water-assisted reactions along the brittle structures.

J

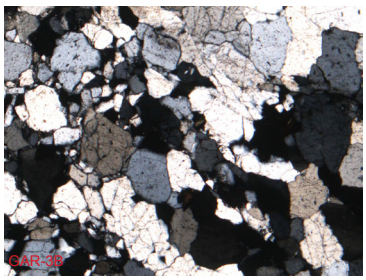

Transgranular fractures in quartzes. Absence of recovery processes. The fractures cut the Variscan microstructures.

J

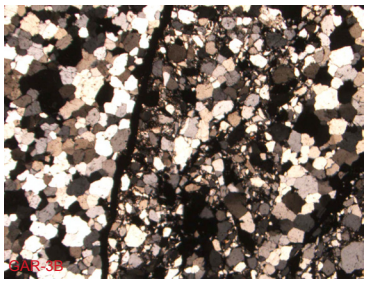

In the fault rocks, cataclastic flow occurs in corridors. Outside the corridor the quartz are fractured. There is no recovery process. It shows that the detachment developed at shallow levels (<300ºC).

I

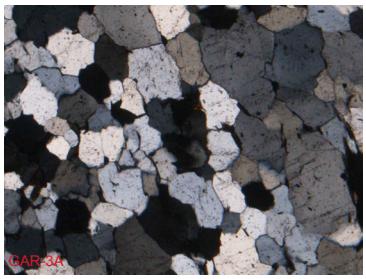

Quartz grains in an amphibolite, absence of undulose extinction. These rocks were not affected by the detachment.

H

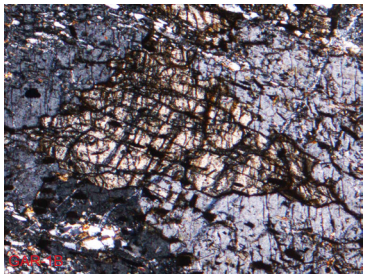

Andalusite after staurolite that can evidence the exhumation of this unit before the detachment activity. This is evidenced by the fact that new low-temperature structures formed by the detachment activity cut the high temperature schistosity. The andalusite forms bellow 3 kbars and 350 ºC (~12 km). Cooling ages of biotite on these rocks is 200 Ma, showing that they were at 10 km at this age. The formation of the andalusite probably occurs during exhumation in the Triassic.

H

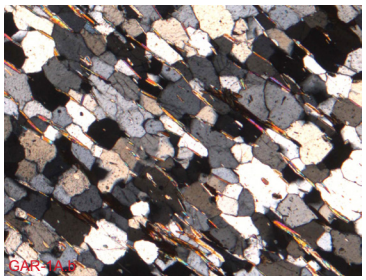

Absent or very weak undulose extinction. The foliation and the GBM is related to the Variscan orogeny. It was not affected by posterior low grade deformation.

Figure A12. Structures and microstructures of fault rocks from the NMD system. These figures show some characteristics of the fault rocks of the NMD system. On the left, from bottom to top: the unaffected Paleozoic basement, sub-vertical brittle shear zone and foliated cataclasite overlain by tectono-sedimentary breccias. On the right, from bottom to top: the gradual deformation observed in thin sections. The temperature is based on the same assumption from previous figures.

RÉSUMÉ ÉTENDU

RÉSUMÉ ÉTENDU

L'évolution et la formation des marges passives riftées, et des océans, sont intimement liées à des processus magmatiques, tectoniques, structuraux et sédimentaires, aussi bien qu'à des changements climatiques et d'ouvertures de nouvelles mers. L'étude de ces marges documente de constants changements de la Terre au cours des temps géologiques. Les fluides sont des constituants fréquemment associés à ces processus ou sont formés par eux, par exemple, les fluides métamorphiques, magmatiques, météoriques, biogènes et diagénétiques. Les relations entre processus dynamiques et fluides sont souvent étudiées localement dans des sites spécifiques, par exemple dans des zones de cisaillement, fumeurs hydrothermaux, et volcans. Ceux-ci sont souvent associés à la formation de veines métamorphiques, de biométhanogenèse et à l'activité des fumeurs noirs (black smokers).

Les fluides jouent un rôle majeur dans le refroidissement de la croûte le long des rides médio-océaniques, dans les formations des gîtes minéraux mais aussi dans la formation des ressources énergétiques. Ils sont probablement importants dans la formation des premiers composés organiques et par conséquence pour l'évolution de la vie primitive.

Bien que les marges passives constituent une grande part de la surface de la planète, les fluides qui se sont développés lors des premiers stades de leur formation et les transferts eau-roche qui en résultent ont été peu étudiés. Cela est principalement dû aux difficultés d'accès aux données car la formation et la circulation actuelle des fluides ont lieu dans les fonds marins, dans les bassins sédimentaires, ou en grande profondeur dans la croûte terrestre. De plus, dans bon nombre de ces systèmes, les flux de fluides sont déjà inactifs, limitant de fait l'étude et compréhension de ces processus.

Cependant, des empreintes et marques de flux de fluides (Figure 1) sont fréquemment observées le long des zones de failles (ex. formation de veines), dans les roches sédimentaires (ex. silicification) et dans le manteau exhumé (ex. serpentinisation). Bien que ces observations soient faites, leur origine, leurs processus de formation ainsi que leur distribution n'ont pas été suffisamment étudiées. Par ailleurs, ces marques sont peu analysées à grande échelle, en particulier à l'échelle d'une marge continentale. D'importantes questions sont fréquemment posées par la communié scientifique, certaines d'entre elles sont abordées dans cette thèse.

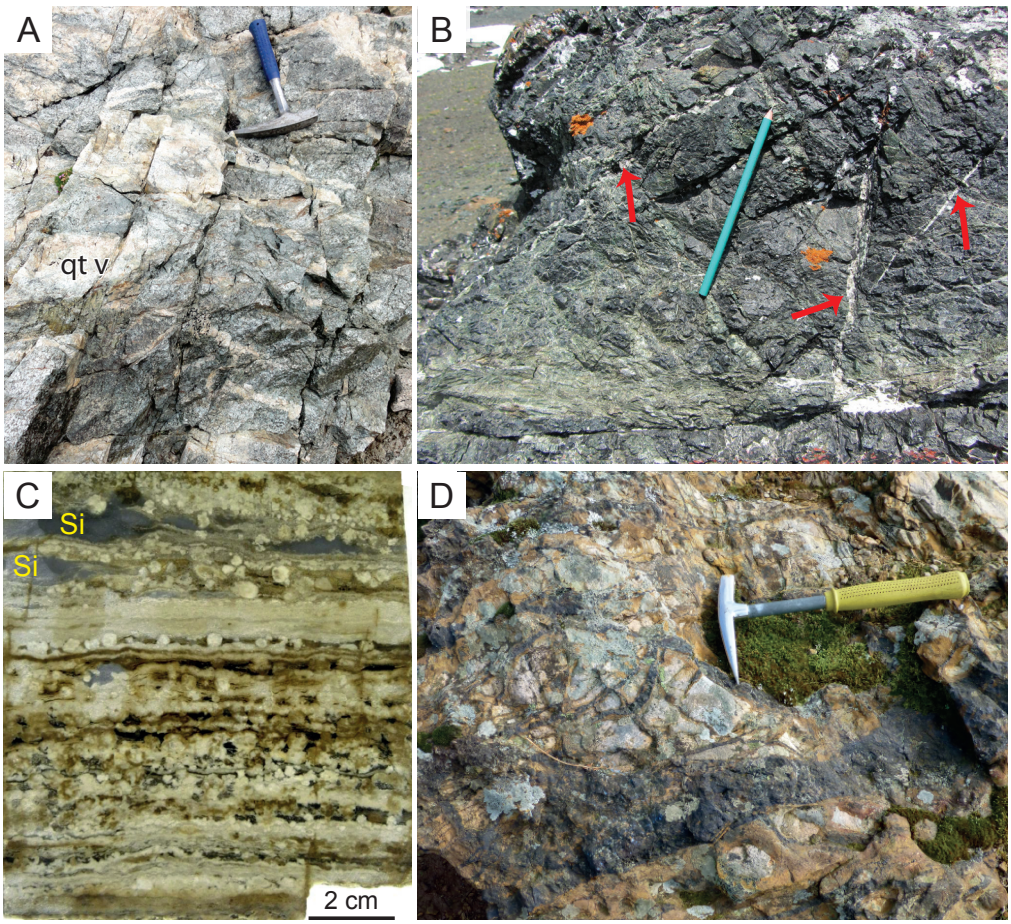

Figure 1. Des empreintes de fluides dans les roches caractéristiques des marges passives riftées. A: veines de quartz et minéraux hydratés (ex. chlorites) dans la zone de faille du détachement d'Err, Alpes Suisse. B: veines de serpentines et calcite formés par la serpentinisation pendant la exhumation du manteau, nappe de Platta, Alpes Suisse. C: silicification des roches carbonatées dans la section «pré-sel» de la marge sud-est brésilienne [Petersohn et al., 2013]. D: veines d'oxydes et dhydroxydes de fer dans les séries pré-rift de la partie hyper-amincie du bassin de Mauléon, Pyrénées de l'ouest.

Quelle est la source des fluides? Comment et quand ont-ils été formés? Quels sont les chemins de migration? Quels sont la source et le piège des ces fluides? Ont-ils interagi avec les roches du socle et du bassin sédimentaire? Quelle est leur composition et sont leurs signatures chimiques préservées? Pouvons-nous quantifier le volume des fluides ayant circulé dans les marges et l'importance des transferts eau-roche? Quel est le rôle des fluides sur l'évolution des marges riftées?

La difficulté d'étudier la trace et la signature des fluides dans les marges actuelles est due à la rareté des données, en particulier dans la partie distale des marges (actuellement en eau profonde). Actuellement, les forages de ces objets géologiques sont limités par la technologie et/ou pour leur coût élevé. De plus, même lorsque les données sont disponibles, elles peuvent être insuffisantes pour comprendre l'évolution des systèmes de fluides à l'échelle d'une marge. Les

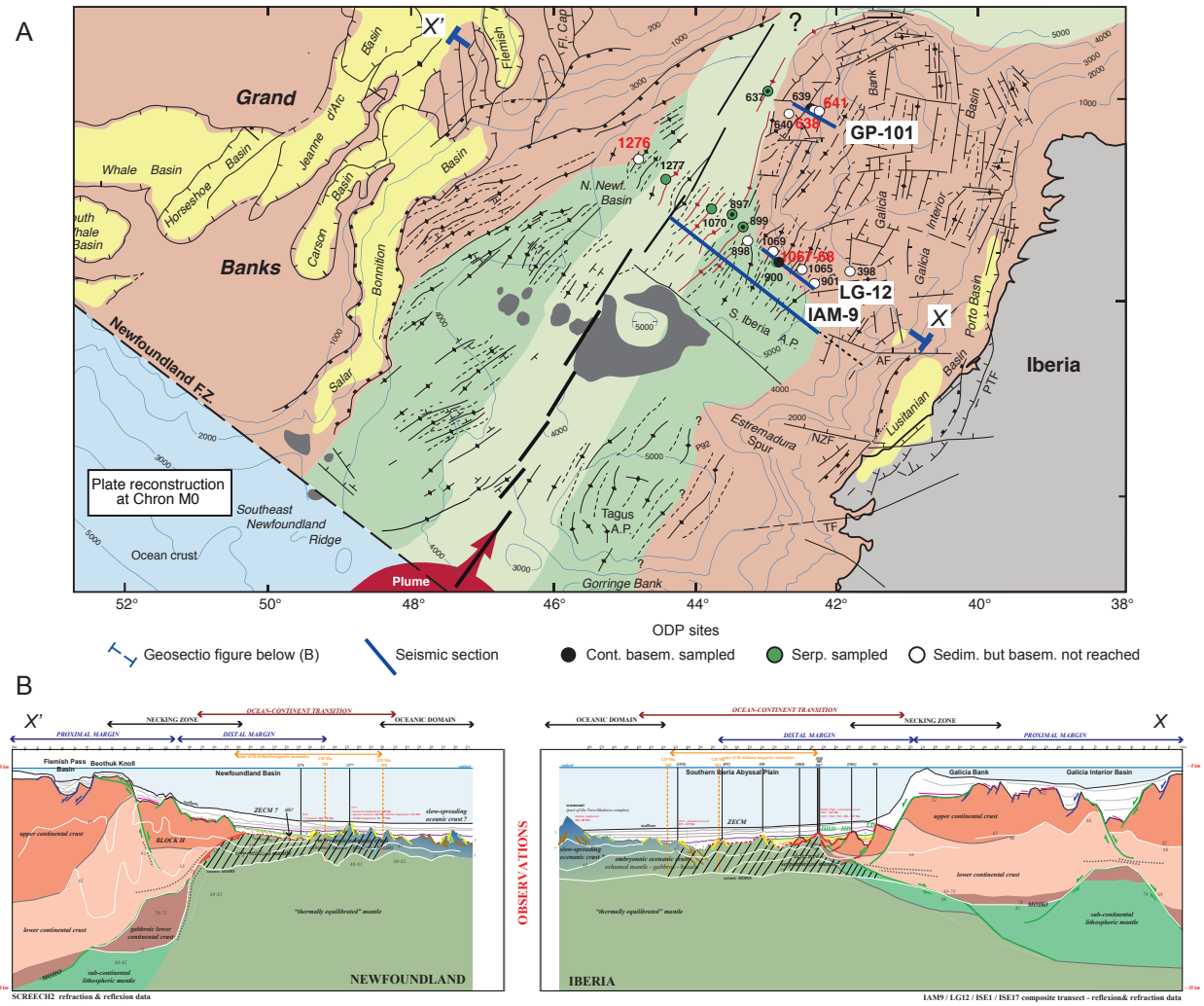

Figure 2. Les marges conjugué d'Ibérie et Terre Neuve . A: reconstruction paleogeographic à l'Aptian (anomalie magnétique M0). Les principaux forage et ligne sísmique utilisée dans cet étude. B: section de la marge conjugué. Les marge d'Ibérie et Terre-Neuve ont de donné unique pour étudier les roche du socle et sédimentaire de la partie hyper-aminci d'un système riftée.

problèmes d'échelle peuvent être résolus par l'utilisation des données sismiques par réfraction et réflexion qui permettent d'imager des structures profondes. Cependant, d'épaisses couches sédimentaires peuvent en limiter la visualisation dans des nombreuses marges. Ainsi, les marges conjuguées de l'Ibérie et de Terre-Neuve (Figure 2) font partie des meilleurs sites pour répondre à ces questions, de par leur caractère pauvre en magma et leurs bassins à faible taux de sédimentation (starved basin). Ainsi, l'acquisition sismique n'est pas influencée par d'épaisses sections sédimentaires, des couches évaporitiques ou d'épaisses séquences volcaniques. De plus, plusieurs forages de l'Ocean Drilling Program (ODP) ont été réalisés lors des trois dernières décennies. Ils ont permis à l'acquisition d'un ensemble de données uniques bien que locales, et très importantes pour la communauté scientifique. Afin de résoudre le problème de continuité

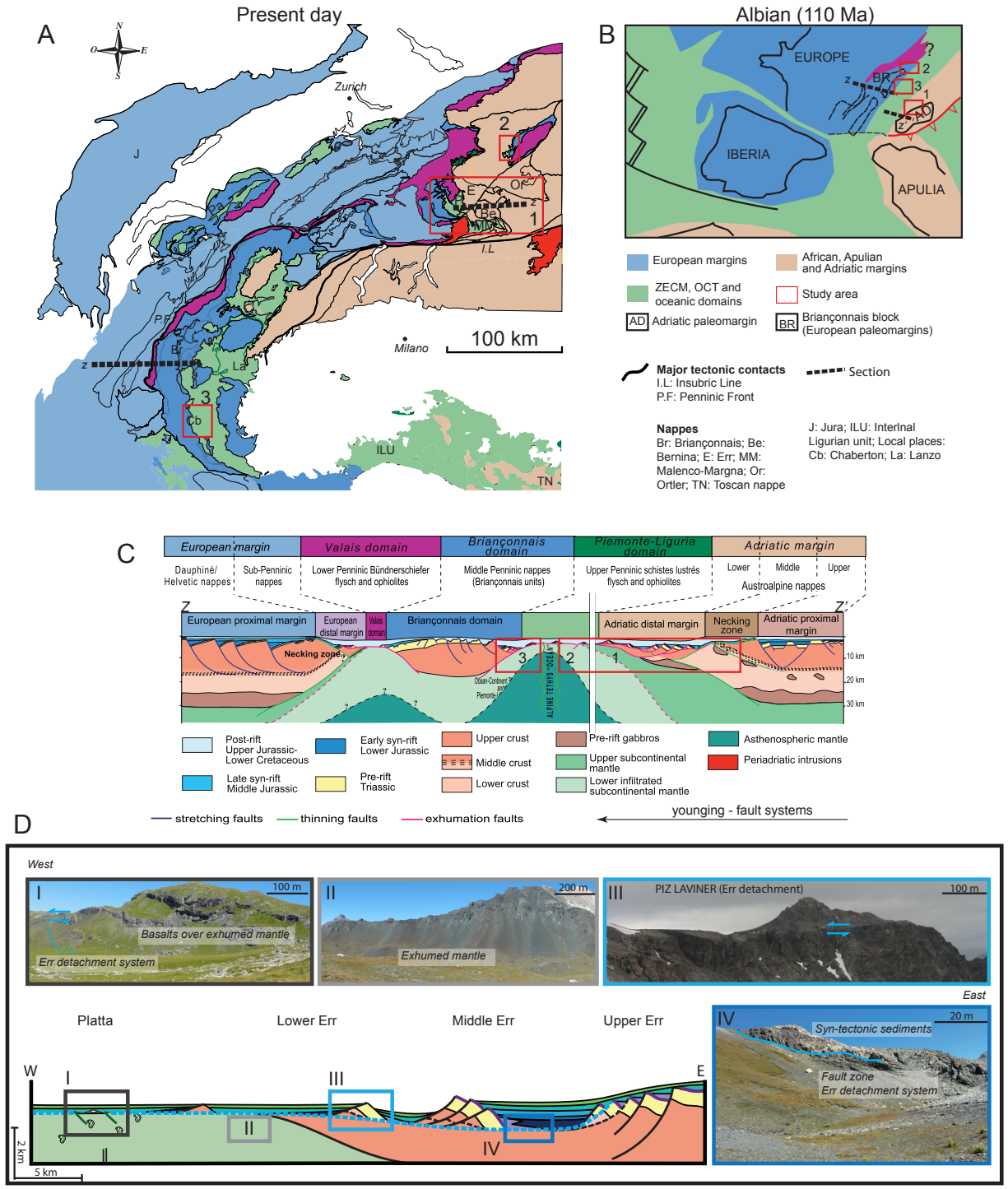

Figure 3. Cartes tectonique, paleogéographique et sections géologique à travers les marges fossiles de la Téthys alpine.(A) Carte tectonique avec la division simplifiée des domaines de la Téthys alpine. (B) carte paleogéographique de la Téthys alpine à l'Albien. Les figures A et B sont modifiées de Schmid et al. [2004] et Mohn et al. [2010]. (C) section composée (z-z') à travers les paleo-marges conjuguées d'Adria et de l'Europe/Briançonnais [Mohn et al., 2010]. Les carrés rouge de A à C marquent la position des sites étudiés: 1-la zone de Necking, la marge distale et la zone de manteau exhumée dans les nappes Austroalpine et Penninique, (Alpes suisse et italienne); 2- La transition continent-ocean (OCT) exposée dans la nappe de Tasna (Alpes suisse); 3- la marge distale et le manteau exhumée exposés dans la nappe Pennique (Alpes française); (D) La marge distale exposée dans les nappes d'Err et de Platta. Les photos correspondantes: I- la faille de détachement extensive et des unités basaltiques dans la zone de manteau exhumé. II- le manteau exhumée de la nappe de Platta. III- le détachement d'Err exposée dans la nappe d'Err. IV: brèches sédimentaires syn-tectonique sur le détachement d'Err.

des structures et des séquences sédimentaires, ces données ont été utilisées dans cette thèse conjointement à deux exemples de systèmes anciens de rift appauvris en magma, de la Téthys alpine et des Pyrénées de l'ouest. Ces systèmes fossiles préservent des bassins sédimentaires et des structures liés au rifting, qui permettent de faire des observations de l'empreinte des fluides et de leur circulation dans un domaine plus large, en comparaison à celui des marges conjuguées Ibérie-Terre Neuve. Les marges de la Téthys alpine exposées dans les Alpes de l'Est Suisse et Sud-Est Français présentent des structures et des bassins jurassiques qui ont été préservés de la déformation et du métamorphisme entre le Crétacé supérieur et le Cénozoïque (Figure 3). Il est important de mentionner que plusieurs similitudes ont été identifiées entre les Alpes et la marge ibérique concernant leur caractéristique tectono-sédimentaire (ex. des bassins à faible taux de sédimentation, des bassins supra-détachements, des failles de détachements extensifs et des systèmes de rift pauvres en magma). Par conséquence, ces marges peuvent être utilisées comme des analogues de systèmes de rift pauvres en magma dont l'évolution des fluides peut être similaire. Le bassin de Mauléon dans les Pyrénées de l'ouest préserve des structures crétacées liées au rifting (Figure 4), et est moins affecté par la compression cénozoïque que les sites des Alpes. Néanmoins, à cause de sections sédimentaires épaisses et d'altérations météoriques intenses, les affleurements sont moins bien exposés et exploitables que ceux des sites des Alpes.

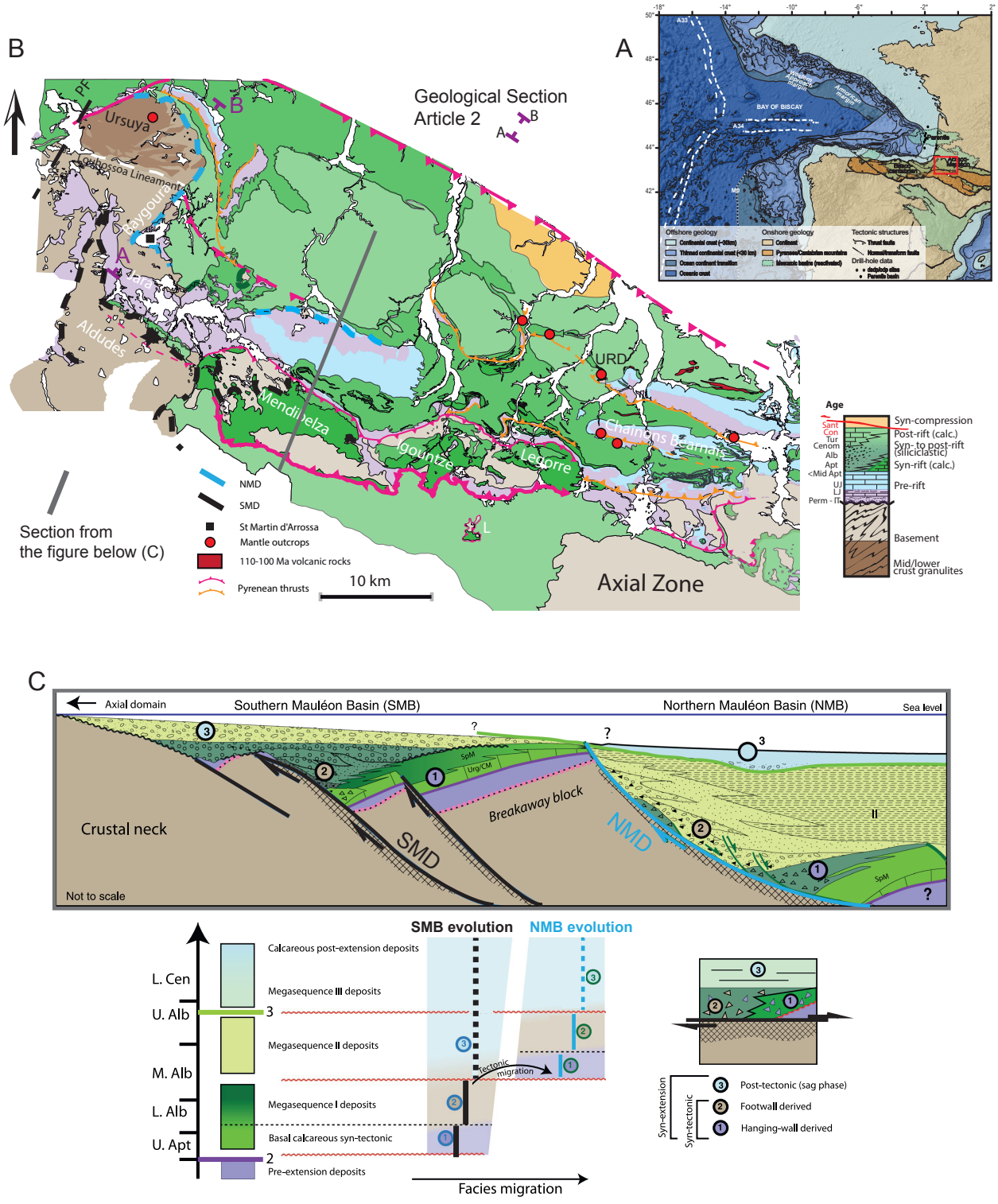

Figure 4. Le bassin de Mauléon dans l'ouest des Pyrénées. A: Contexte général du bassin de Mauléon par rapport au système de rift du Golf de Gascogne et de la chaîne pyrénéenne [Tugend, 2013]. (B) La carte géologique du bassin de Mauléon, modifiée de Masini [2011]. Les points rouge représentent les affleurements de manteau. (C) La section géologique est indiquée sur la carte (B) par la ligne grise. La section recoupe les bassins Sud et Nord de Mauléon, dont le développement est contrôlé par l'activité de leur détachements respectif (SMD et NMD) comme représenté sur le schéma du bas [Masini et al., 2014].

Ainsi, des évidences de circulation de fluides sont présentées et discutées dans cette thèse. J'utilise des exemples des «marges» fossiles riftées exposées dans la Téthys alpine et dans les Pyrénées de l'ouest, ainsi que des marges riftées actuelles d'Ibérie-Terre Neuve. Par les analyses et leurs interprétations, et leur discussion, j'aborde les questions de l'origine et de l'évolution des fluides (c.-à-d. modifiés et enrichis en éléments au cours des réactions eau-roche) dans différents domaines des ces marges au moment de leur formation.

Un résultat majeur est celui de la démonstration que les fluides sont avant tout liés à des structures profondes intimement associées à l'évolution des systèmes hyper-amincis, qui peuvent évoluer dans une marge riftée pauvre en magma. Les fluides migrent au travers de ces structures, provoquent des échanges eau-roche, pour revenir ensuite interagir avec l'eau de mer et les dépôts des bassins sédimentaires sus-jacents (Figure 5). Ces interactions ont de nombreuses implications pour le budget chimique de l'eau de mer, le contrôle de la nature des sédiments, aussi bien que pour les processus diagénétiques.

Ces observations ont permis de proposer des modèles expliquant le lien entre l'histoire de la migration de fluide et l'évolution tectonique des marges riftées. Ces interactions ont un rôle majeur dans les changements rhéologiques de la croûte continentale et du manteau supérieur lors de la phase finale de l'extension, phase qui peut éventuellement résulter en la formation d'une marge riftée pauvre en magma.

La combinaison des différentes méthodes et types de données, comprenant des données structurales/ microstructurales, des études minéralogiques, des analyses chimiques et des données géophysiques, ont permis de caractériser d'anciennes zones de circulation de fluides à grande échelle, dans la partie distale des marges riftées.

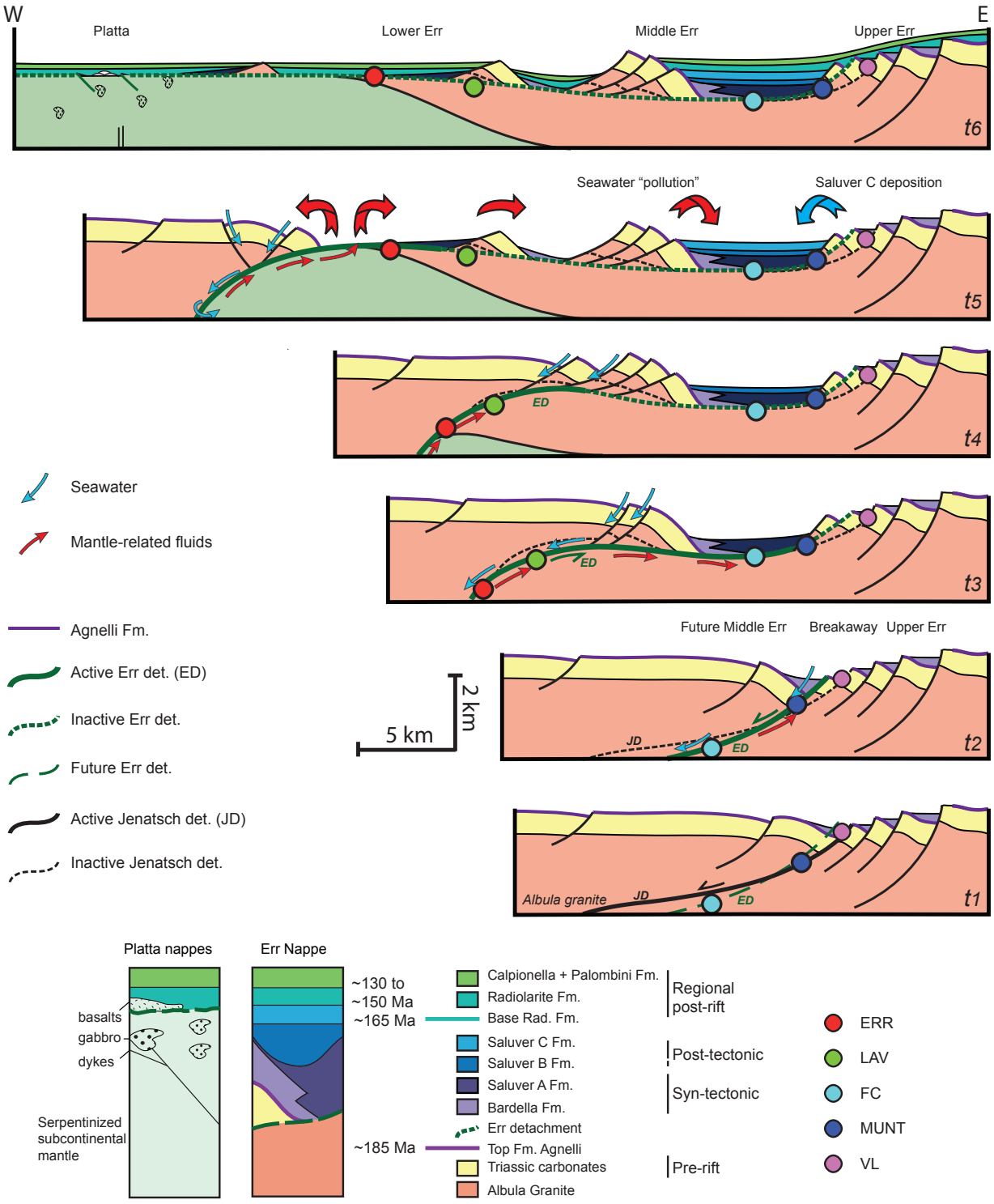

Figure 5. Migration des fluides dans le système hyper-aminci. Exemple de la partie distale de la Téthys alpine, Alpes Suisse. Stage initial (t1): le faille listrique coupe à travers la croûte hyper-aminci (<10 km). À ce moment, l'eau de mer qui circule dans le zone de faille est enrichis en éléments chimique d'origine crustale et mantellique. Ces interactions forment deux types de fluides, un avec une signature de la croûte continentale et un autre avec une signature du manteau. Pendant l'activité du système de détachement, les fluides migrent le long des failles et affectent les sédiments syn-tectonique (t2 and t3). En t3, le détachement devient convexe vers le haut à cause du «upwarping» du pied de la faille. Quand la déformation migre vers la partie distale (ZECM), le segment du détachement situé sous le basin devient inactif. À ce moment les fluides s'échappent vers le fond de la mer, leur signature chimique est ainsi enregistrée dans les sédiments post-tectonique (t4 et t5). A partir de t6, l'activité hydrothermale liée au manteau devient plus faible ce qui est observable dans les enregistrements chimiques des ces sédiments.

Les résultats montrent l'existence de deux types de fluides (Figure 6). Un premier type est dominé par l'interaction entre l'eau de mer et les roches du socle de la croûte continentale, un deuxième type est dominé par l'interaction entre l'eau de mer et des roches mantéliques.

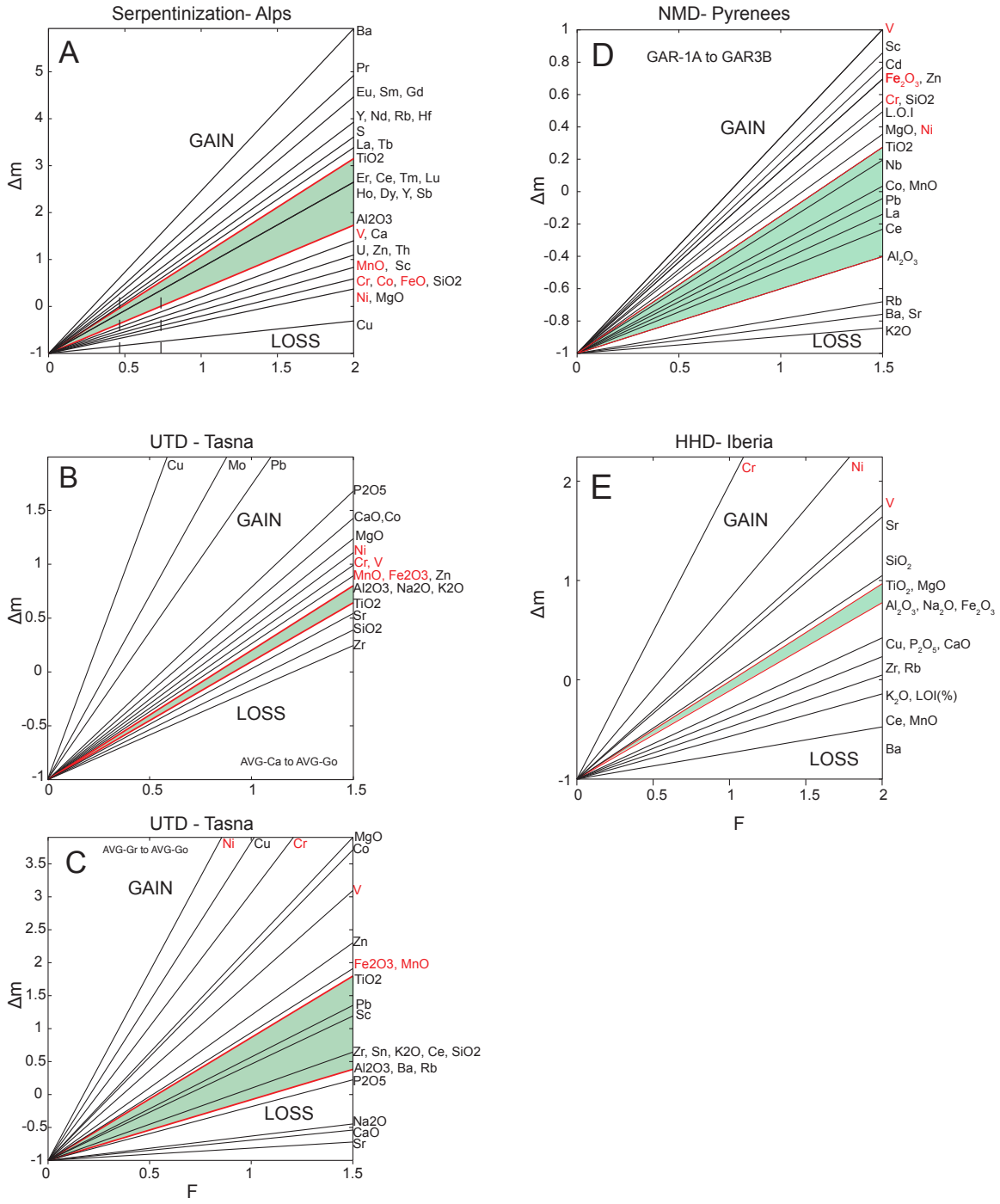

Figure 6. Gains et pertes d'éléments chimiques. La serpentinisation est responsable d'importantes pertes d'éléments (A) pendant l'exhumation du manteau, celle-ci commence en-dessous de la croûte hyper-aminci. Le fluide relié au manteau «mantle-related fluids» peut migrer à travers la zone de faille et ainsi enrichir les roches de faille (gain des élément dans la figure de A-E).

La saussuritisation des roches de la croûte continental peut aussi entraîner des pertes d'éléments (surtout Si et Ca). Ces éléments précipitent sous forme de veines de quartz et de calcite le long de la zone de faille.

Le premier type, lié à la croûte continentale (continental crust related-fluids), est un fluide enrichi en Si et Ca provenant des pertes des éléments causées par l'ensemble des processus de saussuritisation sous l'influence de réactions eau-roche. L'empreinte de ce type de fluide est mise en évidence par la forte chloritisation aussi bien que par les nombreuses occurrences de veines quartz et calcite le long de la zone de faille des systèmes de détachement extensifs. Le deuxième type de fluide, relié au manteau (mantle-related fluids), est enrichi en Si, Mg, Fe, Mn, Ca, Ni, Cr et V provenant des pertes des éléments en réponse aux processus de serpentinisation, produits par l'interaction l'eau de mer-manteau. La serpentinisation produit d'importants changements minéralogiques menant par exemple à la formation de chrysotile, lizardite et chlorite, et résultant en l'augmentation volumétrique et en la diminution de densité des roches mantéliques. Le fluide relié au manteau peut être tracé par les éléments Ni-Cr-V et Fe-Mn le long des zones des failles des grands détachements extensifs mais aussi dans les roches sédimentaires sus-jacentes. Le fait que les signatures des fluides peuvent être documentées dans tous les systèmes extensifs étudiés m'a permis de conclure que la percolation des fluides est un processus important et caractéristique de ces domaines, intervenant au cours de l'évolution des marges riftées pauvres en magma (Figure 7). Tandis que les fluides liés à la croûte continentale sont actifs lors des stades initiaux à tardifs de l'extension, les fluides liés au manteau sont uniquement actifs pendant le stade tardif de l'évolution de systèmes hyper-amincis et au moment de l'exhumation du manteau. Ensuite, la percolation des ces fluides se produit le plus souvent dans des bassins restreints, qui ne sont pas complètement connectés à des domaines océaniques ouverts, causant ainsi une amplification des interactions chimiques entre l'eau de mer et les sédiments contemporains. Les flux de fluides dans les bassins sédimentaires peuvent également influencer l'évolution diagénétique (précoce) des sédiments et par conséquence leurs propriétés physiques (ex. porosité, perméabilité et densité).

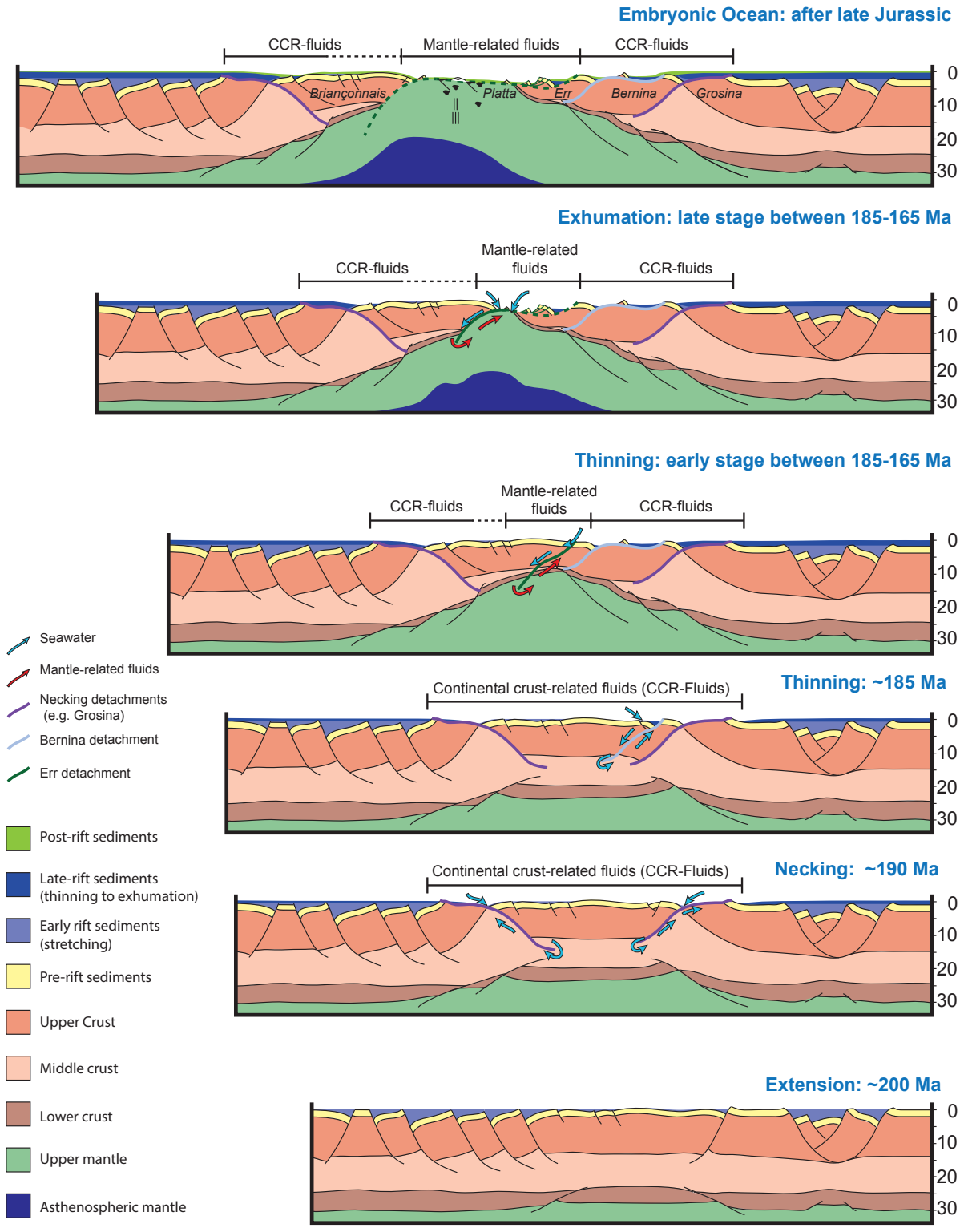

Figure 7. Relation des deux types de fluides avec l'évolutions des marges riftées pauvre en magma. Pendant les phases initiales du système de rift, on trouve seulement des «continental crust-related fluid».

Quand la croûte est hyper-aminci un nouveau système de détachement la recoupe jusqu'à au manteau. A ce moment les «mantle-related fluids» migrent successivement dans la zone de faille, le bassin sédimentaire et finalement dans l'eau de mer. Ces processus change les caractéristiques des roches du socle, des sédiments ainsi que la composition chimique de l'eau de mer.

Le flux de fluides dans les domaines hyper-amincis peuvent jouer un rôle majeur dans la rupture crustale, influencer la focalisation des magmas et la rupture lithosphérique postérieure des marges riftées de type pauvre en magma (Figure 8). Comme l'hydratation de la croûte et du manteau est de grande importance dans les marges riftées pauvres en magma, elle peut également avoir un rôle important au cours de leur réactivation et donc sur la formation de zones de subduction, de l'évolution initiale des orogènes aussi bien que sur le magmatisme le long d'arcs orogéniques. Le cycle de l'exhumation mantélique, d'abord suivie par la serpentinisation, l'absorption d'eau et de pertes d'éléments spécifiques (Ni, Cr, V, Si, Fe, Mn), puis la subduction de ces roches modifiées, doit avoir des impacts majeurs dans les changements et budgets géochimiques des grands réservoirs de la Terre au cours de son évolution.

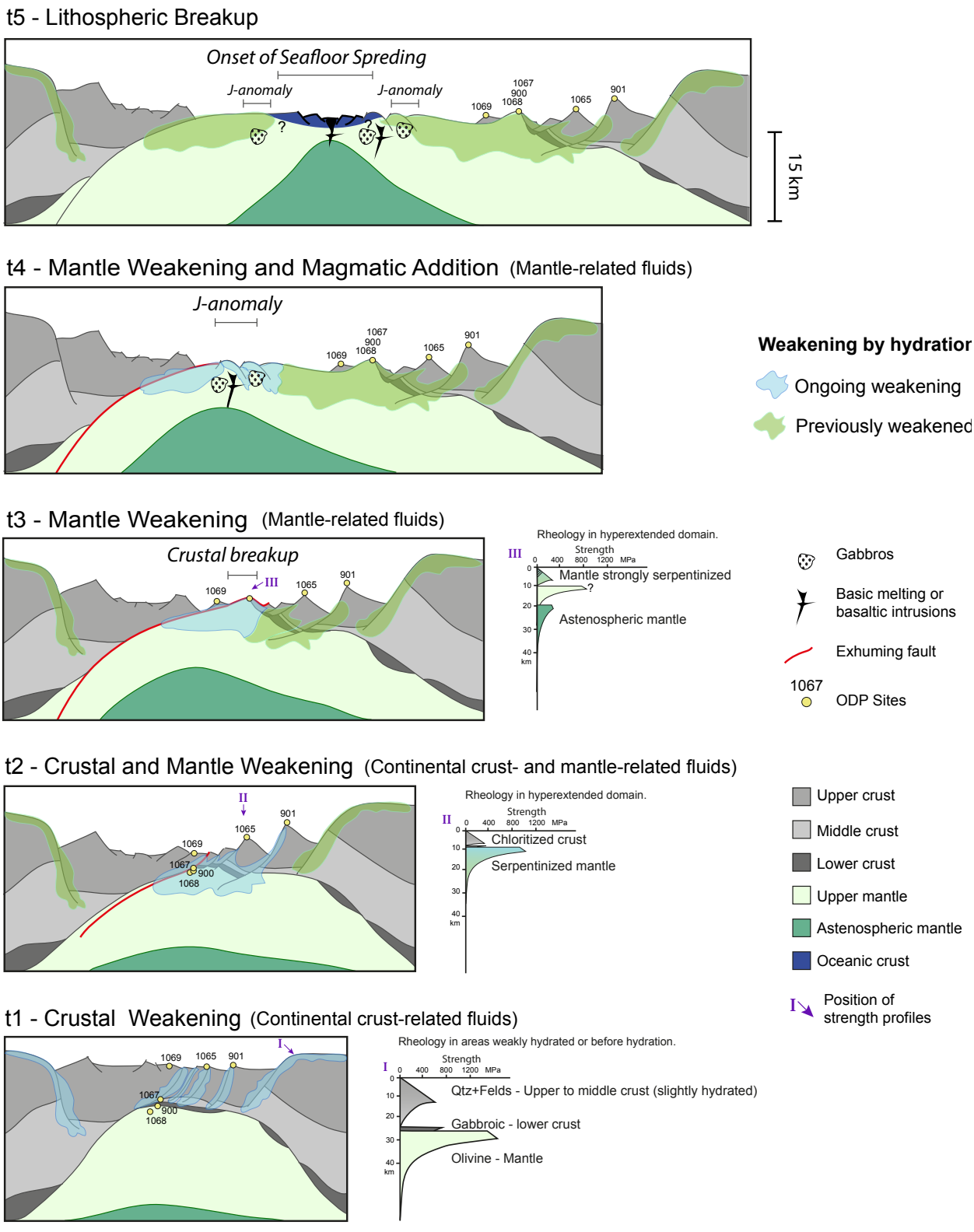

Figure 8. L'influence des fluides sur l'évolution des marges riftées pauvre en magma, l'exemple des marges conjuguées Ibérie-Terre Neuve. L'hydratation des roches de la croûte continentale et du manteau forme des phyllosilicates qui induisent des changements rhéologiques dans ces domaines.

Ce processus peut faciliter le développement de systèmes de détachements, l'exhumation du manteau, les additions magmatiques et l'emplacement d'une ride médio-océanique.

UNIVERSITÉ DE STRASBOURG

Linking tectonic evolution and fluid history in hyperextended rifted margins

IPGS Institut de Physique du Globe de Strasbourg

Résumé

Des évidences de circulation de fluides sont fréquemment observées dans les marges «riftées». Néanmoins, la nature de la plupart de ces fluides est peu comprise. En plus, les effets et les *empreintes* des fluides qui se développent pendant l'évolution des marges distales riftées sont peu discutés ou étudiés. Cette thèse est centrée sur la caractérisation des traceurs des fluides qui interagissent avec les roches du socle et les roches sédimentaires dans les systèmes hyper-amincis. L'étude de ces fluides est basée sur les observations géologiques, les analyses géochimiques et les données géophysiques de laboratoires naturels (sites privilégiés) des systèmes hyper-amincis exposés dans les marges distales riftées de la Téthys alpine, dans le basin de Mauléon (Ouest des Pyrénées) et dans les marges actuelles d'Ibérie et Terre Neuve.

Deux types des fluides ont été identifiés. Le premier, les *fluides associés à la croûte continentale*, est lié à des interactions eau de mer-croûte continentale qui provoquent le processus de saussuritisation responsable de pertes de Si et Ca. Le deuxième type, les *fluides associés au manteau*, est lié aux interactions entre l'eau du mer et le manteau qui induisent la serpentinisation des roches mantélliques responsable des transferts de Si, Mg, Fe, Mn, Ca, Ni, Cr et V vers le milieu marin et sédimentaire. Les interactions fluide-roche ne sont pas uniquement responsables de l'altération et des pertes des éléments mais aussi de l'enrichissement des fluides qui percolent dans les roches de socle puis dans les roches sédimentaires. La migration des fluides dans les systèmes étudiés résulte en une forte *empreinte* qui est fréquemment identifiée par la formation de nouvelles phases minérales et par une importante création de *veines.* Ces *empreintes* de transferts sont vérifiées par les données et les budgets géochimiques.

La percolation des fluides est fortement liée à la formation des failles de détachements extensifs et à l'évolution des systèmes hyper-amincis. Les flux de fluides marquent un évènement important au cours des phases finales d'évolution des systèmes hyper-amincis (exhumation du manteau) et des futurs domaines des marges distales riftées (bassins sédimentaires).

Le flux de fluides dans ces systèmes a des implications importantes pour les changements rhéologiques, pour la nature des sédiments et pour les modifications chimiques des réservoirs de la Terre au cours des étapes majeures de leur évolution.

Mots-clefs: fluides, tectonique des marges riftées, évolutions des domaines hyper-amincis, failles de détachement, serpentinisation, saussuritisation.

Abstract

Fluids are common components observed in rifted margins. However, the nature of many existing fluids in distal rifted margins and hyperextended systems are poorly understood. Moreover, how fluids evolve during the development of distal rifted margins is rarely discussed. This thesis addresses the effects and traces of fluids that interact with basement and sedimentary rocks in hyperextended systems. The investigation of such fluids is based on geological observation, geochemical analyses and geophysical data from natural laboratories of hyperextended systems exposed in the fossil distal rifted margins of the Alpine Tethys, Mauléon Basin in the West Pyrenees and the present-day distal margins of Iberia and Newfoundland.

Two types of fluids were identified during this study. The first type, referred to as *continental crust-related fluids,* is associated with seawater-continental crust interaction leading to saussuritization processes responsible for losses of Si and Ca. The second type, referred to as *mantle-related fluids,* is related to seawater-mantle interaction resulting in serpentinization of mantle rocks, which causes losses of Si, Mg, Fe, Mn, Ca, Ni, Cr and V. These fluid-rock interactions are not only responsible for element losses and leaching but also for the enrichment of fluids that percolate in basement and sedimentary rocks. The fluid migration in the studied systems resulted in a strong *imprint* that is often characterized by new mineralogical phases and strong veining, which are constrained by geochemical data.

The fluid percolation is strongly related to the formation of extensional detachment faults and the evolution of hyperextended systems. Fluid flow marks an important event during the final evolution of hyperextended systems and future domains of distal rifted margin. Fluid flow in these systems has major implications for the nature of sediments, rheological changes and chemical modifications of the Earth's reservoirs throughout its evolution.

Keywords: fluids, tectonics of rifted margins, evolutions of hyperextended domains, detachment faults, serpentinization, saussuritization